

2015

FLOOD RISK ASSESSMENT UNDER HISTORICAL AND PREDICTED LAND USE CHANGE USING CONTINUOUS HYDROLOGIC MODELING

Jonathan T. Nelson
Michigan Technological University

Follow this and additional works at: <https://digitalcommons.mtu.edu/etds>



Part of the [Engineering Commons](#), [Land Use Law Commons](#), and the [Water Resource Management Commons](#)

Copyright 2015 Jonathan T. Nelson

Recommended Citation

Nelson, Jonathan T., "FLOOD RISK ASSESSMENT UNDER HISTORICAL AND PREDICTED LAND USE CHANGE USING CONTINUOUS HYDROLOGIC MODELING", Master's Thesis, Michigan Technological University, 2015.

<https://digitalcommons.mtu.edu/etds/917>

Follow this and additional works at: <https://digitalcommons.mtu.edu/etds>



Part of the [Engineering Commons](#), [Land Use Law Commons](#), and the [Water Resource Management Commons](#)

FLOOD RISK ASSESSMENT UNDER HISTORICAL AND PREDICTED LAND USE
CHANGE USING CONTINUOUS HYDROLOGIC MODELING

By

Jonathan T. Nelson

A THESIS

Submitted in partial fulfillment of the requirements for the degree of

MASTER OF SCIENCE

In Civil Engineering

MICHIGAN TECHNOLOGICAL UNIVERSITY

2015

© 2015 Jonathan T. Nelson

This thesis has been approved in partial fulfillment of the requirements for the Degree of
MASTER OF SCIENCE in Civil Engineering.

Department of Civil and Environmental Engineering

Thesis Advisor: *Dr. Veronica L. Webster*

Committee Member: *Dr. Ann L. Maclean*

Committee Member: *Dr. Alex S. Mayer*

Department Chair: *Dr. David W. Hand*

Table of Contents

List of Figures	vii
List of Tables	xvii
Acknowledgements.....	xx
Abstract	xxii
Chapter 1. Introduction	1
1.1 Research Motivation	2
1.2 Research Objectives.....	9
Chapter 2. Watershed Selection and Characteristics	11
2.1 Watershed Selection Process	13
Chapter 3. Historical Land Use Maps.....	25
3.1 Data Preparation	25
3.1.1 Georeferencing and Rectifying Images	27
3.1.2 Mosaic Images	33
3.1.3 Segmentation and Classification.....	38
3.2 Change Analysis	44
Chapter 4. Land Use Projection	53
4.1 SRES Scenario Storylines	54
4.1.1 A1B Scenario	56
4.1.2 B1 Scenario.....	56

4.1.3 B2 Scenario.....	57
4.1.4 A2 Scenario.....	57
4.1.5 Selected SRES Scenarios.....	58
4.2 FORE-SCE Model Description	58
4.3 FORE-SCE Model Results	66
Chapter 5. Hydrologic Modeling using ArcSWAT	76
5.1 Model Description	76
5.2 Model Input and Current Conditions.....	84
5.3 Historical Flood Series	87
5.3.1 Generalized NLCD Comparison.....	90
5.3.2 Historical LULC Comparison.....	92
5.4 Projected Future Flood Series.....	96
5.5 Overall Flood Series Trends	104
Chapter 6. Conclusions and Recommendations.....	106
Chapter 7. References	110
Appendix A . Current Watershed Characteristics.....	122
Appendix B . Historical Land Use Procedure and Results	128
Appendix C . Future Predictions of LULC Conditions	139
Appendix D . Hydrologic SWAT Model.....	155

List of Figures

Figure 2.1: Locations of 235 USGS streamflow gauging stations defining the study area for unimpaired watersheds in the Upper Midwest and Northeastern U.S. (Data Source: Fritsch, 2012).....	12
Figure 2.2: Locations of 143 USGS streamflow gauging stations defining the study area for moderately impaired watersheds in the Upper Midwest and Northeastern U.S. (Data Source: Salvadori, 2013).....	13
Figure 2.3: Locations of four unimpaired to moderately impaired USGS streamflow gauging stations selected for LULC change analysis.	14
Figure 2.4: Location of Great Egg Harbor River Watershed and associated streamflow gauging station (USGS Station 1411000) with 2011 National Land Cover Database (NLCD). (Data Source: USDA, 2014).....	16
Figure 2.5: Location of Pond Creek Watershed and associated streamflow gauging station (USGS Station 03302000) with 2011 National Land Cover Database (NLCD). (Data Source: USDA, 2014).	17
Figure 2.6: Location of Deer Creek Watershed and associated streamflow gauging station (USGS Station 03329700) with 2011 National Land Cover Database (NLCD). (Data Source: USDA, 2014).	18
Figure 2.7: Location of Pigeon Creek Watershed and associated streamflow gauging station (USGS Station 04099510) with 2011 National Land Cover Database (NLCD). (Data Source: USDA, 2014).....	19
Figure 2.8: Annual maximum flood series from 1945 to 2013 for USGS gauging station 03302000 (Pond Creek Watershed, KY).	23
Figure 2.9: Annual maximum flood series from 1946 to 2013 for USGS gauging station 04099510 (Pigeon Creek Watershed, IN).	23
Figure 2.10: Probability of non-exceedance plot with LP3 distribution fit to observed	

AMF series from 1945 to 2013 for USGS station 03302000 (Pond Creek Watershed, KY).	24
Figure 2.11: Probability of non-exceedance plot with LP3 distribution fit to observed AMF series from 1946 to 2013 for USGS station 04099510 (Pigeon Creek Watershed, IN).	24
Figure 3.1: Depiction of three different orders of polynomial transformations before and after the transformation is implemented (Modified from ArcGIS, 2008).	29
Figure 3.2: Four possible distortion changes while implementing a 1 st order polynomial affine transformation (Modified from ArcGIS Resources, 2014).	29
Figure 3.3: Georeferencing two 1971 aerial images for Pond Creek Watershed, KY (USGS station 03302000) using ArcMap. (Image data source: EROS, 2015. Full image created by author).	32
Figure 3.4: Comparison of a historical image (ca. 1971) to 2006 orthoimagery for station 03302000 (Pond Creek, KY). Circled areas indicate possible coordinate locations of GCPs for georeferencing. (Image data source: EROS, 2015. Full image created by author).	35
Figure 3.5: Mosaic 1971 historical image georeferenced to 2006 orthoimagery, coordinate system NAD 1983 UTM Zone 16N for USGS station 03302000 (Pond Creek, KY). (Image data source: EROS, 2015. Full image created by author).	36
Figure 3.6: Mosaic historic aerial image (ca. 1971) for USGS station 03302000 (Pond Creek, KY) – full image (top), clipped to watershed (bottom). (Image data source: EROS, 2015. Full image created by author).	37
Figure 3.7: Image segmentation utilizing SPRING for Pond Creek Watershed, KY (USGS station 03302000). Red lines are segmented area boundaries.	40
Figure 3.8: Image classification utilizing SPRING for Pond Creek Watershed, KY (USGS station 03302000). Green (light/dark) represents forested areas, brown (light/dark) represents agricultural areas, and white represents urban developed areas.	40

Figure 3.9: Image classification of generalized historical land use types for Pond Creek Watershed, KY (USGS station 03302000) utilizing SPRING.....	43
Figure 3.10: Historical LULC change progression from 1959 to 2011 for Pond Creek, KY (USGS station 03302000).....	46
Figure 3.11: Historical LULC change progression from 1952 to 2011 for Pigeon Creek, IN (USGS station 04099510).....	47
Figure 3.12: Transition from agricultural to urban developed LULC type (in RED) between 1957 and 2011 for Pond Creek, KY (USGS station 03302000) determined using LCM change analysis.....	48
Figure 3.13: Transition from agricultural to urban developed LULC type (in RED) between 1952 and 2011 for Pigeon Creek, KY (USGS station 04099510) determined using LCM change analysis.....	49
Figure 3.14: Net change (mi ²) of generalized LULC types observed between 1952 and 2011 for Pigeon Creek, KY (USGS site 04099510) determined using LCM change analysis.....	50
Figure 3.15: Graphical representation of LULC change between 1957 and 2011 for Pond Creek, KY (USGS station 03302000).....	51
Figure 3.16: Graphical representation of LULC change between 1951 and 2011 for Pigeon Creek, IN (USGS station 04099510).....	51
Figure 4.1: IPCC scenario based models with two axes: 1) economic vs. environmental priorities, and 2) global vs. regional development (Data Source: Nakicenovic, 2000; Solomon et al., 2007. Modified by author).....	55
Figure 4.2: Input variables and driving forces implemented in FORE-SCE (Adapted from USGS, 2014).....	60
Figure 4.3: United States Environmental Protection Agency (EPA) Level III ecological regions. (Data Source: Omernik, 1987).....	65
Figure 4.4: Location of Land Cover Trend ecoregions, with the locations of sample	

blocks used to characterize each ecoregion in the conterminous U.S. Sample blocks have areas of either 10 km x 10 km or 20 km x 20 km (Data Source: USGS, 2014).	65
Figure 4.5: Overall FORE-SCE LULC projection for the year 2100 in the Midwest and Northeast U.S. (Data Source: USGS, 2014).	69
Figure 4.6: FORE-SCE scenario based spatial LULC model projection for the year 2100 for Great Egg Harbor River Watershed, NJ (USGS station 01411000). (Data Source: USGS, 2014).	70
Figure 4.7: FORE-SCE scenario based spatial LULC model projection for the year 2100 for Pond Creek Watershed, KY (USGS station 03302000). (Data Source: USGS, 2014).	71
Figure 4.8: FORE-SCE scenario based spatial LULC model projection for the year 2100 for Deer Creek Watershed, IN (USGS station 03329700). (Data Source: USGS, 2014).	72
Figure 4.9: FORE-SCE scenario based spatial LULC model projection for the year 2100 for Pigeon Creek Watershed, IN (USGS station 04099510). (Data Source: USGS, 2014).	73
Figure 5.1: Soil and Water Assessment Tool GIS integrated model (ArcSWAT) Hydrologic Response Unit (HRU) layer used to separate areas with similar hydrologic response characteristics.	78
Figure 5.2: SWAT command loop for HRU/Subbasin process simulating the land phase of the hydrologic cycle. Modified from (Neitsch et al., 2005).	79
Figure 5.3: Probability of non-exceedance plot with LP3 distribution fit to the base period simulation and observed data from 1980 to 1999 for Pond Creek Watershed, KY (USGS station 03302000). Data include 1992 NLCD and 1978-1999 CMIP3 climate data.	86
Figure 5.4: Probability of non-exceedance plot with LP3 distribution fit to the base period simulation and observed data from 1980 to 1999 for Pigeon Creek Watershed, IN	

(USGS station 04099510). Data include 1992 NLCD and 1978-1999 CMIP3 climate data.....	86
Figure 5.5: Probability plot for LP3 distributions fit over base period (1980–1999) for comparison of observed AMF, simulated AMF with 1992 NLCD, and simulated AMF with generalized 1992 NLCD for Pond Creek Watershed, KY (USGS station 03302000).....	91
Figure 5.6: Probability plot of LP3 distributions fit over base period (1980–1999) for comparison of simulated AMF with 2006 NLCD and simulated AMF with generalized 2006 NLCD for Pond Creek Watershed, KY (USGS station 03302000).	91
Figure 5.7: Probability plot of LP3 distributions fit over base period (1980–1999) for comparison of observed AMF, simulated AMF with 1992 NLCD, and simulated AMF with generalized 1992 NLCD for Pigeon Creek Watershed, IN (USGS station 04099510).....	92
Figure 5.8: Probability plot for comparison of LP3 distributions fit to simulated AMF series obtained using 1992 NLCD, generalized 1992 NLCD, and results of aerial imagery for historic periods in Pond Creek Watershed, KY (USGS station 03302000).	95
Figure 5.9: Probability plot for comparison of LP3 distributions fit to simulated AMF series obtained using 1992 NLCD, generalized 1992 NLCD, and results of aerial imagery for historic periods in Pigeon Creek Watershed, KY (USGS station 04099510).	96
Figure 5.10: Probability plot of LP3 distributions fit to simulated AMF series under A1B, A2, B1, and B2 FORE-SCE LULC scenarios for 2080-2100 in Pond Creek Watershed, KY (USGS station 03302000).	100
Figure 5.11: Probability plot of LP3 distributions fit to simulated AMF series under A1B, A2, B1, and B2 FORE-SCE LULC scenarios for 2080-2100 in Pigeon Creek Watershed, IN (USGS station 04099510).....	100

Figure 5.12: Probability plot of LP3 distribution fit to simulated AMF series under the A2 FORE-SCE LULC scenario for 2080-2100 compared to results for ‘base’ simulation period 1980-1999 for Pond Creek Watershed, KY (USGS station 03302000).	101
Figure 5.13: Probability plot of LP3 distribution fit to simulated AMF series under the A2 FORE-SCE LULC scenario for 2080-2100 compared to results for ‘base’ simulation period 1980-2000 for Pigeon Creek Watershed, IN (USGS station 04099510).	101
Figure 5.14: Moving window plot of percentiles for the FORE-SCE A1B scenario simulating a repeating 20 year climate period and shifting LULC data for Pigeon Creek Watershed (USGS station 04099510) from 2000-2100.	103
Figure 5.15: Moving window plot of percentiles for the FORE-SCE A2 scenario simulating a repeating 20 year climate period and shifting LULC data for Pigeon Creek Watershed (USGS station 04099510) from 2000-2100.	103
Figure 5.16: Probability plot comparing LP3 distributions fit to simulated AMF series for the base period (1980-1999), an early historical period, and the future A2 FORE-SCE LULC scenario (2080-2100) for Pond Creek Watershed, IN (USGS station 03302000).	104
Figure 5.17: Probability plot comparing LP3 distributions fit to simulated AMF series for the base period (1980-1999), an early historical period, and the future A2 FORE-SCE LULC scenario (2080-2100) for Pigeon Creek Watershed, IN (USGS station 04099510).	105
Figure A.1: Watershed characteristics including soil (STATSGO), Digital Elevation Model (DEM), slope, and 2011 NLCD for USGS station 01411000. (Data Source: USDA, 2014).	122
Figure A.2: Watershed characteristics including soil (STATSGO), Digital Elevation Model (DEM), slope, and 2011 NLCD for USGS station 03302000. (Data Source: USDA, 2014).	123

Figure A.3: Watershed characteristics including soil (STATSGO), Digital Elevation Model (DEM), slope, and 2011 NLCD for USGS station 03329700. (Data Source: USDA, 2014).	124
Figure A.4: Watershed characteristics including soil (STATSGO), Digital Elevation Model (DEM), slope, and 2011 NLCD for USGS station 04099510. (Data Source: USDA, 2014).	125
Figure A.5: Annual maximum flood series from 1926 to 2013 for USGS gauging station 01411000 (Great Egg Harbor River Watershed, NJ).....	126
Figure A.6: Annual maximum flood series from 1943 to 2013 for USGS gauging station 03329700 (Deer Creek Watershed, IN).	126
Figure A.7: Probability of non-exceedance plot with LP3 distribution fit to observed AMF series from 1926 to 2013 for USGS station 01411000 (Great Egg Harbor River Watershed, NJ)	127
Figure A.8: Probability of non-exceedance plot with LP3 distribution fit to observed AMF series from 1943 to 2013 for USGS station 03329700 (Deer Creek Watershed, IN).....	127
Figure B.1: Flowchart depicting the geometric transformation process on an image-to-image transformation. (Method developed by author).	129
Figure B.2: Step-by-step flow chart instructions on segmentation and classification of an image. (Method developed by author).	130
Figure B.3: Flowchart depicting the process to create a mosaic image using ERDAS IMAGINE. (Method developed by author).	131
Figure B.4: 1959 mosaic aerial image clipped to watershed boundary for USGS station 03302000. (Image data source: EROS, 2015. Full image created by author). ...	132
Figure B.5: 1952 mosaic aerial image clipped to watershed boundary for USGS station 03329700. (Image data source: EROS, 2015. Full image created by author). ...	132
Figure B.6: 1952 mosaic aerial image clipped to watershed boundary for USGS station	

04099510. (Image data source: EROS, 2015. Full image created by author). ...	133
Figure B.7: 1979 mosaic aerial image clipped to watershed boundary for USGS station 04099510. (Image data source: EROS, 2015. Full image created by author). ...	134
Figure B.8: 1979 mosaic aerial image clipped to watershed boundary for USGS station 04099510, with any open water or urban developed land use class types erased from the image. (Image data source: EROS, 2015. Full image created by author).	135
Figure B.9: Land use progression from 1952 to 2011 for USGS station 03329700. Maps for 1992 to 2011 employ generalized NLCD LULC classes.	136
Figure B.10: Graphical representation of LULC change between 1957 and 2011 for Great Egg Harbor River, NJ (USGS station 01411000).	137
Figure B.11: Graphical representation of LULC change between 1952 and 2011 for Deer Creek, IN (USGS station 03329700).	137
Figure B.12: Net change (mi ²) of generalized LULC types observed between 1957 and 2011 for Great Egg Harbor River, NJ (USGS station 01411000) using LCM change analysis.	138
Figure B.13: Net change (mi ²) of generalized LULC types observed between 1957 and 2011 for Deer Creek, IN (USGS station 03329700) using LCM change analysis.	138
Figure B.14: Change analysis transition from agricultural to urban developed LULC type (in RED) between 1957 and 2011 for Deer Creek, IN (USGS station 03329700).	138
Figure C.1: Projected LULC conditions from FORE-SCE Scenario A1B for Great Egg Harbor River, NJ (USGS station 01411000). (Data Source: USGS, 2014).	139
Figure C.2: Projected LULC conditions from FORE-SCE Scenario A2 for Great Egg Harbor River, NJ (USGS station 01411000). (Data Source: USGS, 2014).	140
Figure C.3: Projected LULC conditions from FORE-SCE Scenario B1 for Great Egg	

Harbor River, NJ (USGS station 01411000). (Data Source: USGS, 2014).....	141
Figure C.4: Projected LULC conditions from FORE-SCE Scenario B2 for Great Egg Harbor River, NJ (USGS station 01411000). (Data Source: USGS, 2014).....	142
Figure C.5: Projected LULC conditions from FORE-SCE Scenario A1B for Pond Creek, KY (USGS station 03302000). (Data Source: USGS, 2014).....	143
Figure C.6: Projected LULC conditions from FORE-SCE Scenario A2 for Pond Creek, KY (USGS station 03302000). (Data Source: USGS, 2014).....	144
Figure C.7: Projected LULC conditions from FORE-SCE Scenario B1 for Pond Creek, KY (USGS station 03302000). (Data Source: USGS, 2014).....	145
Figure C.8: Projected LULC conditions from FORE-SCE Scenario B2 for Pond Creek, KY (USGS station 03302000). (Data Source: USGS, 2014).....	146
Figure C.9: Projected LULC conditions from FORE-SCE scenario A1B for Deer Creek, IN (USGS station 03329700). (Data Source: USGS, 2014).	147
Figure C.10: Projected LULC conditions from FORE-SCE scenario A2 for Deer Creek, IN (USGS station 03329700). (Data Source: USGS, 2014).	148
Figure C.11: Projected LULC conditions from FORE-SCE scenario B1 for Deer Creek, IN (USGS station 03329700). (Data Source: USGS, 2014).	149
Figure C.12: Projected LULC conditions from FORE-SCE scenario B2 for Deer Creek, IN (USGS station 03329700). (Data Source: USGS, 2014).	150
Figure C.13: Projected LULC conditions from FORE-SCE scenario A1B for Pigeon Creek, IN (USGS Station 0499510). (Data Source: USGS, 2014).....	151
Figure C.14: Projected LULC conditions from FORE-SCE scenario A2 for Pigeon Creek, IN (USGS Station 0499510). (Data Source: USGS, 2014).	152
Figure C.15: Projected LULC conditions from FORE-SCE scenario B1 for Pigeon Creek, IN (USGS Station 0499510). (Data Source: USGS, 2014).	153
Figure C.16: Projected LULC conditions from FORE-SCE scenario B1 for Pigeon Creek,	

IN (USGS Station 0499510). (Data Source: USGS, 2014). 154

List of Tables

Table 2.1: Physical characteristics of selected USGS watersheds located in the Upper Midwest and Northeast U.S.	15
Table 2.2: Climatic and anthropogenic characteristics of selected USGS watersheds located in the Upper Midwest and Northeast U.S.	15
Table 2.3: AMF statistics (cms) and associated LP3 parameters for selected USGS gauging stations.	21
Table 3.1: Historical aerial image characteristics for watersheds associated with select USGS gauging stations.	27
Table 3.2: ERDAS IMAGINE 2014 mosaic image overlay function options and descriptions (Pouncey et al., 1999).	34
Table 3.3: 1992 NLCD generalized LULC breakdown for classification in SPRING.	42
Table 3.4: Percentage of total watershed area covered by each generalized LULC type over historical period for each case study site.	50
Table 4.1: SRES scenario based model driving force characteristics and level of change for the future (Data Source: Nakicenovic, 2000. Modified by author).....	55
Table 4.2: USGS Land Use Trends Project LULC categories.....	63
Table 4.3: FORE-SCE land use/land cover classification descriptions.....	64
Table 4.4: LULC (mi ²) projected for 2100 using the A1B FORE-SCE scenario relative to current conditions (2011) for the four case study watersheds.	74
Table 4.5: Percent change in LULC projected for 2100 using the A1B FORE-SCE scenario relative to current conditions (2011) for the case study watersheds.....	75
Table 5.1: Calibration and validation periods, as well as model efficiency measures for validation period for USGS stations selected for SWAT simulations.....	82
Table 5.2: Optimal hydrological parameter values used in ArcSWAT simulation for	

Pond Creek Watershed, KY (USGS station 03302000).	82
Table 5.3: Optimal hydrological parameter values used in ArcSWAT simulation for Pigeon Creek Watershed, IN (USGS station 04099510).	83
Table 5.4: 1992 NLCD classification for runoff curve number (RCN) values, averages, and chosen generalized LULC classification values.	88
Table 5.5: SWAT geodatabase urban land use table with RCN values.	89
Table 5.6: AMF (cms) statistics and LP3 parameters for simulations based on historical LULC change in Pond Creek Watershed, KY (USGS station 03302000). All 20- year simulations were completed with consistent CMIP3 climate data.	94
Table 5.7: AMF (cms) statistics and LP3 parameters for simulations based on historical LULC change in Pigeon Creek Watershed, IN (USGS station 04099510). All 20- year simulations were completed with consistent CMIP3 climate data.	94
Table 5.8: AMF (cms) statistics and LP3 parameters for simulations based on future predicted LULC change in Pond Creek Watershed, KY (USGS station 03302000). All 20-year simulations were completed with consistent CMIP3 climate data. .	102
Table 5.9: AMF (cms) statistics and LP3 parameters for simulations based on future predicted LULC change in Pigeon Creek Watershed, IN (USGS station 04099510). All 20-year simulations were completed with consistent CMIP3 climate data.	102
Table D.1: NRCS hydrologic soil groups (NRCS, 2007).	155
Table D.2: SWAT simulation output for current (base period) and historical AMF series (cms) for Pond Creek Watershed (USGS station 03302000).	156
Table D.3: SWAT simulation output for current (base period) and historical AMF series (cms) for Pigeon Creek Watershed (USGS station 04099510).	157
Table D.4: Instantaneous AMF series (cms) based on SWAT simulation output for FORE-SCE scenarios for Pond Creek Watershed (USGS station 03302000)....	158
Table D.5: Instantaneous AMF series (cms) based on SWAT simulation output for	

predicted FORE-SCE scenarios for Pigeon Creek Watershed (USGS station
04099510). 159

Acknowledgements

I would like to first start out thanking my parents for their immense support, encouragement, words of advice, and prayers throughout my time at Michigan Tech. They always pushing me to always do my best, to not stress about the little things, and trust the Lord in all that I do. I would also like to thank my fiancé Mel, whose light heartedness, joy and encouragement lifted my spirits each and every day. I would also like to express my deep thanks to all of my sisters and family members who supported me throughout my time here.

My deepest thanks to Dr. Veronica Webster for her endless help on this project. Although there were many times throughout the last two years when models refused to run, Dr. Webster gave great support and advice through all of these trials. Without her immense help with reviewing my thesis, endless advice regarding modeling, and patience, this project would never have been possible. Also, for advocating for my position continuing to teach CE3620 for four semesters and help fund my time here I am immensely grateful.

I would like to thank my committee members Ann Maclean and Alex Mayer, for their guidance and with the review of my thesis. Many eyes make light work, and I would like to thank them for their help revising and suggestions along the way.

Further, I especially want to give a big thanks to Ann Maclean, who's exceeding willingness to go out of her way to find time to help me advance my skills in GIS and immense help with beginning my research and guiding me in the right direction was not taken for granted. My hope is that Michigan Tech pushes all of their professors to strive to her level of excellence and willingness to help any and all students.

Thank you Keenan Murray for helping me get my feet on the ground teaching, and the endless hours of work put in by Jennie Tyrrell helping with lab and giving invaluable advice about job searching, career help, and life lessons. Thanks to Kaye LaFond and

Patricia Spellman for providing calibrated SWAT models, as this research builds on their work, and would not have been possible to proceed with a new topic in this research project without their work. Lastly I would like to give a big thanks to Rob Fritz, whose lab assistance for the past two years was invaluable.

Abstract

Current procedures for flood risk estimation assume flood distributions are stationary over time, meaning annual maximum flood (AMF) series are not affected by climatic variation, land use/land cover (LULC) change, or management practices. Thus, changes in LULC and climate are generally not accounted for in policy and design related to flood risk/control, and historical flood events are deemed representative of future flood risk. These assumptions need to be re-evaluated, however, as climate change and anthropogenic activities have been observed to have large impacts on flood risk in many areas. In particular, understanding the effects of LULC change is essential to the study and understanding of global environmental change and the consequent hydrologic responses. The research presented herein provides possible causation for observed nonstationarity in AMF series with respect to changes in LULC, as well as a means to assess the degree to which future LULC change will impact flood risk.

Four watersheds in the Midwest, Northeastern, and Central United States were studied to determine flood risk associated with historical and future projected LULC change. Historical single framed aerial images dating back to the mid-1950s were used along with Geographic Information Systems (GIS) and remote sensing models (SPRING and ERDAS) to create historical land use maps. The Forecasting Scenarios of Future Land Use Change (FORE-SCE) model was applied to generate future LULC maps annually from 2006 to 2100 for the conterminous U.S. based on the four IPCC-SRES future emission scenario conditions. These land use maps were input into previously calibrated Soil and Water Assessment Tool (SWAT) models for two case study watersheds. In order to isolate effects of LULC change, the only variable parameter was the Runoff Curve Number associated with the land use layer. All simulations were run with daily climate data from 1978-1999, consistent with the 'base' model which employed the 1992 NLCD to represent 'current' conditions. Output daily maximum flows were converted to instantaneous AMF series and were subsequently modeled using a Log-Pearson Type 3 (LP3) distribution to evaluate flood risk.

Analysis of the progression of LULC change over the historic period and associated SWAT outputs revealed that AMF magnitudes tend to increase over time in response to increasing degrees of urbanization. This is consistent with positive trends in the AMF series identified in previous studies, although there are difficulties identifying correlations between LULC change and identified change points due to large time gaps in the generated historical LULC maps, mainly caused by unavailability of sufficient quality historic aerial imagery. Similarly, increases in the mean and median AMF magnitude were observed in response to future LULC change projections, with the tails of the distributions remaining reasonably constant. FORE-SCE scenario A2 was found to have the most dramatic impact on AMF series, consistent with more extreme projections of population growth, demands for growing energy sources, agricultural land, and urban expansion, while AMF outputs based on scenario B2 showed little changes for the future as the focus is on environmental conservation and regional solutions to environmental issues.

Chapter 1. Introduction

Location and distance to bodies of water can be a major attraction for developers and home owners, but can also have considerable consequences. Flooding is one of the largest natural disasters in the world. Over the past 30 years in the United States, floods have caused an average of \$8.2 billion in damages/year and 89 fatalities/year (NOAA, 2014). As population in the U.S. increases and densely populated urban development expands, engineers and planners must consider structural and non-structural approaches to reduce flood risk and the consequent economic losses, environmental damages and loss of life (Griffis and Stedinger, 2008; IFMRC, 1994). Flood control and associated water resources planning and management policies must be implemented appropriately, ensuring that floodplain habitat and biodiversity are not compromised (Interagency Floodplain Management Review Committee, 1994), long term economic damages are limited, and public safety is ensured. In order to implement these plans economically and efficiently with potential climate change and anthropogenic activities, a universal understanding of flood risk must be attained (Griffis and Stedinger, 2008).

Today, the United States uses the guidelines established within Bulletin 17B (Interagency Floodplain Management Review Committee, 1982) to estimate flood risk based on the underlying assumption that annual maximum flood (AMF) series follow a Log-Pearson Type III (LP3) distribution. This report allows uniform estimates of the potential for flood damage to be produced nationwide. The need for a recommended procedure for flood risk assessment can best be stated as follows:

“Further, there is an acute need for a consistent approach to such estimates because management of the nation’s water and related land resources is shared among various levels of government and private enterprise. To obtain both a consistent and accurate estimate of flood losses requires development, acceptance, and widespread application of a uniform, consistent and accurate technique for determining flood-flow frequencies.”

(Bulletin 17B, Interagency Committee on Water Data, 1982)

Over the past 30 years, this document has served as the basis for the evaluation of flood risk to inform watershed planning and management, agricultural practices, and infrastructure planning and design, including transportation systems, housing developments, and river control structures. Recently, however, it has come to attention that aspects of this document may be inappropriate, and must be evaluated, and possibly modified, in order to obtain a more accurate basis for future flood risk estimation. The procedures in Bulletin 17B currently assume AMF series to be stationary or constant throughout time, meaning they are not affected by climate variability, land use change or any other trend (for example, Fritsch, 2012; Griffis and Stedinger, 2008; Hirschboeck et al., 2000; Olsen et al., 1999). In the study presented herein, land use change and associated impacts on flood risk will be examined.

1.1 Research Motivation

Changes in the long-term surface water discharge from a watershed can be caused by many variables such as climate variability, land use and land cover (LULC) change, soil management practices, introduction of large detention ponds or artificial lakes, or diversion of water for irrigation. The two most influential drivers for changes in long-term discharge from a large watershed are precipitation variability and LULC changes in the upstream basins (Costa et al., 2003). Due to an increase in large flood events in the past two decades, a substantial amount of research is focused on the effect of LULC change on discharge and flood events (e.g. Archer et al., 2010; Bronstert et al., 2002; Costa et al., 2003; Fohrer et al., 2001; Kuntiyawichai et al., 2011; O'Connell et al., 2007; Palamuleni et al., 2011; Sullivan et al., 2004; Tollan, 2002). It is clearly stated in these articles, and many others, that LULC change such as urbanization and deforestation, affects the hydrologic response in a watershed and can increase the frequency and severity of flood events. Fohrer (2001) clearly states that land use change has a direct effect on hydrologic processes due to the degree and type of LULC, and associated impacts on evapotranspiration (ET) and surface runoff. Furthermore, if the changes in LULC result in infiltration change which override the decrease in ET, shifts in the flow regime of a river can be expected, with increasing

peak flows during the wet season and lower flows during the dry season (Bruijnzeel, 1990). Increased understanding of the degree to which LULC change affects hydrologic processes could be extremely useful for water resources planning and management, and engineering design.

It has been contended that a variety of land use changes, such as deforestation (e.g. Bradshaw et al., 2007), urbanization (Sheng et al., 2009; Zhang et al., 2008), and increased cultivated land (Tollan, 2002) can contribute to increased flood risk. In the past, the response was to implement an engineering solution such as constructing a dam (Brown and Damery, 2007). The problem with these conventional solutions, however, is that they are not sustainable. With regards to riverine ecosystems, conventional measures for flood control have extensive consequences. Habitat biodiversity, sediment transport, biota, water energy, riverine wetland health, and nutrient levels within streams are all altered by the implementation of dams (Ligon et al, 1995). According to the US Army Corps of Engineers' (Corps) National Inventory of Dams (NID), U.S. rivers are currently controlled by approximately 75,000 dams (Engineers, 2013). The impacts of these hydraulic structures need to be addressed in order to identify more sustainable approaches to flood control for community safety, as well as river conservation for preservation of environmental and stream health. Additionally, land management that attempts to preserve a watershed/river system or return it to its natural state should be the goal of decision-makers. An understanding of the beneficial aspects of rural land management (Boardman et al., 2003; Carroll et al., 2004; Hess et al., 2010; O'Connell et al., 2007; Schilling et al., 2013), soil management (Holman et al., 2003), and flood management techniques (Kuntiyawichai et al., 2011) on the reduction of storm runoff and flood risk needs to be considered while making these decisions.

A more thorough understanding of anthropogenic influences, mainly changes in LULC patterns, as well as knowledge of the environmental, hydrologic, and socioeconomic effects that such changes promote, is critical for many fields. Unfortunately, investigations of impacts of LULC changes are hindered by the limited amount of accurate data on

historical land use and management practices. In the past, many methods have been used to determine land cover change, namely land surveying and evaluation of historical literature, statistical data, existing maps, and remote sensing images. The use of remote sensed imagery, such as historical aerial images, has been found to be the most successful tool in determining how land use is changing through time (Hedge, 2003).

In this study, an integrated approach using geographic information systems (GIS), digital image processing, remote sensing, and future prediction models was applied to (1) identify how LULC has changed historically, (2) analyze how land use change will continue into the future, (3) identify the main driving forces behind this change, and (4) assess how this change affects hydrologic parameters, namely those associated with flood risk. Predicting future land use change and the associated consequences will give decision-makers the justification they need to make design and legislative decisions to counteract the consequences of land use change on flood potential. It would also be useful to understand how land use types and patterns, along with climate change, impact watershed runoff and streamflow, as well as to identify which LULC patterns would minimize adverse hydrologic impacts.

Due to the complexity of the hydrologic process coupled with land use change, climate variability/change and spatial variation, it is exceedingly difficult to identify single factors as the cause of hydrologic effects at a watershed level. Furthermore, once all of these variables have been introduced into a model, the results are overwhelmingly difficult to analyze. Although many studies have found the task of modeling climate variability/change coupled with LULC change daunting, Barlage et al. (2002) studied the effects on surface runoff characteristics due to future climate and land use changes on the Huron River Watershed located in southeastern Michigan. The watershed is primarily agricultural and urban, and has experienced rapid population growth, resulting in the historical wetlands and forest land use types to be nearly eliminated. The study projected future climate and land use changes to 2100, resulting in an increase in the percentages of precipitation and impervious surface due to continued urban development, which in turn

increased surface runoff from 17.1% to 21.4%. Climate change comprised 2.5% of this increase, while 1.6% was attributed to land use change. Other studies could not identify direct impact due to either land use or climate change, mainly due to the fact that natural year-to-year climate variation impedes identification of the true causes of the impact (Institute of Hydrology, 1999; O' Connell et al., 2007; Robson et al., 1998). Although further studies are needed including both of these variables, this thesis focuses on isolating LULC change to model the hydrologic response, with particular attention to flood risk.

Relatively few studies have analyzed impacts on hydrology and water quality from coupled climate and land use changes (Chang, 2004; Choi, 2008; Franczyk and Chang, 2009; Qi et al., 2009; Tong et al., 2012; Tu, 2009). Tu (2009) studied the effects on streamflow and water quality in eastern Massachusetts. Using AVGWLF, a GIS-based watershed simulation model, it was concluded that the impact of land development will be enhanced with climate change; however, the combination of these two changes was observed to have a greater impact on seasonal streamflow and water quality changes than on average annual changes. Tong et al. (2012) used a spatial analytical approach, integrating mathematical modeling and GIS, to examine relations between coupled climate/land use changes and impacts on hydrologic and water quality in the Little Miami River watershed in Ohio. Overall, it was concluded that these changes would increase streamflow and nutrient levels under the 2050 projected date. Tong et al. (2012) provides an effective approach to simulate hydrologic and water quality changes due to climate and generalized land use changes, however, the approach is limited by the use of generalized land use classes rather than the finer classification typically employed (NRCS, 2015). With impending climate change and continual LULC change, it is necessary to establish new integrative approaches to model hydrologic impacts due to both combined and individual changes (Tong et al., 2012).

Many studies have focused research on only limited types of land use in order to isolate the variables influencing shifts in the response to a hydrologic event (e.g. Tong et al., 2012). By isolating one or two parameters, changes in the water balance in a watershed can be

directly linked to individual variables. If too many variables are simultaneously added to the model (e.g. climate variation, concurrent changes in multiple land use types, socioeconomic changes), changes in streamflow, runoff or other hydrologic outputs cannot be linked to a single variable as the sole cause of that change. In order to eliminate the complex interactions within a watershed, Fohrer et al. (2001) used SWAT to consider changes in the annual water balance with regards to one underlying soil type and a single crop type. It was found that the effect of change in land use on the annual water balance was relatively small although a decrease of forest due to an increase in grassland did subsequently increase peak flows rates, and therefore increase flood risk.

O'Connell et al. (2007) noted that there is substantial evidence that modern land-use management practices have enhanced surface runoff generation at the local scale, frequently creating impacts through 'muddy floods'. However, there is very limited evidence that these local changes would affect larger scale watersheds. The subject of land drainage has also been extensively discussed, debated and studied (Robinson, 1990). An extensive amount of research supports that in predominantly rural areas, soil compaction, reduction in infiltration and groundwater recharge has resulted from agricultural land use changes, namely changes in cultivation practices and increased grazing pressure (Fohrer et al., 2001; Holman et al., 2003; Schilling et al., 2014). By understanding how changes in agricultural practices alter hydrologic response to a storm, more management practices can be put into place to prevent higher flows, excess sediment loading into streams/rivers, pollutants discharged into waterbodies, and flashy floods.

The Defra FD2120 project (Beven et al., 2008) investigated impacts on flood events for agricultural watersheds that experienced dramatic land use and management changes over the past 50 years. The Dynamic Harmonic Regression (DHR) method was used to analyze changes in long term trends in monthly rainfall and flows, and a Data Based Mechanistic (DBM) model with a State Dependent Parameter (SPD) nonlinear filtering of rainfall inputs was employed to diagnose storm responses using hourly data. Only 2 out of 9 watersheds under investigation showed hydrologic trends that could be directly related to land use

change or management. This study confirmed that while land use and land management changes are an important aspect of the hydrologic response in a watershed, due to watershed complexity it is difficult to identify the specific parameters that contribute to this change through physical modeling (Archer et al., 2010).

Rural land areas consist primarily of agricultural and forested land with scattered houses; urban utilities and development are not present and are typically not planned for the future. If development is necessary, rural land management decisions are based on the most appropriate locations for development as a function of land use, soil condition and type, and climate. Rural land management practices (i.e. field and soil condition improvements) may be a good option for flood risk management in areas where structural measures are not cost effective relative to their likely beneficial effects, or are otherwise implausible. If implemented effectively, rural land management changes may also help offset some of the forecasted increases in flood risk due to climate change (Hess et al., 2010).

Within the last quarter of the 20th century, urban population increased by 100% at a global scale (Chin, 2006), while U.S. population increased by only 24% between 1980 and 2000 (USDC Census Bureau, 2001). While this is a substantial increase in U.S. population, the majority of population growth presided in developed and urbanized land, as within approximately the same time period, there was a 34% increase in the area of U.S. land comprised of urban and build-up uses (USDA Natural Resources Conservation Services, 2001). This trend in population growth is expected to continue over the next 30 years and is projected to occur in urban areas (Alig et al., 2004). One study pattern projects that with current development trends and population projections, urban land in the U.S. will more than double between 2000 and 2050, increasing from 3% to 8% (Nowak and Walton, 2005). A negative effect of this expansion of urban area and population will be the inherent impact on local water resources and water supply systems, as well as the possible increase in vulnerability to flood risk at a watershed level (see for example, Rose and Peters, 2001; Schueler, 1994).

Historical, current and projected population rates are a significant indicator of how land cover has and/or will change through time. Based on a study by Pew Research Center, population growth from 1950 to 2010 was rapid; almost doubling in the U.S., and nearly tripling globally (Kochhar et al., 2014). Population projection for 2010 to 2050, however, is expected to be substantially slower with an increase in the U.S. of 28%, from 312.2 million to 400.9 million, corresponding to a 0.6% average annual rate of increase. This rapid urban growth has spurred major environmental concerns and has motivated researchers to study the effects of these changes to aid in the development of efficient and effective land use management practices, as well as planning policies that will preserve natural land more effectively (Araya and Cabral, 2010).

Shaw (1994) presents five major effects of urbanization:

1. An increase in the amount of precipitation that appears as surface runoff.
2. The time to peak flow at the outlet of the watershed is decreased, and the lag time between precipitation and runoff is decreased.
3. An increase in peak flow magnitude for all but the largest storm events.
4. A decrease in groundwater storage resulting in a decrease in low flows.
5. A decrease in water quality.

Urbanization in the U.S. has resulted in removal of vegetation and soil, replacing natural land cover with impervious surfaces, and consequently replacing natural river channels with drainage systems. Pinter et al. (2008) studied the effects of river engineering on the Mississippi River and concluded that although climate and/or land use change is related to increased risk of flooding, this increased risk could also be attributed to the introduction of major levees, dikes, and navigational structures. Such changes at a watershed level can affect surface water runoff, groundwater and evapotranspiration. First, introducing more impervious surface or compacted soil results in increasing the volume and duration of surface runoff. This occurs as the time between the peak of the precipitation hyetograph and peak of the flow hydrograph (i.e. basin lag time) is decreased. Second, as permeable surface transforms into impervious surface, the volume of water infiltrating decreases,

thereby effecting groundwater recharge and baseflow in streams. Third, by reducing the amount of vegetation cover and infiltration, the rate of evapotranspiration decreases (Chang, 2007; Mansell, 2003). Due to these anthropogenic effects, the capacity of stormwater management/detention structures to capture storm runoff must increase, further resulting in decreased infiltration, as well as an increase in streamflow magnitude if stormwater runoff is discharged directly into the river system (Mansell, 2003; McCuen, 1998; Rose and Peters, 2001). This discovery reiterates the urgency for further hydrologic research isolating land use and climate change on relatively unimpaired watersheds.

1.2 Research Objectives

The overall objective of this thesis is to identify the effects of LULC change on annual maximum flood (AMF) series, using models applied over both historical and predicted future land use scenarios. This will be achieved through completion of the following tasks:

- 1) Creation of historical land use maps using historical aerial imagery and modeling of LULC change over time;
- 2) Utilization of a scenario based spatial model to project LULC change for future time periods;
- 3) Determination of the effects of LULC change, mainly on flood risk, at a watershed level; and,
- 4) Evaluation of whether generalizing land use classifications dramatically affects hydrologic model parameters and projected/estimated flood risk as compared to use of existing NLCD classifications.

The direct outcomes of this research will provide insight as to how to properly implement management or design measures to reduce flood risk. This research is necessary as anthropogenic activity is increasing and/or continuously changing in watersheds throughout the U.S., thereby creating nonstationary streamflow in watersheds classified as unimpaired and moderately impaired. Increased understanding of the effects of LULC change on flood risk is also needed in order to update current models for flood frequency analysis (i.e.,

Bulletin 17B).

This study builds on previous efforts which employed statistical analyses to identify non-stationary behavior in AMF series for hundreds of sites throughout the Northeastern and Upper Midwestern U.S. (Fritsch, 2012; Salvadori, 2013), as well as LaFond (2014) who explored effects of projected climatic variation/change on AMF series and flood risk. Due to insufficient research regarding LULC change in the U.S., only cursory attempts were made therein to relate nonstationarity in AMF series to anthropogenic activities within the watershed. Therefore, with regards to LULC change, this thesis seeks to determine the appropriate drivers of a statistical model appropriate for creation of flood risk projections over extended time horizons (up through 2100) to assist in long term and/or large scale water resource planning and management.

Chapter 2. Watershed Selection and Characteristics

This study builds on previous research in which the annual maximum flood (AMF) series of 399 United States Geological Survey (USGS) gauged watersheds within the Northeastern and Upper Midwestern United States were analyzed (Fritsch 2012, Salvadori 2013). Fritsch (2012) studied nonstationarity in AMF series for 256 unimpaired watersheds, while Salvadori (2013) similarly studied 143 moderately impaired watersheds. The locations of these watersheds are seen in Figure 2.1 and Figure 2.2, respectively. These watersheds were chosen based on availability of at least 65 years of continuous AMF records and because they are relatively unimpaired. In this study, the term unimpaired refers to watersheds that do not have major anthropogenic influences such as major structural diversions or controls (e.g., dams), water withdrawals and land use changes. Data regarding gauged sites that are relatively unimpaired are compiled within the Hydro-Climatic Data Network (HCDN) Streamflow Dataset (Slack and Landwehr, 1992). Due to the HCDN not having been updated since 1988, the Geospatial Attributes of Gages for Evaluating Streamflow (GAGES) was published in 2010, with a more recent version, GAGES II, published in 2011. The latter dataset provides geospatial information and characteristics for hundreds of gauged watersheds within the U.S. These characteristics include the level at which the watersheds are impaired, as well as length of continuous flow records and basin characteristics (e.g., % impervious surface) (Falcone et al., 2010).

Present assumptions for design and regulation of water resources applications assume that instantaneous AMF series are stationary over time. Parameters of probability distributions fit to AMF series are subsequently presumed to be stable, regardless of land use change or climatic trends (Hirschboeck et al., 2000; Olsen et al., 2007). However, nonstationary behavior in the form of trends and change points (abrupt shifts) has been identified with respect to both the magnitude and timing of AMF events (Fritsch 2012, Salvadori 2013). Possible causes for this behavior, such as climate variability, land use change and other anthropogenic activities, were considered; however, these efforts were cursory, as they were conducted at a regional level. Analyses at the watershed level were needed to fully

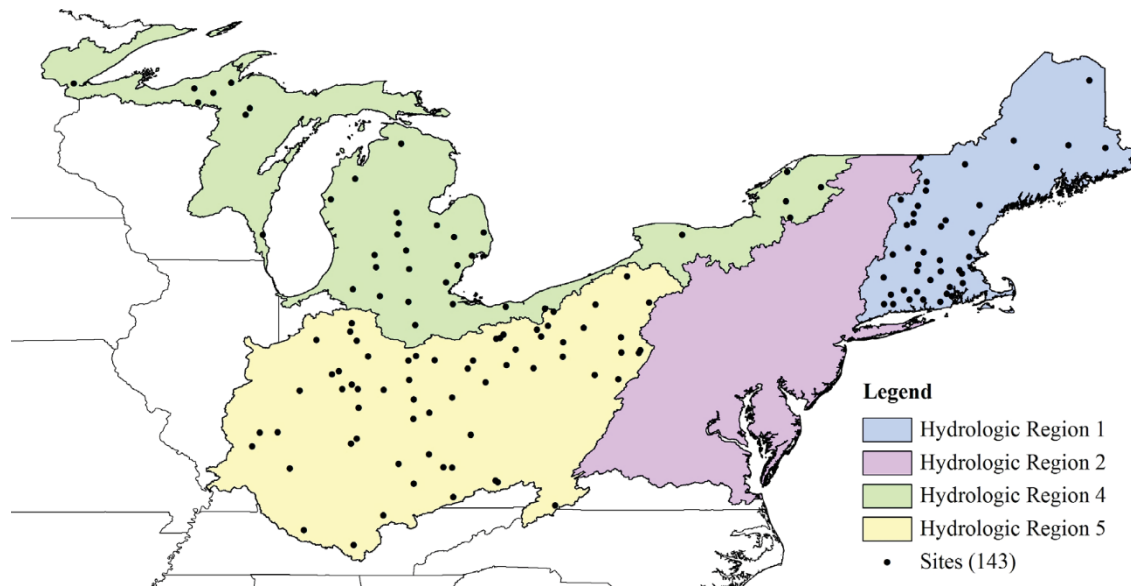


Figure 2.2: Locations of 143 USGS streamflow gauging stations defining the study area for moderately impaired watersheds in the Upper Midwest and Northeastern U.S. (Data Source: Salvadori, 2013).

2.1 Watershed Selection Process

In the interest of furthering understanding of the impacts of land use change on the hydrologic response in a watershed and associated flood risk, a smaller set of case study watersheds was selected for more detailed analysis herein. Watersheds were selected based on results of Fritsch (2012) and Salvadori (2013), and were chosen to be representative of a wide range of physical, demographic, climatic, and hydrologic characteristics. The predominant LULC type of each watershed was also heavily considered during the selection process. The locations of the four gauged watersheds to be explored herein are illustrated in Figure 2.3. Three of the sites are moderately impaired, and USGS station 0411000 located in New Jersey is unimpaired.

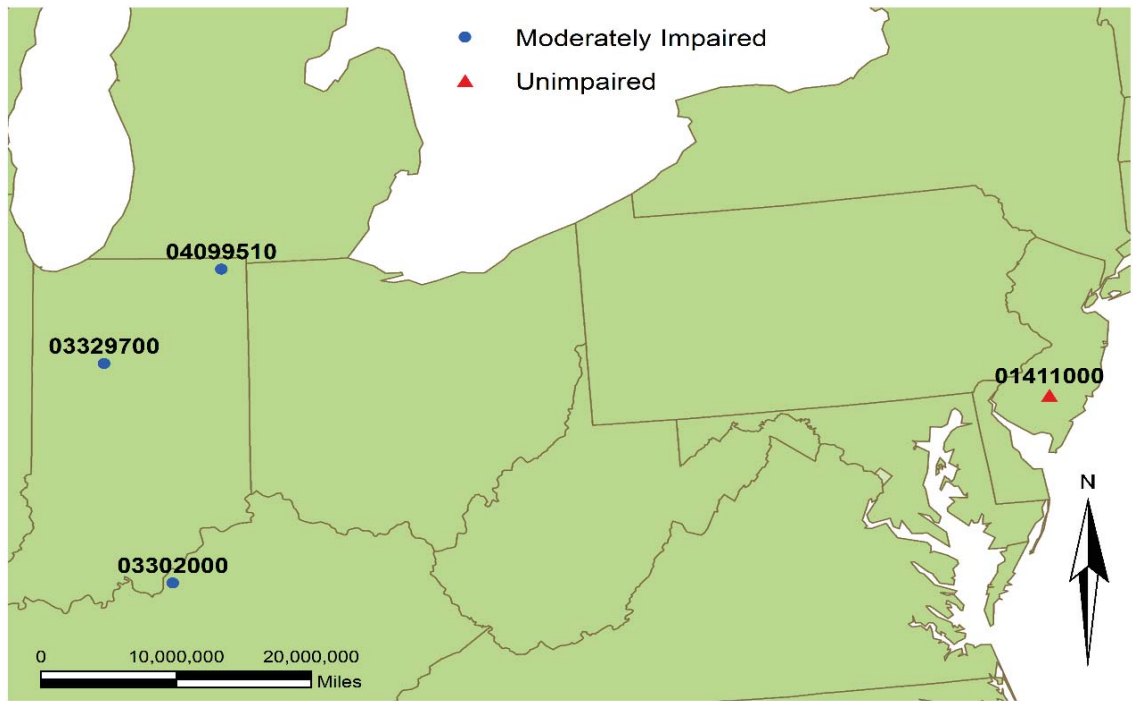


Figure 2.3: Locations of four unimpaired to moderately impaired USGS streamflow gauging stations selected for LULC change analysis.

As the primary focus of this study is effects of land use change, watersheds with a variety of principal land use types were chosen. Figure 2.4 through Figure 2.7 show the selected watershed boundaries overlaid on the current 2011 National Land Cover Dataset (NLCD). For each of the four chosen watersheds, Table 2.1 presents the location, area, and general land use percentages; Table 2.2 provides information related to climate, anthropogenic impairment, and possible trends in AMF series as identified by Fritsch (2012) and Salvadori (2013). While both watersheds located in Indiana are primarily agricultural, Great Egg Harbor Watershed contains mostly forested land and Pond Creek Watershed resembles a heavily urbanized area. To prevent excessive data processing, relatively smaller watersheds were selected. In addition, stations where a large portion of the annual precipitation is in the form of snowfall were not selected, as snowfall/snowmelt significantly affect watershed hydrology, thereby increasing parameter complexity in modeling. Further, degree of impairment was assessed based on GAGES II (Falcone, 2011), and sites with major flow regulations or diversions, including major dams or control

structures were not considered due to complexity of modeling and isolating variables. Finally, two sites were chosen that exhibit both a positive long-term trend and a change point at a 10% significance level; corresponding p-values indicating the actual significance level are reported in Table 2.2.

Table 2.1: Physical characteristics of selected USGS watersheds located in the Upper Midwest and Northeast U.S.

USGS Station	Watershed Name	State	Area (mi ²)	LULC (%)		
				Urban	Forest	Agriculture
01411000	Great Egg Harbor River	NJ	56	36	56	8
03302000	Pond Creek	KY	64	68	29	3
03329700	Deer Creek	IN	276	7	4	89
04099510	Pigeon Creek	IN	105	10	22	66

Table 2.2: Climatic and anthropogenic characteristics of selected USGS watersheds located in the Upper Midwest and Northeast U.S.

Station	Mean Annual Temperature [†]	Mean Annual Precipitation [†]	% of Precipitation as Snow ^{††}	Impaired?	Modified MK		Pettitt Test	
	(°C)	(cm)			P	Year	P	
01411000	12.16	117.01	14%	No				
03302000	13.37	117.09	11%	Yes	+	0.008	1962	< 0.0001
03329700	10.07	99.86	17%	Yes				
04099510	8.68	94.19	21%	Yes	+	0.071	1975	0.001

[†]Period of record 1971 – 2000; ^{††}Period of record 1901 – 2000

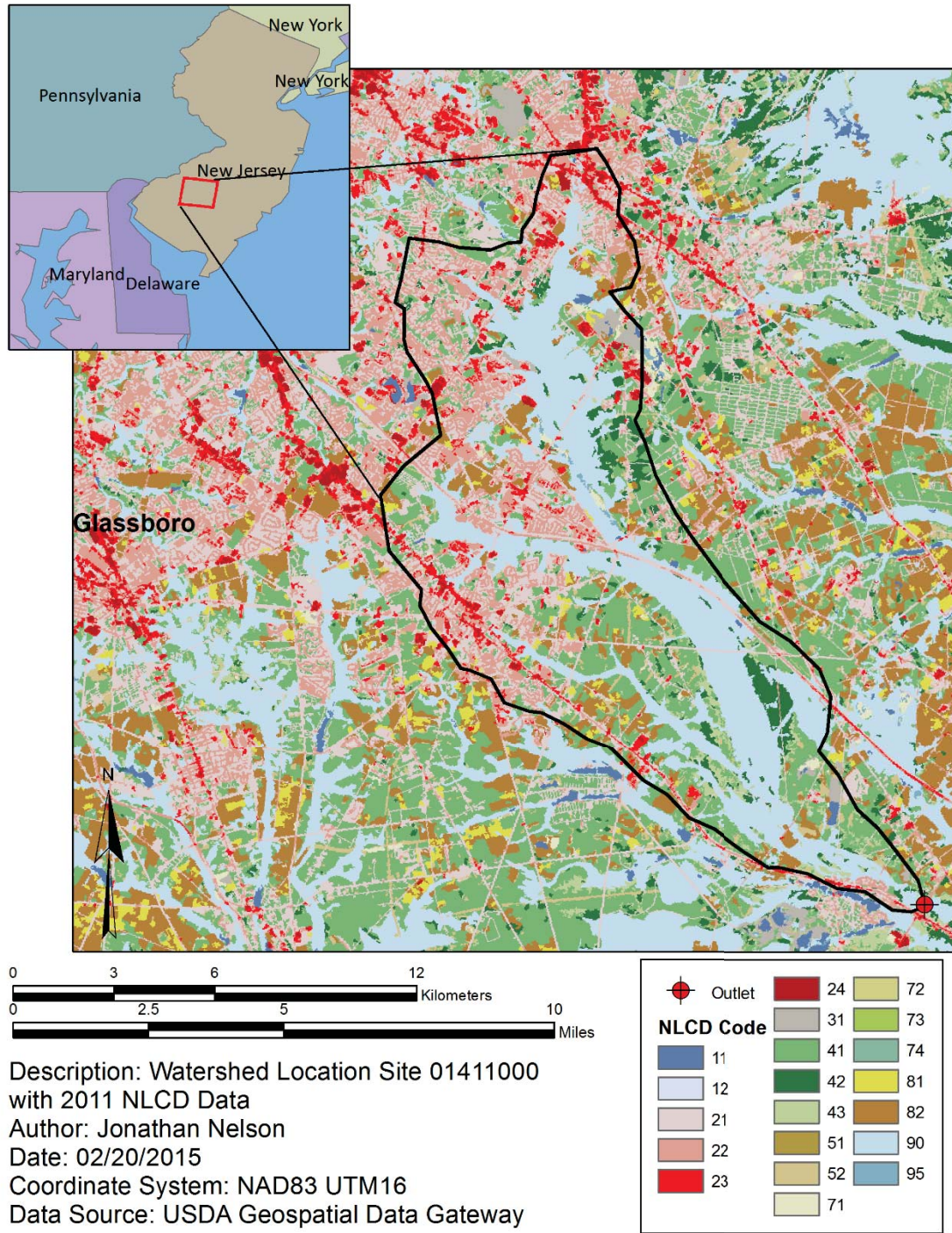


Figure 2.4: Location of Great Egg Harbor River Watershed and associated streamflow gauging station (USGS Station 1411000) with 2011 National Land Cover Database (NLCD). (Data Source: USDA, 2014).

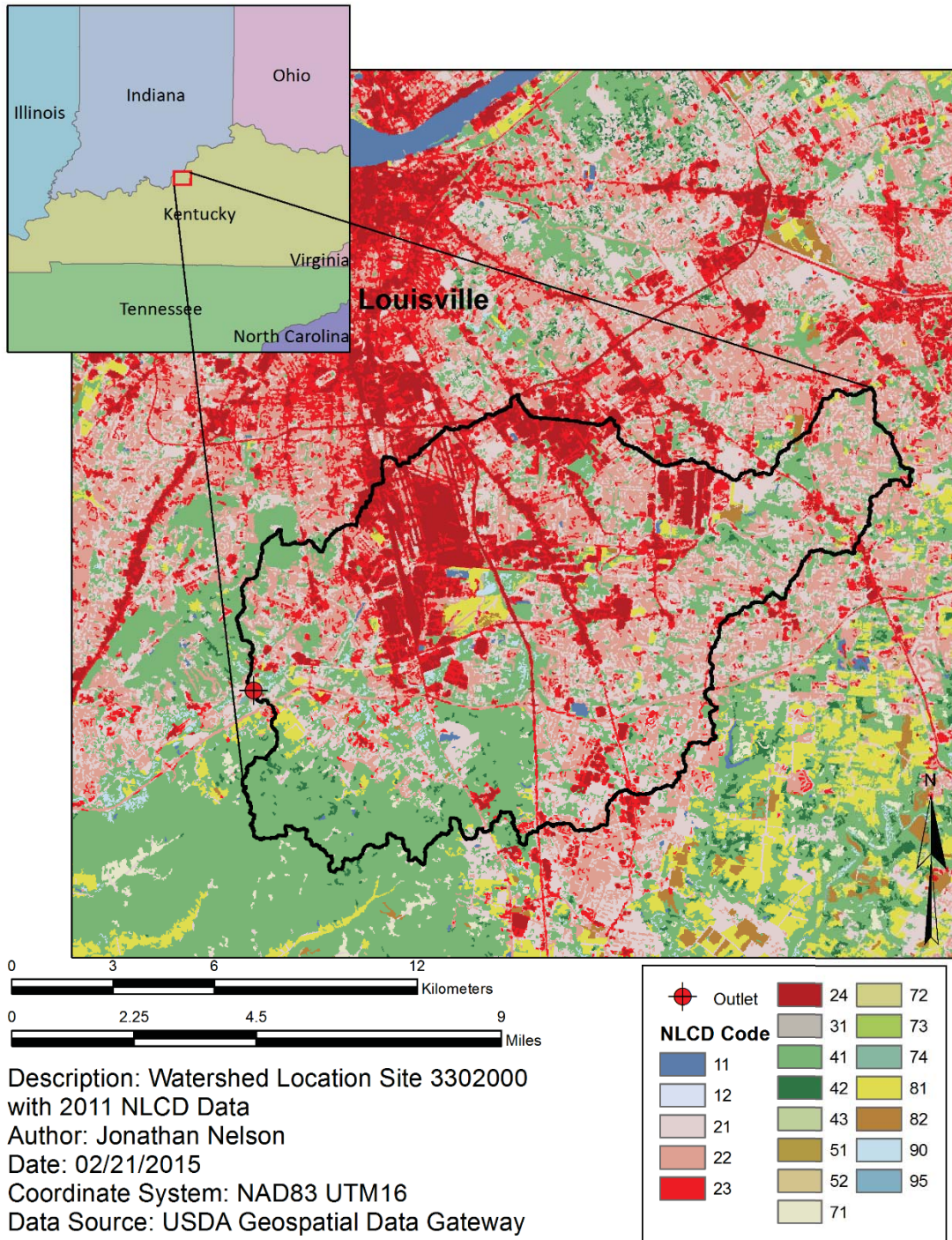


Figure 2.5: Location of Pond Creek Watershed and associated streamflow gauging station (USGS Station 03302000) with 2011 National Land Cover Database (NLCD). (Data Source: USDA, 2014).

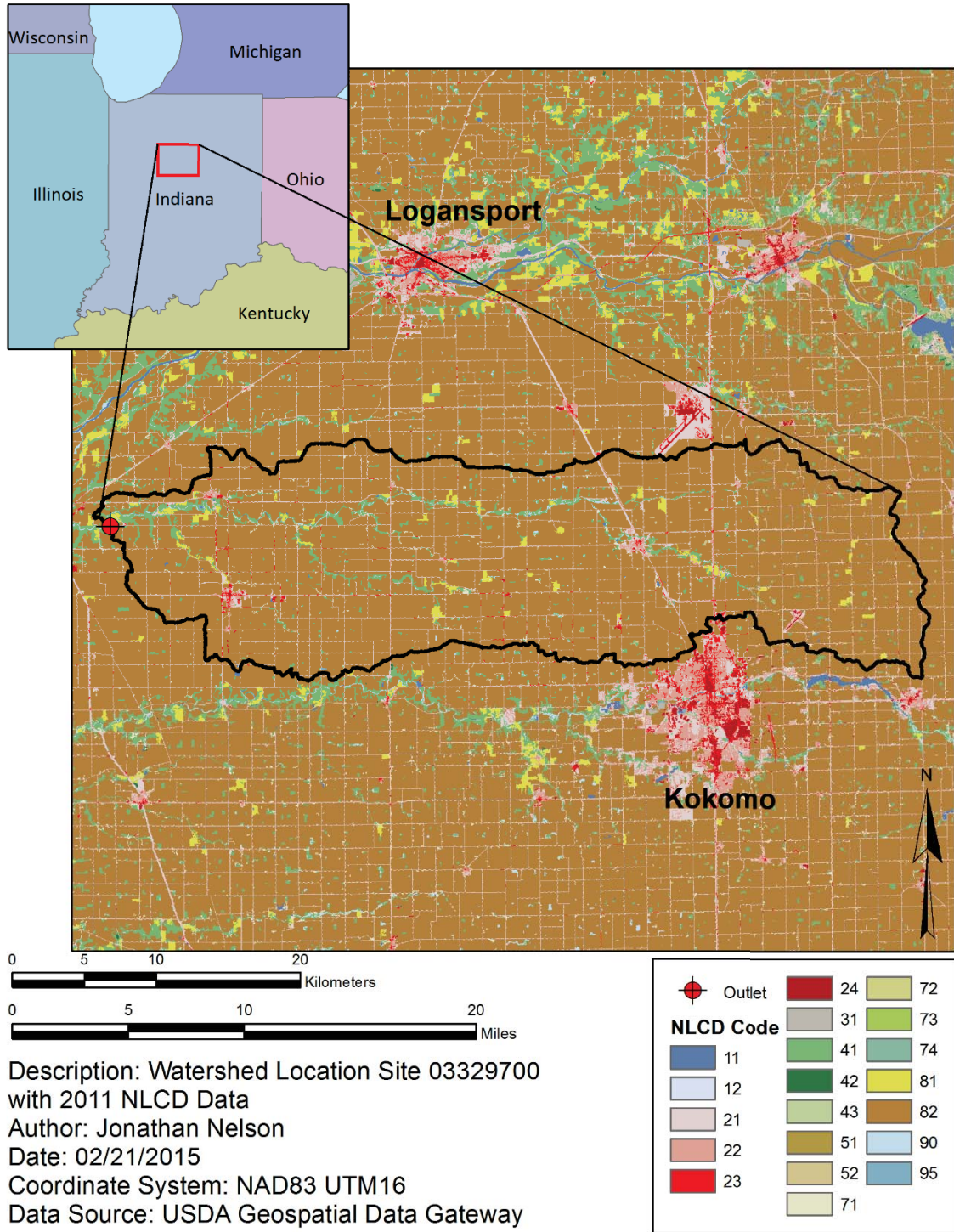


Figure 2.6: Location of Deer Creek Watershed and associated streamflow gauging station (USGS Station 03329700) with 2011 National Land Cover Database (NLCD). (Data Source: USDA, 2014).

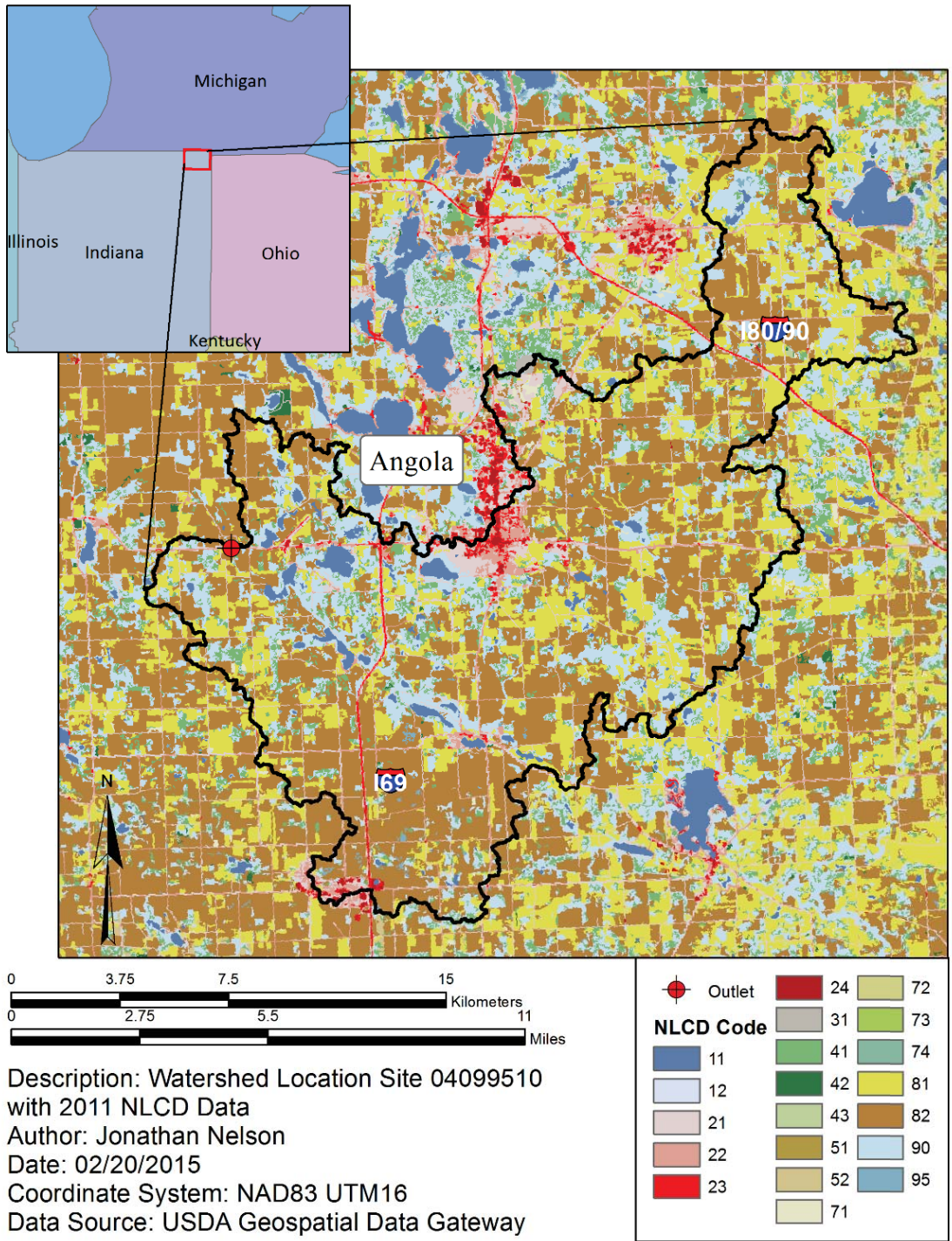


Figure 2.7: Location of Pigeon Creek Watershed and associated streamflow gauging station (USGS Station 04099510) with 2011 National Land Cover Database (NLCD). (Data Source: USDA, 2014).

With its close proximity to Louisville, population of 600,000, USGS gauging station 03302000 is susceptible to further urban development at the expense of agricultural and forested land. This watershed is the first of two watersheds that will serve in further hydrologic analyses. The southwest corner of the watershed is located in a high elevation area, and topographically has higher changes in slope (see Figure A.2). In areas of high slope, development becomes more challenging and may be less susceptible to rapid urbanization in the future.

USGS station 03329700 is located near Delphi, Indiana, with the southern border of the Deer Creek watershed adjacent to the town of Kokomo, Indiana. Of the four watersheds, Deer Creek presently has the least amount of urban cover; however, with the city of Kokomo's proximity to the watershed boundary, future urbanization could extend inside the watershed boundary, and would likely result in effects on the watershed hydrology. Due to time constraints, hydrologic modeling of the latter two sites will not be discussed herein.

The second watershed to be modeled in more detail is associated with USGS gauge 04099510 located along a relatively unimpaired river in Steuben County Indiana near the Michigan/Indiana border. Although the major land use class within this watershed is agricultural, future urban development is projected due to the proximity to Angola, Indiana, as well as two major interstate highways (I69 and I90/80) that run through the watershed.

For each watershed, a Log-Pearson Type III (LP3) distribution was fit to the observed AMF data series using Method of Moments (MOM) in log-space as recommended in Bulletin 17B. The LP3 distribution has three parameters (α , β , τ) representing the shape, scale, and location, respectively, of the fitted distribution. To obtain these parameters, the sample size (N), mean (\bar{Q}), standard deviation (S_Q) and skew (G_Q) were computed. Percentiles of the fitted LP3 distribution, denoted Q_p , represent the flow magnitude with 1-p probability of exceedance in a given year. For example, $Q_{0.99}$ represents the flow magnitude which has a 1% chance of being exceeded in a given year, also referred to as the 100-year flow event.

Flow percentiles and summary statistics are reported for all four case study watersheds in Table 2.3. The mean of the AMF flow series for USGS stations 03302000 and 03329700 are quite large compared to stations 01411000 and 04099510. The larger mean flow of USGS station 03329700 can be explained by the relatively large area that it extends; however, when scaling to account for watershed size, the largest flows are observed at USGS station 03302000, presumably due to it being predominantly urban (see Table 2.1).

Table 2.3: AMF statistics (cms) and associated LP3 parameters for selected USGS gauging stations.

	Station	01411000	03302000	03329700	04099510
Statistics & Parameters	N	88	69	71	68
	Area (km ²)	145	167	714	273
	Q (cms)	10.53	91.68	162.69	12.97
	Q/Area	0.073	0.549	0.228	0.048
	S _Q	6.82	39.16	142.02	7.81
	G _Q	2.52	1.05	3.45	3.96
	α	18.25	10.74	90.59	614.85
	β	0.12	-0.14	0.07	0.02
	τ	-0.04	5.90	-1.48	-9.33
Flow Parameters	Q _{0.99}	36.76	193.91	670.02	35.79
	Q _{0.98}	30.30	180.61	543.23	31.20
	Q _{0.90}	18.17	143.25	305.81	21.27
	Q _{0.50}	8.72	87.49	125.53	11.46
	Q _{0.10}	4.78	46.02	55.63	6.30
	Q _{0.02}	3.54	28.90	35.31	4.44
	Q _{0.01}	3.21	24.17	30.26	3.93

Probability plots were used to assess the fit of the LP3 distribution to the gauged AMF data. The empirical cumulative distribution function (CDF) was generated by plotting the ordered data in log-space with the incremental plotting position (p_i) computed using Blom's formula:

$$p_i = \frac{(i - 3/8)}{(N + 1/4)} \quad (1)$$

where i is the rank of an individual observation over the record length of N years (Blom, 1958). The historical AMF series for USGS stations 03302000 (Pond Creek) and 04099510 (Pigeon Creek) are presented in Figure 2.8 and Figure 2.11, respectively, and plots of the fitted LP3 distributions relative to the observed data are provided in Figure 2.10 and Figure 2.11, respectively. Figures for the additional case study watersheds are contained in Appendix A. Overall, the plots demonstrate the suitability of the LP3 distribution for modeling AMF flow data. By observing the shape of the CDFs, an understanding of the range and likelihood of the flows can be obtained. Pond Creek Watershed presents quite high AMF flows compared to Pigeon Creek Watershed. In addition, the LP3 distribution for Pond Creek has a much wider spread, representing a very wide range of AMF flows compared to the steeper shaped LP3 curve in Pigeon Creek. As such, the tails of the distribution are more gradual in Pond Creek as compared to a quite dramatic shift in the shape of the tails for Pigeon Creek.

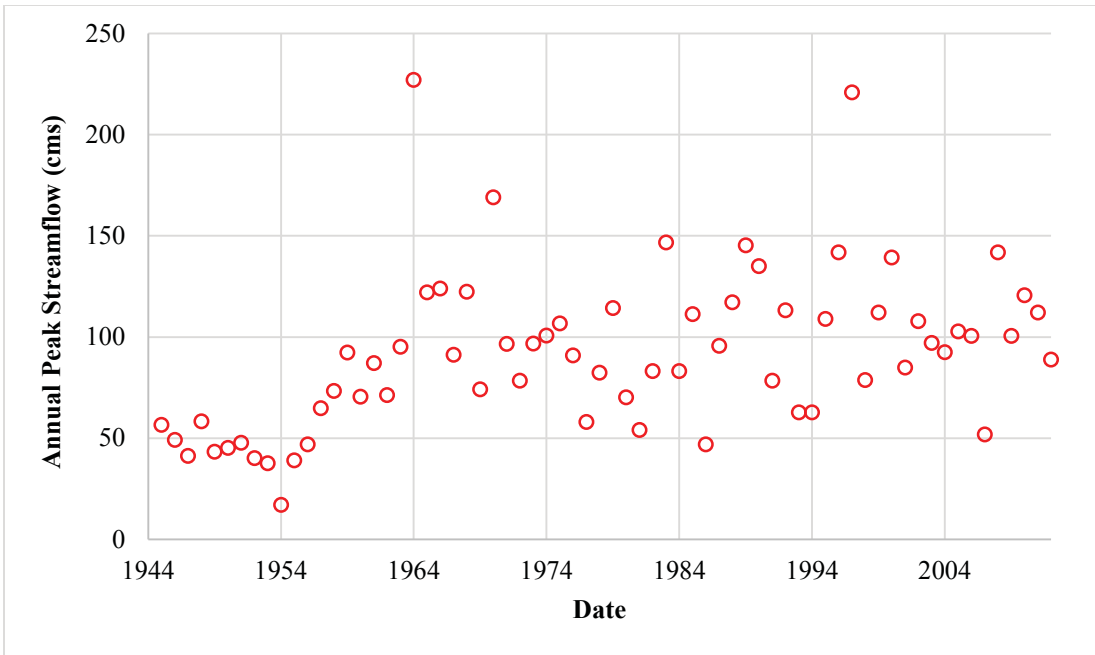


Figure 2.8: Annual maximum flood series from 1945 to 2013 for USGS gauging station 03302000 (Pond Creek Watershed, KY).

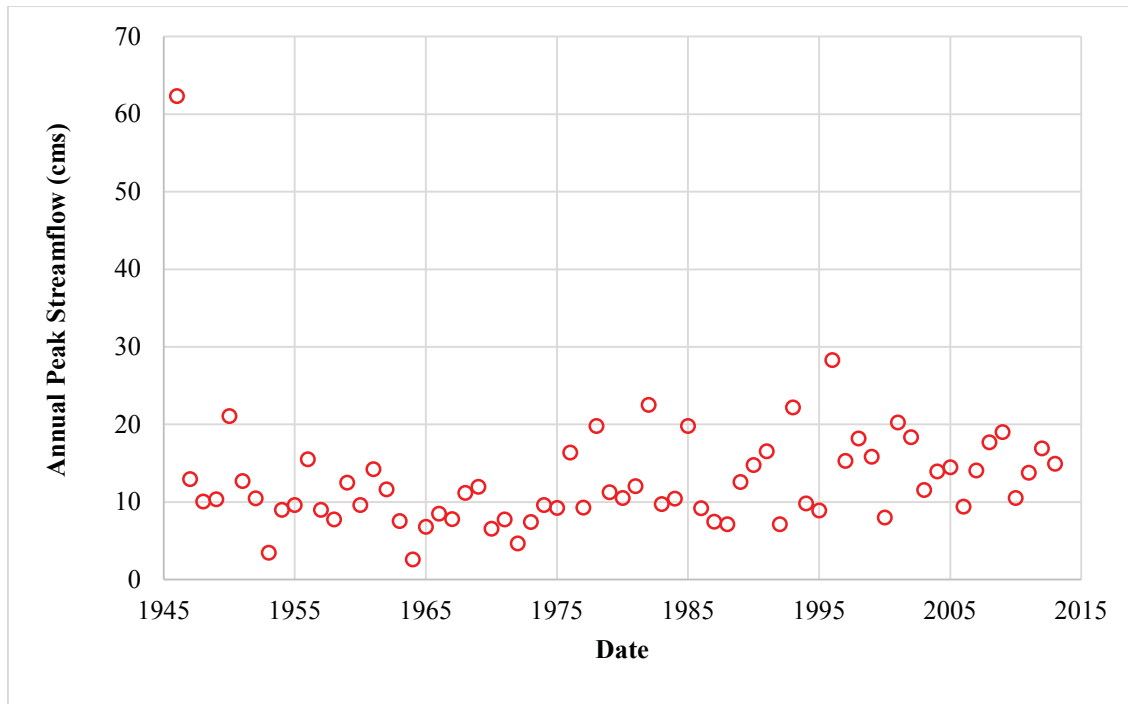


Figure 2.9: Annual maximum flood series from 1946 to 2013 for USGS gauging station 04099510 (Pigeon Creek Watershed, IN).

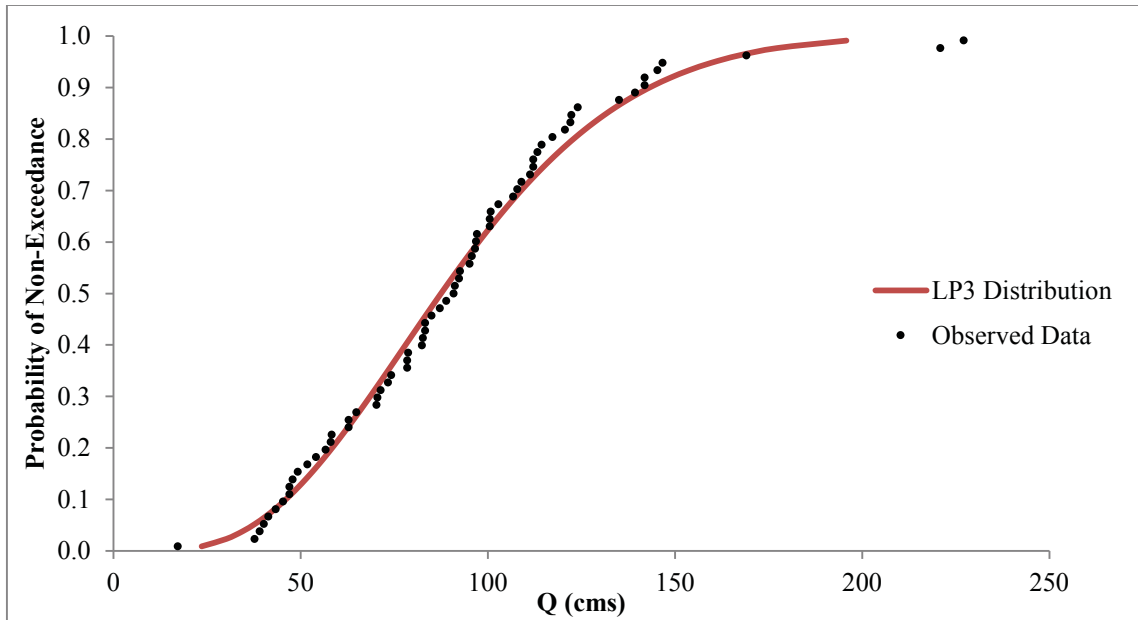


Figure 2.10: Probability of non-exceedance plot with LP3 distribution fit to observed AMF series from 1945 to 2013 for USGS station 03302000 (Pond Creek Watershed, KY).

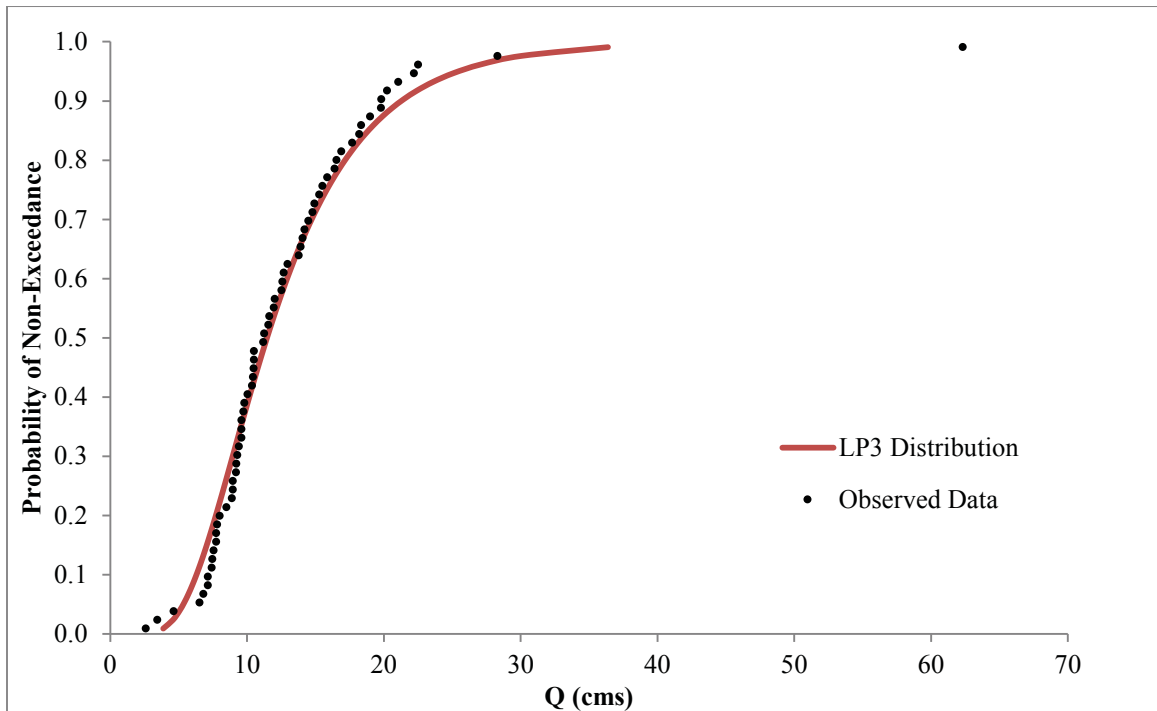


Figure 2.11: Probability of non-exceedance plot with LP3 distribution fit to observed AMF series from 1946 to 2013 for USGS station 04099510 (Pigeon Creek Watershed, IN).

Chapter 3. Historical Land Use Maps

A limited amount of accurate historical land use data over long time periods is available in the United States due to a lack of historical data sources (Rhemtulla et al., 2007). The National Land Cover Database (NLCD) is the major source for relevant land use data, but only extends back to 1992. The NLCD was derived from the Landsat Thematic Mapper (TM) sensor in the early 1990s, replacing the original Multispectral Scanner (MSS) in 1992 and creating usable LULC maps. The Landsat program began in 1972 (Landsat 1) as one of NASA's earth observation programs. MSS images prior to Landsat TM may be converted to LULC data manually. In addition, aerial photographs may be processed to create historical land use maps extending further back in time. Panchromatic aerial imagery (single band image) is often the only source of historical land use dating back to earlier time periods. Compared to modern image technology (i.e. multispectral and hyperspectral aerial imaging), it is significantly more difficult to use panchromatic aerial imagery to gather accurate data/information regarding land use (Porter, 2011). Advancements in image processing, GIS, and remote sensing techniques, mainly image segmentation and object-based classification, have allowed researchers to study historical images more accurately with respect to land use (Berberoglu and Curran, 2004).

Historical trends in land use change can be linked to a variety of physical (distance from roads, urban areas, etc.) and socioeconomic (e.g. population) indicators. In this chapter, single frame aerial photographs are used to create historical land use maps, from which impacts on hydrologic response and changes in flood risk over the historic period can be inferred. Depending on data availability, images dating back to the 1950s were desired in order to correspond to the time period considered by Fritsch (2012) and Salvadori (2013). This historical LULC data will also serve as a basis for predicting future LULC change (Chapter 4), and to understand associated implications on future flood risk (Chapter 5).

3.1 Data Preparation

Historical land use change is typically determined using remote sensing to interpret and

analyze the data, and then GIS is employed for further spatial analysis (Hudak and Wessman, 1998). Many studies utilize LandSat data to generate historical land use maps and study the environmental consequences of LULC change (Alves et al., 1996; Comber et al., 2012; Rhemtulla et al., 2007; Skirvin et al., 2005; Valeriano et al., 2004). The earliest Landsat data available dates to 1972, and while very limited historical agricultural census data is available with percentages of croplands at a county level, data describing the land use spatially during the mid-1900s is not available. Although analysis post-1972 is often sufficient, an understanding of historical land use extending to the 1950s is preferable herein, as this study builds on previous efforts (Fritsch, 2012; LaFond, 2014; Salvadori, 2013) which examined nonstationarity in AMF series dating back to the mid-20th century.

In this study, historic aerial images were used to create generalized land use maps for the selected case study watersheds. All of the historical aerial images were obtained from USGS Earth Explorer which can be accessed at <http://earthexplorer.usgs.gov/>, an interactive website where the user specifies the bounding extent, search dates, and image type. Many types of data sets are available through this website, such as DEMs, land cover maps, Landsat archive, radar, vegetation monitoring, and aerial imagery. In order to obtain images from the 1950s, data was retrieved from Aerial Photo Single Frames, National Aerial Photography Program (NAPP), and the National High Altitude Program (NHAP). Each USGS gauging site had a variety of images with various image scales, years obtained, focal length, and quality of image as seen in Table 3.1. The image scale is the ratio of the distance on the image compared to the equivalent distance on the ground. Many images were of poor quality, and either the scale was too large, resulting in a loss of accuracy due to the resolution in the image, or too small, thereby requiring extensive data preparation for larger watersheds. Another issue that arose was the size of many of the watersheds, resulting in an unrealistic number of images to be processed if the image scale was small. For each site, images from the earliest date with reasonable scale and image quality were obtained.

The aerial images were connected using ArcMap 10.2 (IDRISI), segmented and classified

through SPRING 5.1.8, analyzed for change with the Land Change Modeler (IDRISI), an extension of ArcMap, and finally implemented in calibrated SWAT models to simulate the effects of land use change on hydrologic response. Details associated with image processing are provided below; SWAT modeling is discussed in more detail in Chapter 5. (Plieninger, 2006) similarly studied the effects of land use change on habitat loss and biodiversity in Spain using single framed aerial images.

Table 3.1: Historical aerial image characteristics for watersheds associated with select USGS gauging stations.

USGS Station	Acquisition Year	Acquisition Date	Scale	Focal Length (mm)	Image Quality	Cloud Cover
01141000	1957	4/30	1 : 60000	155	Good	0 - 9%
03302000	1959	4/4 & 4/5	1 : 24000	151		
	1971	4/15	1 : 24000	152		
03329700	1952	10/8	1 : 69000	154		
04099510	1952	9/28	1 : 69000	132		
	1979	11/18	1 : 80000	152		

3.1.1 Georeferencing and Rectifying Images

As the extents of the historical images do not align with watershed boundaries, they must be joined prior to analysis of land use/cover change. This process of spatially joining images together is known as georeferencing. In addition, scanned historical aerial images usually do not contain spatial reference information, meaning the image is not tied to a coordinate system and the spatial reference of the image is unknown. Therefore, in order to use the historical images along with other datasets and layers contained in ArcMap, the images must also be aligned or georeferenced to a map coordinate system. In this case, the images must be georeferenced to each other (image-to-image) before the image can be assigned a coordinate system, because most of the images have a 30-60% overlap with other photos. An example is provided in Figure 3.3.

For images to be correctly linked to each other, a transformation shift of the images must take place to correct for distortion of the images around the edges due to the elliptical shape

of the lens. Transformations are often used to convert an image with an unknown coordinate system to real-world coordinates. The geometric transformation implemented herein transform points from one location to another, and can range from simple scaling of points, to complex non-linear twisting and bending. They may also be used, as in this study, to link two adjacent images which both lack a coordinate system. ArcMap offers three types of transformations during an image-to-image transformation or a transformation to a known coordinate system: affine, similarity, and projective, as seen in Figure 3.1. In this study, an affine transformation (1st order) was used as it is the most widely implemented when dealing with scanned data. This polynomial transformation can model six kinds of distortions in the imagery or scanned map, including translation in x and y, scale changes in x and y, skew and rotation. Figure 3.2 provides graphics representing each distortion. The affine transformation is defined in Equation 2. The starting location of a point is represented by coordinates (x, y) with the ending transformed location coordinates (x', y'). Coefficients a₀, a₁, a₂, b₀, b₁, b₂ are determined based on the starting and ending coordinates, and will scale, skew, translate and rotate the image coordinates in order to match (ArcGIS Resources, 2014).

$$\begin{aligned}x' &= a_0 + a_1x + a_2y \\y' &= b_0 + b_1x + b_2y\end{aligned}\tag{2}$$

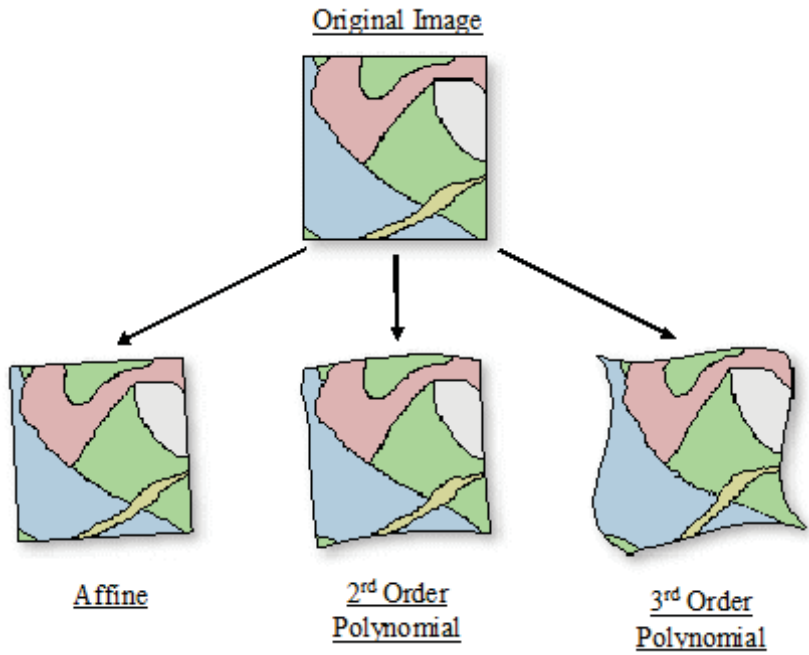


Figure 3.1: Depiction of three different orders of polynomial transformations before and after the transformation is implemented (Modified from ArcGIS, 2008).

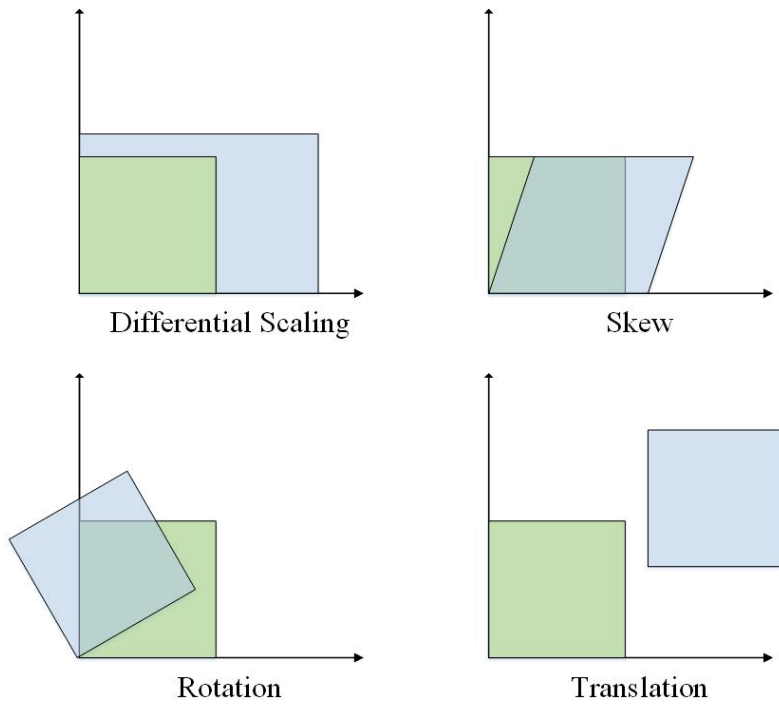


Figure 3.2: Four possible distortion changes while implementing a 1st order polynomial affine transformation (Modified from ArcGIS Resources, 2014).

In order to implement these transformations, ground control points (GCPs) are used to link the images together. GCPs, also referred to as the destination and transformed source control points, are locations in both images with shared coordinates. These can be physical locations such as road intersections, building corners, or even tree line corners. Because the images may be tilted, flipped, or reversed, the user must manually input the first few GCPs. Once this is complete, ArcMap allows the user to either continue manually inputting GCPs or to complete registration of the points automatically. The latter option creates the points for the user by identifying the GCPs, and generates substantially greater number of links (GCPs) compared to a manual insertion by the user. For the affine transformation, at least 3 GCPs must be selected in order to perform the 1st order transformation, although typically 15 to 20 GCPs are required to increase accuracy.

While the transformation/georeferencing process continues, error can occur due to radiometric and geometric distortions in the images. Radiometric errors involve distortions of the image brightness or shade due to the sensitivity of the camera sensor, the angle of the sun and topography, and atmospheric conditions. Geometric distortions refer to error in the image based on the actual image coordinates versus the ideal image coordinates. In basic terms, geometric distortion stems from images that are skewed in some way, usually due to the elliptical shape of the camera lens as described previously (Woodham and Gray 1987). Due to these inaccuracies, each link created between images has a corresponding residual, or error between the two location points, denoted e_i where $i = 1, \dots, n$ for n GCPs defined. ArcMap will output the total residual, or Total Root Mean Square Error (RMSE), for each pair of georeferenced images within/containing the specified watershed. This measure of error between the destination control points and the transformed locations of the source control is computed as:

$$RMSE = \sqrt{\frac{e_1^2 + e_2^2 + \dots + e_n^2}{n}} \quad (3)$$

In this case, the RMSE is in units of pixels, as the images have not yet been assigned a coordinate system, and thus do not have an associated unit of measurement. In this study,

an initial 3 to 5 GCPs were manually created by the user, and then ArcMap was allowed to create the rest of the points automatically. Once the appropriate number of GCPs were created, manual modifications were made to improve how the images overlapped and to decrease the RMSE. A flowchart of the step-by-step instructions to complete the image-to-image georeferencing process is provided in Appendix B (Figure B.1).

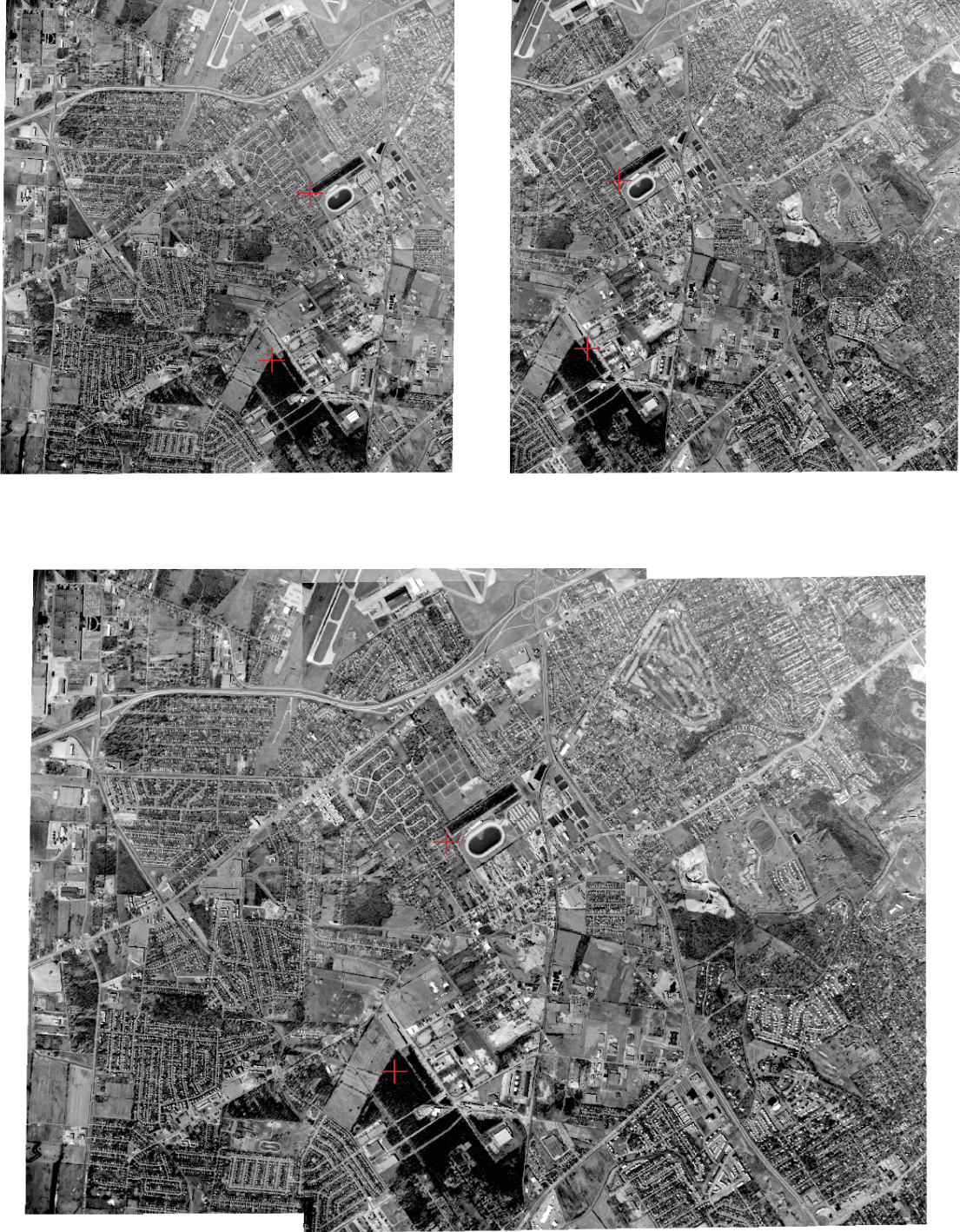


Figure 3.3: Georeferencing two 1971 aerial images for Pond Creek Watershed, KY (USGS station 03302000) using ArcMap. (Image data source: EROS, 2015. Full image created by author).

Following completion of georeferencing, the images must be rectified. As georeferencing is only a temporary method, rectification will permanently transform the images based on the ground control points. This will create a new raster feature of the georeferenced image in the correct spatial location based on the map coordinate system, if one exists. This process of georeferencing/rectification continues until all of the individual images are spatially connected to each other, yet physically are still separated.

3.1.2 Mosaic Images

Although the images are spatially connected, a physical permanent join of the rectified images has not yet occurred. The rectified images were imported into ERDAS IMAGINE 2014, a remote sensing application program used for geospatial raster data processing. ERDAS is used to physically meld/join the images together creating a mosaic image. By doing this, all of the images defining a given watershed are ‘smoothed over’ and combined into a single raster image. A variety of overlap functions are available to join the images (see Table 3.2). Overlap functions define how ERDAS deals with overlapping areas in the images, and if the images do not match perfectly, attempts to make the transition between images look natural. In this study, the quality, resolution and amount of overlap between each image determined the overlap function that would create the most accurate mosaic; therefore, selected functions varied from site to site.

The mosaic image is still not registered to a known coordinate system; therefore, the mosaic images were imported into ArcMap wherein an image-to-map transformation was used to register the image. A 2006 orthoimage was imported from USDA Geospatial Data Gateway and used to perform the image-to-map transformation using NAD 1983 UTM Zone 16N coordinate system. As previously described for image-to-image transformation, GCPs were used to link the mosaic image with an unknown coordinate system to the orthoimage with real-world coordinates. These locations are chosen assuming that the coordinates of the locations have not changed over time, and therefore is based on the user’s judgment. An example of an area that has not changed historically can be seen in

Figure 3.4. Auto registration was used to complete the georeferencing once initial links were complete as seen in Figure 3.5.

Table 3.2: ERDAS IMAGINE 2014 mosaic image overlay function options and descriptions (Pouncey et al., 1999).

Overlay Function	Description
Overlay	The last image opened (image at the top of the stacking order) will have precedence of the overlapping area. The images at the top of the order will overlap those below it.
Average	An average value will replace any pixels overlapping each other.
Minimum	The value in each pixel is replaced by the minimum value of the overlapping pixels.
Maximum	The value in each pixel is replaced by the maximum value of the overlapping pixels.
Feather	The overlap area is replaced by a linear interpolation of all overlapping pixels.

Once the mosaic images were registered to a coordinate system, the area of interest (i.e. the watershed) was used to clip the image as seen in Figure 3.6. The watershed boundaries used for clipping were obtained from GAGES II, and were generated based on a variety of DEMs (National Hydrography Dataset NHDPlus vs. National Elevation Dataset NED) and/or using a variety of different methods and tools.¹ Mosaic historical clipped images for all selected watersheds are provided in Appendix B (Figure B.2 through Figure B.3). In order to simplify image processing, any open water and urban developed areas were erased from the images manually, to be introduced back into the images during later procedures. This was completed in ArcMap using the polygon drawing tool to manually identify these areas. An example of this is provided in Appendix B (Figure B.8).

¹ GAGESII point location shapefiles and watershed boundary shapefiles may be downloaded at http://water.usgs.gov/GIS/metadata/usgswrd/XML/gagesII_Sept2011.xml. Metadata, information regarding criteria for inclusion, methods for watershed delineation, boundary quality assurance, and data assembly and organization can be obtained from Falcone (2011).

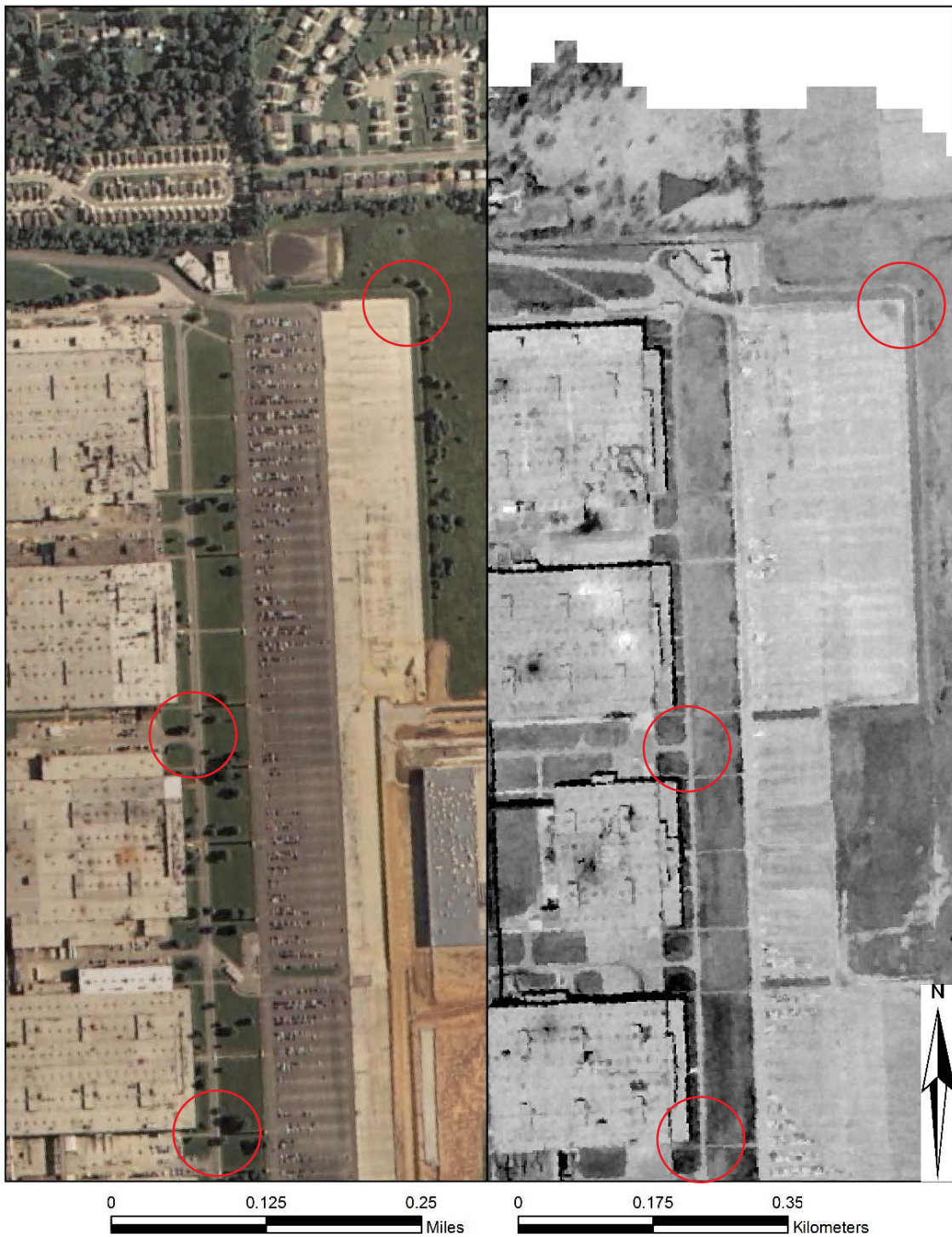


Figure 3.4: Comparison of a historical image (ca. 1971) to 2006 orthoimagery for station 03302000 (Pond Creek, KY). Circled areas indicate possible coordinate locations of GCPs for georeferencing. (Image data source: EROS, 2015. Full image created by author).

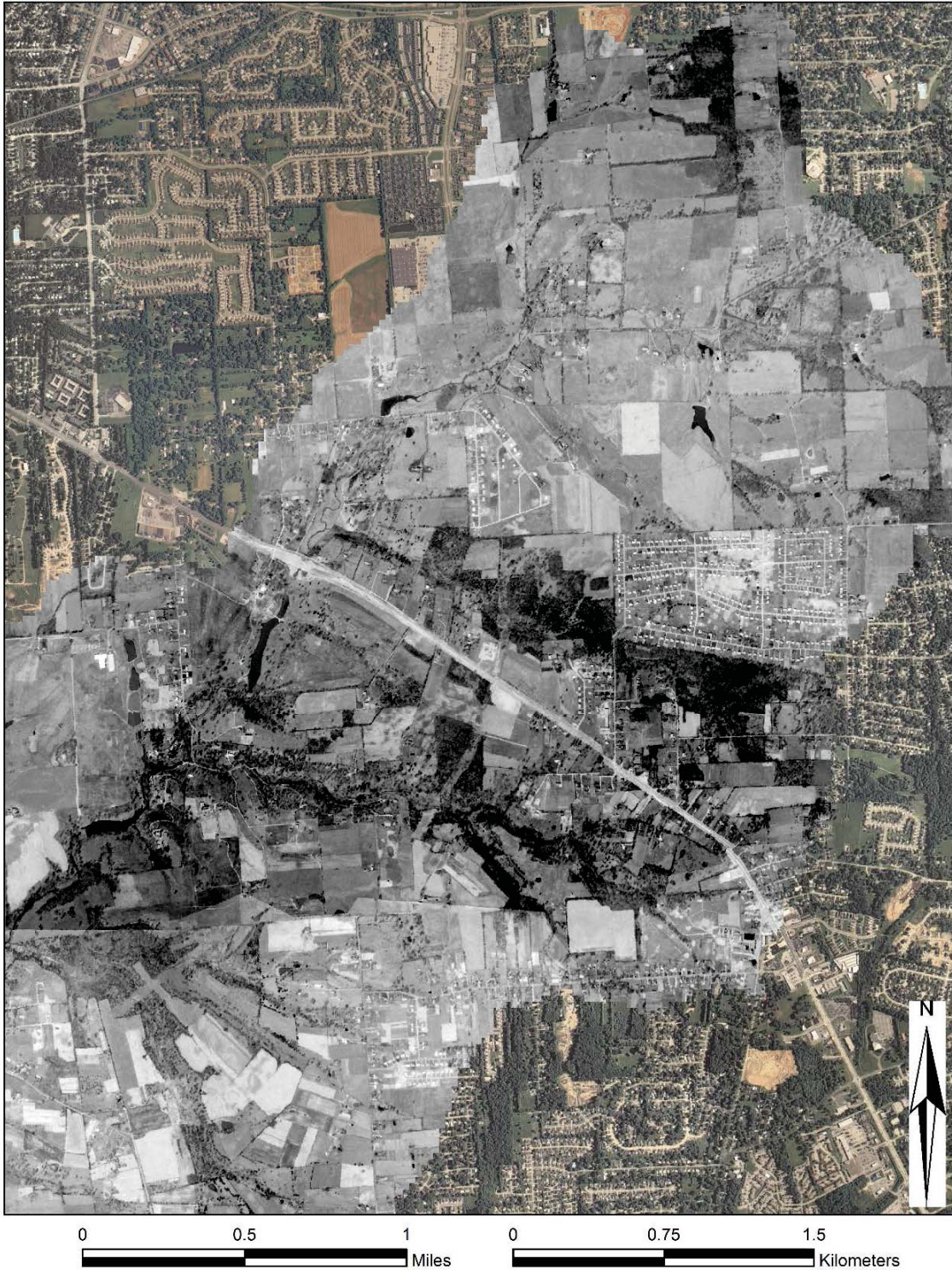


Figure 3.5: Mosaic 1971 historical image georeferenced to 2006 orthoimagery, coordinate system NAD 1983 UTM Zone 16N for USGS station 03302000 (Pond Creek, KY). (Image data source: EROS, 2015. Full image created by author).

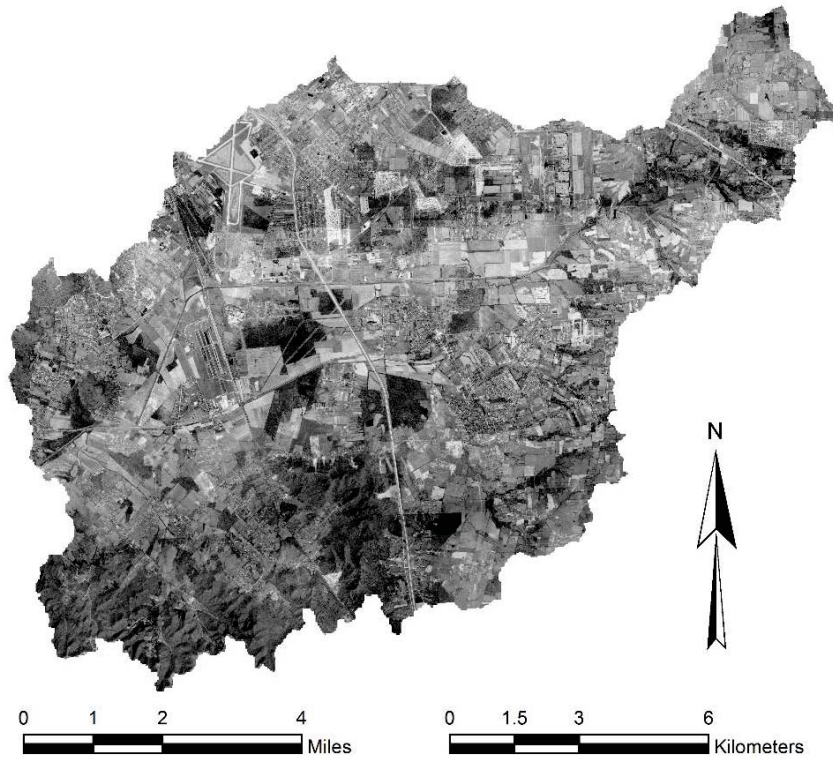
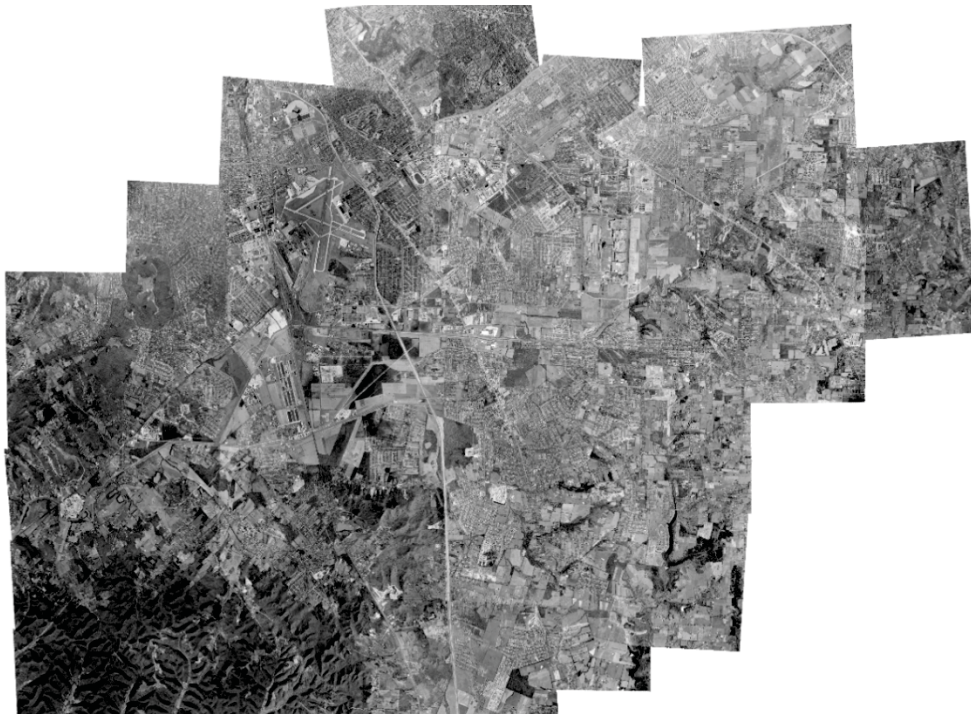


Figure 3.6: Mosaic historic aerial image (ca. 1971) for USGS station 03302000 (Pond Creek, KY) – full image (top), clipped to watershed (bottom). (Image data source: EROS, 2015. Full image created by author).

3.1.3 Segmentation and Classification

In order to transform aerial images to land use maps, the mosaic images were separated (or segmented) into polygons based on similar properties such as texture and hue. This process, referred to as image segmentation, is used frequently in image processing and remote sensing image analysis (Bins et al., 1996; Porter, 2011). Each segmented area is then classified to a specific land use type. There are a variety of image processing programs which implement segmentation in order to categorize an image. Porter (2011) utilized ENVI Zoom 4.5, a remote sensing program, to create detailed historical LULC maps using a variety of methods. In this study, segmentation was completed using SPRING, a GIS and remote sensing processing system developed in Brazil by the National Institute for Space Research (INPE) and Image Processing Division (DPI). SPRING integrates raster and vector data in a single location (Camara et al., 1996). SPRING has been used in many studies and for many purposes, although the main function of the model is land use change detection (Alves et al., 1996; Bins et al., 1996; Valeriano et. al., 2004). Figure B.2 outlines the segmentation and classification methodology implemented herein.

There are two types of segmentation techniques: region-based segmentation and basin detection. Region-based segmentation separates the image into areas with homogeneous properties, while edge detection finds the dividing line between homogeneous polygons with different properties (Bins et al., 1996). In this study, a region growing segmentation method was implemented, as previous studies have determined that this method is reasonable for images consisting of forest and agriculture (Alves et al., 1996; Bins et al., 1996), and has been extensively used in the Amazon region to analyze LULC change (Valeriano et. al., 2004).

The segmentation technique involves regions being grouped together, starting with individual pixels, and grows iteratively until the whole image or all of the pixels have been processed. The process can be described as follows (Bins et al., 1996):

1. Separate or segment the image into pattern cells consisting of 1 or more pixels.

2. Compare each pattern cell to neighboring cells to determine if they are similar enough to merge together to form a fragment. Once a cell is joined with the fragment, the property of the fragment is updated for further comparison.
3. Proceed growing the fragment section by comparing to neighboring cells until no more joinable regions remain. The completed individual fragments are then labeled.
4. Move to the next incomplete cell, and repeat until all cells/fragments are labeled.

The segmentation process was completed herein through trial and error by considering a range of similarity and area (pixels) input values. Similarity values were on the order of 10 pixels, while area values ranged from 10 to 35 pixels. Similarity refers to how 'strict' SPRING segments the image. Higher similarity values will produce polygons with less similar pixels (less similar brightness values), usually producing larger segments, while lower similarity values will produce smaller segments with more homogeneous pixels. Area (pixels) will set the minimum region, or polygon area, that SPRING will delineate in the image. Areas that were segmented incorrectly in SPRING were later corrected manually using ArcMap. Figure 3.7 presents an example of how SPRING segments an image.



Figure 3.7: Image segmentation utilizing SPRING for Pond Creek Watershed, KY (USGS station 03302000). Red lines are segmented area boundaries.



Figure 3.8: Image classification utilizing SPRING for Pond Creek Watershed, KY (USGS station 03302000). Green (light/dark) represents forested areas, brown (light/dark) represents agricultural areas, and white represents urban developed areas.

Once segmentation was complete, the segmented fragments within the image were assigned to (or classified as) specific land use classes. The first process for classification is to extract attributes of the regions in the image, which includes the area and mean brightness values for each segment, and a covariance matrix (Antonova, 2014). SPRING will classify individual image segments on the basis of these parameters. The classification is performed by “training” the image, a technique wherein the user specifies which segmented areas are to be assigned to a given land use type based on the texture and hue of the pixels inside the segment. The data was trained using SPRING by identifying segments into six general land use types: light, medium and dark shaded agricultural and forested land as seen in Figure 3.8. Once the user completed training, SPRING automatically classified the entirety of the image based on the user training.

Although a wider variety of distinct land use types are desired in analysis, the segmentation and classification process employed herein grouped general land use types together, due to limited resources, knowledge, and user expertise in the field of remote sensing and image processing. Many studies have analyzed land use change using finer classifications with more LULC classes (Rhemtulla et al., 2007), however, due to the limited accuracy of the panchromatic aerial imagery, this study found it suitable and more appropriate to use four generalized land use classes similar to (Alves et al., 2003; Porter, 2011). The generalization of the 1992 NLCD can be seen in Table 3.3. An example of SPRING classifying an image is shown in Figure 3.9. Finally, the images were imported into ArcGIS, where the variety of differently shaded agricultural classes and forested classes (see Figure 3.8) were merged to provide the four general land use types considered in subsequent analyses.

Table 3.3: 1992 NLCD generalized LULC breakdown for classification in SPRING.

NLCD 1992 Code	Land Cover Classification	General Land Cover Type	Assigned Code
71	Grassland/Herbaceous		
81	Pasture/Hay		
82	Cultivated Crops	Small Grains (AGRR)	83
83	Small Grains		
84	Fallow		
41	Deciduous Forest		
42	Evergreen Forest		
43	Mixed Forest	Shrubland (RNGB)	51
51	Shrubland		
91	Woody Wetlands		
92	Emergent Herbaceous Wetlands		
11	Open Water	Open Water (WATR)	11
21	Low Intensity Residential		
22	Heavy Intensity Residential		
23	Commercial/Industrial/Transportation	Commercial/Industrial/ Transportation	23
31	Barren Land (Rock/Sand/Clay)		
85	Urban/Recreational Grasses		



Figure 3.9: Image classification of generalized historical land use types for Pond Creek Watershed, KY (USGS station 03302000) utilizing SPRING.

3.2 Change Analysis

The Land Use Change Model (LCM) was implemented to quantify the level of LULC change historically and to visually represent the change spatially. LCM is a relatively new model, which is primarily employed for predictions of future land use change, mainly urbanization, and identification of driving change variables (Jiang, 2007; Pérez-Vega et al., 2012; Tewolde and Cabral, 2011), but has also been used to predict the impacts of urbanization on runoff and non-point source pollutants (Tang et al., 2005). LCM was also used in conjunction with the Soil and Water Assessment Tool (SWAT) to estimate total suspended solids and phosphorus concentrations in the Des Plaines River watershed in Chicago, Illinois (Wilson and Weng, 2011), where it was found that LCM was a useful tool in determining various future land use/planning scenarios.

For each study site considered herein, an examination of historical land use change was performed using the historical land use maps dating back to the 1950s or early 1960s, created as discussed in Section 3.1. These land use maps were generally categorized into four land use types: agriculture/grassland, forest/woody wetlands, open water, and urban/built-up areas. Figure 3.10 and Figure 3.11 give a spatial overview of the LULC change observed over the historic period for the Pond Creek and Pigeon Creek watersheds, respectively, with the 1992 through 2011 NLCD LULC generalized for comparison purposes; the progression of historical LULC change for other watersheds can be seen in Appendix B.

To quantify LULC change for a given watershed, inputs into the LCM included the land use map from the earliest obtained date and the generalized form of the 2011 NLCD map. LCM provides a variety of analysis options for the user to display the LULC change; however, further spatial representation of the LULC change was needed first. Figure 3.12 and Figure 3.13 represent examples of the spatial transition from agricultural/grassland to urban developed land from the earliest historical time period to present in the Pond Creek and Pigeon Creek watersheds, respectively. For all four case study watersheds, Table 3.4

shows quantitatively how general LULC has changed over the historic period. For Pigeon Creek watershed, Figure 3.14 shows the net change for each generalized LULC type and Figure 3.15 provides a graphical representation of the changes in percent coverage of each LULC class throughout the historical period. The main transition in this watershed was agricultural land converted to urbanized area. Figure 3.16 provides a graphical representation of the changes in percent coverage of each LULC class in Pigeon Creek Watershed. As the most data regarding historical LULC change was gathered for the Pond Creek and Pigeon Creek watersheds, they will be employed in subsequent analyses regarding impacts on the hydrology of the watersheds. Additional information regarding change analysis in the remaining case study sites is provided in Appendix B.

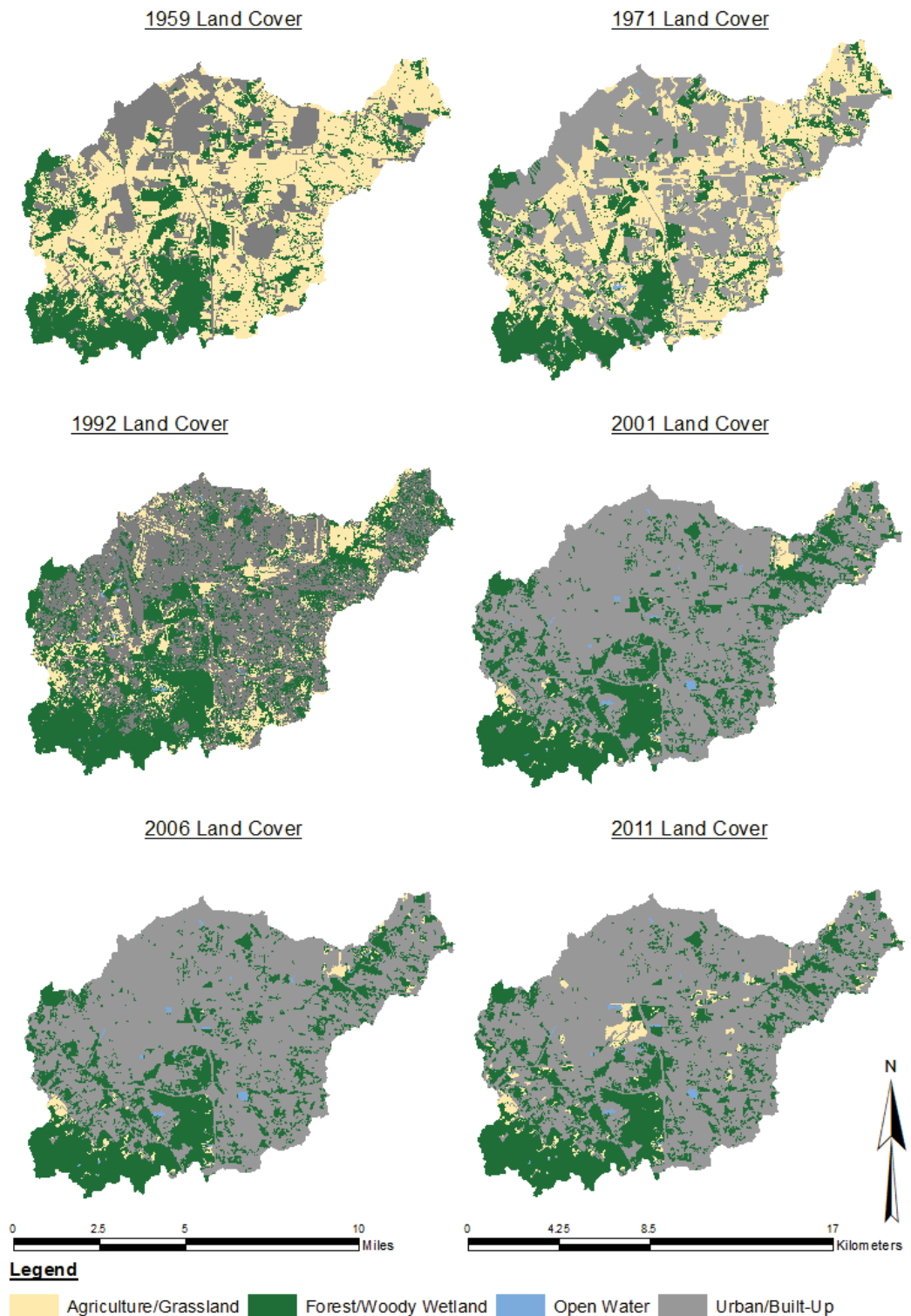


Figure 3.10: Historical LULC change progression from 1959 to 2011 for Pond Creek, KY (USGS station 03302000).

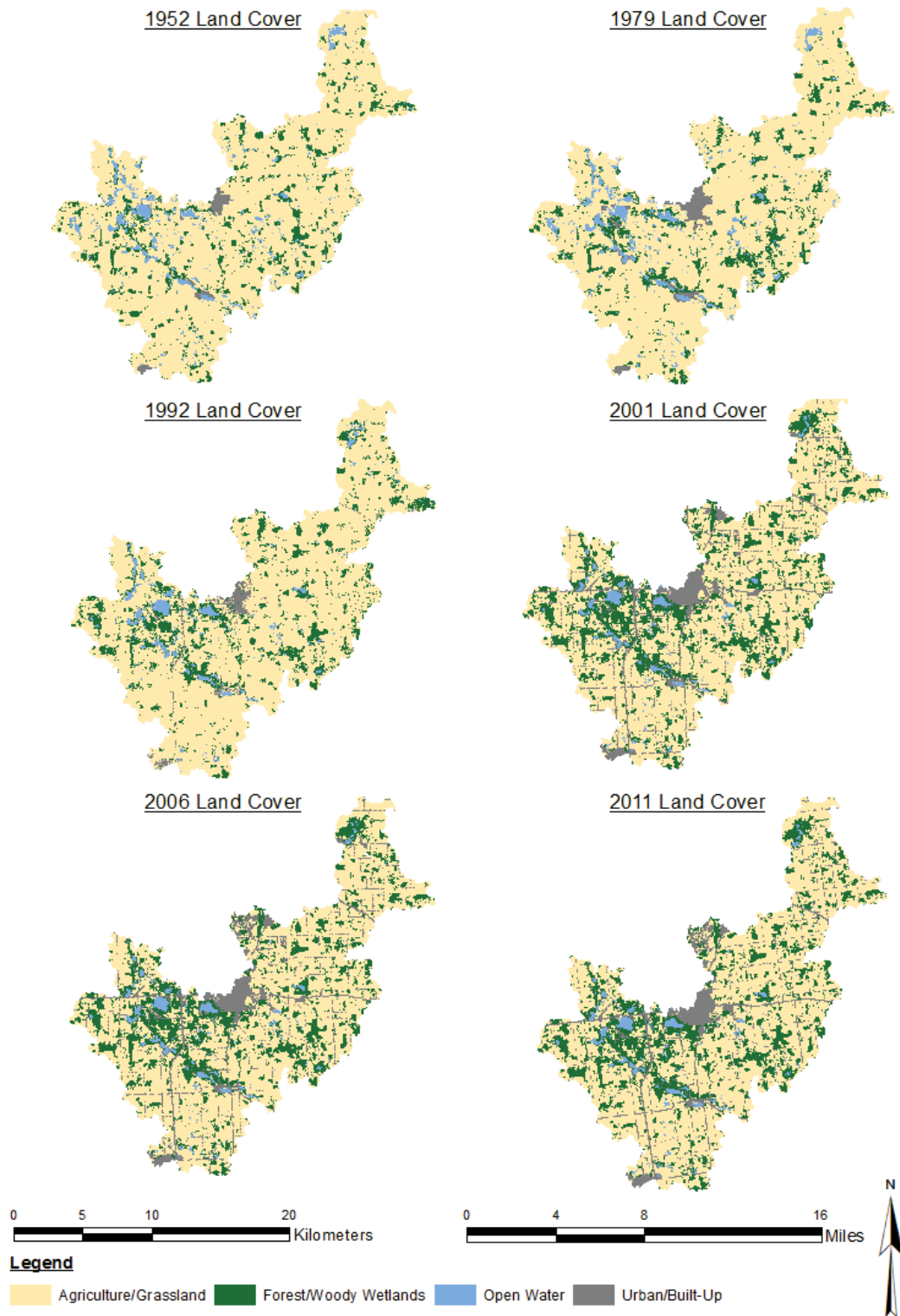


Figure 3.11: Historical LULC change progression from 1952 to 2011 for Pigeon Creek, IN (USGS station 04099510).

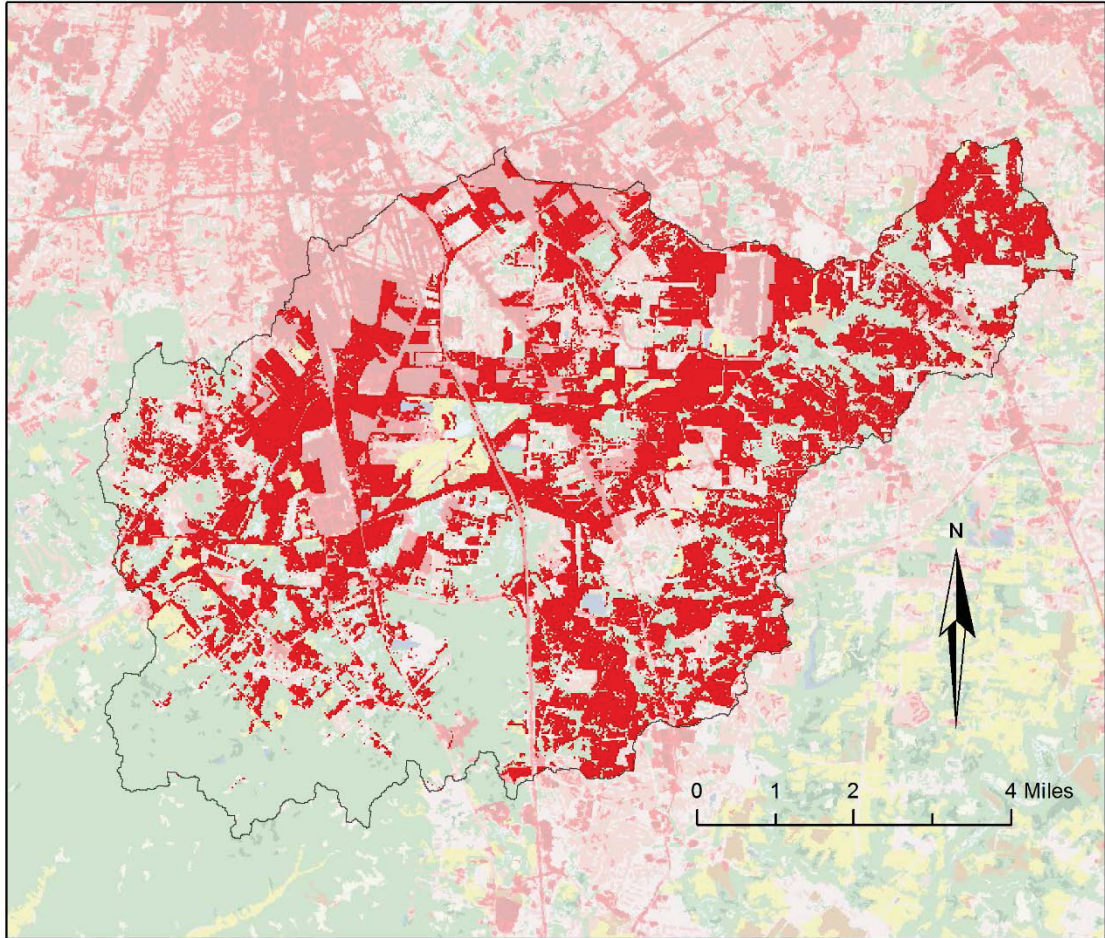


Figure 3.12: Transition from agricultural to urban developed LULC type (in RED) between 1957 and 2011 for Pond Creek, KY (USGS station 03302000) determined using LCM change analysis.

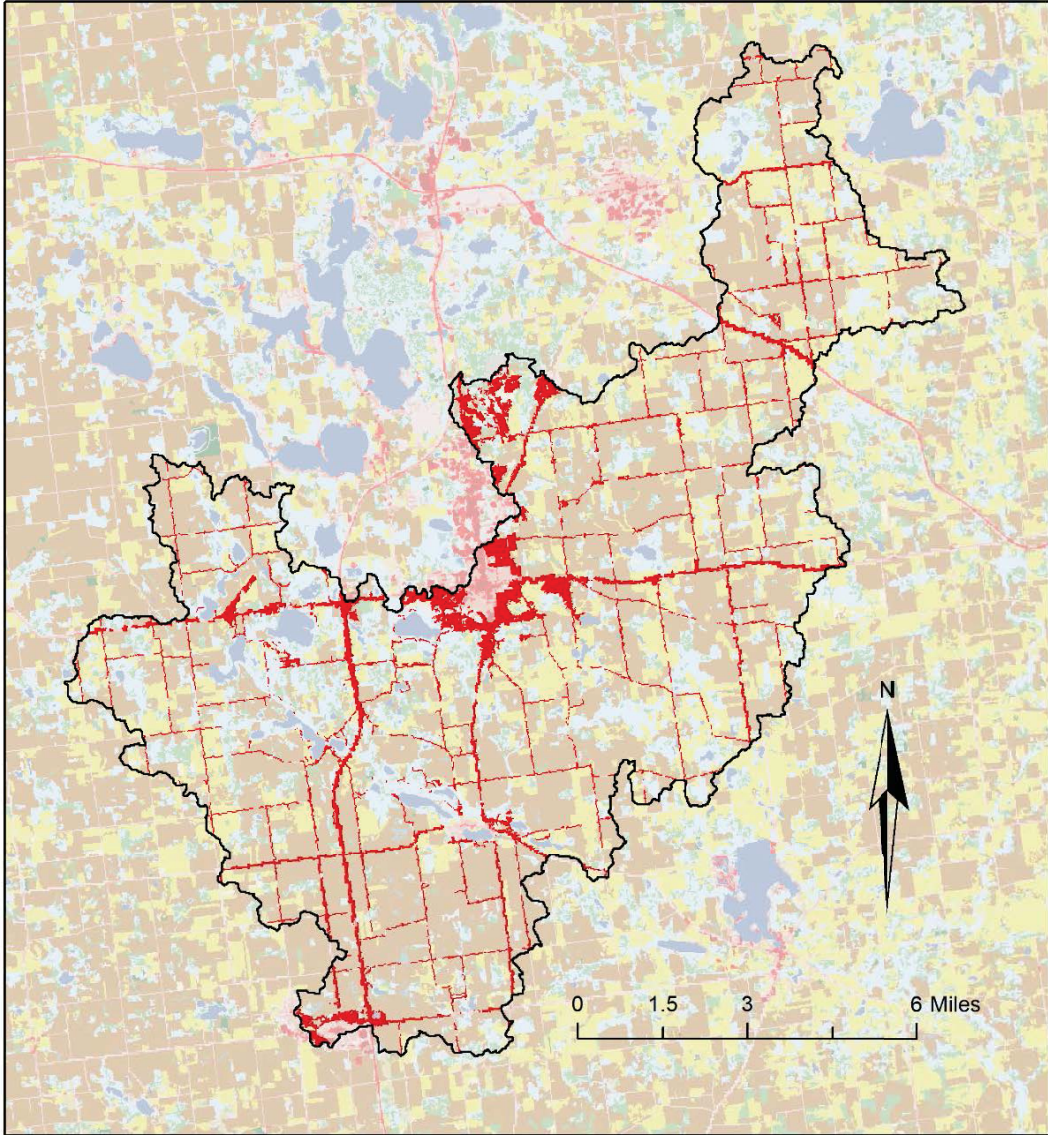


Figure 3.13: Transition from agricultural to urban developed LULC type (in RED) between 1952 and 2011 for Pigeon Creek, KY (USGS station 04099510) determined using LCM change analysis.

Table 3.4: Percentage of total watershed area covered by each generalized LULC type over historical period for each case study site.

Land Use Type	Year							
	1952	1957	1971	1979	1992	2001	2006	2011
Great Egg Harbor River, NJ (USGS Station 01411000)								
Agriculture		14%			15%	8%	8%	8%
Forest		76%			62%	60%	58%	56%
Urban		10%			22%	32%	34%	36%
Open Water		0%			1%	0%	0%	0%
Pond Creek, KY (USGS Station 03302000)								
Agriculture		50%	38%		14%	2%	1%	3%
Forest		27%	23%		39%	31%	29%	28%
Urban		23%	39%		47%	67%	69%	68%
Open Water		0%	0%		0%	0%	0%	0%
Deer Creek, IN (USGS Station 03329700)								
Agriculture	94%				95%	89%	89%	89%
Forest	5%				3%	4%	4%	4%
Urban	1%				1%	7%	7%	7%
Open Water	0%				0%	0%	0%	0%
Pigeon Creek, IN (USGS Station 04099510)								
Agriculture	83%			81%	80%	65%	65%	66%
Forest	11%			12%	12%	23%	22%	22%
Urban	1%			2%	2%	10%	10%	10%
Open Water	5%			5%	6%	2%	2%	2%

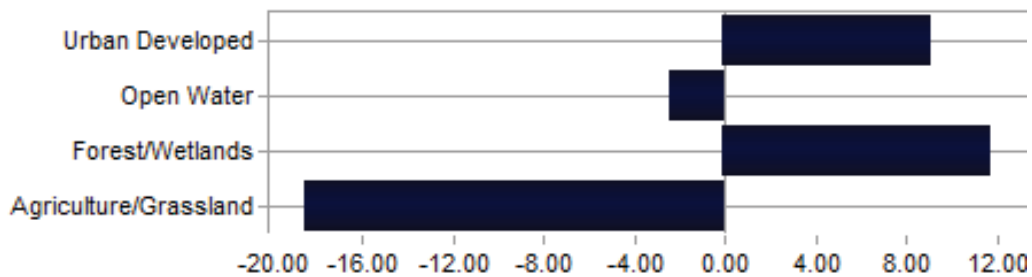


Figure 3.14: Net change (mi²) of generalized LULC types observed between 1952 and 2011 for Pigeon Creek, KY (USGS site 04099510) determined using LCM change analysis.

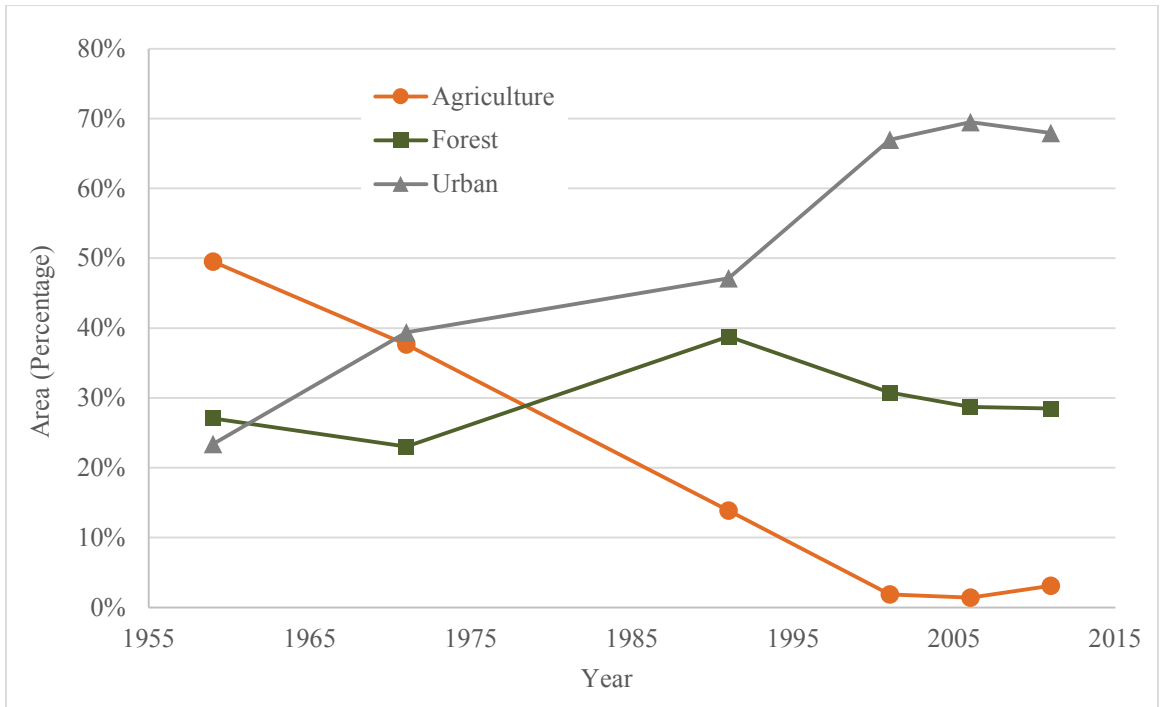


Figure 3.15: Graphical representation of LULC change between 1957 and 2011 for Pond Creek, KY (USGS station 03302000).

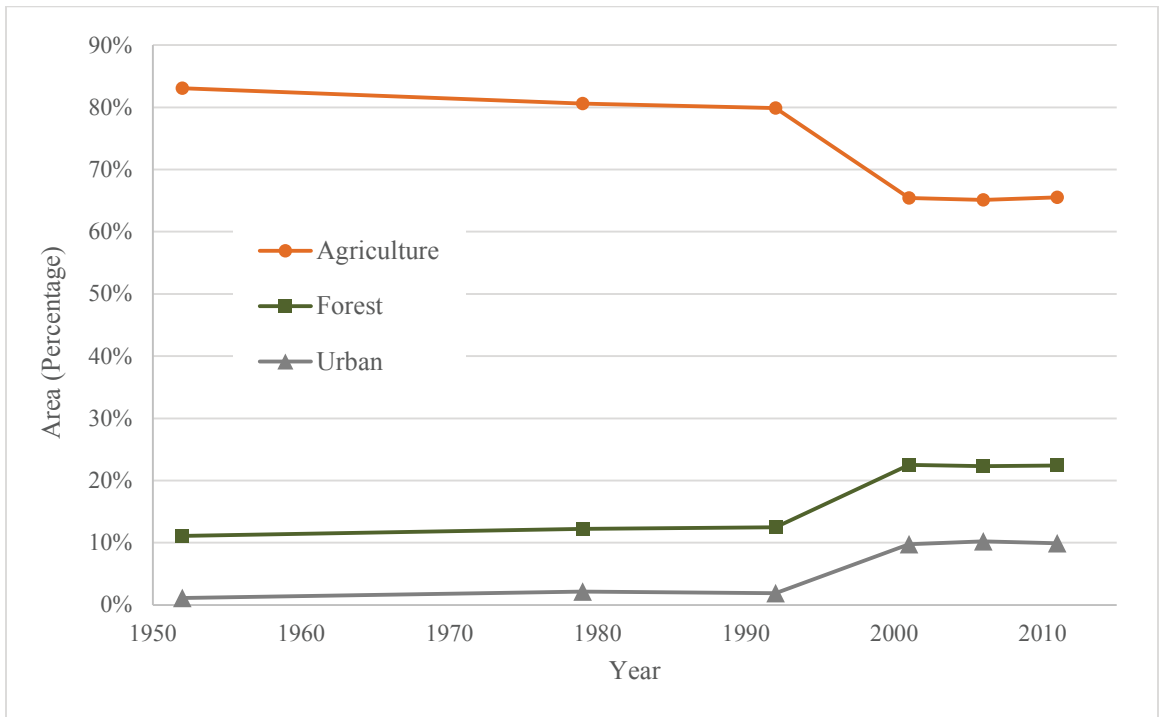


Figure 3.16: Graphical representation of LULC change between 1951 and 2011 for Pigeon Creek, IN (USGS station 04099510).

As seen in Table 2.2 (Section 2.1), Fritsch (2012) and Salvadori (2013) found that the historical AMF series for USGS stations 03302000 and 04099510 exhibit both positive trends and change points (abrupt shifts) in 1962 and 1975, respectively. Urban developed land in Pond Creek watershed (USGS station 03302000) has transitioned from the lowest LULC type within the watershed at 23.4% in 1957, to covering approximately 70% of the watershed area at present. This drastic conversion of LULC may be one of the driving factors for a positive trend in the AMF series. As seen in Figure 3.15, forested land remained nearly constant between 1957 and 1971, while 7.5% of the watershed area was converted from agricultural to urban developed land. This change in LULC may support the presence of the 1962 change point identified in the AMF flow series. As many of the cities surrounding Pigeon Creek watershed (USGS station 04099510) had not begun to extend beyond existing urban borders prior to 1992, relatively little change in LULC is observed in Figure 3.16; therefore, the cause of the trend and abrupt shift at this station is not yet apparent. Admittedly, these are only cursory observations based on the results presented thus far; further analysis will be conducted for both stations in Chapter 5 using SWAT to identify whether spatial variability of LULC yielded shifts or trends in the AMF flow series.

Chapter 4. Land Use Projection

Projecting land use change into the future is of the utmost importance when considering how the hydrology of a watershed and associated flood risk will be affected by future anthropogenic activities. However, land use projection is highly complex, due to: (1) the variety of parameters that must be considered, as well as their spatial variability and interactions; (2) the ability to determine driving forces for change, factoring in both spatial change and quantity of change; (3) implementation of socioeconomic factors; and, (4) unforeseen anthropogenic disturbances. Shifts in land use types with regards to urbanized, croplands, and forested lands can be attributed to population density, housing values, personal income, and even timber prices (Sun et al., 2008). Economic and environmental driving forces, as well as the global or regional focus in future policy, can merely be speculated. Understanding these factors, changes, and drivers will assist engineers and decision makers in accurately forecasting flood risk as LULC changes into the future.

Land use/cover change (LUCC) is recognized as one of the major contributors to global environmental change (Hudak and Wessman, 1998; Meyer and Turner, 1994). In the past century, human modifications of the environment have increased exponentially in order to keep up with inflated population and increased standards of living. Over the next century, this trend will likely continue, resulting in expanding agriculture, urban growth, and extraction of Earth's natural resources in excess just to maintain our shockingly high standard of living (DeFries and Eshleman, 2004).

Multiple approaches have been adopted for prediction of LULC change. Models predict land use change spatially (i.e. location for change) and/or statistically (i.e. rate of change). These two factors are referred to as the location issue versus the quantity issue (Pontius and Schneider, 2001). The task of determining the location for change only requires proximate causes for change, while the projection of the rate of change becomes more involved, as it requires a deep understanding of the underlying driving forces for change (Riebsame et al., 1994).

The study presented herein implemented the Forecasting Scenarios of Future Land Use Change (FORE-SCE) model (Sohl et al., 2007; Sohl and Saylor, 2008). FORE-SCE is a unique land use change prediction framework created by the USGS Earth Resources Observation and Science (EROS) Center to develop LULC projections for the contiguous United States. The FORE-SCE model has extensive applications, ranging from biochemical cycling and greenhouse gas fluxes, habitat biodiversity and conservation, climate and weather variability and cycles, and hydrology (Alves et al., 1996; USGS, 2014). The model projects four future LULC scenarios through 2100 based on emission scenarios developed by the Intergovernmental Panel on Climate Change (IPCC). The FORE-SCE model was selected based on its use in previous similar studies, the complexity and wide range of driving forces included in the model, and the ability to simulate a variety of scenarios as future social, economic and climatic change becomes increasingly unknown and difficult to project.

4.1 SRES Scenario Storylines

Emissions scenarios developed by the IPCC are detailed in the Special Report on Emission Scenarios (SRES). Descriptions of the IPCC-SRES scenarios (A1b, A2, B1, and B2) are presented in Figure 4.1, with Table 4.1 describing the level of change each characteristic in the model encounters for the future. These scenarios are hypothetical versions for future conditions based on extensive driving forces for future emissions (i.e. demographic, technologic advancement, economic growth/decline, land use change, etc.). The scenarios are a tool used to link qualitative stories and quantitative models for assessing future variables (Nakicenovic, 2000). Changes in carbon and greenhouse gas fluxes can be influenced by LULC change, and for this reason, projections in LULC from 2006 to 2100 were modeled herein for all four IPCC-SRES scenarios.

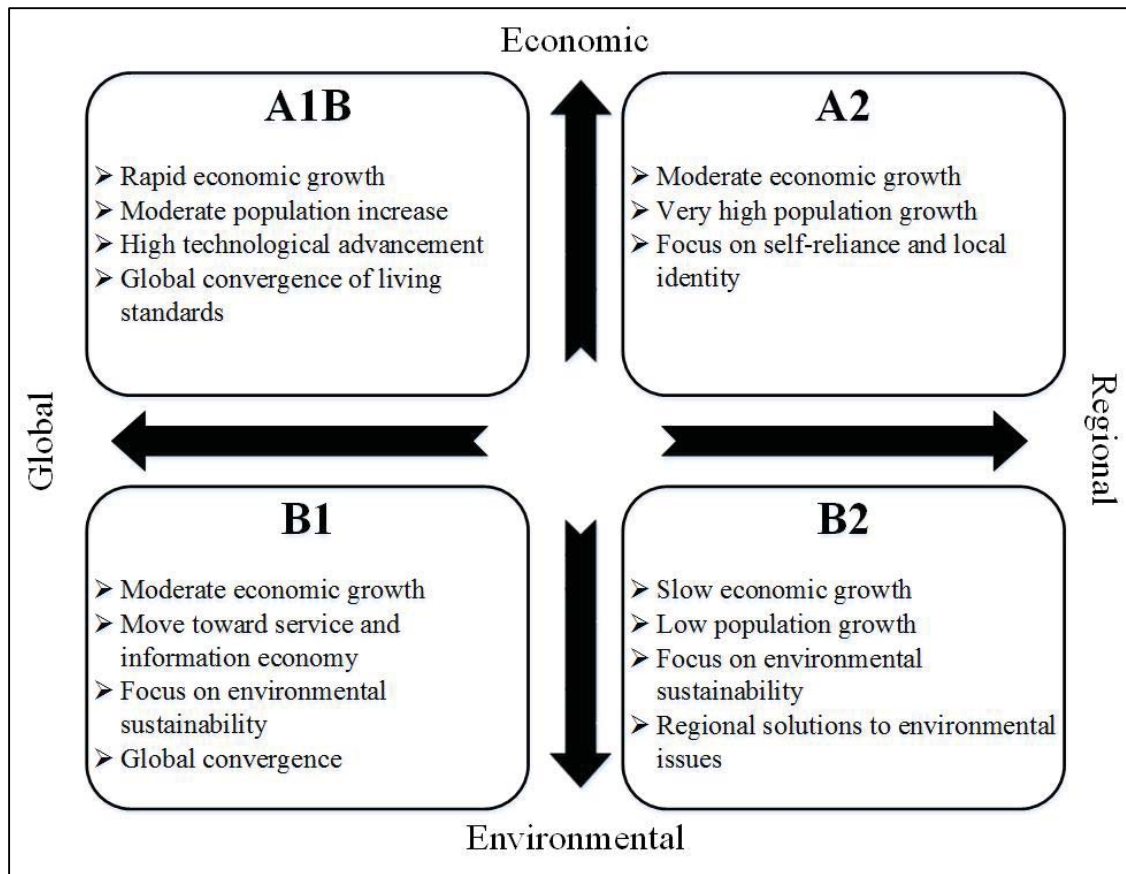


Figure 4.1: IPCC scenario based models with two axes: 1) economic vs. environmental priorities, and 2) global vs. regional development (Data Source: Nakicenovic, 2000; Solomon et al., 2007. Modified by author).

Table 4.1: SRES scenario based model driving force characteristics and level of change for the future (Data Source: Nakicenovic, 2000. Modified by author).

Scenario Group	A1B	A2	B1	B2
Population growth	low	high	low	medium
GDP growth	very high	medium	high	medium
Energy use	very high	high	low	medium
Land use changes	low	medium/high	high	medium
Resource availability [†]	medium	low	low	medium
Pace and direction of technological	rapid	slow	medium	medium
Change favoring	balanced	regional	efficiency & dematerialization	"dynamics as usual"

[†] Resource availability of conventional oil and gas

4.1.1 A1B Scenario

The A1 storyline is representative of rapid and successful economic development, where regional average income per capita converge, and current differences between “poor” and “rich” countries eventually disintegrate as a result of increases in transport and communication technology, shifts in national policy regarding immigration and education, and international cooperation. With economic growth at such a high rate, energy demand is subsequently extremely high. Continued use of fossil fuels coupled with the increase in technologic advances results in increased use of renewable energy sources. Population growth is moderate with a global population of 9 billion by the year 2050, followed by a decrease in population through 2100. Environmental protection remains moderate with the moderate increase in population and successful economic growth, although focuses have shifted from a ‘conservation’ approach to ‘active management’ approach. The primary dynamics of this scenario are (Nakicenovic, 2000):

- 1) Strong commitment to market-based solutions.
- 2) High savings and commitment to education at the household level.
- 3) High rates of investment and innovation in education, technology, and institutions at the national and international levels.
- 4) International mobility of people, ideas, and technology.

4.1.2 B1 Scenario

This scenario focuses on environmental conservation and global cooperation regarding socioeconomic conditions. This leads to high rates of technologic advances and global convergence of per capita Gross Domestic Product (GDP). Population increase is moderate at 9 billion by 2050, followed by a decrease to 2100. With an emphasis on environmental conservation, innovations regarding renewable energy result in a reduction in the use of fossil fuels. The primary dynamics of this scenario are (Nakicenovic, 2000):

- 1) Moderate economic growth.

- 2) Move toward service and information economy.
- 3) Focus on environmental sustainability.
- 4) Global convergence.

4.1.3 B2 Scenario

The B2 scenario is based on environmental conservation and regional growth. This leads to a reduction in global cooperation and self-reliance, which results in regional disparities in prosperity and living standards. Technologic advances slow with the lack of global cooperation, and economic growth is moderate, due to lack of growth potential stemming from environmentally friendly lifestyles. Population growth is slow, although global populations reach 10 billion by the year 2100. The primary dynamics of this scenario are (Nakicenovic, 2000):

- 1) Slow economic growth.
- 2) Low population increases.
- 3) Focus on environmental sustainability.
- 4) Regional solutions to environmental issues.

4.1.4 A2 Scenario

Compared to scenario A1, which focuses on interacting and working with other regions in the world, storyline A2 has more of a regional, self-reliance focus in terms of economic, social, and technological advances. This subsequently results in moderate economic growth, slower increases in technologic advances, and greater diversity regarding policy, resource dependency, and social structure. With the emphasis on community and family centered values, population growth rates remain high (15 billion in 2100). Energy demands also remain high, while the development and implementation of renewable energy is quite low. Global concerns for the environment are low due to regional reliability, while regions that are more developed and have ample funds may focus on environmental protection (Nakicenovic, 2000).

4.1.5 Selected SRES Scenarios

The FORE-SCE model is implemented based on these scenarios, or unique hypothetical sets of socioeconomic and environmental conditions for the future. These scenarios can form a basis for constructing future proportions for LULC change, and can be in the form of existing modeling frameworks, or a more subjective scenario based workshop with land use experts. These scenarios drive decisions for input variables into the model, and will be discussed further in subsequent sections. As the stations studied herein are located in the Midwest and Northeast U.S., much of this area is primarily agricultural based. However, many of the selected watersheds include or are located adjacent to urban developed land, which if it begins to encompass a larger area of land in response to population growth, can be directly linked to increases in flood magnitude. For the purposes of this study, interest is in scenarios with high economic and/or urban growth. As described previously, the A1B scenario projects rapid economic growth in the future, with increasingly high technological advances resulting in high energy demands. The demand for increased agricultural land will result in a loss of forest and grassland, along with rapid growth in urban development. While population growth is low with scenario A1B, growth rates for scenario A2 are relatively high, and thus urban expansion is likely. The A1B and A2 FORE-SCE scenarios were thus chosen to be the focused scenarios, as these hypothetical situations are anticipated to have the largest consequences on the hydrology of the watersheds. As a source of reference, FORE-SCE scenarios B1 and B2 were also observed and integrated into the results.

4.2 FORE-SCE Model Description

The FORE-SCE model was part of the USGS LandCarbon project, the overall goal of which was to assess the potential storage and emissions of carbon and other greenhouse gas emissions in the U.S., as well as to study the effects of anthropogenic and major natural processes such as climate change, land use change, wildfire, and land management activities (Zhu, 2014). The model is an integrated assessment tool, incorporating existing data collected by multiple national agencies, monitoring programs, historical land use data

from the USGS Land Cover Trends project, remote sensing programs and expert knowledge. As part of the assessment, FORE-SCE was applied to generate future LULC maps annually from 1992 to 2100 for the conterminous U.S. based on the four IPCC-SRES future emission scenario conditions. The study implements extensive multidisciplinary methods, along with both qualitative and quantitative scenario storylines useful for a wide range of purposes including hydrologic modeling, land use studies, wetland ecology, wildfire mapping, aquatic assessment, and biogeochemical modeling.

FORE-SCE has been implemented in a variety of studies focused on flood risk and environmental impact from LULC change. Tao et al. (2014) studied the effects of climate, land use, and atmospheric CO₂ change on the Mississippi River discharge and found that land use change along with human induced atmospheric CO₂ increases have a larger effect on river discharge compared to climate change expectations based on the high-emission scenario (A2). Wu et al. (2013) used FORE-SCE along with the Soil and Water Assessment Tool (SWAT) to study the impacts of land use change on the water cycle, water quality, and surface runoff in the Cedar River Basin. All inputs, excluding land use, were kept constant to isolate the effects of LULC change. A significant increase in surface runoff (approximately 10.5%) along with a drop in baseflow (approximately 7.3%) was found due to projected urban expansion using the A1B FORE-SCE scenario.

LULC trends can be based off of large-scale driving forces (demographic change, economic variation) or local-based drivers for change (soil type, climatic, topographic) (Lambin and Helmut, 2006). These driving forces for change are known as top-down (large scale) and bottom-up (local spatial pattern), and are both utilized in the FORE-SCE model. The FORE-SCE model sets up scenario-based proportion models for land use change based on ‘demands’ at a regional scale given top-down drivers. The model then inputs these future proportion ‘demands’ into a ‘spatial designation’ component to produce spatial predictions that are driven by local or bottom-up driving forces (Wu et al., 2013). This ‘demand’ assists the model in determining what land use is most appropriate, or needed, in a given area.

The simplest form for inputting a ‘demand’ value within FORE-SCE is to determine proportions of change based on historical data. FORE-SCE is supported by an integrated modeling framework called IMAGE version 2.2 (Integrated Model to Assess the Global Environment). This framework models socioeconomic and biophysical driving forces for LULC, and helps provide the future proportions for change at the regional level (USGS, 2014). An overview of the FORE-SCE model including the framework and drivers for change can be seen in Figure 4.2, which shows that the future emission scenarios encompass all aspects for change, dictating local, national, and global drivers. As each scenario varies, more emphasis may be placed on different drivers. For example, the A2 scenario focuses on regional sustainability with economic, technological and social growth centered on self-reliance, and thus local community centered focus will drive change more heavily.

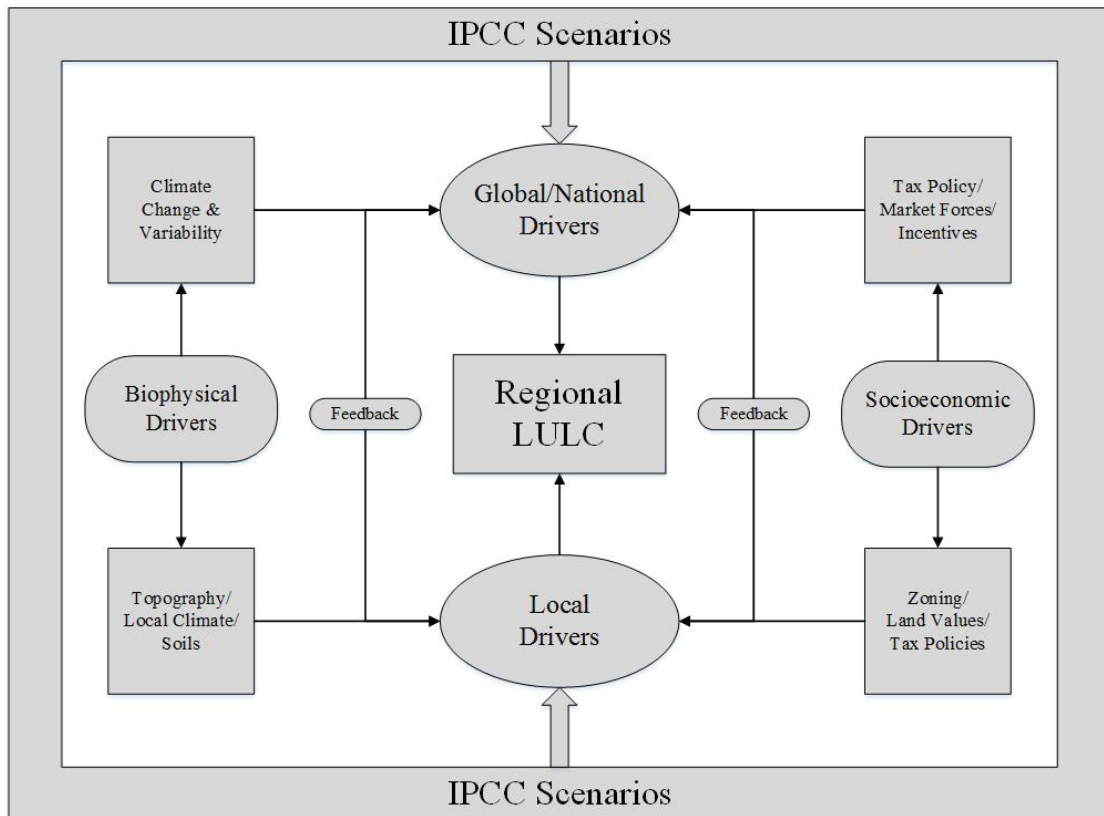


Figure 4.2: Input variables and driving forces implemented in FORE-SCE (Adapted from USGS, 2014).

The FORE-SCE model uses the ‘demand’ module, or proportions for change, to produce spatially explicit LULC maps within the ‘spatial allocation’ module. While considering suitability for various land use classes, a dispersion variable is used to regulate how clustered or spread-out land use classes are allowed to be established. This dispersion variable is based on the suitability of an area, and will place a greater probability for change for a given land use class based on this suitability. Suitability values are created based on statistical relationships between existing LULC distributions and variables such as climate, soil characteristics, topography, and distance from roads. For example, while predicting future development, areas with a close proximity to existing urban land are given a higher suitability or probability for change to urban development than areas farther away. For the case study watersheds considered herein, Figure 4.6 through Figure 4.9 illustrate how urban development tends to extend away from existing urban areas, justifying that these areas have higher suitability for urban change. On the other hand, areas that are protected (wetlands, National Parks, etc.) are given a very low probability for change, based on the specified scenario. Scenarios which focus on economic growth compared to environmental conservation will have significantly fewer restrictions for LULC change in protected areas (Wu et al., 2013).

The regional scale of the ‘demand’ module is based on EPA Level III ecoregions (Omernik, 1987; USEPA, 2013). These ecoregions consist of areas where similar characteristics are present such as climate, geology, physiography, soils, vegetation, and hydrology (USGS, 2014). 182 ecoregions for the conterminous U.S. are illustrated in Figure 4.3. USGS (2014) provides justification for dividing the U.S. into these ecoregions as follows:

“... ecoregions (1) provide a means to localize estimates of the rates and driving forces of change, (2) play a significant role in determining the range of current LULC types, and the trajectories of land use and land cover that may take place in the future, and (3) provide a framework that can be extended globally.”

For each ecoregion, the Land Use Trend project analyzed trends and patterns in the rate of change in LULC based on historic Landsat imagery from 1973 to 2000 (Loveland et al.,

2002) for 11 general land use classes as described in Table 4.2. Within each ecoregion, finer sample blocks (10 km x 10 km or 20 km x 20 km) were selected to represent the characteristics of the ecoregions, as seen in Figure 4.4. The results of the USGS Land Use Trend project were used to determine the land use demands for each ecoregion, and subsequent future proportions for land use change. These demands and proportions were used in the spatial allocation component of FORE-SCE to create spatial land use maps at the local scale, with a more specific breakdown of LULC classes using 17 LULC classes as seen in Table 4.3. The FORE-SCE model implemented patch-based modeling to characterize the land use of an ecoregion by using the results from the Land Use Trend project, altering the land use in the area based on statistical suitability until the ‘demand’ of an area has been satisfied (Wu et al., 2013).

Table 4.2: USGS Land Use Trends Project LULC categories.

Class	Description
Water	Areas persistently covered with water, such as streams, canals, lakes, reservoirs, bays, or oceans.
Developed/urban	Areas of intensive use with much of the land covered with structures (e.g., high density residential, commercial, industrial, transportation, mining, confined livestock operations), or less intensive uses where the land cover matrix includes both vegetation and structures (e.g., low density residential, recreational facilities, cemeteries, etc.), including any land functionally attached to the urban or built-up activity.
Mechanically disturbed*	Land in an altered and often non-vegetated state that, due to disturbances by mechanical means, is in transition from one cover type to another. Mechanical disturbances include forest clear-cutting, earthmoving, scraping, chaining, reservoir drawdown, and other similar human-induced changes.
Barren	Land comprised of natural occurrences of soils, sand, or rocks where less than 10% of the area is vegetated.
Mining	Areas with extractive mining activities that have a significant surface expression. This includes (to the extent that these features can be detected) mining buildings, quarry pits, overburden, leach, evaporative, tailing, or other related components.
Forests/woodlands	Tree-covered land where the tree-cover density is greater than 10%. Note that cleared forest land (i.e., clear-cut logging) will be mapped according to current cover (e.g., disturbed or transitional, shrubland/grassland).
Grassland/shrubland	Land predominately covered with grasses, forbs, or shrubs. The vegetated cover must comprise at least 10% of the area.
Agriculture	Cropland or pastureland in either a vegetated or non-vegetated state used for the production of food and fiber. Note that forest plantations are considered as forests or woodlands regardless of the use of the wood products.
Wetland	Lands where water saturation is the determining factor in soil characteristics, vegetation types, and animal
Nonmechanically disturbed*	Land in an altered and often non-vegetated state that, due to disturbances by nonmechanical means, is in transition from one cover type to another. Nonmechanical disturbances are caused by wind, floods, fire, animals, and other similar phenomenon.
Ice/snow	Land where the accumulation of snow and ice does not completely melt during the summer period.

Table 4.3: FORE-SCE land use/land cover classification descriptions.

Land Use Class	LULC Code	Description
Water	WATR	Areas of open water, generally with less than 25% vegetation/land cover.
Developed	UIDU	Areas characterized by a high percentage (20% or greater) of constructed material (concrete, asphalt, buildings, etc.)
Mechanically Disturbed National Forest	FRST	Forested lands within National Forests that have been mechanically disturbed (cleared, thinned, etc.)
Mechanically Disturbed Public Land	FRST	Forested lands within all other publicly owned property (excluding National Forests) that have been mechanically disturbed (cleared, thinned, etc.)
Mechanically Disturbed Private Land	FRST	Mechanically disturbed (cleared, thinned, etc.) forested lands on privately-owned property.
Mining	BARR	Areas of extractive mining activities with surface expressions
Barren	BARR	Areas characterized by bare rock, gravel, sand, silt, clay, or other earthen material, with little or no "green" vegetation present regardless of its inherent ability to support life. Vegetation, if present, is more widely spaced and scrubby than that in the green vegetated categories; lichen cover may be extensive
Deciduous Forest	FRSD	Areas dominated by trees where 75% or more of the tree species shed foliage simultaneously in response to seasonal change
Evergreen forest	FRSE	Areas dominated by trees where 75% or more of the tree species maintain their leaves all year. Canopy is never without green foliage
Mixed Forest	FRST	Areas dominated by trees where neither deciduous nor evergreen species represent more than 75% of the cover present
Grassland	RNGE	Areas dominated by grasses and forbs. In rare cases, herbaceous cover is less than 25%, but exceeds the combined cover of the woody species present. These areas are not subject to intensive management, but they are often utilized for grazing.
Shrubland	RNGB	Areas dominated by shrubs; shrub canopy accounts for 25 to 100% of the cover. Shrub cover is generally greater than 25% when tree cover is less than 25%. Shrub cover may be less than 25% in cases when the cover of other life forms (e.g. herbaceous or tree) is less than 25% and shrubs cover exceeds the cover of the other life forms
Cropland	AGR	Areas dominated by vegetation that has been planted or is intensively managed for the production of food, feed, or fiber; or is maintained in developed settings for specific purposes. Includes cultivated crops, row crops, small grains, and fallow fields
Hay/Pasture	HAY	Areas of grasses, legumes, or grass-legume mixtures planted for livestock grazing or the production of seed or hay crops
Herbaceous Wetland	WETN	Areas where perennial herbaceous vegetation accounts for 75% to 100% of the cover and the soil or substrate is periodically saturated with or covered with water.
Woody Wetland	WETF	Areas where forest or shrubland vegetation accounts for 25% to 100% of the cover and the soil or substrate is periodically saturated with or covered with water
Ice/Snow	WATR	Areas characterized by a perennial cover of ice and/or snow, generally greater than 25% of total cover.

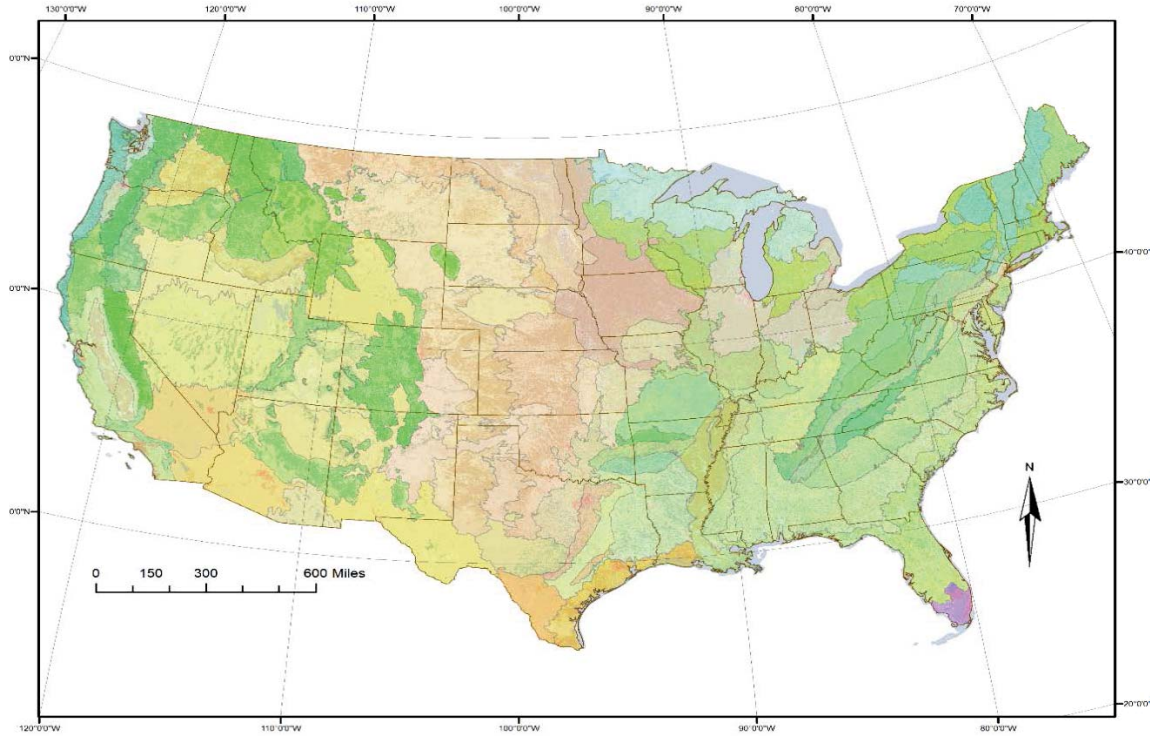


Figure 4.3: United States Environmental Protection Agency (EPA) Level III ecological regions. (Data Source: Omernik, 1987).

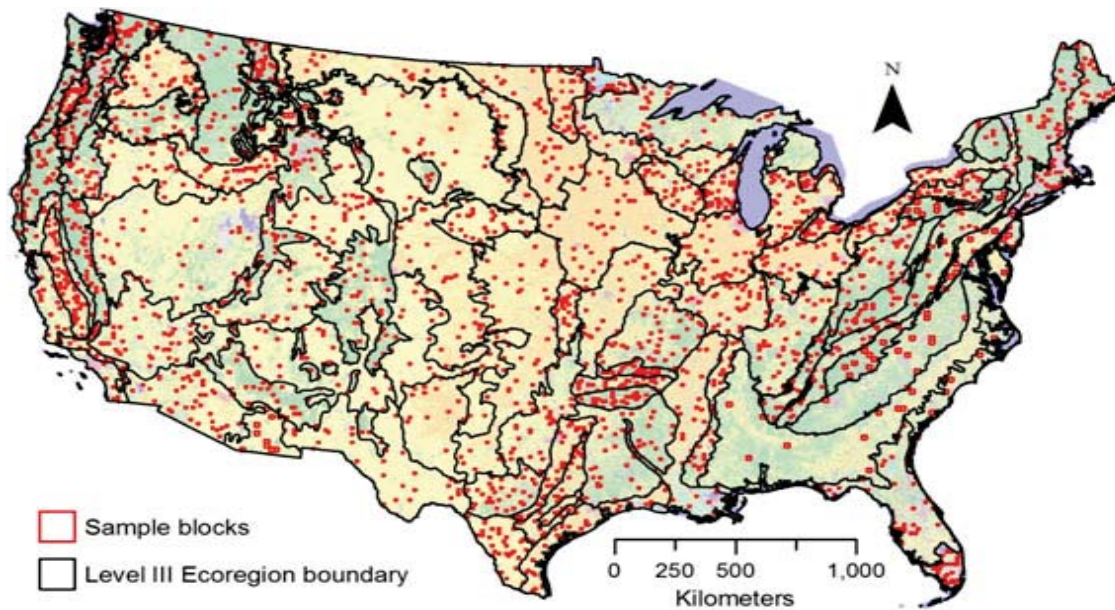


Figure 4.4: Location of Land Cover Trend ecoregions, with the locations of sample blocks used to characterize each ecoregion in the conterminous U.S. Sample blocks have areas of either 10 km x 10 km or 20 km x 20 km (Data Source: USGS, 2014).

4.3 FORE-SCE Model Results

Each FORE-SCE scenario is based on a variety of socioeconomic, environmental, and political drivers specified by the SRES scenario storylines, thereby resulting in a wide range of projected LULC types and subsequent proportions of LULC. As the SRES emission scenarios A1B and A2 were chosen for application herein, the assumption for the future is representative of highly expansive growth in technology and economy, with a large need for further energy sources. With the continued urban expansion of many areas, the LULC types with the largest area lost are deciduous forest, cropland and hay/pasture. This is observed in the 2100 FORE-SCE projection LULC maps for the four watersheds studied herein, as seen in Figure 4.6 through Figure 4.9. Urban developed land in the A1B and A2 scenarios can be seen to propagate around existing developed land more intensely compared to scenarios B1 and B2. In scenarios A1B and A2, forested land is lost rapidly to urbanization, as well as agricultural land being preserved due to high energy and food demands, stemming from population growth and the focus on sustaining a strong growing economic foundation. In contrast, scenarios B1 and B2 can be seen to preserve forested land and have limited urban development as a result of focuses on sustainability, environmental preservation, and alternative energy sources.

As an example, results of change projected under scenario A1B are presented in Table 4.4 and Table 4.5, quantifying the decrease in agricultural and forested lands associated with increased developed area in terms of actual land area (mi²) and as a percent change, respectively. Urban areas are projected to increase for all watersheds in scenario A1B, although station 04099510 is the only watershed where agricultural land increases by the year 2100. This may be due to the heavy percentage of the watershed's current LULC consisting of agricultural land, and with limited large cities within or surrounding Pigeon Creek, this watershed would likely provide supportive crops for the growing energy and population demands. Similarly, urban development is limited in Deer Creek Watershed (station 03329700) as it is presently dominated by agricultural land. For each case study watershed, Appendix C provides graphical representations of the progression of spatial

LULC change projected from 2025 to 2100 under the all four FORE-SCE scenarios.

The FORE-SCE projection results also correlate with historical LULC changes. As Great Egg Harbor River Watershed (USGS station 0411000) is adjacent to heavily urbanized land, FORE-SCE scenarios A1B and A1 are representative of a loss in forested land to urban development, similar to the historical LULC change in this watershed. As Pond Creek Watershed (USGS station 0332000) is located in such close proximity to Louisville, KY with a large urban footprint at present, further urban development in the watershed is inevitable as the boundary of the city expands. This can also be seen in the historical LULC data, as loss of agricultural and forest land has been taking place since the late 1950s. It is also interesting to note the interactions of the surrounding LULC classes extending beyond Louisville, KY, as each scenario paints a very different picture of the surrounding LULC. Scenario A2 can be seen to have a heavy agricultural basis in the surrounding areas, as the demand for agricultural commodities results in an expansion in cropland and hay/pasture, while scenario B2 presents a heavy focus on environmental conservation with thriving forest, grassland, and shrubland. This phenomenon in LULC can also be seen in the agriculturally dominated Pigeon Creek Watershed (USGS station 04099510). Historically, Deer Creek Watershed (USGS station 03329700) has been quite stagnant with regards to LULC change. As a primarily rural based watershed, agricultural land has remained quite constant, with urban developed land increasing minimally. Future projections for LULC in Deer Creek Watershed show a mere five percent increase in developed land for scenario A1B, although many of the surrounding towns and cities have expanded quite heavily by 2100 under scenarios A1B and A2, resulting in increased impact on the watershed. On the contrary, scenarios B1 and B2 which focus on conservation, seem to preserve this watershed quite close to current LULC conditions.

While reviewing all scenarios, it was determined that scenario A1B is the most realistic scenario for future LULC change. This can be seen in Figure 4.5, which includes a spatial representation of the LULC predicted within the Midwest and Northeast for 2100 under all four FORE-SCE scenarios. Current shifts in urbanization seem to be moderately

increasing, with demands for further energy sources staying quite high. Moderate population growth would be an appropriate assumption, and as environmental awareness may be growing within the United States, little action is being taken to make drastic policy changes, as seen in scenario A1B. Overall, engineers, politicians, and policy makers should view FORE-SCE scenario A1B as a realistic scenario for change.

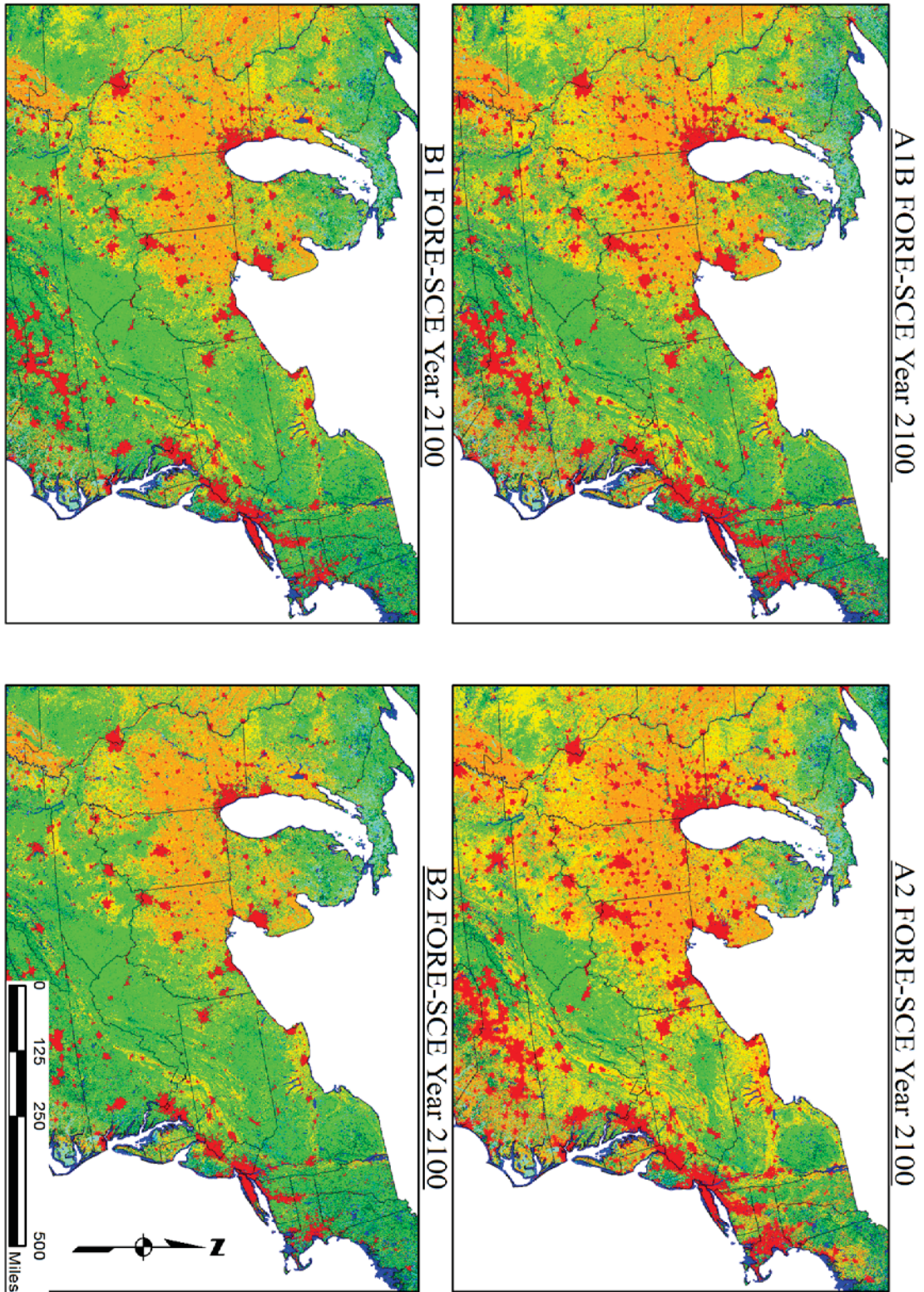


Figure 4.5: Overall FORE-SCE LULC projection for the year 2100 in the Midwest and Northeast U.S. (Data Source: USGS, 2014).

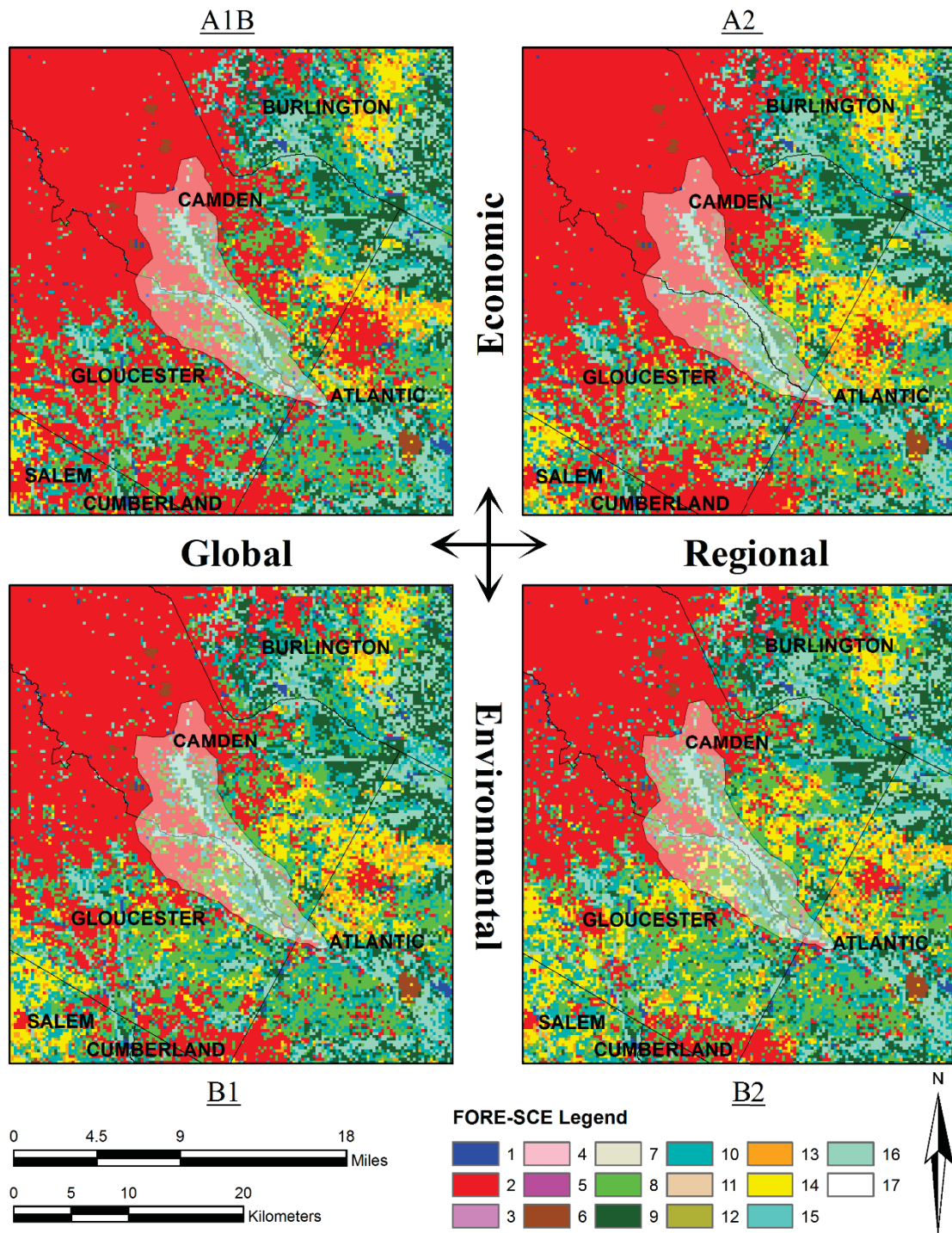


Figure 4.6: FORE-SCE scenario based spatial LULC model projection for the year 2100 for Great Egg Harbor River Watershed, NJ (USGS station 01411000). (Data Source: USGS, 2014).

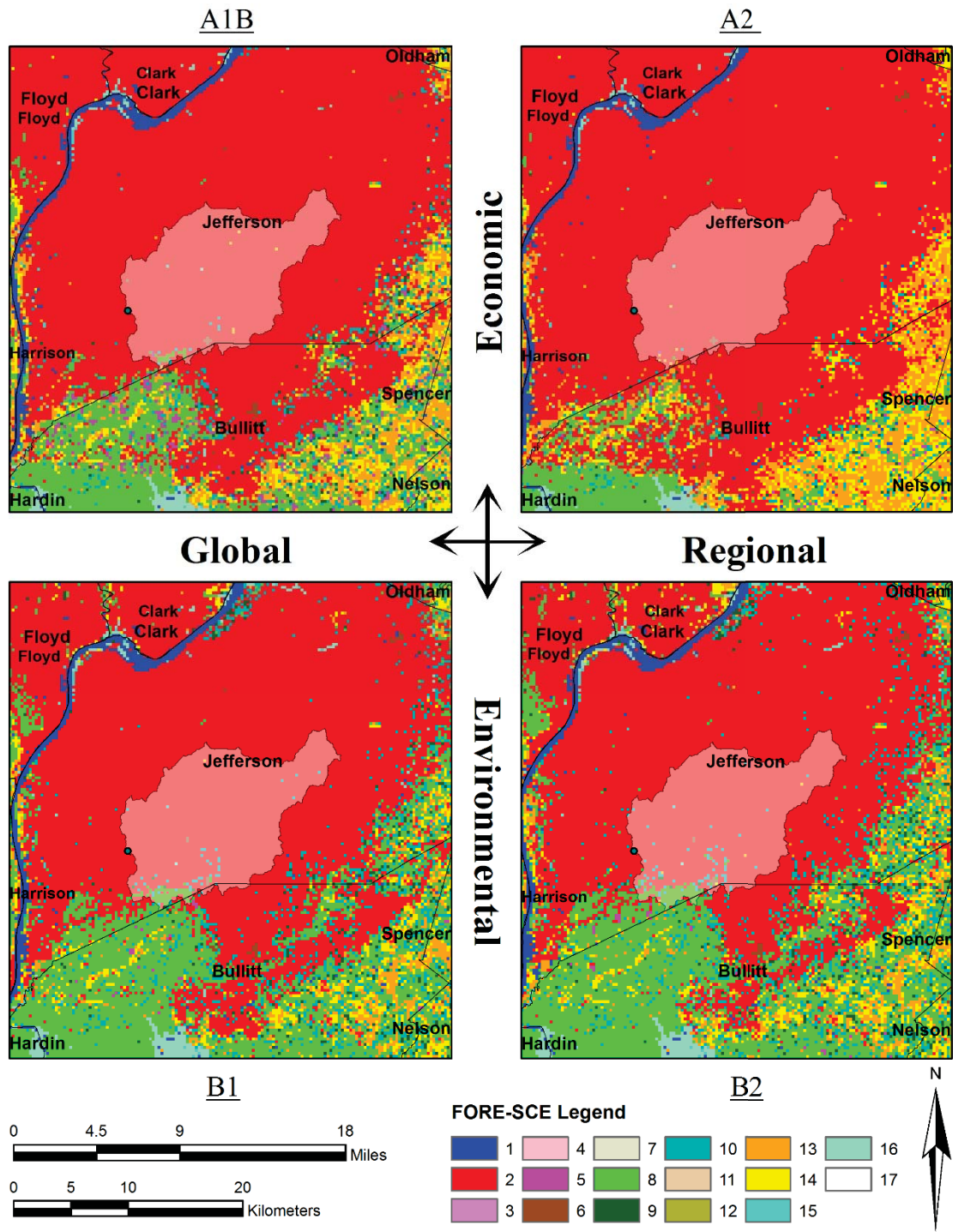


Figure 4.7: FORE-SCE scenario based spatial LULC model projection for the year 2100 for Pond Creek Watershed, KY (USGS station 03302000). (Data Source: USGS, 2014).

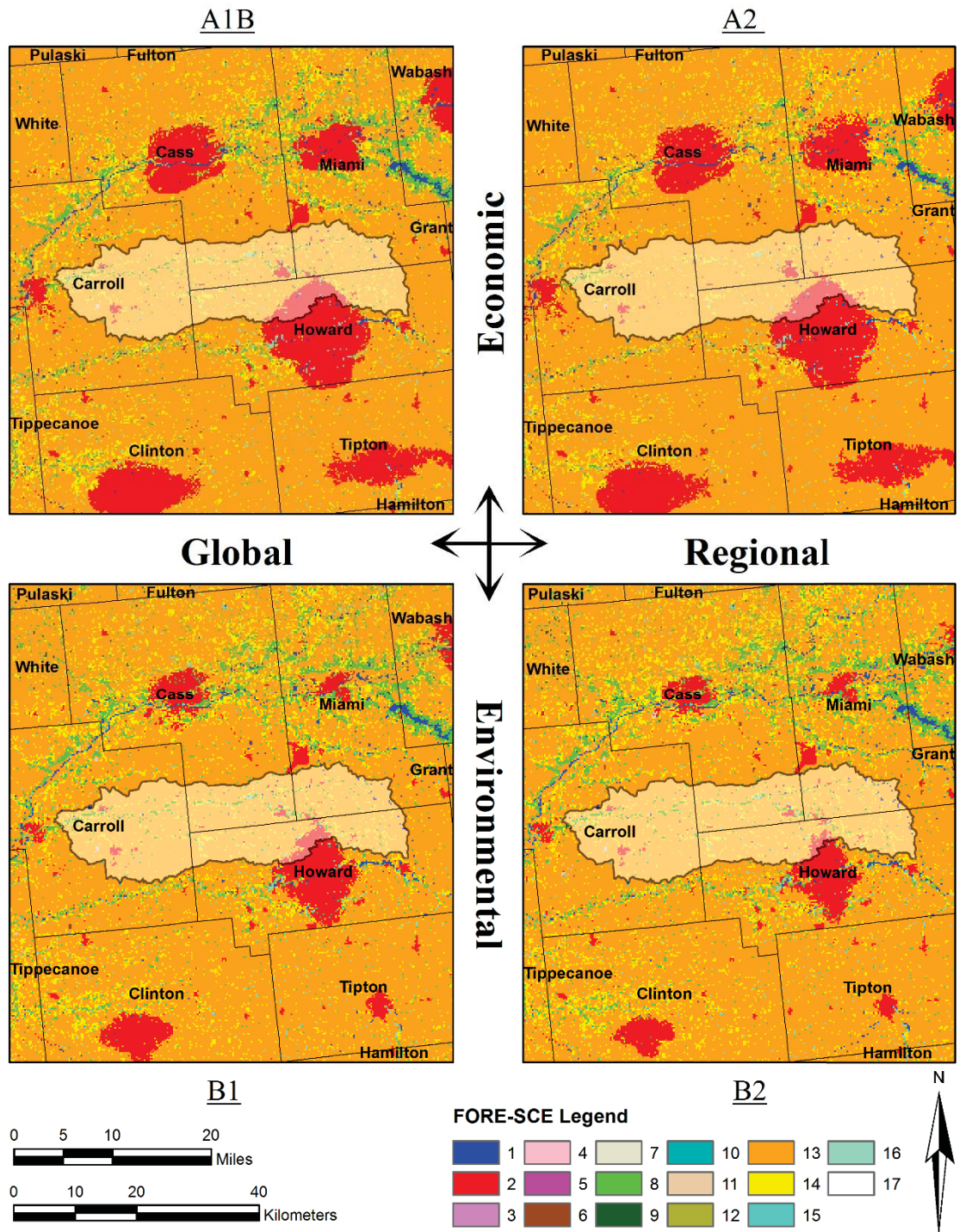


Figure 4.8: FORE-SCE scenario based spatial LULC model projection for the year 2100 for Deer Creek Watershed, IN (USGS station 03329700). (Data Source: USGS, 2014).

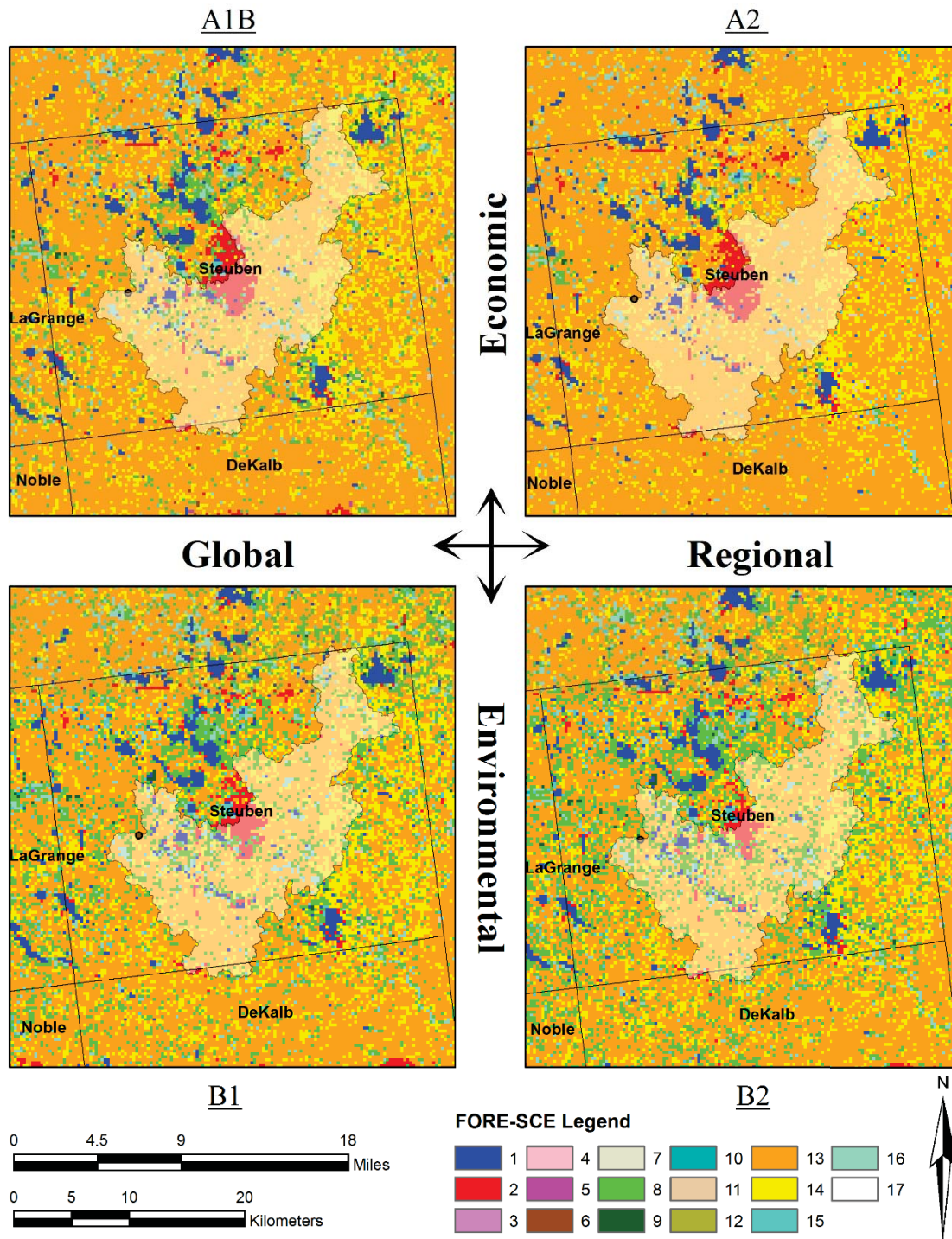


Figure 4.9: FORE-SCE scenario based spatial LULC model projection for the year 2100 for Pigeon Creek Watershed, IN (USGS station 04099510). (Data Source: USGS, 2014).

Table 4.4: LULC (mi²) projected for 2100 using the A1B FORE-SCE scenario relative to current conditions (2011) for the four case study watersheds.

Description	FORE-SCE Code	Area (mi ²)							
		01411000		03302000		03329700		04099510	
		2011	2100	2011	2100	2011	2100	2011	2100
Water	1	0.1	0.1	0.1	-	0.4	0.6	2.3	2.4
Developed	2	15.8	25.8	55.1	63.1	5.6	18.3	2.5	5.6
Mechanically Disturbed National Forest	3	-	-	-	-	-	-	-	-
Mechanically Disturbed Public Land	4	-	-	-	-	-	-	-	-
Mechanically Disturbed Private Land	5	0.2	0.0	0.1	0.1	-	-	0.1	0.1
Mining	6	1.1	1.3	0.1	0.2	0.2	1.2	0.0	0.1
Barren	7	-	-	-	-	-	-	-	-
Deciduous Forest	8	11.7	8.1	5.4	0.5	6.4	4.4	11.8	6.4
Evergreen forest	9	5.0	4.4	0.3	-	0.0	-	0.1	0.0
Mixed Forest	10	8.2	6.5	2.6	0.2	-	-	0.0	0.0
Grassland	11	-	-	-	-	0.2	0.2	0.0	0.0
Shrubland	12	-	-	-	-	-	-	-	-
Cropland	13	0.9	0.2	0.4	0.2	237.2	231.8	65.7	69.1
Hay/Pasture	14	4.1	0.7	0.1	0.0	24.2	17.8	18.0	17.4
Herbaceous Wetland	15	0.1	0.1	0.0	0.0	0.2	0.2	1.4	1.1
Woody Wetland	16	8.8	8.7	0.1	0.0	1.4	1.4	3.7	3.2
Ice/Snow	17	-	-	-	-	-	-	-	-

Table 4.5: Percent change in LULC projected for 2100 using the A1B FORE-SCE scenario relative to current conditions (2011) for the case study watersheds.

Description	FORE-SCE Code	Percent of Area Change (%)			
		01411000	03302000	03329700	04099510
Water	1	-	-0.08%	0.06%	0.07%
Developed	2	17.86%	12.47%	4.61%	2.96%
Mechanically Disturbed National Forest	3	-	-	-	-
Mechanically Disturbed Public Land	4	-	-	-	-
Mechanically Disturbed Private Land	5	-0.30%	-0.11%	0.00%	0.02%
Mining	6	0.36%	0.05%	0.34%	0.08%
Barren	7	-	-	-	-
Deciduous Forest	8	-6.51%	-7.63%	-0.71%	-5.08%
Evergreen forest	9	-1.07%	-0.42%	-0.01%	-0.08%
Mixed Forest	10	-2.93%	-3.75%	-	-
Grassland	11	-	-	-0.01%	-
Shrubland	12	-	-	-	-
Cropland	13	-1.20%	-0.34%	-1.96%	3.27%
Hay/Pasture	14	-5.99%	-0.08%	-2.32%	-0.57%
Herbaceous Wetland	15	-	-	-	-0.21%
Woody Wetland	16	-0.16%	-0.12%	-	-0.46%
Ice/Snow	17	-	-	-	-

Chapter 5. Hydrologic Modeling using ArcSWAT

To study the effect of LULC change on hydrologic response and flood risk during both historical and future periods, the Soil and Water Assessment Tool (SWAT) (Arnold et al., 1998) was implemented herein. SWAT is a physically based hydrologic model designed to simulate water quantity and quality of surface and groundwater. As opposed to use of statistical regression models (for example, Gyawali et al., 2014), the benefit of a physically based model is that the effects of alternative input data (e.g. management practices, vegetation cover change, or climate variability) on water quality and other parameters can be directly quantified (Neitsch et al., 2005). SWAT's capabilities for modeling the hydrologic impacts of LULC change, land management practices, and climate change has provided researchers the ability to simulate complex environmental impacts. SWAT has also been widely used for the study of non-point source pollution control, soil erosion and sediment transport control and prevention, as well as watershed management and planning (Arnold et al., 1998). The version of SWAT used in this study was ArcSWAT 2012, which is compatible with ArcGIS version 10.2. This version of SWAT enables the program to exist as an extension in ArcMap, making the interface more user-friendly, allowing models to be built more quickly, and for output layers to be viewed simultaneously.

5.1 Model Description

SWAT requires inputs including LULC data, soil characteristics, a digital elevation model (DEM), and climate data, namely precipitation and temperature. SWAT initially processes the DEM, locating flow accumulation paths and direction, and then delineates a watershed boundary based on a user defined outlet location. ArcSWAT was chosen to delineate the watershed, as to minimize possible processing difficulties if another method for delineation was chosen. The watershed is then separated into subwatersheds or subbasins based on the topography and flow patterns. Separation into subbasins is particularly useful when various areas within a watershed are dramatically different with regards to soil and land use properties, so that impact on hydrology are difficult to identify spatially within the

watershed (Neitsch et al., 2005). Information and input values regarding each subbasin is separated into the following categories: groundwater, main reach of the subbasin, ponds/wetlands, climate, and hydraulic response units (HRUs). As seen in Figure 5.1, hydrological response units (HRUs) are finer subdivisions of the subbasins created based on the LULC, land slope, and soil characteristics; areas sharing the same HRU are assumed to have unique hydrologic responses (Neitsch et al., 2005). This is a critical piece in the model as the land use layer in this study will be changing, thereby resulting in changes in HRU values and associated response to a storm event.

SWAT simulations regarding the hydrology of a watershed can be separated into two groups. The first is the land phase of the hydrologic cycle, meaning the process that controls the quantity of water, sediment, and nutrients reaching the stream channel. The second group is the method with which the water, sediment and nutrients are routed, or moved, through the channel networks to the watershed outlet (Neitsch et al., 2005). With regards to the land phase, all calculations in SWAT are based on the water balance equation applied on an annual time scale with daily climate input:

$$SW_t = SW_o + \sum_{i=1}^t (R_{day} - Q_{surf} - E_a - w_{seep} - Q_{gw}) \quad (4)$$

where SW_t represents the final soil water content (mm), SW_o is the initial soil water content on day i (mm), t is the total period (days), R_{day} is the precipitation (mm) on day i , Q_{surf} is the surface runoff depth (mm) on day i , E_a is the depth (mm) of evapotranspiration on day i , w_{seep} is the depth (mm) of water entering the vadose zone from the soil profile on day i , and Q_{gw} is the depth (mm) of return flow on day i . By separating the watershed into subbasins as described previously, the model can detect differences in evapotranspiration for a range of LULC and soil types. Based on the HRUs, runoff depths are generated and routed through the entire watershed to obtain an overall runoff value. This approach to the water balance increases the accuracy of the model and gives a more thorough description of the physical model (Neitsch et al., 2005). A schematic of the land phase process of the hydrologic cycle as implemented by SWAT can be seen in Figure 5.2. The SWAT model

has the capability to model all hydrological components therein, including evapotranspiration (ET), surface runoff, percolation, and groundwater flow (return flow) (Arnold et al., 1998).

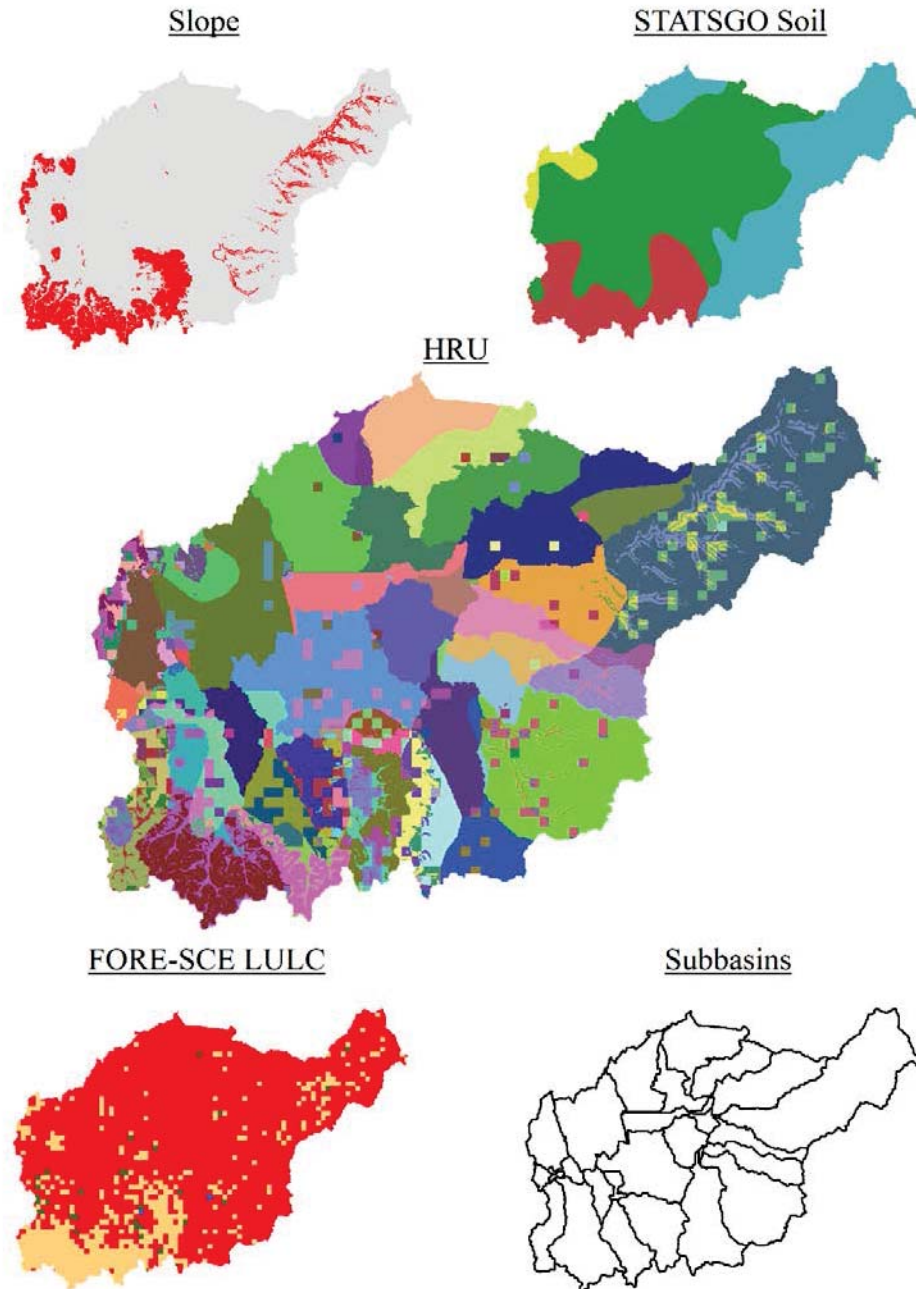


Figure 5.1: Soil and Water Assessment Tool GIS integrated model (ArcSWAT) Hydrologic Response Unit (HRU) layer used to separate areas with similar hydrologic response characteristics.

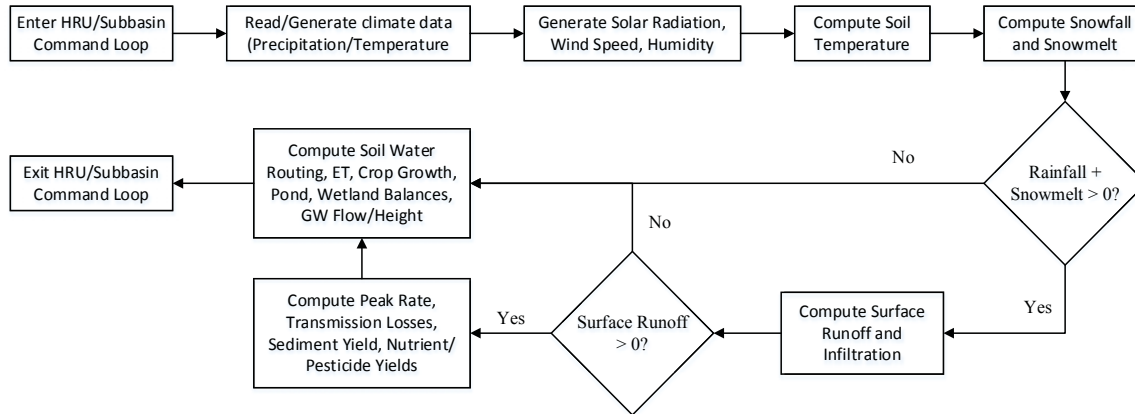


Figure 5.2: SWAT command loop for HRU/Subbasin process simulating the land phase of the hydrologic cycle. Modified from (Neitsch et al., 2005).

The Natural Resources Conservation Service (NRCS, previously Soil Conservation Service, SCS) runoff curve number method (Soil Conservation Service, 1972) is utilized to estimate surface runoff based on daily rainfall data. The runoff curve number (RCN) values are an estimation of the level of permeability of the watershed, based on soil type, land use classes, and land management conditions (Rallison and Miller, 1981), and are adjusted for antecedent soil moisture conditions (AMC) (Arnold et al., 1993). RCN values range from 0 to 100, with low values representative of a high infiltration/low runoff potential, corresponding with type A soils and/or LULC types that enable infiltration. Adversely, higher RCN values are characteristic of type D soils and/or LULC types with low infiltration potential (e.g. pavement), thereby having a high runoff potential. Descriptions of the NRCS hydrologic soil groups (A, B, C, and D) are provided in Appendix D.

In this study, the RCN will be a variable parameter due to historical/projected LULC change. To find the total runoff depth, the SCS curve number equation is used (USGS 1972):

$$Q_{surf} = \frac{(R_{day} - I_a)^2}{(R_{day} - I_a + S)} \quad (5)$$

where Q_{surf} is the accumulated surface runoff depth (mm), R_{day} is the precipitation depth (mm) on day i , I_a is the initial abstraction depth including surface storage, interception and infiltration prior to runoff (mm), and S is the retention parameter (mm). The retention parameter changes both temporally due to varying soil water content and spatially as a function of land use, soil, slope and management as computed in Equation 6. Runoff in the subbasins will not begin until the rainfall depth (R_{day}) exceeds the initial abstraction (I_a), approximated as $0.2S$.

$$S = 25.4 \left(\frac{1000}{RCN} - 10 \right) \quad (6)$$

Evaporation and transpiration are modeled separately in SWAT, wherein evaporation is simulated using exponential functions based on soil depth and water content, and transpiration is modeled using a linear function based on leaf area index and potential evapotranspiration (PET) (Wu et al., 2013). The default method for determining PET in SWAT--the Penman-Monteith method--was implemented in this study. Percolation is determined using a storage routing method and a crack-flow model (Arnold et al., 1998), while lateral flow is estimated along with percolation using a kinematic storage model (Solan et al., 1983). Baseflow into the river (groundwater) is estimated based on the hydraulic conductivity of a shallow aquifer, the distance from each subbasin to the watershed outlet and the water table height (Wu et al., 2013).

Two methods are available to route the flow through each subbasin, and subsequently to the watershed outlet: the Muskingum method and the variable storage routing method. In this study, the variable storage routing method was implemented. Once the model is run, SWAT determined the overland and subsurface flows through each HRU in the watershed, routing the flow using Manning's Equation (Arnold et al., 1998). SWAT provides the option to model the watershed as a single unit, or subdivided into multiple HRUs as was done in the study herein, thereby resulting in a more accurate output.

For the purpose of this study, simulated daily flows output from SWAT must closely

resemble observed (gauged) daily flow data. Initial parameter values are first specified for each process, and then model calibration is performed, in which the parameters of the model are altered in order to ensure that the simulated model gives an appropriate representation of the response of the study area (i.e. watershed). Once calibration is complete, validation of the data must be run with an alternative time period, in order to review the calibrations accuracy. For this study, it must be recognized that the models employed were previously calibrated and validated by others in this research group (Kaye LaFond and Patricia Spellman). Due to the extensiveness of the calibration and validation process, watersheds were chosen to have this task previously completed to save time.

In order to optimize the model and calibrate associated parameter values, goodness-of-fit was evaluated using the Nash-Sutcliffe model efficiency (NSE) coefficient as the objective function, as performed in previous studies and applications of SWAT (e.g. LaFond, 2014; Yang et al., 2008; Zhang et al., 2007). The coefficient of determination (R^2), defining the extent to which variability in the dataset is captured by the model, was also used to determine the quality of fit to observed events. The ideal value of each metric is 1 indicating a perfect fit. The calibration and validation periods, as well as the resulting model efficiency measures are reported in Table 5.1. These time periods were chosen based on the availability of continuous daily flow data, as well as to be consistent with use of the 1992 NLCD. Calibration efficiency values for USGS station 04099510 measure quite high compared to those of USGS station 03302000, and although neither model yields an impressive fit, these values are comparable to results of other studies in the literature (see LaFond, 2014).

Table 5.2 and Table 5.3 report the final optimal parameter values of the calibrated and validated SWAT models for Pond Creek and Pigeon Creek Watersheds, respectively, to be used in subsequent analyses herein.

Table 5.1: Calibration and validation periods, as well as model efficiency measures for validation period for USGS stations selected for SWAT simulations.

USGS Station	Calibration Period	Validation Period	NSE Value	R² Value
03302000	1996-1999	1980-1992	0.395	0.435
04099510	1987-1993	1994-1999	0.53	0.53

Table 5.2: Optimal hydrological parameter values used in ArcSWAT simulation for Pond Creek Watershed, KY (USGS station 03302000).

Parameter	File Name	Description	Mathematical Operation	Optimal Values
CN2	.mgt	SCS runoff curve number (AMC II)	Multiply by	1.127220
ALPHA_BF	.gw	Baseflow recession constant (days)	Replace	0.782844
GW_DELAY	.gw	Groundwater delay (days)	Replace	52.843522
GWQMN	.gw	Threshold water level in shallow aquifer for return flow (mm H ₂ O)	Replace	1.2566475
GW_REVAP	.gw	Groundwater reevaporation coefficient (ability of water to transfer from shallow quifer to root zone)	Replace	0.138289
ESCO	.hru	Soil evaporation compensation factor	Replace	0.839671
CH_N2	.rte	Manning's n value for the main channel	Replace	0.272970
CH_K2	.rte	Main channel effective hydraulic conductivity (mm/hr)	Replace	43.640442
SOL_AWC	.sol	Available water capacity of the soil layer	Multiply by	1.206014
SOL_K	.sol	Saturated hydraulic conductivity (mm/hr)	Multiply by	3.420647

Table 5.3: Optimal hydrological parameter values used in ArcSWAT simulation for Pigeon Creek Watershed, IN (USGS station 04099510).

Parameter	File Name	Description	Mathematical Operation	Optimal Values
CN2	.mgt	SCS runoff curve number (AMC II)	Multiply by	0.833000
ALPHA_BF	.gw	Baseflow recession constant (days)	Replace	0.644000
GW_DELAY	.gw	Groundwater delay (days)	Replace	24
GWQMN	.gw	Threshold water level in shallow aquifer for return flow (mm H ₂ O)	Replace	1.225000
GW_REVAP	.gw	Groundwater revaporation coefficient (ability of water to transfer from shallow aquifer to root zone)	Replace	0.087900
ESCO	.hru	Soil evaporation compensation factor	Replace	0.552000
CH_N2	.rte	Manning's n value for the main channel	Replace	0.100000
CH_K2	.rte	Main channel effective hydraulic conductivity (mm/hr)	Replace	116.849998
ALPHA_BNK	.rte	Bank flow recession constant or constant of proportionality	Replace	0.350000
SOL_AWC	.sol	Available water capacity of the soil layer	Multiply by	1.208144
SOL_K	.sol	Saturated hydraulic conductivity (mm/hr)	Multiply by	0.986500
SFTMP	.bsn	Snowfall temperature (°C)	Replace	0.820000
SURLAG	.bsn	Surface runoff lag coefficient	Replace	6.250000
EPCO	.bsn	Plant uptake compensation factor	Replace	0.912500
SMTMP	.bsn	Snowmelt temperature (°C)	Replace	1.080000
SNOCVMX	.bsn	Max snow cover	Replace	0.500000
REVAPMN	.gw	Threshold water level in shallow aquifer for revap (mm H ₂ O)	Replace	0.137000
RCHRG_DP	.gw	Aquifer percolation coefficient	Replace	0.090000
TIMP	.bsn	Snow temperature lag factor	Replace	0.290000
SMFMX	.bsn	Melt factor for snow on June 21 (mm H ₂ O/°C-day)	Replace	4.460000
SMFMN	.bsn	Melt factor for snow on December 21 (mm H ₂ O/°C-day)	Replace	1.485000

5.2 Model Input and Current Conditions

As described previously, data input to the SWAT model includes soil data, land use data, a digital elevation model (DEM), and climate data. To simulate current (or ‘base’) conditions more in line with the calibration and validation periods, the soil data was obtained from the Stat Soil Geographic (STATSGO) Database (NRCS), the 1992 National Land Cover Database (NLCD) was used for the land use layer, and the DEM with resolution of 1/3 arc-second (10 meters) was gathered from the USGS National Elevation Dataset (NED) (Gesch et al., 2002; Gesch, 2007). Land slope for input into HRU generation was derived based on the 10 meter DEM, separated into two groups: “mild” (1-10% slopes) and “sloped” (10% slopes and greater). This decision for separation of the slope layer is based on previous research demonstrating the acceptability in model accuracy while implementing limited slope separation (Yacoub and Foguet, 2013). For each study site, the approximate watershed boundary location was gathered from GAGES II (Falcone, 2011). All input layers were ‘clipped’ to the watershed with a 1 mile buffer (see Appendix A). Climate data for 1978 to 1999 was obtained from the World Climate Research Programme’s (WCRP’s) Coupled Model Intercomparison Project Phase 3 (CMIP3) multi-model dataset (http://gdo-dcp.ucllnl.org/downscaled_cmip_projections/dcpInterface.html), a fine spatial resolution climatic projection dataset. Temperature and precipitation data from 1987 to 1999 was inputted into all models, and was held constant in all simulations presented herein so as to isolate the effects of LULC change. A 20 year assessment period was chosen, beginning with a 2 year warm up period for a total simulation length of 22 years.

As a basis for determining the hydrologic effects of LULC change, a 20 year ‘base’ model simulation was run from 1978 to 1999, including the two year warm up period. This ‘base’ simulation employed the 1992 NLCD dataset, and will act as the foundation against which to compare results of simulations under historical and future LULC conditions. To isolate the hydrologic effects of LULC change, the LULC layer is the sole data input to be varied; all other simulation inputs for historical and future periods were consistent with the ‘base’

simulation. By this procedure, the only parameter value being altered is the RCN value, and as such, HRU area fractions are altered, changing the land area response to a rain event.

As discussed in previous sections, the focus of this research regards flood risk based on instantaneous AMF series, or the maximum instantaneous flow rates the gauge recorded in each water year over the period of record. However, the SWAT model outputs daily maximum flows, which subsequently need to be converted to instantaneous AMF peaks using the procedure defined by Fill and Steiner (2003). This procedure analyzes a three day period of flow values, calculating the instantaneous flow for the second day using a simple statistical conversion. This is done for each day within a given water year, and the maximum value constitutes the instantaneous AMF peak for that year. To evaluate flood risk, a LP3 distribution was then fit to the simulated instantaneous AMF series using the Method of Moments (MOM) in log space, as discussed in Section 2.1. The LP3 parameters (α , β , τ) and AMF statistics for the ‘base’ model are reported in Table 5.6 and Table 5.7 for Pond Creek and Pigeon Creek Watersheds, respectively. Note that the year corresponding to the inputted LULC is assumed to represent the simulated period.

A comparison of the probability of non-exceedance based on LP3 distributions fit to the simulated AMF series for the ‘base’ period (1980 – 1999) and the AMF data series observed for the same period is plotted in Figure 5.3 and Figure 5.4 for Pond Creek and Pigeon Creek Watersheds, respectively. Overall, the simulated AMF series for the Pigeon Creek Watershed and the associated LP3 distribution tend to underestimate flood risk with greater deviations observed in the middle of the distribution; larger events with less than a 10% probability of exceedance are overestimated by the SWAT model for the Pond Creek Watershed. To minimize effects of error in the SWAT model and further isolate impacts of LULC change, the LP3 distribution fit to simulated AMF series for the base period will serve as the benchmark for comparison of simulated AMF under both historic and future LULC conditions.

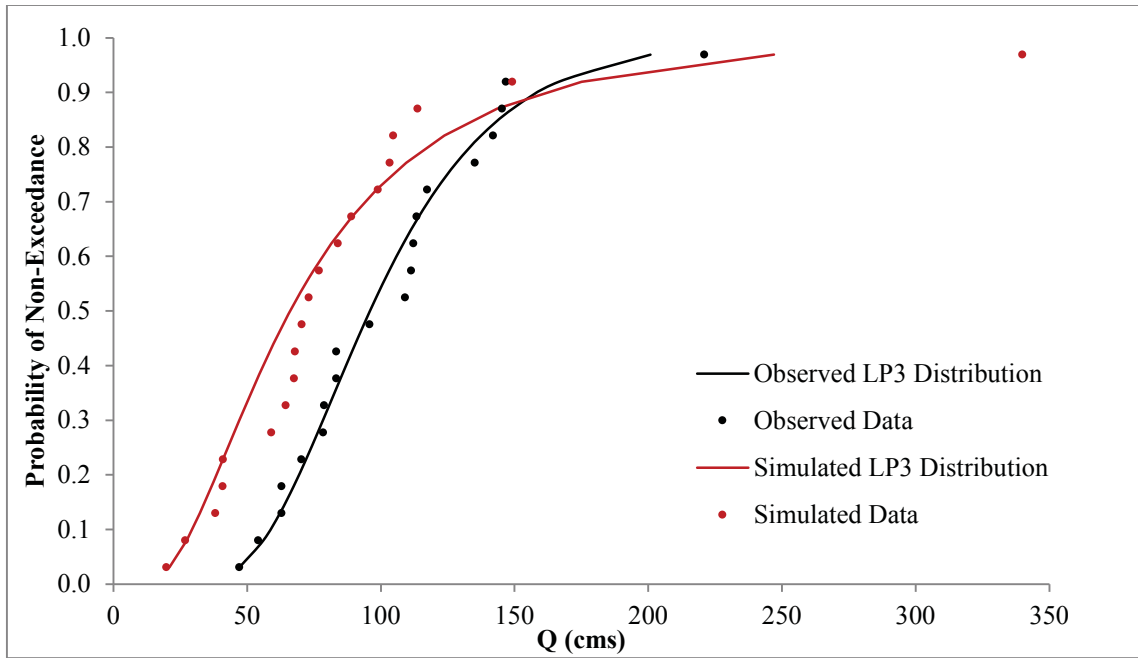


Figure 5.3: Probability of non-exceedance plot with LP3 distribution fit to the base period simulation and observed data from 1980 to 1999 for Pond Creek Watershed, KY (USGS station 03302000). Data include 1992 NLCD and 1978-1999 CMIP3 climate data.

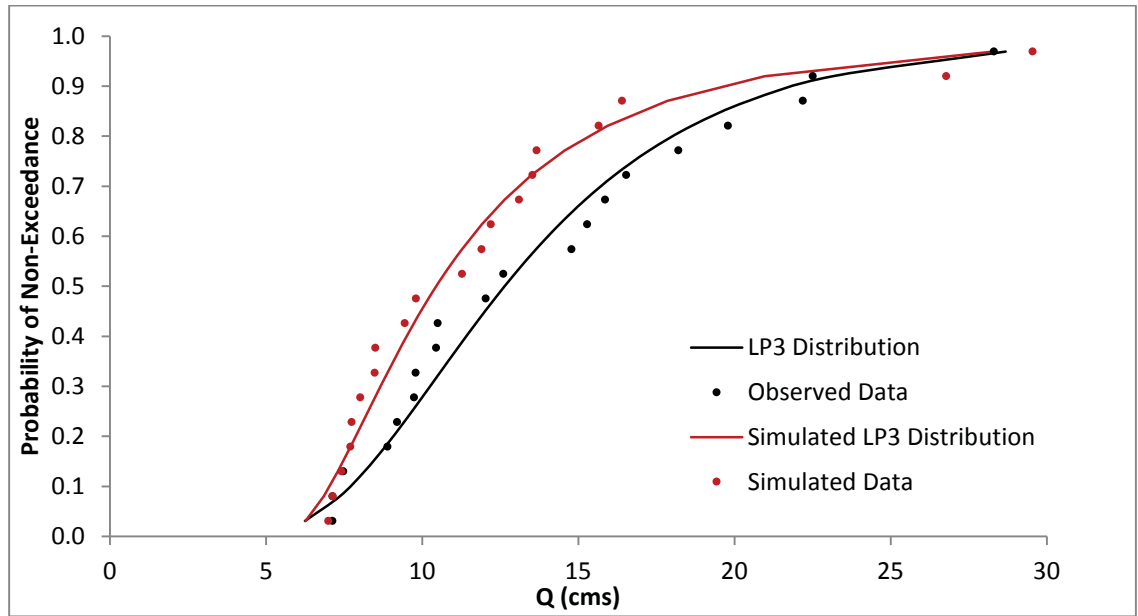


Figure 5.4: Probability of non-exceedance plot with LP3 distribution fit to the base period simulation and observed data from 1980 to 1999 for Pigeon Creek Watershed, IN (USGS station 04099510). Data include 1992 NLCD and 1978-1999 CMIP3 climate data.

5.3 Historical Flood Series

Before historical LULC maps could be input into the SWAT model, each generalized land cover had to be assigned to a specific NLCD classification value in order for the SWAT model to be able to reference input values, primarily the runoff curve number (RCN), from the geodatabases. RCN values from the 1992 NLCD classification were considered for the generalized LULC classes, consistent with operations done in Section 3.1. The 1992 NLCD RCN values were averaged within each generalized LULC class for all four soil groups and used as a basis for assigning the appropriate RCN values. Once the average RCN values were calculated, specific NLCD LULC types were chosen to represent the generalized land use types of the historical maps, as seen in Table 5.4. For purposes of display, only soil groups A and D are shown.

The curve number values were not the only values used in the decision of what NLCD classification type would be used for each generalized land use type. With regards to the generalized urban areas, RCN values within the urban SWAT geodatabase table are considered to be the same for a given soil group, as seen in Table 5.5 under the headings CN2A, CN2B, CN2C, and CN2D. These unique urban land use types in reality have varying CN values. SWAT accounts for the realistic difference in CN values by including the percentage of that specific land use type that would typically have impervious surface within it and assigning that given area a CN of 98, as seen in Table 5.5 under the heading URBCN2. During the generation of the historical land use maps (see Section 3.1), urban areas were removed manually by the user. These areas denoted as urban development were those that were visually distinguishable as mostly impervious. While considering the percentage of the area identified as urban land use, NLCD code 23 (Commercial/Industrial/Transportation) land use class was chosen as it has a range of impervious surface percentages (i.e. 67%, 84%, 98%) with an average impervious percent equal to 83%, typical for areas in which the majority of the land contains impervious surface. Therefore, using both the average RCN values from Table 5.4 and typical percentage of impervious surface of the urban areas within the historical land use maps, specific NLCD LULC types

were assigned. The generalized 1992 NLCD determined here is directly related to the general LULC types in Chapter 3, where agricultural, forested, open water, and urban developed land was generated from historical aerial images.

Table 5.4: 1992 NLCD classification for runoff curve number (RCN) values, averages, and chosen generalized LULC classification values.

NLCD 1992 Code	Land Cover Classification	RCN (Soil A)	Average RCN	RCN (Soil D)	Average RCN	Assigned Land Use (Abbreviation /Code)
71	Grassland/Herbaceous	49		84		
81	Pasture/Hay	40		82		
82	Row Crops	67	59	89	87	Small Grains (AGRC - 83)
83	Small Grains	62		84		
84	Fallow	77		94		
41	Deciduous Forest	45		83		
42	Evergreen Forest	25		77		
43	Mixed Forest	36		79		
51	Shrubland	39	40	80	81	Shrub/Scrub (RNGB - 51)
91	Woody Wetlands	45		83		
92	Emergent Herbaceous Wetlands	49		84		
11	Open Water	100	100	100	100	
21	Low Intensity Residential	31		79		
22	Heavy Intensity Residential	31		79		
23	Commercial/Industrial/ Transportation	31	44	79	83	Commercial/ Industrial/ Transportation (UIDU - 23)
31	Barren Land (Rock/Sand/Clay)	77		94		
85	Urban/Recreational Grasses	49		84		

Table 5.5: SWAT geodatabase urban land use table with RCN values.

URBNAME	URBFLNM	FIMP	FCIMP	CN2A	CN2B	CN2C	CN2D	URBCN2
URHD	Residential-High Density	0.6	0.44	31	59	72	79	98
URMD	Residential-Medium Density	0.38	0.3	31	59	72	79	98
URML	Residential-Med/Low Density	0.2	0.17	31	59	72	79	98
URLD	Residential-Low Density	0.12	0.1	31	59	72	79	98
UCOM	Commercial	0.67	0.62	31	59	72	79	98
UIDU	Industrial	0.84	0.79	31	59	72	79	98
UTRN	Transportation	0.98	0.95	31	59	72	79	98
UINS	Institutional	0.51	0.47	31	59	72	79	98
URBN	Residential	0.38	0.3	31	59	72	79	98

URBNAME: The 4-letter codes in the plant growth and urban databases are used by the GIS interfaces to link land use/land cover maps to SWAT plant types. This code is printed to the output files. When adding a new urban category, the four letter code for the new urban land type must be unique.

FIMP: Fraction total impervious area in urban land type. This includes directly and indirectly connected impervious areas. Urban areas differ from rural areas in the fraction of total area that is impervious. Construction of buildings, parking lots and paved roads increases the impervious cover in the watershed and reduces infiltration. With development, the spatial flow pattern of water is altered and the hydraulic efficiency of flow is increased through artificial channels, curbing, and storm drainage and collection systems.

FCIMP: Fraction directly connected impervious area in urban land type. Impervious areas can be differentiated into two groups - the area that is hydraulically connected to the drainage system and the area that is not directly connected. As an example, assume there is a house surrounded by a yard where runoff from the roof flows into the yard and is able to infiltrate into the soil. The rooftop is impervious by it is not hydraulically connected to the drainage system. In contrast, a parking lot whose runoff enters a storm water drain is hydraulically connected. When modeling urban areas the connectedness of the drainage system must be quantified. The best methods for determining the fraction total and directly connected impervious areas is to conduct a field survey or analyze aerial photographs.

CN2A: Curve number associated with soil group A for AMC II conditions.

URBCN2: Curve number for AMC II in impervious areas of urban land type (Arnold, Kiniry et al. 2012).

5.3.1 Generalized NLCD Comparison

While considering the impacts of historical LULC change with generalized LULC classifications, investigations regarding current (base) conditions using generalized 1992 NLCD with a broad classification occurred. This can then be used as a basis for comparison and insight to the consequences and possible changes in the results of output flows obtained using a general LULC classification. Generalizing the 1992 and 2006 NLCD for Pond Creek results in an increase in AMF magnitudes corresponding to lower probability z-values, and a decrease in AMF magnitudes at higher probability z-values, as seen in Figure 5.5 and Figure 5.6, respectively. Overall, generalization of the NLCD decreases the spread (standard deviation) of the data, as reported in Table 5.6 and Table 5.7. This effect is also observed in Pigeon Creek (see Figure 5.7), although the differences are less dramatic. These results indicate that the use of generalized LULC data in SWAT modeling typically results in a decrease in the standard deviation of the instantaneous AMF flow series, with increases in the magnitude of smaller return period events and decreases in higher return period events. For this reason, it must be noted that if this study were to simulate historical LULC change implementing finer classified LULC, resulting AMF series would have a higher average and higher standard deviation, and would likely be more representative of actual observed flow distributions.

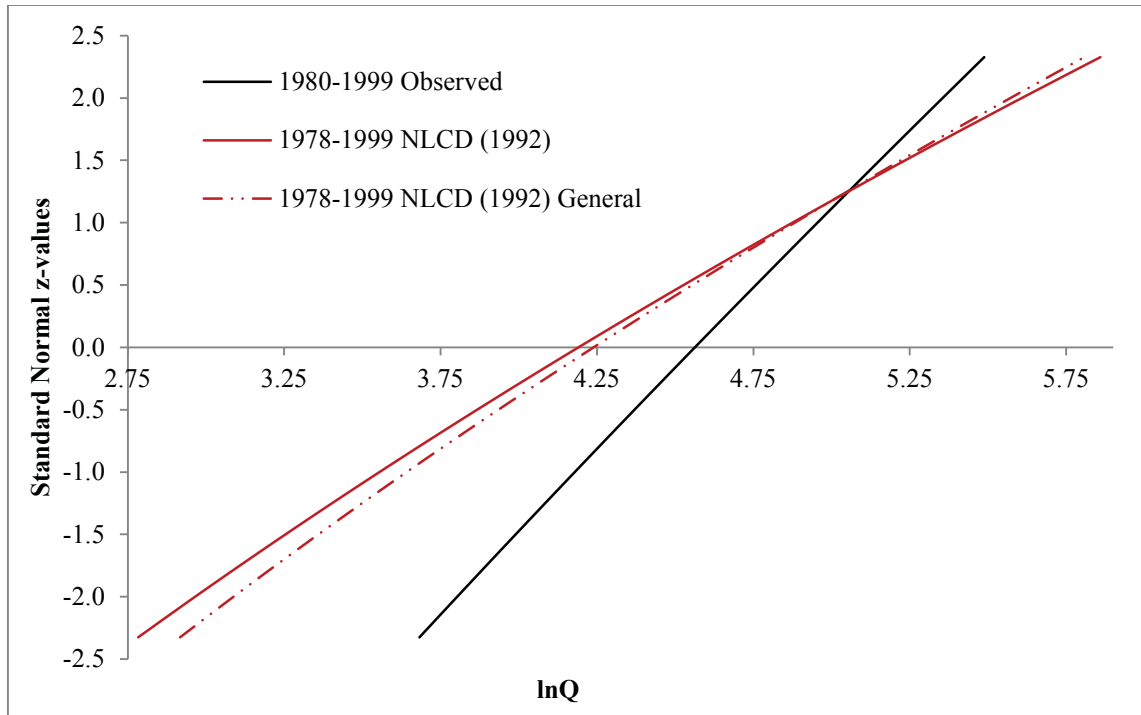


Figure 5.5: Probability plot for LP3 distributions fit over base period (1980–1999) for comparison of observed AMF, simulated AMF with 1992 NLCD, and simulated AMF with generalized 1992 NLCD for Pond Creek Watershed, KY (USGS station 03302000).

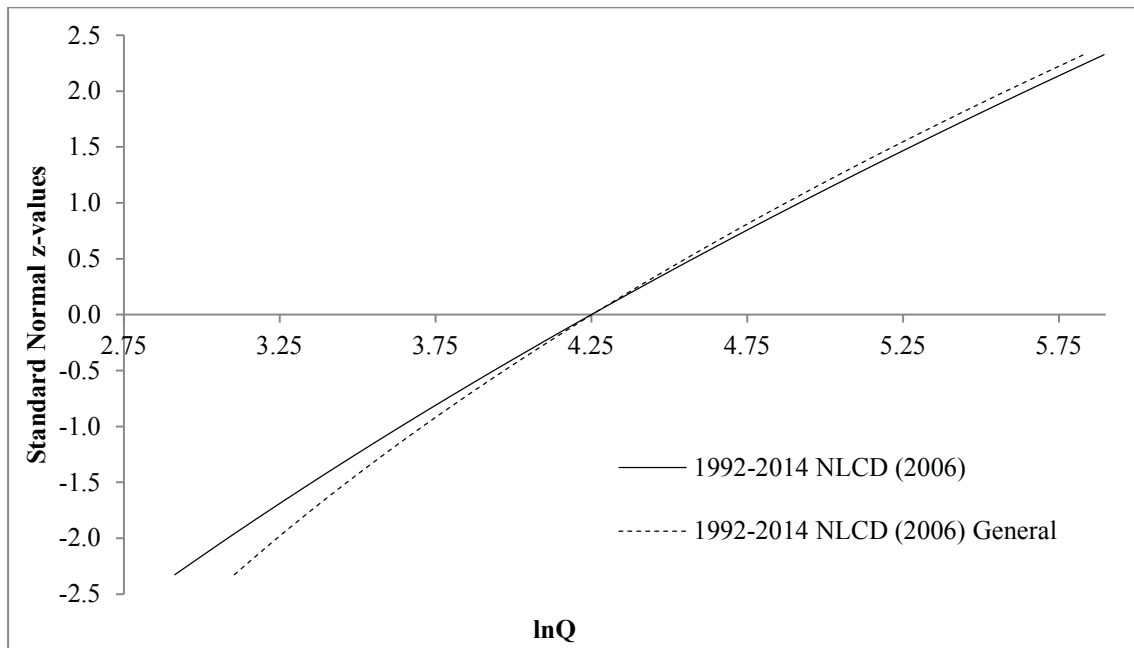


Figure 5.6: Probability plot of LP3 distributions fit over base period (1980–1999) for comparison of simulated AMF with 2006 NLCD and simulated AMF with generalized 2006 NLCD for Pond Creek Watershed, KY (USGS station 03302000).

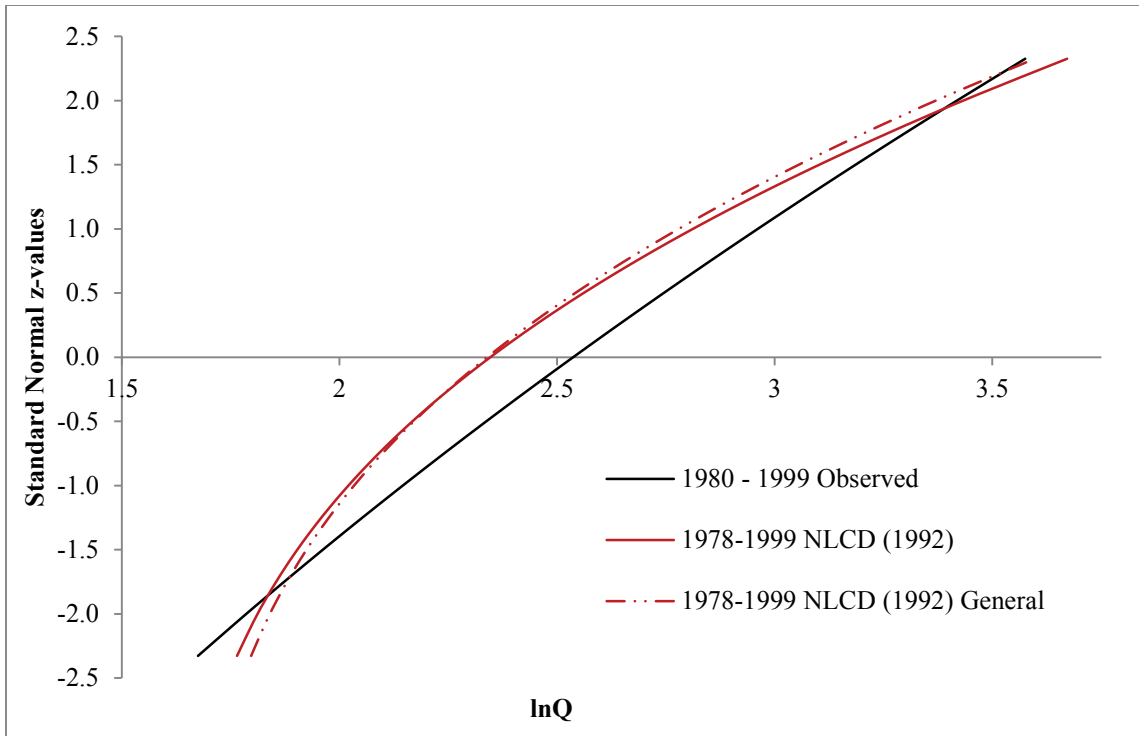


Figure 5.7: Probability plot of LP3 distributions fit over base period (1980–1999) for comparison of observed AMF, simulated AMF with 1992 NLCD, and simulated AMF with generalized 1992 NLCD for Pigeon Creek Watershed, IN (USGS station 04099510).

5.3.2 Historical LULC Comparison

The historical LULC data created in Chapter 3 was used as input to the SWAT models and the resulting simulated AMF series were compared with the results for the base period (1980 – 1999) obtained using both specific and generalized NLCD. To reiterate, the historical LULC data was classified into four general categories, and thus the latter comparison will likely be more appropriate. Summary statistics of the simulated AMF series and parameters of the associated LP3 distributions for each historic period are presented in Table 5.6 and Table 5.7 for Pond Creek and Pigeon Creek Watersheds, respectively. The fitted LP3 distributions are illustrated in Figure 5.8 and Figure 5.9.

For both case study watersheds, magnitudes of lower return period events are estimated to be higher in the historic periods than in the ‘base’ period. This is not consistent with

expectations given LULC change, and is likely due to use of the generalized LULC, as the LULC types chosen may be overestimating the hydrologic response compared to more specific LULC types as seen in the NLCD. For larger return periods, results are more consistent with expected effects of increased urbanization, with the earliest simulation period having the lowest magnitude for a given probability, and the 1992 simulation period being the highest.

A possible reason for these discrepancies and clear source of error may be the generalized LULC types selected from the 1992 NLCD to represent the historical classified images. An assumption made in this study is that the specified NLCD LULC type chosen to represent a general area will encompass its properties effectively. This is not always the case, as up to six LULC types can be generalized into just one LULC classification. This will affect the inferred hydrologic response of the watershed. For example, if an area historically was merely residential, the amount of impervious surface is only 38%, resulting in a greater volume of runoff able to infiltrate, as opposed to the selected industrial LULC type which contains 84% impervious surface. Because these urban areas were manually classified, the specific properties of the watershed are lost, resulting in skewed or inaccurate data. This may result in a larger volume of runoff and consequent AMF events, shifting the LP3 distribution of the simulated data to the right. This may be the reason for the simulated historical AMF series having higher average values than the ‘base’ 1992 NLCD simulation. Similarly, the standard deviations of the simulated historical AMF series tend to be lower than that of the base period simulation, which is consistent with the results found comparing generalized NLCD simulations.

Overall, these results show the difficulty in identifying correlations between change points identified in observed AMF series and changes in LULC, as the availability for quality resolution historic aerial imagery is limited, and there are large time period gaps between generated LULC maps, in some cases 20 to 30 years. With gaps this large, accuracies, shifts, and change points related to specific years are overlooked. Therefore, further research is needed to map LULC at 5 to 10 year periods in order to correlate these shifts in

the AMF series.

Further information of historical conditions for the selected watersheds is also necessary. All assumptions and information used in analysis of the watershed area and characteristics are based on quantitative information regarding climatic predictions, observed AMF series, and historical aerial images, which provide little detailed information about land management, agricultural practices, and presence of stormwater management. With regard to Pigeon Creek Watershed, further information would be needed regarding agricultural practices, cattle grazing patterns, construction of irrigation methods, as well as the location and amount of drain tiles within croplands in order to perform a more comprehensive and detailed analysis. For Pond Creek, more information regarding urban development practices, designs of channelized flow, stormwater structures or diversions would be necessary to obtain accurate results and make reliable associations/correlations. Even with the quantity and quality of advanced technologic models, methods, and equipment currently implemented in similar studies today, much of this information requires on-site inspection and surveying to gather accurate data, and therefore is nearly unattainable for historical periods.

Table 5.6: AMF (cms) statistics and LP3 parameters for simulations based on historical LULC change in Pond Creek Watershed, KY (USGS station 03302000). All 20-year simulations were completed with consistent CMIP3 climate data.

Source	Simulation Period	LULC Year	AMF Statistics			LP3 Parameters		
			\bar{Q}	S_Q	G_Q	α	β	τ
Aerial	1952 - 1972	1957	85.49	66.64	3.00	1586.31	0.02	-20.93
Aerial	1961 - 1981	1971	88.70	67.52	2.98	107.92	0.06	-2.02
NLCD	1980 - 2000	1992	84.51	70.83	3.03	84.37	0.07	-1.86
NLCD ²	1980 - 2000	1992	86.36	67.52	2.98	83.10	0.07	-1.41

Table 5.7: AMF (cms) statistics and LP3 parameters for simulations based on historical

² NLCD is generalized into broad category classes, as seen in Table 5.4

LULC change in Pigeon Creek Watershed, IN (USGS station 04099510). All 20-year simulations were completed with consistent CMIP3 climate data.

Source	Simulation Period	LULC Year	AMF Statistics			LP3 Parameters		
			\bar{Q}	S_Q	G_Q	α	β	τ
Aerial	1952 - 1972	1952	12.14	5.84	1.92	3.48	0.21	1.68
Aerial	1970 - 1990	1979	12.07	5.84	1.90	3.78	0.21	1.63
NLCD	1980 - 2000	1992	12.27	6.17	1.88	3.84	0.21	1.61
NLCD ²	1980 - 2000	1992	12.03	5.68	1.88	3.68	0.20	1.66

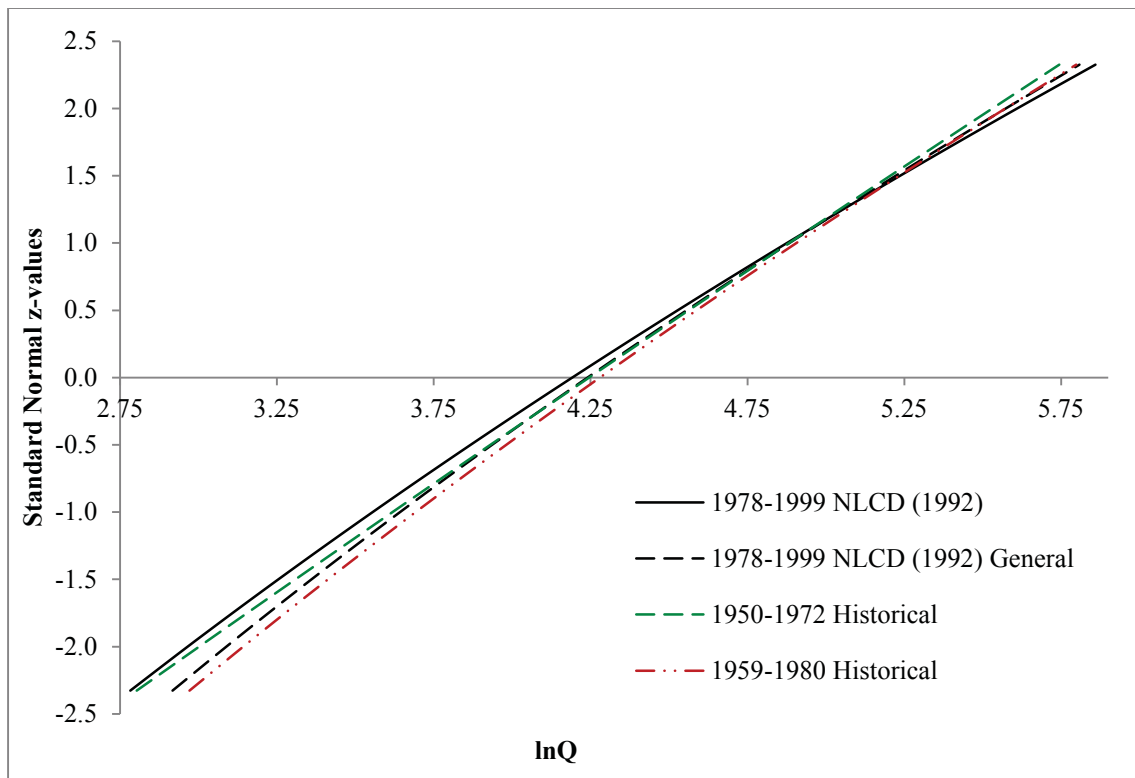


Figure 5.8: Probability plot for comparison of LP3 distributions fit to simulated AMF series obtained using 1992 NLCD, generalized 1992 NLCD, and results of aerial imagery for historic periods in Pond Creek Watershed, KY (USGS station 03302000).

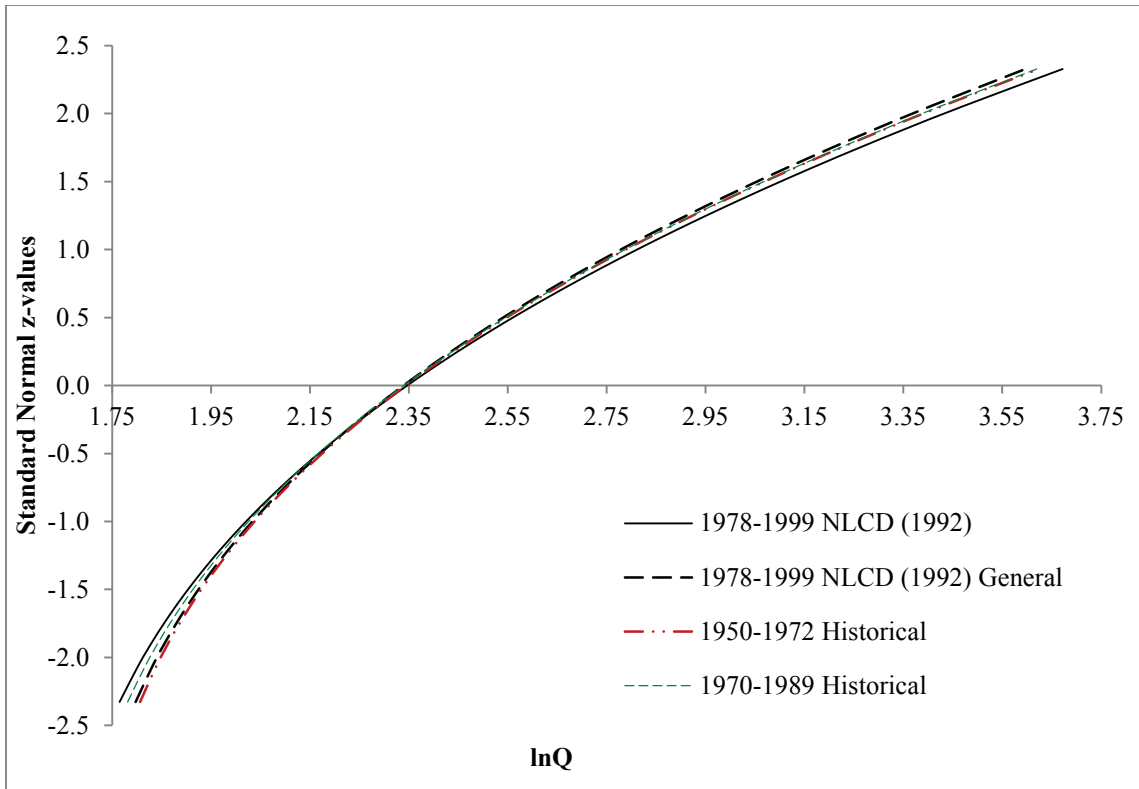


Figure 5.9: Probability plot for comparison of LP3 distributions fit to simulated AMF series obtained using 1992 NLCD, generalized 1992 NLCD, and results of aerial imagery for historic periods in Pigeon Creek Watershed, KY (USGS station 04099510).

5.4 Projected Future Flood Series

While engineers use existing methods, past experiences, and current conditions to design engineered structures, create policies, and determine risk related to various issues for future events, further emphasis must be placed on accounting for future physical and/or climatic changes, either caused naturally or anthropogenically induced. This study has focused on physical changes, mainly regarding land use due to anthropogenic activities. As discussed in Chapter 4, to simulate changes in LULC for future events, the FORE-SCE modeled scenarios were implemented to model future instantaneous AMF series related to future predicted LULC change. Similar to the methods performed for historical simulations, all models ran a 22-year simulation period, including a 2 year warm up period with the same corresponding 1978 – 1999 climate data. LP3 distributions were fit to the simulated future

AMF series using the Method of Moments (MOM) in log space. The probability plots for five 20 year simulation periods spanning from 2000 to 2100 were compared to each other, as well as against results of the simulation for the base period (1980-1999). Each 20 year period simulation was based on the FORE-SCE LULC map projected at the midpoint of the simulation period (for example, a simulation period from 2040-2060 included a 2050 LULC layer), acting as a general representation of the LULC over that 20 year period.

Probability plots for all four FORE-SCE scenarios from 2080 to 2100 are presented in Figure 5.10 and Figure 5.11 for Pond Creek and Pigeon Creek Watersheds, respectively. For clarity, results using the most extreme future scenario (A2) can be compared against results for the base period (1980-1999) using Figure 5.12 and Figure 5.13. As discussed previously, scenarios A2 and B2 represent the most dramatic future scenarios for change, with scenario A2 suggesting intensive urban expansion, population growth, moderate technologic advances, and regional solutions to issues pushing demands for energy and agricultural land, and scenario B2 focusing on environmental preservation, with slow economic and population growth and a focus on regional sustainability and solutions to environmental issues. As expected, the results of scenario A2 represent the most dramatic increases in instantaneous AMF series, while scenario B2 resulted in very small increases to outlet peak flows.

Overall, more significant differences are observed in the AMF series and associated flood risk under future LULC scenarios for Pigeon Creek Watershed than for Pond Creek Watershed. As the latter watershed is in close proximity with Louisville, KY, it currently has a very high concentration of urban developed land. With limited area for dramatic changes in non-urbanized land, effects of further urbanization to the remaining area are quite insignificant. The more significant differences observed in Pigeon Creek Watershed are due to the ability/capacity for this watershed to experience drastic changes in urban development, as well as deforestation and increased agricultural land, as anticipated under scenario A2, thereby creating a noticeable gap between simulated AMF distributions using the A2 scenario compared to the B2 scenario.

Table 5.8 and Table 5.9 report summary statistics for the simulated AMF series and the associated LP3 parameter values for both case study watersheds. Results are reported for the base period and three future 20-yr periods for scenario A1B; results from scenarios A2, B1, and B2 are limited to the simulation periods 2040-2060 and 2080-2100, as the intended purpose of the analysis is to gather general trends and impacts on AMF series resulting from LULC projections out to 2100. Similar to the results for historical LULC change, each FORE-SCE scenario resulted in an overall increase in the average of the AMF series, and a decrease in the spread of the data for Pond Creek (USGS station 03302000). On the contrary, the average of the AMF series increased for all but the B2 scenario in the Pigeon Creek watershed (USGS station 04099510), and the spread increased under the A1B and A2 scenarios, although decreased variability out to the 2100 projection date was observed under the more conservative B1 and B2 scenarios. As scenario A1B represents the most realistic scenario at this time, with a focus on economic development, results are very similar to those of the more extreme development scenario A2, although shifts in AMF series are not quite as dramatic under scenario A1B. For this reason, it is suggested that while engineers and policy makers account for shifts in climate change, similar scenario projections related to FORE-SCE scenario A1B should be used as a basis for future LULC change.

To understand the shifts and trends in AMF series simulated under various future scenarios and to understand what level of flood flows will be affected most by future LULC change, it is essential to view what flow magnitudes are shifting the most, thereby changing the average of the AMF series. It was observed in the Pond Creek Watershed (Figure 5.12), that the AMF magnitudes corresponding to larger z-values (upper tail of the fitted LP3 distribution) are quite constant through time; however, the magnitude of flows corresponding to lower z-values increase over time, thereby increasing the median and average of the AMF series, as well as decreasing the variability. On the contrary, in the Pigeon Creek Watershed (Figure 5.13), the lower tail of the fitted LP3 distributions remains reasonably constant through time, while in the upper tail increased magnitudes of flow corresponding to a given return period are observed through time for the development

based A1B and A2 scenarios, although increased magnitudes are more dramatic in the middle of the distribution. This results in the observed increases in the average and standard deviation of the AMF series predicted under these future scenarios. These results are further illustrated in Figure 5.14 and Figure 5.15, which show a variety of probability percentiles for the simulated AMF series with a 20 year moving window over the entire projection period (2000-2100) for scenarios A1B and A2, respectively, for Pigeon Creek Watershed. As the same climate data is used to simulate flows, any trends or patterns observed should be due to LULC change over time. In both cases, the lower end of the distribution remains quite stable through time as seen through lower percentiles. Similarly, the upper tail is reasonably constant for the A1B scenario with a slight increase observed under the more extreme scenario A2. The most dramatic change is observed in the middle section of the plots, subsequently shifting the averages for AMF series.

While considering the accuracy and error involved with modeling future LULC change using the FORE-SCE model, concerns arose regarding the spatial resolution of the LULC maps. Due to the FORE-SCE project having a nationwide scale, modeling change at a cell size of 250 meters by 250 meters would be appropriate for a wide range of practical applications with larger scaled projects. However, a cell size of that magnitude is quite large relative to the size of watersheds studied herein, and will therefore reduce the accuracy of the results. This may be the result in the dramatic shift in the lower tail of the fitted distribution for Pond Creek Watershed seen in Figure 5.12. While this watershed is mainly urban developed, FORE-SCE overestimates the amount of urban land, due to the large spatial resolution. Within each pixel, in reality there are a variety of land use types, but is mainly urbanized and therefore is classified as fully urban within that pixel. This will lead to overestimating urban developed land, and therefore will result in higher simulated flows, especially at the lower ends of the probability plots. Further analysis of future LULC change with finer resolution data is recommended for producing more accurate projections of flood risk.

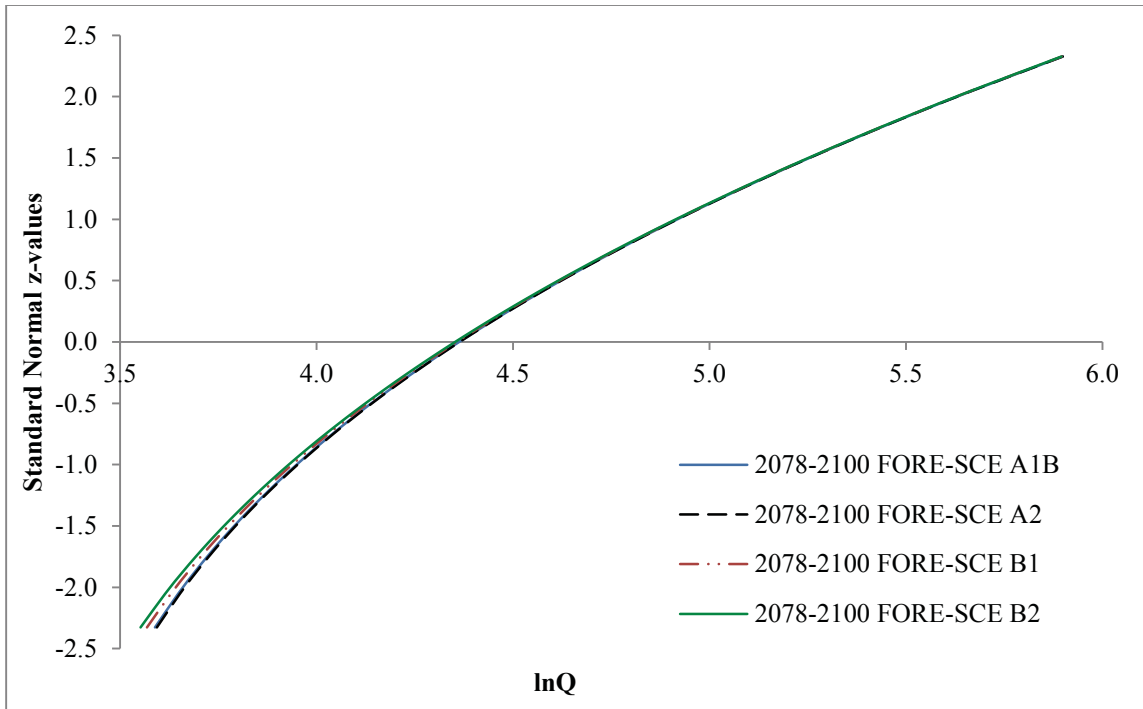


Figure 5.10: Probability plot of LP3 distributions fit to simulated AMF series under A1B, A2, B1, and B2 FORE-SCE LULC scenarios for 2080-2100 in Pond Creek Watershed, KY (USGS station 03302000).

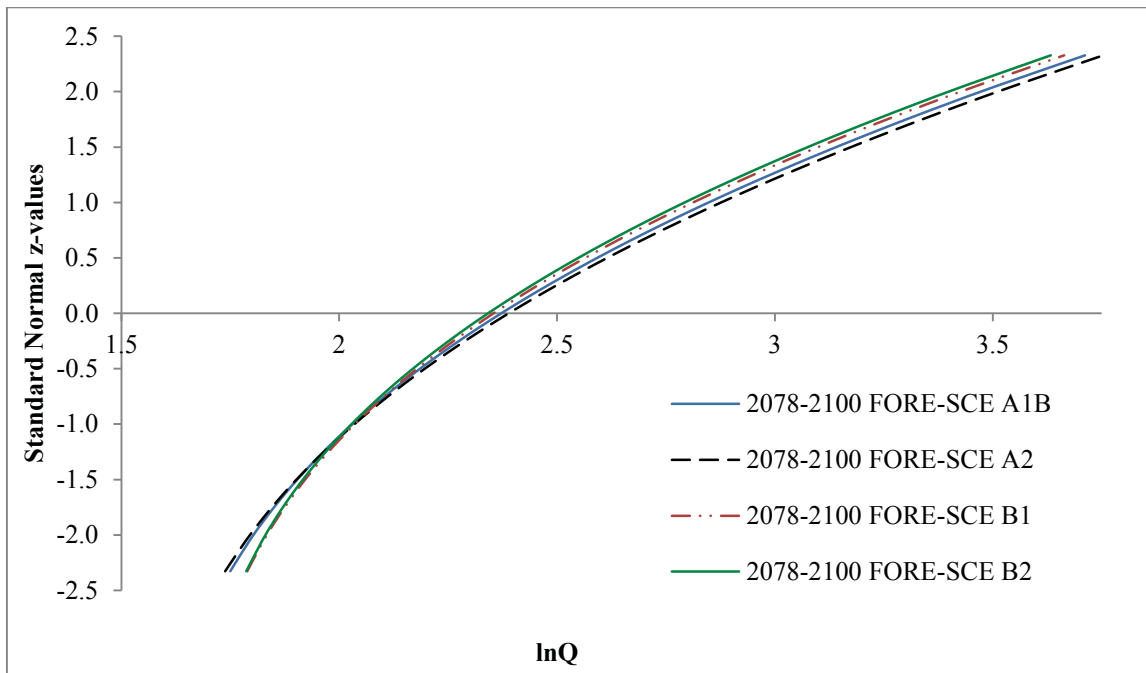


Figure 5.11: Probability plot of LP3 distributions fit to simulated AMF series under A1B, A2, B1, and B2 FORE-SCE LULC scenarios for 2080-2100 in Pigeon Creek Watershed, IN (USGS station 04099510).

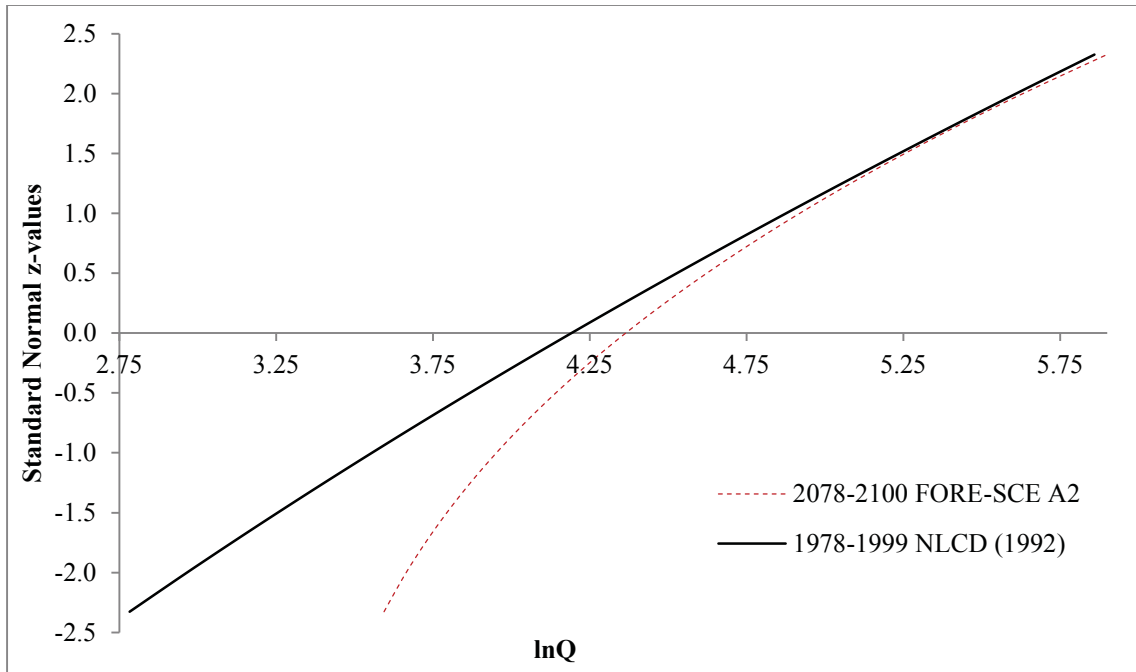


Figure 5.12: Probability plot of LP3 distribution fit to simulated AMF series under the A2 FORE-SCE LULC scenario for 2080-2100 compared to results for 'base' simulation period 1980-1999 for Pond Creek Watershed, KY (USGS station 03302000).

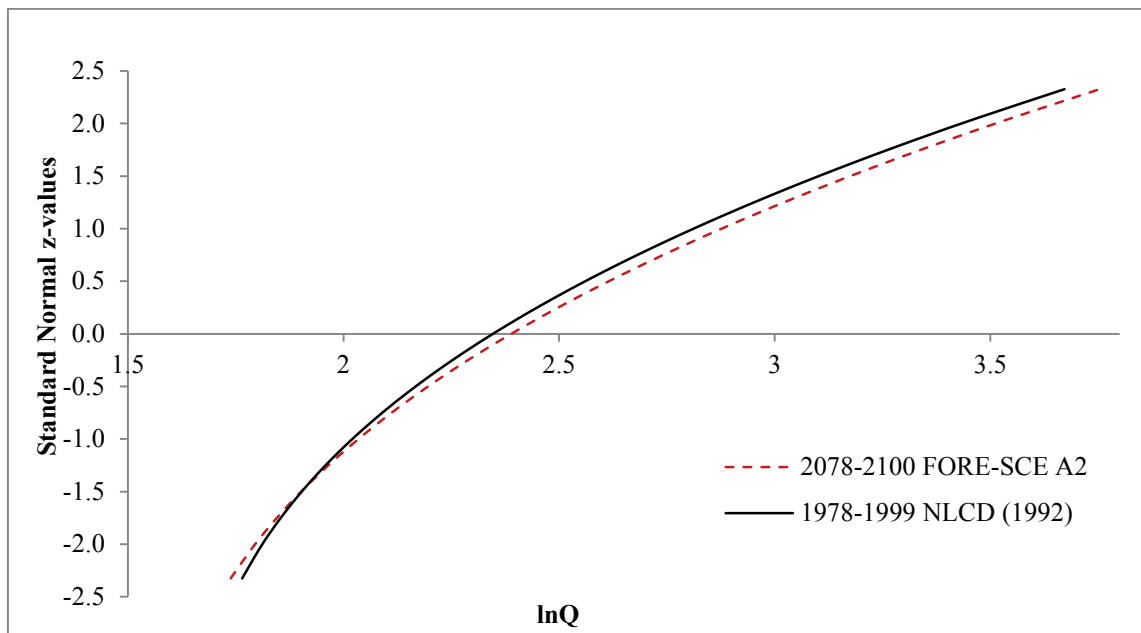


Figure 5.13: Probability plot of LP3 distribution fit to simulated AMF series under the A2 FORE-SCE LULC scenario for 2080-2100 compared to results for 'base' simulation period 1980-2000 for Pigeon Creek Watershed, IN (USGS station 04099510).

Table 5.8: AMF (cms) statistics and LP3 parameters for simulations based on future predicted LULC change in Pond Creek Watershed, KY (USGS station 03302000). All 20-year simulations were completed with consistent CMIP3 climate data.

Scenario	Simulation Period	AMF Statistics			LP3 Parameters		
		\bar{Q}	S_Q	G_Q	α	β	τ
A1B Hindcast	1980 - 2000	93.39	66.88	2.89	11.58	0.16	2.49
	2000 - 2020	94.79	64.40	2.83	6.73	0.20	3.06
A1B	2040 - 2060	96.18	63.50	2.80	5.61	0.21	3.24
	2080 - 2100	96.54	63.44	2.80	5.42	0.21	3.27
A2	2040 - 2060	96.16	63.52	2.80	5.63	0.21	3.23
	2080 - 2100	96.62	63.39	2.80	5.36	0.22	3.28
B1	2040 - 2060	95.55	63.66	2.81	5.91	0.21	3.18
	2080 - 2100	96.01	63.50	2.81	5.66	0.21	3.23
B2	2040 - 2060	95.53	63.79	2.81	6.03	0.21	3.17
	2080 - 2100	95.67	63.62	2.81	5.88	0.21	3.19

Table 5.9: AMF (cms) statistics and LP3 parameters for simulations based on future predicted LULC change in Pigeon Creek Watershed, IN (USGS station 04099510). All 20-year simulations were completed with consistent CMIP3 climate data.

Scenario	Simulation Period	AMF Statistics			LP3 Parameters		
		\bar{Q}	S_Q	G_Q	α	β	τ
A1B Hindcast	1980 - 2000	12.26	6.14	1.88	3.76	0.21	1.62
	2000 - 2020	12.28	6.12	1.87	3.71	0.21	1.63
A1B	2040 - 2060	12.39	6.26	1.78	4.55	0.20	1.52
	2080 - 2100	12.61	6.43	1.75	4.38	0.20	1.55
A2	2040 - 2060	12.40	6.27	1.82	4.18	0.20	1.57
	2080 - 2100	12.89	6.70	1.68	4.69	0.20	1.51
B1	2040 - 2060	12.27	6.09	1.86	3.74	0.21	1.63
	2080 - 2100	12.33	6.08	1.85	3.70	0.21	1.64
B2	2040 - 2060	12.15	5.97	1.87	3.80	0.21	1.62
	2080 - 2100	12.13	5.90	1.88	3.66	0.21	1.64

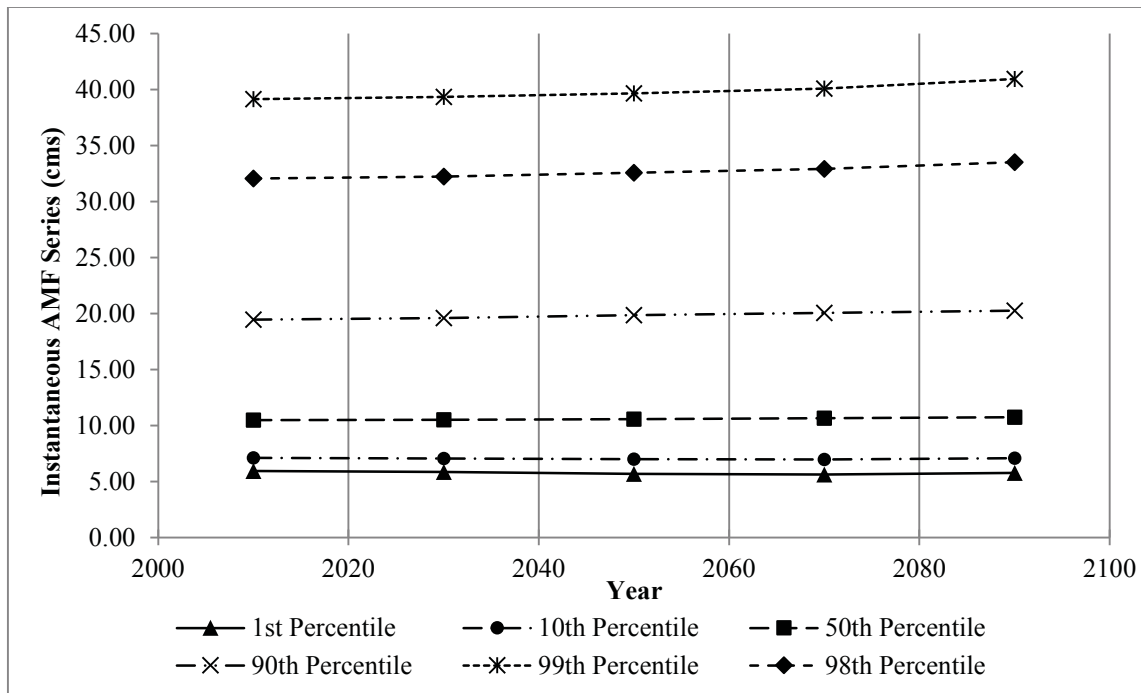


Figure 5.14: Moving window plot of percentiles for the FORE-SCE A1B scenario simulating a repeating 20 year climate period and shifting LULC data for Pigeon Creek Watershed (USGS station 04099510) from 2000-2100.

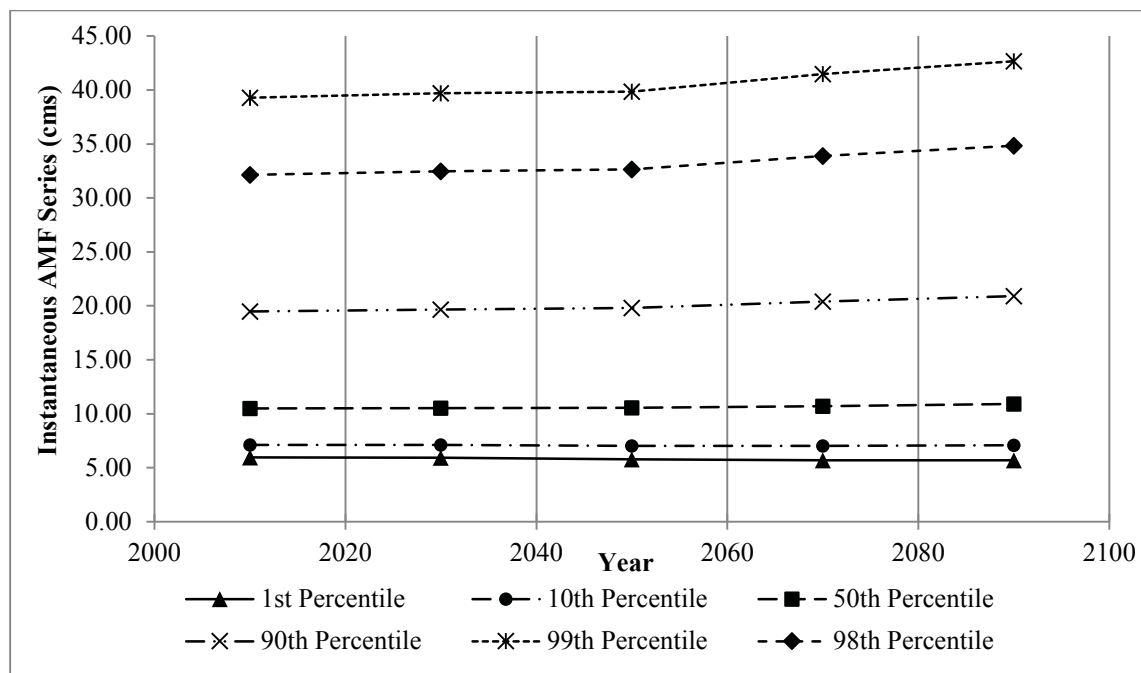


Figure 5.15: Moving window plot of percentiles for the FORE-SCE A2 scenario simulating a repeating 20 year climate period and shifting LULC data for Pigeon Creek Watershed (USGS station 04099510) from 2000-2100.

5.5 Overall Flood Series Trends

To observe overall trends in flood distributions resulting from LULC change through the historic, base and future periods, probability plots are presented in Figure 5.16 and Figure 5.17 for the Pond Creek and Pigeon Creek Watersheds, respectively. Results suggest larger changes and shifts in the instantaneous AMF series between the base period and simulations under FORE-SCE future scenario, especially results for scenario A2, than when considering the historical impact of LULC change. As discussed previously, greater impacts are observed in the Pond Creek Watershed than for the Pigeon Creek Watershed, as the former is located in an area which is presently predominantly urban, and there is greater potential for continued urbanization into the future.

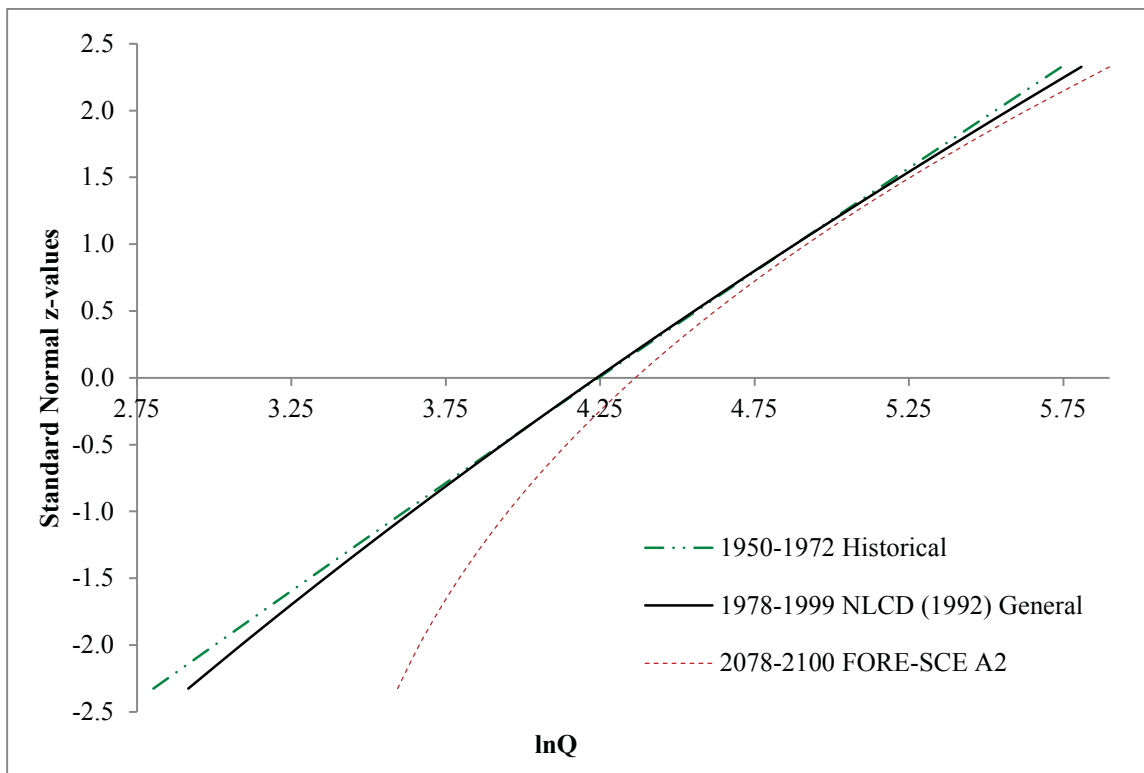


Figure 5.16: Probability plot comparing LP3 distributions fit to simulated AMF series for the base period (1980-1999), an early historical period, and the future A2 FORE-SCE LULC scenario (2080-2100) for Pond Creek Watershed, IN (USGS station 03302000).

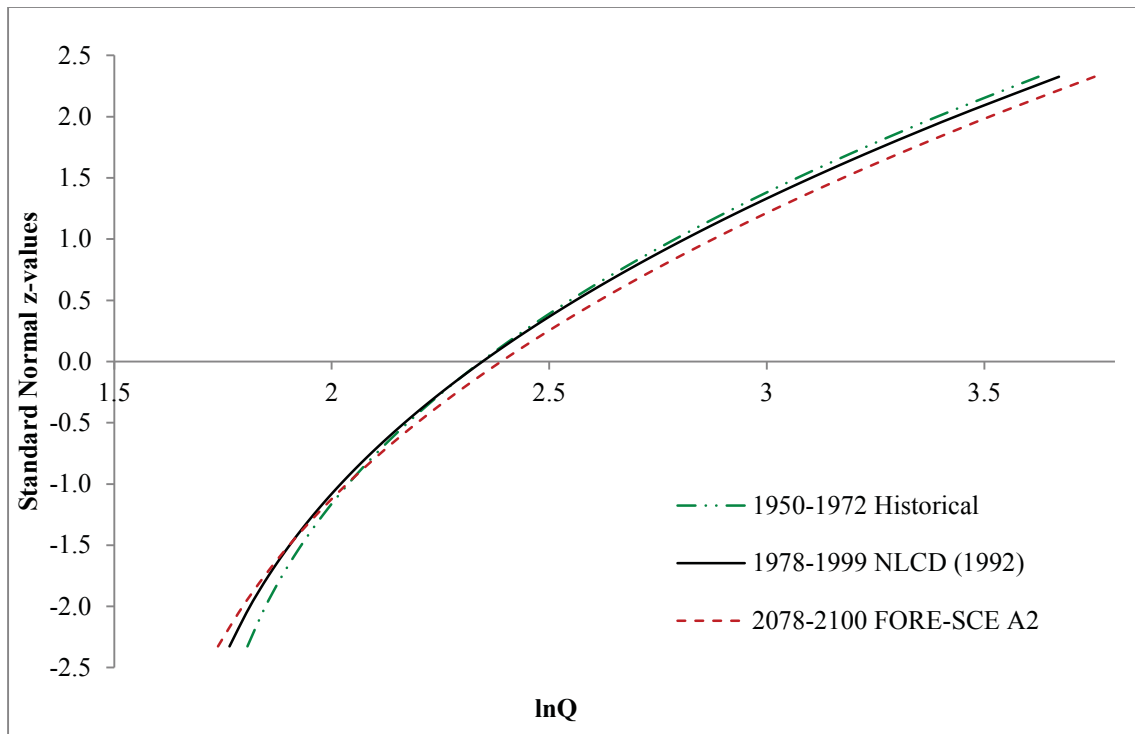


Figure 5.17: Probability plot comparing LP3 distributions fit to simulated AMF series for the base period (1980-1999), an early historical period, and the future A2 FORE-SCE LULC scenario (2080-2100) for Pigeon Creek Watershed, IN (USGS station 04099510).

Chapter 6. Conclusions and Recommendations

Current approaches for estimating flood risk assume that annual maximum flood (AMF) series are stationary, and thus past observations are representative of future flood events, and the flood distribution is unaffected by climate variability, climate change, and/or land use change. It has come to attention, however, that AMF series exhibit nonstationary behavior even in unimpaired watersheds. Further, population is expected to continue to rise over the next century despite the actual emissions and/or economic scenario considered for the future. Land use/land cover (LULC) change will accompany the growth of the population/economy in order to meet the needs of future generations. As such, standard approaches for flood frequency analysis (e.g., Bulletin 17B) need to be adapted to account for nonstationarity in the AMF series induced by future climate changes and/or anthropogenic activities. Previous efforts had focused on analyzing nonstationary behavior in the AMF series and evaluating effects of climate change. Only cursory attempts were made to relate nonstationarity to historical land use change and other anthropogenic activities. As such, the study presented herein, examined both historical and projected land use change and associated impacts on flood risk for four case study watersheds located in the Upper Midwest and Northeastern U.S.

Unfortunately, investigations of LULC changes are hindered by the limited amount of accurate data on historical land use and management practices. Herein, historical aerial images were processed and converted to usable spatial LULC maps of the selected watersheds dating back to the 1950s. The LULC data created provides general LULC classifications for the study areas, and while this data is useful and applicable in modeling, provides inaccuracies due to the generalization of the data and lack of specified LULC types. By analyzing generalized land use data, identifying specific shifts in land use change may be overlooked. There is a need to identify the degree of vulnerability to change of specific NLCD classification types and the actual location of the change within the watershed, as this information will be beneficial in future land use planning and management.

Also, the availability of quality historic aerial imagery is limited and inconsistent, making it difficult to create LULC maps with limited gaps of time between them. To better understand the progression of LULC change over the historical period, future analyses should consider use of Landsat imagery from 1972 to 1992 with specific NLCD classification types. The quality of the images employed may also limit accuracy of the analysis herein. The position of the satellite/plane, environmental conditions while the images are being captured, such as sun angle, humidity, and cloud cover, can all be sources for imperfect aerial images. This can also include what type of instrument took the image, scale and resolution of the image. As described previously, human and model error was also present during the segmentation and classification of the images. These errors should be acknowledged when interpreting results presented herein.

Overall, AMF series simulated over the historical period (early 1950s – 2000) suggest that low flows have been increasing; however, the magnitudes of large events (e.g. the 100-yr event) have remained reasonably constant. Further, the simulated AMF series for earlier decades based on generalized LULC types presented a decrease in the spread of the data (i.e. standard deviation) relative to the current ‘base’ conditions. This decrease was also observed when comparing results based on both generalized and specific 1992 NLCD data, and thus is more likely due to inaccuracies of the historical LULC maps than an actual effect of LULC change on flood risk. Further analysis of future LULC change with finer resolution data is recommended for producing more accurate results, especially studies that create LULC data consistent with the NLCD classification.

Projected LULC changes based on the FORE-SCE model were consistent with expectations, as decreases in agricultural and forested land coupled with increases in urbanized development were observed in most of the case study watersheds. Further, the extent of the urban development was appropriately dependent on the location of the watershed and the proximity to towns and cities. Heavily rural land with small surrounding cities observed less percent of LULC change compared to watersheds adjacent to larger cities, as seen in Pond Creek Watershed, where already existing urban developed land

within the watershed added to the trend of future urban expansion around those developments. While this study focused mainly on the amount of change within the watersheds through time, future analysis regarding the location of land use change is necessary in determining the level of impact certain LULC change has on flood risk, depending on the proximity of change to areas such as the watershed outlet or stream.

Simulations of AMF series under future emissions/economic scenarios for 2000-2100 showed scenario A2 to have the most dramatic effects on future flood risk as it presents the most extreme scenario for change, while scenario B2 had the most stagnant trends in fitted AMF series as the projects consisted of the most conservative aspects for change. Scenario A1B is observed to be the most realistic projection for future LULC change, showing moderate increases in AMF series and realistic expectations for changes regarding socioeconomic and environmental conditions and policies. It is suggested that future research investigates scenarios similar to A1B, and engineers and policy makers use this scenario as a basis for predictions of LULC for future events. General observations over projected LULC changes found increases over time occurred for the median AMF magnitudes, with the high and low AMF flow values within the distribution remaining quite constant. This has implications for presenting policy and design alternatives based on future predicted LULC changes that will adapt with the changing land use and account for increases in mid-level AMF flows.

Increased understanding of the degree to which LULC change affects hydrologic processes and flood risk would be extremely useful for water resources planning and management, and engineering design. However, much research is still needed with regards to agricultural practices and management effects on hydrology and water quality, and more detailed LULC classifications must be employed. McIntyre and Marshall (2010) point out that rural land management signals have not been unambiguously observed in catchment-scale flood responses, and the lack of evidence about effects remains a major obstacle to developing rural land management policy. If these responses to changing land management strategies can be determined, policies may be put in place to reduce flash

flows, sediment loads, and water quality issues. Further hydrologic research integrating land use and climate change on relatively unimpaired watersheds is also needed, as the research herein only considered effects of LULC change in order to isolate its effects on AMF series.

A better understanding of the effects of urbanization would enable policy-makers to continue to make smarter decisions when it comes to where and how we build. Cities, states, and private sectors need to continue planning and implementing smart growth strategies and other measures in order to counter balance the environmental impact that urbanization and other land use change has induced. Smart growth strategies are development designs that reduce the environmental impact of constructing new developments, by placing developments in convenient locations and making design decisions that are more efficient and environmentally friendly. This will in turn improve quality of life and human health in our communities (Kramer, 2013).

Chapter 7. References

- Alig, R.J., Kline, J.D., Lichtenstein, M., 2004. Urbanization on the US landscape: looking ahead in the 21st century. *Landscape and Urban Planning*, 69(2-3): 219-234. DOI:10.1016/j.landurbplan.2003.07.004.
- Alves, D.S. et al., 1996. Characterizing Land Use Dynamics in Amazon using Multi-Temporal Imagery and Segmentation Techniques. *International Archives of Photogrammetry and Remote Sensing*, XXXI(B7): 5-13.
- Alves, D.S., Escada, M.I.S., Pereira, J.L.G., de Albuquerque Linhares, C., 2003. Land use intensification and abandonment in Rondônia, Brazilian Amazônia. *International Journal of Remote Sensing*, 24(4): 899-903. DOI:10.1080/0143116021000015807.
- Antonova, N., 2014. Image Segmentation with SPRING and ENVI: WorldView-2, 8-band image of Acme, WA, ESCI 442/542: Introduction to Remote Sensing. Spatial Analysis Lab: Western Washington University, Bellingham, WA.
- Araya, Y.H., Cabral, P., 2010. Analysis and Modeling of Urban Land Cover Change in Setúbal and Sesimbra, Portugal. *Remote Sensing*, 2(6): 1549-1563. DOI:10.3390/rs2061549.
- ArcGIS Resources, 2014. How Transform (Coverage) works. ESRI. Accessed 2/10/2015, <<http://resources.arcgis.com/en/help/main/10.2/index.html#//001300000056000000>>.
- ArcGIS, 2008. Transforming the raster, Georeferencing a raster dataset. Environmental Systems Research Institute, Inc. <http://webhelp.esri.com/arcgisdesktop/9.2/?TopicName=Georeferencing_a_raster_dataset>.
- Archer, D.R., Climent-Soler, D., Holman, I.P., 2010. Changes in discharge rise and fall rates applied to impact assessment of catchment land use. *Hydrology Research*, 41(1): 13. DOI:10.2166/nh.2010.092.
- Arnold, J.G., Allen, P.M., Bernhardt, G., 1993. A comprehensive surface-groundwater flow model. *Journal of Hydrology*, 142(1-4): 47-69.
- Arnold, J.G., Srinivasan, R., Mutiah, R.S., Williams, J.R., 1998. Large Area Hydrologic Modeling and Assessment Part I: Model Development, *Journal of the American*

- Water Resources Association (JAWRA), pp. 17. DOI:10.1111/j.1752-1688.1998.tb05961.x.
- Arnold, J.G. et al., 2012. SWAT Input/Output Documentation Version 2012, Texas Water Resources Institute.
- Barlage, M.J., Richards, P.L., Sousounis, P.J., Brenner, A.J., 2002. Impacts of Climate Change and Land Use Change on Runoff from a Great Lakes Watershed. *Journal of Great Lakes Research*, 28(4): 568-582.
- Berberoglu, S., Curran, P.J., 2004. Merging spectral and textural information for classifying remotely sensed images: Remote sensing image analysis: including the spatial domain. Springer, Netherlands, pp. 113-136.
- Beven, K. et al., 2008. FD2120: Analysis of Historical Data Sets to Look for Impacts of Land Use Management Change on Flood Generation, Defra, London.
- Bins, L.S.A., Fonseca, L.M.G., Erthal, G.J., Li, F.M., 1996. Satellite Imagery Segmentation: a region growing approach. *Simposio Brasileiro de Sensoriamento Remoto*, 8: 677-680.
- Blom, G., 1958. *Statistical Estimates and Transformed Beta Variables*. John Wiley and sons, New York, New York.
- Boardman, J., Poesen, J., Evans, R., 2003. Socio-economic factors in soil erosion and conservation. *Environmental Science & Policy*, 6(1): 1-6. DOI:10.1016/s1462-9011(02)00120-x.
- Bradshaw, C.J.A., Sodhi, N.S., Peh, K.S.H., Brook, B.W., 2007. Global evidence that deforestation amplifies flood risk and severity in the developing world. *Global Change Biology*, 13(11): 2379-2395. DOI:10.1111/j.1365-2486.2007.01446.x.
- Bronstert, A., Niehoff, D., Bürger, G., 2002. Effects of climate and land-use change on storm runoff generation: present knowledge and modelling capabilities. *Hydrological Processes*, 16(2): 509-529. DOI:10.1002/hyp.326.
- Brown, J.D., Damery, S.L., 2002. Managing flood risk in the UK: towards an integration of social and technical perspectives. *Transactions of the Institute of British Geographers*, 27(4): 412-427.
- Bruijnzeel, L.A. (1990). *Hydrology of Moist Tropical Forests and Effects of Conversion:*

- a State of Knowledge Review. Humid Tropics Programme, IHP-UNESCO, Paris, and Vrije Universiteit, Amsterdam, 224 pp.
- Camara, G., Souza, R.C.M., Freitas, U.M., Garrido, J., 1996. SPRING: Integrating remote sensing and GIS by object-oriented data modelling. INPE.
- Carroll, Z.L., Bird, S.B., Emmett, B.A., Reynolds, B., Sinclair, F.L., 2004. Can tree shelterbelts on agricultural land reduce flood risk? *Soil Use Management*, 20: 357-359.
- Chang, H., 2004. Water Quality Impacts of Climate and Land Use Changes in Southeastern Pennsylvania. *The Professional Geographer*, 56(2): 240-257. DOI:10.1111/j.0033-0124.2004.05602008.x.
- Chang, H., 2007. Comparative streamflow characteristics in urbanizing basins in the Portland Metropolitan Area, Oregon, USA. *Hydrological Processes*, 21(2): 211-222. DOI:10.1002/hyp.6233.
- Chin, A., 2006. Urban transformation of river landscapes in a global context. *Geomorphology*, 79(3-4): 460-487. DOI:10.1016/j.geomorph.2006.06.033.
- Choi, W., 2008. Catchment-scale hydrological response to climate-land-use combined scenarios: a case study for the Kishwaukee River Basin, Illinois. *Physical Geography*, 29(1): 79-99. DOI:10.2747/0272-3646.29.1.79.
- Comber, A., Fisher, P., Brunson, C., Khmag, A., 2012. Spatial analysis of remote sensing image classification accuracy. *Remote Sensing of Environment*, 127: 237-246. DOI:10.1016/j.rse.2012.09.005.
- Costa, M.H., Botta, A., Cardille, J.A., 2003. Effects of large-scale changes in land cover on the discharge of the Tocantins River, Southeastern Amazonia. *Journal of Hydrology*, 283(1-4): 206-217. DOI:10.1016/s0022-1694(03)00267-1.
- DeFries, R., Eshleman, K.N., 2004. Land-use change and hydrologic processes: a major focus for the future. *Hydrological Processes*, 18(11): 2183-2186. DOI:10.1002/hyp.5584.
- Engineers, A.C.o., 2013. National Inventory of Dams, CorpsMap. Accessed 2/21/2015.
- EROS, 2015. EarthExplorer. U.S. Geologic Survey's (USGS) Earth Resources Observation and Science (EROS) Center. <<http://earthexplorer.usgs.gov/>>

- Falcone, J., 2011. GAGES II: Geospatial Attributes of Gages for Evaluation Streamflow Summary Report, Reston, Virginia. <http://water.usgs.gov/GIS/metadata/usgswrd/XML/gagesII_Sept2011.xml>.
- Falcone, J.A., Carlisle, D.M., Wolock, D.M., Meador, M.R., 2010. GAGES: A stream gage database for evaluating natural and altered flow conditions in the conterminous United States. *Ecology* 91:621–621. <http://dx.doi.org/10.1890/09-0889.1>.
- Fill, H., Steiner, A., 2003. Estimating Instantaneous Peak Flow from Mean Daily Flow Data. *Journal of Hydrologic Engineering*, 8(6): 365-369.
- Fohrer, N., Haverkamp, S., Eckhardt, K., Frede, H.-G., 2001. Hydrologic Response to Land Use Changes on the Catchment Scale. *Physics and Chemistry of the Earth, Parts A/B/C*, 26(7-8): 577-582.
- Franczyk, J., Chang, H., 2009. The effects of climate change and urbanization on the runoff of the Rock Creek basin in the Portland metropolitan area, Oregon, USA. *Hydrological Processes*, 23(6): 805-815. DOI:10.1002/hyp.7176.
- Fritsch, C.E., 2012. Evaluation of Flood Risk in Response to Climate Variability, Michigan Technological University, Houghton, MI.
- Gesch, D.B., Oimoen, M., Greenlee, S., Nelson, C., Steuck, M., and Tyler, D., 2002. The National Elevation Dataset. *Photogrammetric Engineering and Remote Sensing*, 68(1): 5-11.
- Gesch, D.B., 2007. The National Elevation Dataset, in Maune, D., ed., *Digital Elevation Model Technologies and Applications: The DEM User's Manual*, 2nd Edition. Bethesda, Maryland. American Society for Photogrammetry and Remote Sensing, p. 99-118.
- Griffis, V.W., Stedinger, J.R., 2008. Flood Frequency Analysis in the United States: Time to Update. *Journal of Hydrologic Engineering*, 13(4): 199-204.
- Gyawali, R., Griffis, V.W., Watkins, D.W., Fennessey, N.M., 2014. Regional regression models for hydro-climate change impact assessment. *Hydrological Processes*: n/a-n/a. DOI:10.1002/hyp.10312.
- Hegde, S., 2003. *Modelling Land Cover Change: A Fuzzy Approach*, International Institute for Geo-Information Science and Earth Observation, Enschede, Netherlands, 62 pp.

- Hess, T.M., Holman, I.P., Rose, S.C., Rosolova, Z., Parrott, A., 2010. Estimating the Impact of Rural Land Management Changes on Catchment Runoff Generation in England and Wales. *Hydrological Processes*, 24: 1357-1368. DOI:10.1002/hyp.7598.
- Hirschboeck, K.K., Ely, L., Maddox, R.A., 2000. Hydroclimatology of meteorologic floods, in Wohl, Ellen, ed, *Inland Flood Hazards: Human, Riparian and Aquatic Communities*, Cambridge University Press, p. 39-72.
- Holman, I.P., Hollis, J.M., Bramley, M.E., Thompson, T.R.E, 2003. The contribution of soil structural degradation to catchment flooding: a preliminary investigation of the 2000 floods in England and Wales. *Hydrology and Earth System Sciences Discussions*, 7(5): 755-766.
- Hudak, A.T., Wessman, C.A., 1998. Textural Analysis of Historical Aerial Photography to Characterize Woody Plant Encroachment in South African Savanna. *Remote Sensing of Environment*, 66(3): 317-330.
- Institute of Hydrology (1999). *Flood Estimation Handbook*. Institute of Hydrology, Crowmarsh Gifford, UK.
- Interagency Committee on Water Data (IACWD), 1982. Guidelines for Determining flood flow frequency: Bulletin 17B (revised and corrected), Hydrol. Subcomm., Washington, D.C., 28.
- Interagency Floodplain Management Review Committee (IFMRC). 1994. *Sharing the Challenge: Floodplain Management into the 21st Century (Galloway Report)*. U.S. Government Printing Office, Washington, D.C.
- Jiang, Z., 2007. The Road Extension Model in the Land Change Modeler for Ecological Sustainability of IDRISI. *Proceedings of the 15th International Symposium on Advances in Geographic Information Systems*: 1-8.
- Kochhar, R. et al., 2014. *Attitudes about Aging: A Global Perspective*, Pew Research Center.
- Kramer, M.G., 2013. *Our Built and National Environment: A Technical Review of the Interactions among Land Use, Transportation, and Environmental Quality*, EPA.
- Kuntiyawichai, K., Schultz, B., Uhlenbrook, S., Suryadi, F.X., Van Griensven, A., 2011.

- Comparison of flood management options for the Yang River Basin, Thailand. *Irrigation and Drainage*, 60(4): 526-543. DOI:10.1002/ird.596.
- LaFond, K.M., 2014. *Assessment of Flood Risk under Future Climate Conditions*, Michigan Technological University, 174 pp.
- Lambin, E.F., Helmut, J.G., 2008. *Land-use and land-cover change: local processes and global impacts*. Springer Science & Business Media.
- Ligon, F.K., Dietrich, W.E., Trush, W.J., 1995. Downstream Ecological Effects of Dams. *BioScience*, 45(3): 183-192.
- Loveland, T.R. et al., 2002. A Strategy for Estimating the Rates of Recent United States Land-Cover Changes. *Photogrammetric Engineering & Remote Sensing*, 68(10): 1061-1099.
- Mansell, M.G., 2003. *Rural and urban hydrology*. Thomas Telford.
- McCuen, R.H., 1998. *Hydrological Analysis and Design*, Prentice Hall, Englewood Cliffs, NJ.
- McIntyre, N., Marshall, M., 2010. Identification of rural land management signals in runoff response. *Hydrological Processes*, (24): 3521-3534.
- Meyer, V., Turner, B.L., 1994. *Global land-use and land-cover change: an overview*, *Changes in land use and land cover: a global perspective*. Cambridge University Press.
- Nakicenovic, N., 2000. Intergovernmental Panel on Climate Change (IPCC): Special Report on Emissions Scenarios, IPCC, Cambridge, UK.
- Neitsch, S.L., Arnold, J.G., Kiniry, J.R., Williams, J.R., 2005. *Soil and Water Assessment Tool Theoretical Documentation*, Version 2005, Grassland and Water Research Laboratory and Blackland Research Center, Temple, TX, USA.
- NOAA, 2015. *Hydrologic Information Center: Flood Loss Data*. National Weather Service, Silver Spring, MD. Accessed 2/26/2015.
- Nowak, D.J., Walton, J.T., 2005. Projected Urban Growth (2000 - 2050) and Its Estimated Impact on the US Forest Resource. *Journal of Forestry*, 103(9): 383-389.
- NRCS, 2007. Chapter 7 Hydrologic Soil Group, United States Department of Agriculture. Accessed 10/15/2014.

- NRCS, 2015. National Land Cover Database (NLCD) 2011, Geospatial Data Gateway. United States Department of Agriculture (USDA).
- O'Connell, E., Ewen, J., O'Donnell, G., Quinn, P., 2007. Is There a Link Between Agricultural Land-Use Management and Flooding? *Hydrology and Earth System Sciences*, 11(1): 96-107.
- Olsen, J.R., Stedinger, J.R., Matalas, N.C., Stakhiv, E.Z., 2007. Climate Variability and Flood Frequency Estimation for the Upper Mississippi and Lower Missouri Rivers. *Journal of the American Water Resources Association (JAWRA)*, 35(6): 1509-1523. DOI:10.1111/j.1752-1688.
- Omernik, J.M., 1987. Ecoregions of the Conterminous United States. *Annals of the Association of the American Geographers*, 77(9): 118-125.
- Palamuleni, L.G., Ndomba, P.M., Annegarn, H.J., 2011. Evaluating land cover change and its impact on hydrological regime in Upper Shire river catchment, Malawi. *Regional Environmental Change*, 11(4): 845-855. DOI:10.1007/s10113-011-0220-2.
- Pérez-Vega, A., Mas, J.-F., Ligmann-Zielinska, A., 2012. Comparing two approaches to land use/cover change modeling and their implications for the assessment of biodiversity loss in a deciduous tropical forest. *Environmental Modelling & Software*, 29(1): 11-23. DOI:10.1016/j.envsoft.2011.09.011.
- Pinter, N., Jemberie, A.A., Remo, J.W.F., Heine, R.A., Ickes, B.S., 2008. Flood trends and river engineering on the Mississippi River system. *Geophysical Research Letters*, 35(23): 1-5. DOI:10.1029/2008gl035987.
- Plieninger, T., 2006. Habitat loss, Fragmentation, and Alteration – Quantifying the Impact of Land-use Changes on a Spanish Dehesa Landscape by Use of Aerial Photography and GIS. *Landscape Ecology*, 21(1): 91-105. DOI:10.1007/s10980-005-8294-1.
- Pontius, R.G.J., Schneider, L.C., 2001. Land-Cover Change Model Validation by an ROC Method for the Ipswich Watershed, Massachusetts, USA. *Agriculture, Ecosystems & Environment*, 85: 239-248.
- Porter, S.A., 2011. Land cover study in Iowa: analysis of classification methodology and

- its impact on scale, accuracy, and landscape metrics, University of Iowa, Iowa, 131 pp.
- Pouncey, R., Swanson, K., Hart, K., 1999. ERDAS Field Guide: Fifth Edition, Revised and Expanded, Atlanta, Georgia.
- Qi, S., Sun, G., Wang, Y., McNulty, S.G., Moore Myers, J.A., 2009. Streamflow Response to Climate and Landuse Changes in a Coastal Watershed in North Carolina. *Transactions of the ASABE*, 52(3): 739-749.
- Rallison, R.E., Miller, N., 1981. Past, Present and future SCS runoff procedure. Rainfall runoff relationship. Water Resources Publication.
- Rhemtulla, J.M., Mladenoff, D.J., Clayton, M.K., 2007. Regional land-cover conversion in the U.S. upper Midwest: magnitude of change and limited recovery (1850–1935–1993). *Landscape Ecology*, 22(S1): 57-75. DOI:10.1007/s10980-007-9117-3.
- Riebsame, W.E., Meyer, W.B., Turner II, B.L., 1994. Modeling land use and cover as part of global environmental change. *Climatic Change* 28: 45-64.
- Robinson, M., 1990. Impact of Improved Land Drainage on River Flows, Institute of Hydrology, Wallingford, UK.
- Robson, A.J., Jones, T.K., Reed, D.W., Bayliss, A.C., 1998. A Study of National Trend and Variation in UK Floods. *International Journal of Climatology*, 18: 165-182.
- Rose, S., Peters, N.E., 2001. Effects of urbanization on streamflow in the Atlanta area (Georgia, USA): a comparative hydrological approach. *Hydrological Processes*, 15(8): 1441-1457. DOI:10.1002/hyp.218.
- Salvadori, N.M., 2013. Evaluation of Non-Stationarity in Annual Maximum Flood Series of Moderately Impaired Watersheds in the Upper Midwest and Northeastern United States, Michigan Technological University, Michigan.
- Schilling, K.E. et al., 2014. The potential for agricultural land use change to reduce flood risk in a large watershed. *Hydrological Processes*, 28(8): 3314-3325. DOI:10.1002/hyp.9865.
- Schottler, S.P. et al., 2014. Twentieth century agricultural drainage creates more erosive rivers. *Hydrological Processes*, 28(4): 1951-1961. DOI:10.1002/hyp.9738.
- Schueler, T.R., 1994. The Importance of Imperviousness. *Watershed Protection*

Techniques 1(3): 100-111.

- Shaw E.M., 1994. *Hydrology in Practice*. 3rd edn. Chapman & Hall, London.
- Sheng, J., Wilson, J.P., Chen, N., Devinny, J.S., Sayre, J.M., 2007. Evaluating the quality of the National Hydrography Dataset for watershed assessments in metropolitan regions. *GIScience & Remote Sensing* 44: 283–304.
- Skirvin, S.M. et al., 2005. Assessing the Accuracy of Satellite-Derived Land-Cover Classification Using Historical Aerial Photography, Digital Orthophoto Quadrangles, and Airborne Video Data, *Remote Sensing and GIS Accuracy Assessment*, Boca Roton, Florida, pp. 115-133.
- Slack, J.R., Landwehr, J.M., 1992. *Hydro-Climatic Data Network: A U.S. Geological Survey Streamflow Data Set for the United States for the study of Climate Variations*, U.S. Geological Survey, Washington, D.C.
- Sohl, T.L., Sayler, K.L, Drummond, M.A., Loveland, T.R., 2007. The FORE-SCE model: A practical approach for projecting land use change using scenario-based modeling. *Journal of Land Use Science* 2(2): 103-126.
- Sohl, T.L., Sayler, K.L., 2008. Using the FORE-SCE model to project land-cover change in the southeastern United States. *Ecological Modelling*, 219(1-2): 49-65. DOI:10.1016/j.ecolmodel.2008.08.003
- Soil Conservation Service (SCS), 1972. *Hydrology, National Engineering Handbook, Supplement A, Section 4, Chapter 10*, Soil Conservation Service, U.S.D.A. Washington, D.C.
- Solan, P.G., Morre, I.D., Coltharp, G.B., Eigel, J.D., 1983. *Modeling surface and subsurface stormflow on steeply-sloping forested watersheds*, Water Resource Institute, University of Kentucky, Lexington.
- Solomon, S. et al., 2007. *Contribution of Working Group I to the Fourth Assessment Report of the Intergovernmental Panel on Climate Change*, Cambridge University Press, Cambridge, United Kingdom and New York, NY, USA.
- Sullivan, A., Ternan, J.L., Williams, A.G., 2004. Land use change and hydrological response in the Camel catchment, Cornwall. *Applied Geography*, 24(2): 119-137. DOI:10.1016/j.apgeog.2003.11.002

- Sun, G., McNulty, S.G., Myers, M., Cohen, E.C., 2008. Impacts of Climate Change, Population Growth, Land Use Change, and Groundwater Availability on Water Supply and Demand across the Conterminous U.S., USDA Forest Service, Raleigh, NC.
- Tang, Z., Engel, B.A., Pijanowski, B.C., Lim, K.J., 2005. Forecasting land use change and its environmental impact at a watershed scale. *Journal of environmental management*, 76(1): 35-45. DOI:10.1016/j.jenvman.2005.01.006.
- Tao, B. et al., 2014. Increasing Mississippi river discharge throughout the 21st century influenced by changes in climate, land use, and atmospheric CO₂. *Geophysical Research Letters*, 41(14): 4978-4986. DOI:10.1002/2014gl060361.
- Tewelde, M.G., Cabral, P., 2011. Urban Sprawl Analysis and Modeling in Asmara, Eritrea. *Remote Sensing*, 3(12): 2148-2165. DOI:10.3390/rs3102148.
- Tollan, A., 2002. Land-use change and floods: what do we need most, research or management? *Water Science and Technology*, 45(8): 183-190.
- Tong, S.T.Y., Sun, Y., Ranatunga, T., He, J., Yang, Y.J., 2012. Predicting plausible impacts of sets of climate and land use change scenarios on water resources. *Applied Geography*, 32(2): 477-489. DOI:10.1016/j.apgeog.2011.06.014.
- Tu, J., 2009. Combined impact of climate and land use changes on streamflow and water quality in eastern Massachusetts, USA. *Journal of Hydrology*, 379(3-4): 268-283. DOI:10.1016/j.jhydrol.2009.10.009.
- USDA, Natural Resources Conservation Service, 2001. Summary Report: 1997 National Resources Inventory (revised December 2001). US Department of Agriculture, Natural Resource Conservation Service, Washington, D.C.
- USDA, 2014. Geospatial Data Gateway. U.S. Department of Agriculture and Natural Resources Conservation Service. <<https://gdg.sc.egov.usda.gov/GDGHome.aspx>>
- USDC, Census Bureau, 2001. Statistical Abstract of the United States, 2001. Table 1046. <<http://www.census.gov/main/www/cen2000.html>>.
- USEPA, 2013. Ecoregion Maps and GIS Resources, Western Ecology Division. EPA. Accessed 3/2/2015. <<http://www.epa.gov/wed/pages/ecoregions.htm>>.
- USGS, 2014. Ecoregion Framework, Land Cover Trends Project. Accessed 7/24/2014.

- <<http://landcoverrends.usgs.gov/main/ecoFrame.html>>.
- USGS, 2014. Land Cover Trends, Land Cover Trends Project. Accessed 7/23/2014. <<http://landcoverrends.usgs.gov/>>.
- USGS, 2014. Land-cover Modeling at USGS Earth Resources Observation and Science (EROS) Center, Landcover Modeling. Accessed 7/15/2014. <<http://landcover-modeling.cr.usgs.gov/applications.php>>.
- Valeriano, D.M. et al., 2004. Monitoring Tropical Forest from Space: The Prodes Digital Project. *International Archives of Photogrammetry*, 35: 272-275.
- Wilson, C.O., Weng, Q., 2011. Simulating the impacts of future land use and climate changes on surface water quality in the Des Plaines River watershed, Chicago Metropolitan Statistical Area, Illinois. *The Science of the total environment*, 409(20): 4387-405. DOI:10.1016/j.scitotenv.2011.07.001.
- Woodham, R.J., Gray, M.H., 1987. An Analytic Method for Radiometric Correction of Satellite Multispectral Scanner Data. *IEEE Transactions on Geoscience and Remote Sensing*, GE-25(3): 258-272.
- Wu, Y., Liu, S., Sohl, T.L., Young, C.J., 2013. Projecting the land cover change and its environmental impacts in the Cedar River Basin in the Midwestern United States. *Environmental Research Letters*, 8(2): 024025. DOI:10.1088/17489326/8/2/024025.
- Yang, P., Reichert, P., Abbaspour, K.C., Xia, J., Yang, H., 2008. Comparing uncertainty analysis techniques for a SWAT application to the Chaohe Basin in China. *Journal of Hydrology*, 358(1): 1-23.
- Yocoub, C., Foguet, A., 2013. Slope Effects on SWAT Modeling in a Mountainous Basin. *Journal of Hydrologic Engineering*, 18(12), 1663-1673.
- Zhang, H., Ma, W.-c., Wang, X.-r., 2008. Rapid Urbanization and Implications for Flood Risk Management in Hinterland of the Pearl River Delta, China: The Foshan Study. *Sensors*, 8: 2223-2239.
- Zhang, X., Srinivasan, R., Hao, F., 2007. Predicting Hydrological Response to Climate Change in the Luohe River Basin Using the SWAT Model. *Transactions of the American Society of Agricultural and Biological Engineers*, 50(3): 901-910.

Zhu, Z., 2014. Future Land Use and Land Cover Scenarios, National Assessment of Ecosystem Carbon Sequestration and Greenhouse Gas Fluxes.

Appendix A. Current Watershed Characteristics

This appendix contains figures and tables with further information regarding the selected USGS watersheds studied herein, building on the discussion provided in Chapter 2. Data for watershed characteristics include STATSGO soil published in 1994, 30 meter National Elevation Dataset (NED), and 2011 NLCD were obtained from the USDA and NRCS Geospatial Data Gateway (<http://datagateway.nrcs.usda.gov/>). The slope map was generated using ArcMap 10.2 based on the 30 meter DEM. Historical AMF series were obtained from the USGS National Water Information System Web Interface (<http://waterdata.usgs.gov/nwis>).

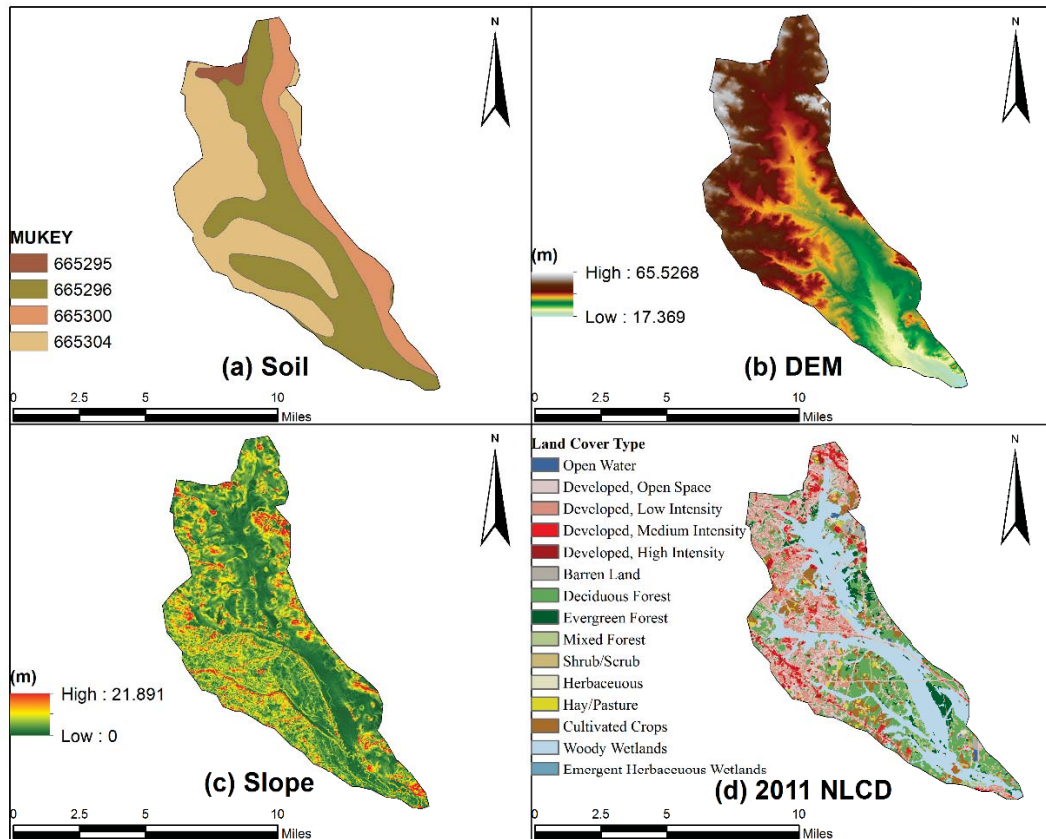


Figure A.1: Watershed characteristics including soil (STATSGO), Digital Elevation Model (DEM), slope, and 2011 NLCD for USGS station 01411000. (Data Source: USDA, 2014).

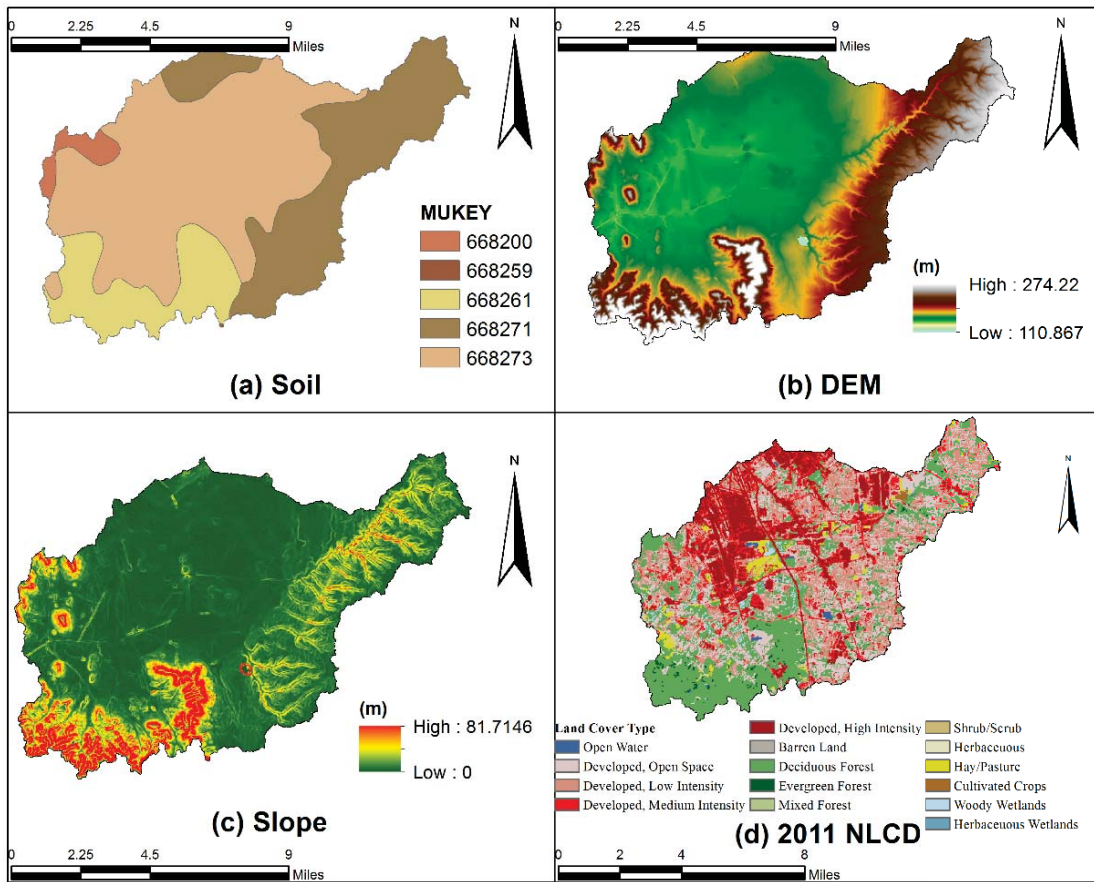


Figure A.2: Watershed characteristics including soil (STATSGO), Digital Elevation Model (DEM), slope, and 2011 NLCD for USGS station 03302000. (Data Source: USDA, 2014).

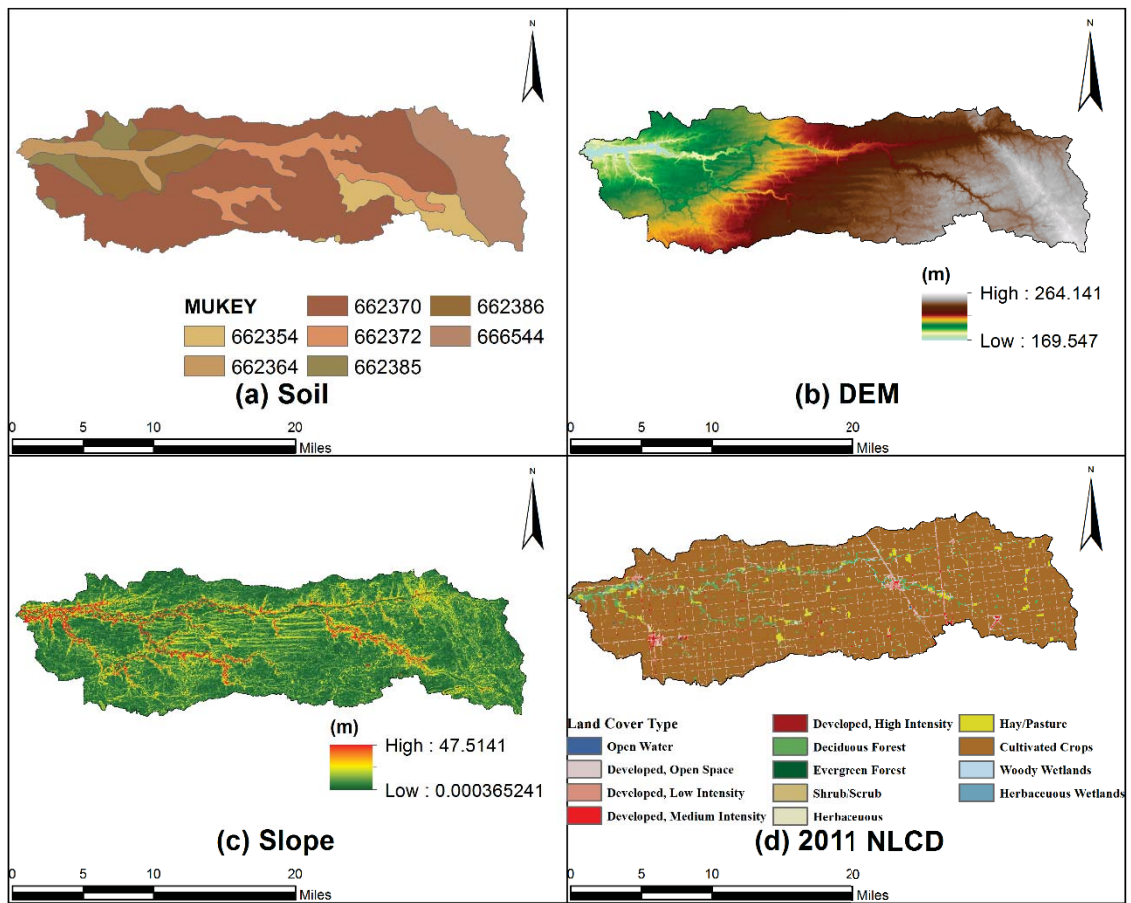


Figure A.3: Watershed characteristics including soil (STATSGO), Digital Elevation Model (DEM), slope, and 2011 NLCD for USGS station 03329700. (Data Source: USDA, 2014).

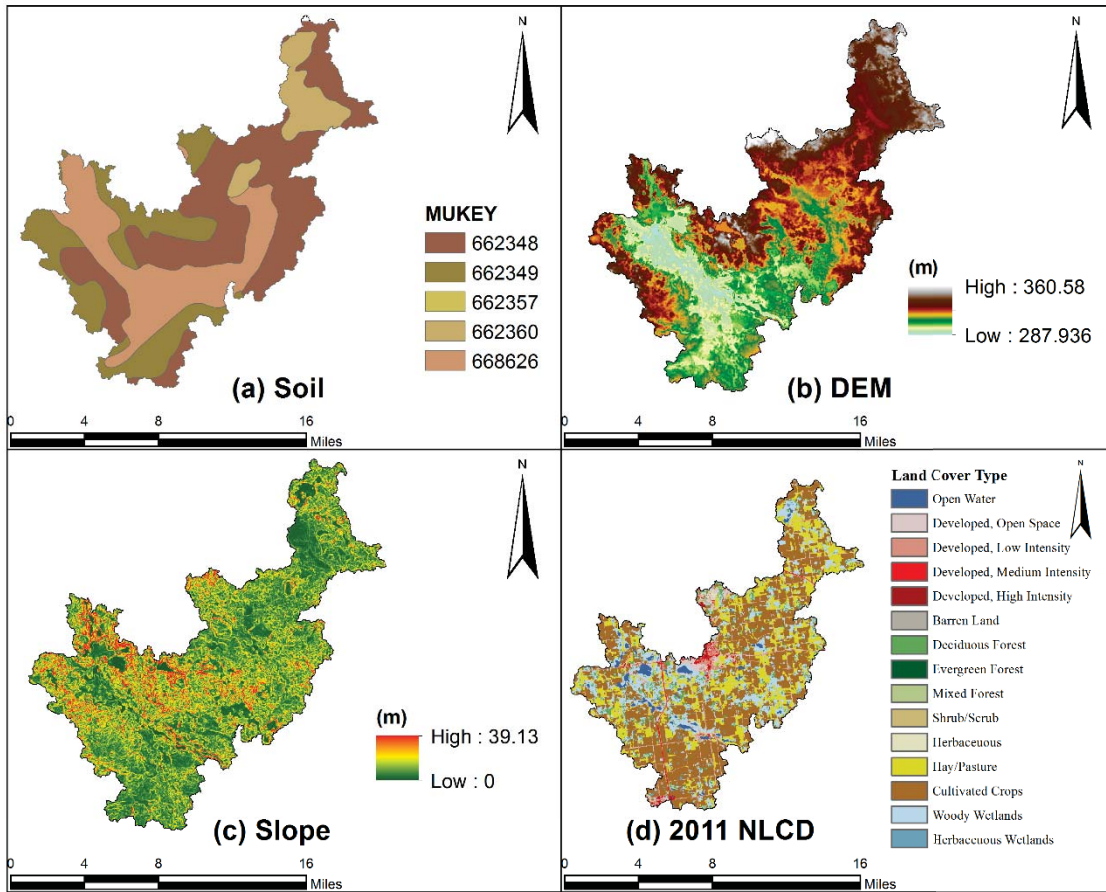


Figure A.4: Watershed characteristics including soil (STATSGO), Digital Elevation Model (DEM), slope, and 2011 NLCD for USGS station 04099510. (Data Source: USDA, 2014).

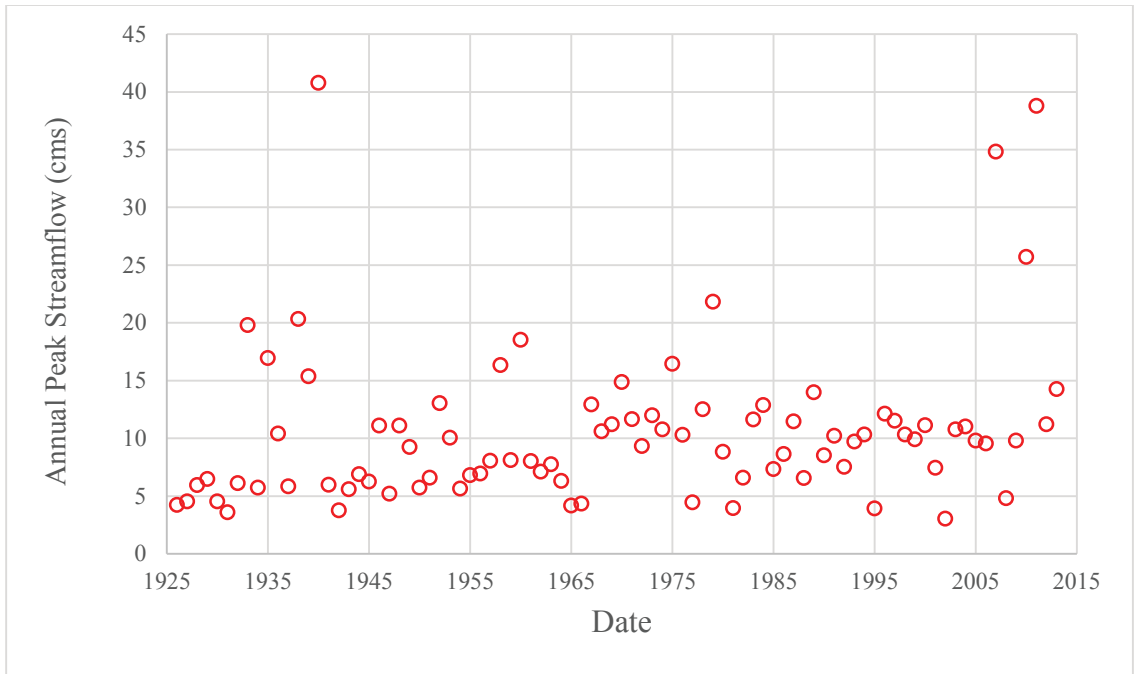


Figure A.5: Annual maximum flood series from 1926 to 2013 for USGS gauging station 01411000 (Great Egg Harbor River Watershed, NJ).

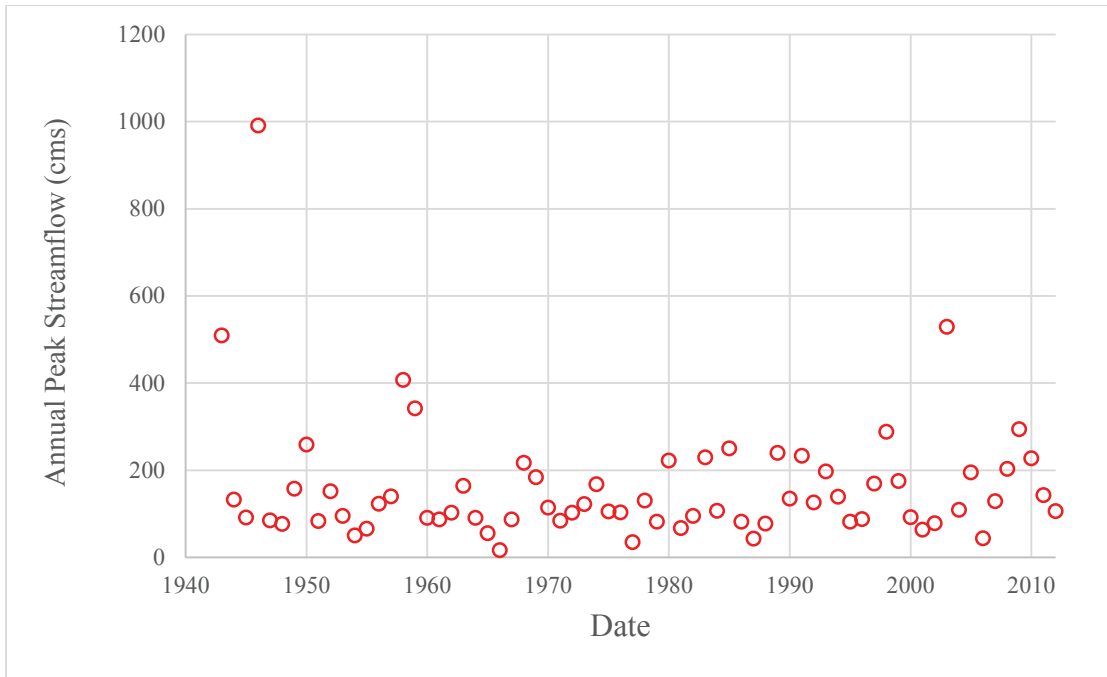


Figure A.6: Annual maximum flood series from 1943 to 2013 for USGS gauging station 03329700 (Deer Creek Watershed, IN).

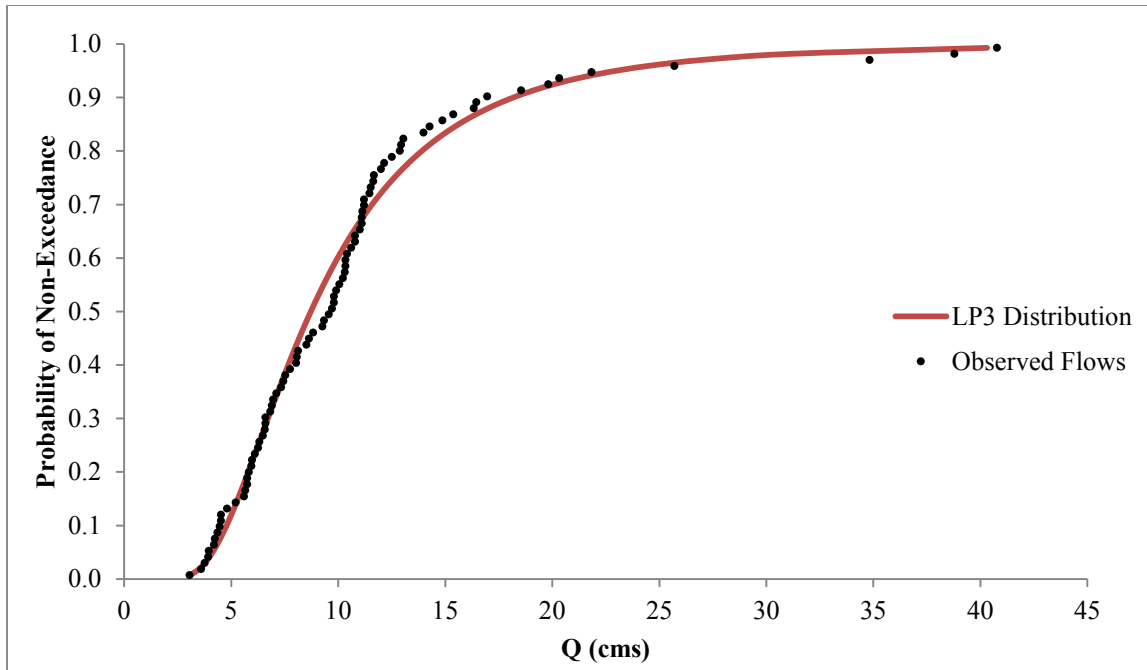


Figure A.7: Probability of non-exceedance plot with LP3 distribution fit to observed AMF series from 1926 to 2013 for USGS station 01411000 (Great Egg Harbor River Watershed, NJ).

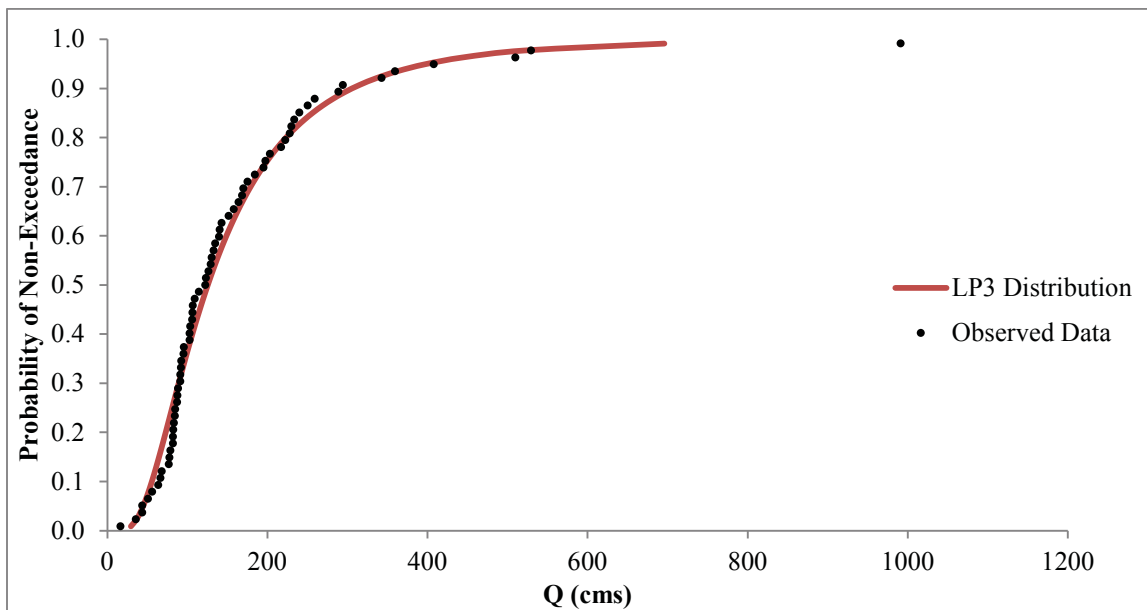


Figure A.8: Probability of non-exceedance plot with LP3 distribution fit to observed AMF series from 1943 to 2013 for USGS station 03329700 (Deer Creek Watershed, IN).

Appendix B. Historical Land Use Procedure and Results

This appendix provides flowcharts created to assist in outlining the methods employed in Chapter 3 for creating historical LULC data. In addition, spatial maps included herein provide general locations and information on historic aerial images clipped to selected watershed boundaries, both graphical and spatially visual historical LULC data, and further information regarding change analysis and transition maps.

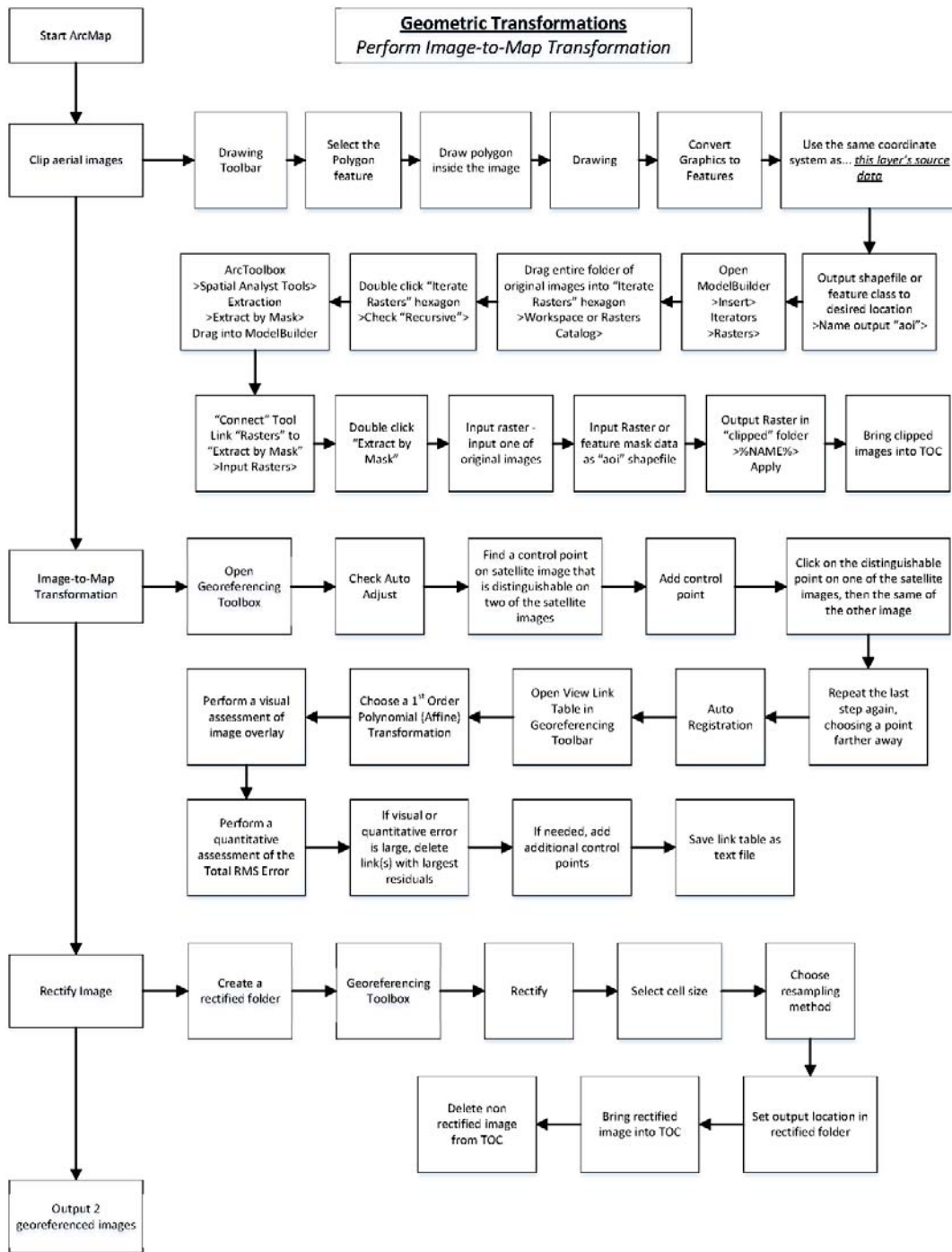


Figure B.1: Flowchart depicting the geometric transformation process on an image-to-image transformation. (Method developed by author).

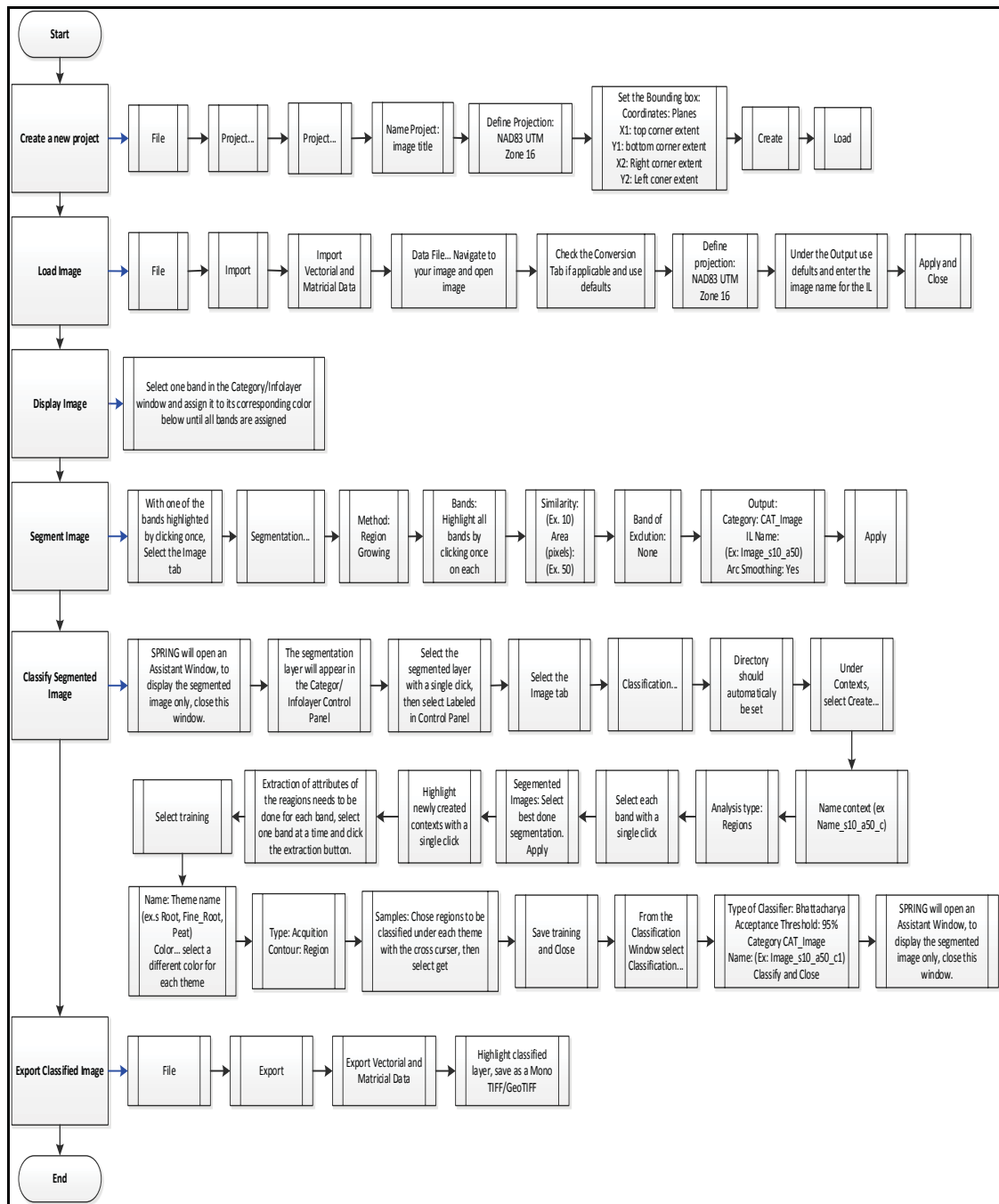


Figure B.2: Step-by-step flow chart instructions on segmentation and classification of an image. (Method developed by author).

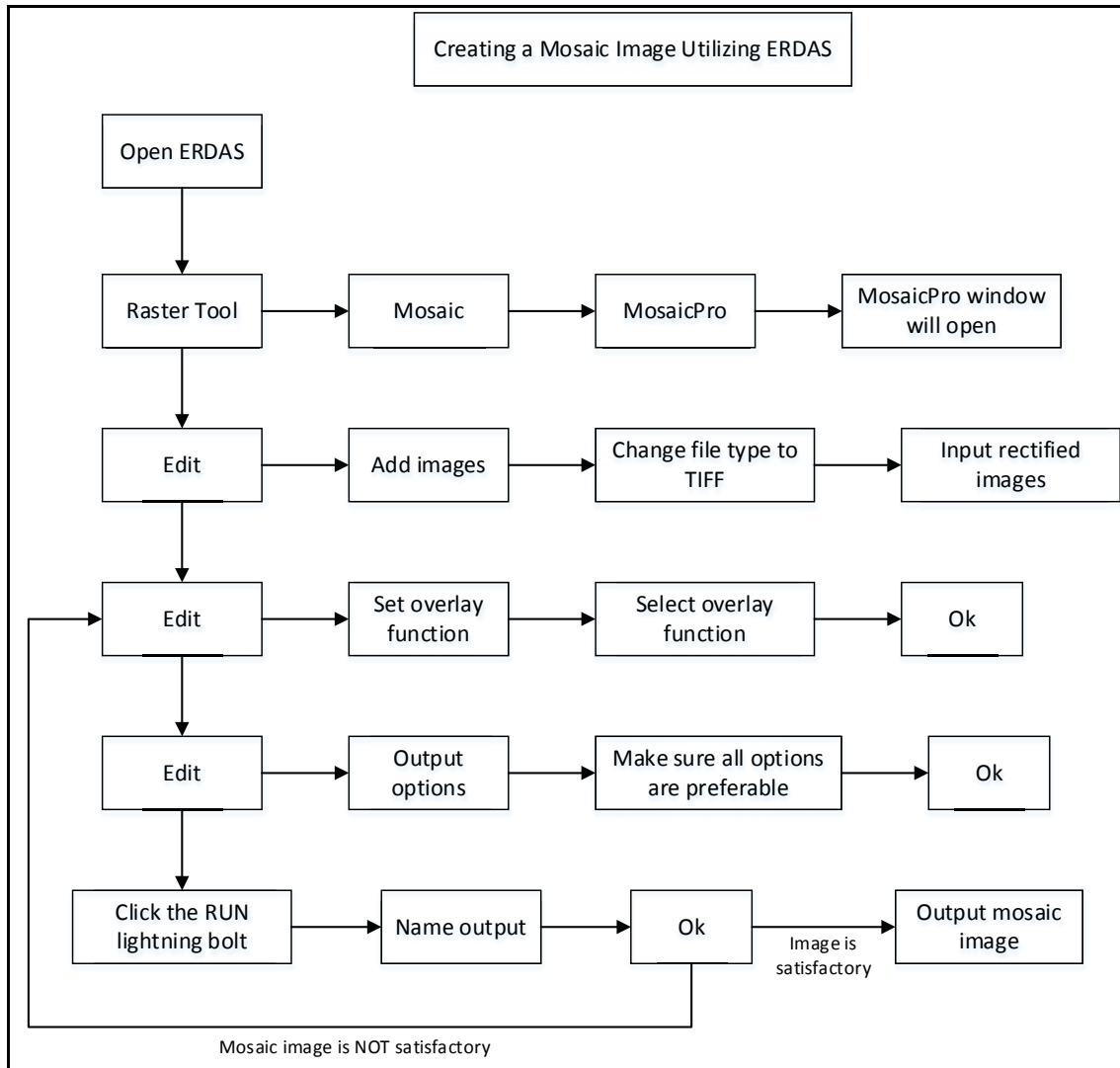


Figure B.3: Flowchart depicting the process to create a mosaic image using ERDAS IMAGINE. (Method developed by author).

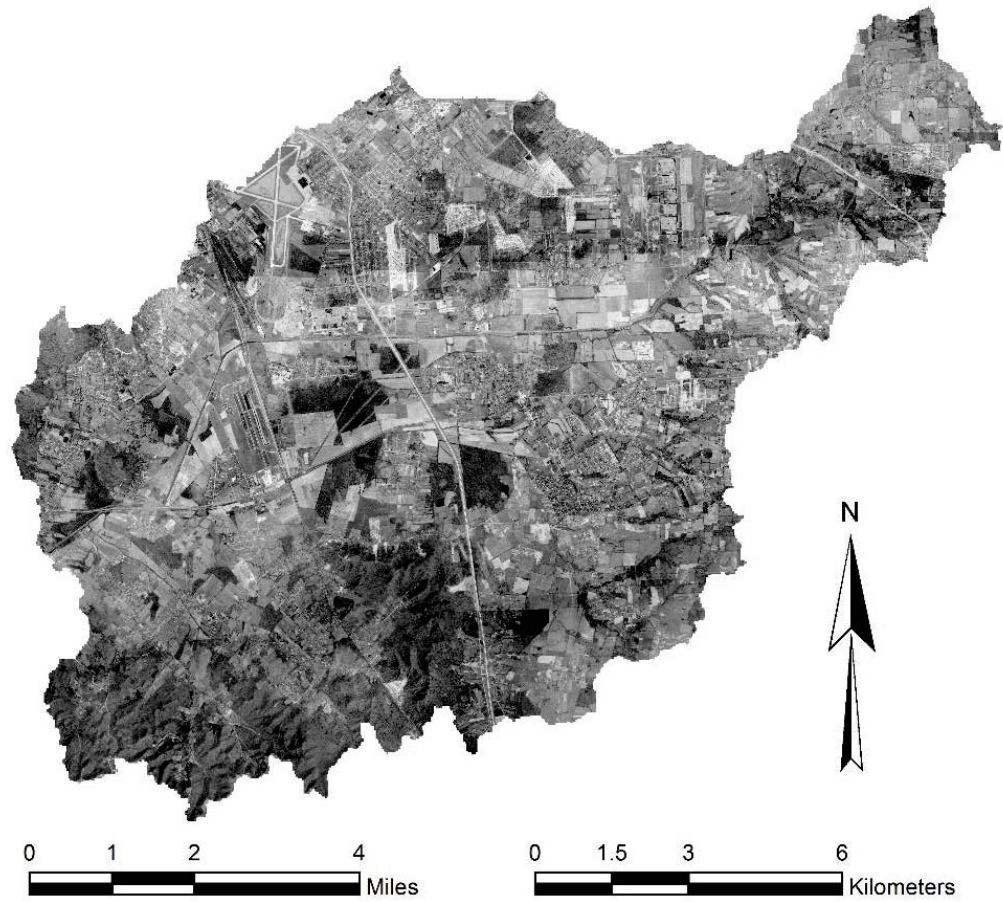


Figure B.4: 1959 mosaic aerial image clipped to watershed boundary for USGS station 03302000. (Image data source: EROS, 2015. Full image created by author).

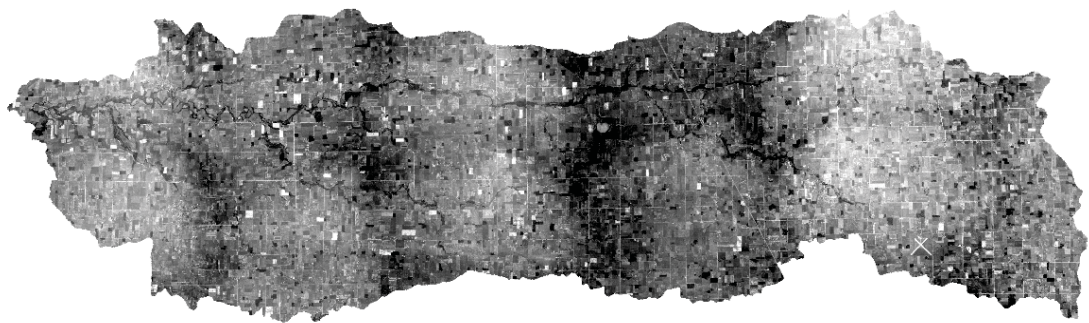


Figure B.5: 1952 mosaic aerial image clipped to watershed boundary for USGS station 03329700. (Image data source: EROS, 2015. Full image created by author).



Figure B.6: 1952 mosaic aerial image clipped to watershed boundary for USGS station 04099510. (Image data source: EROS, 2015. Full image created by author).

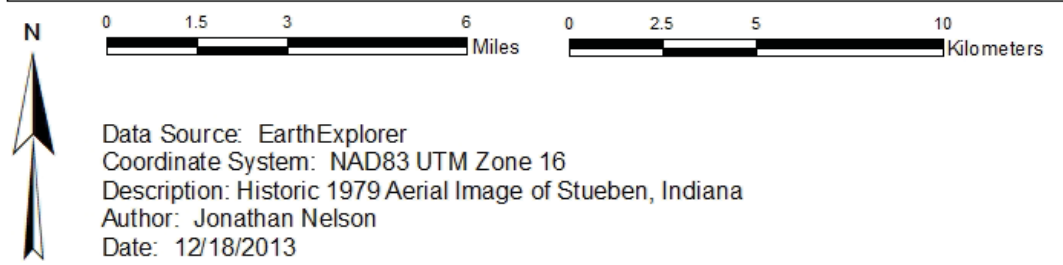
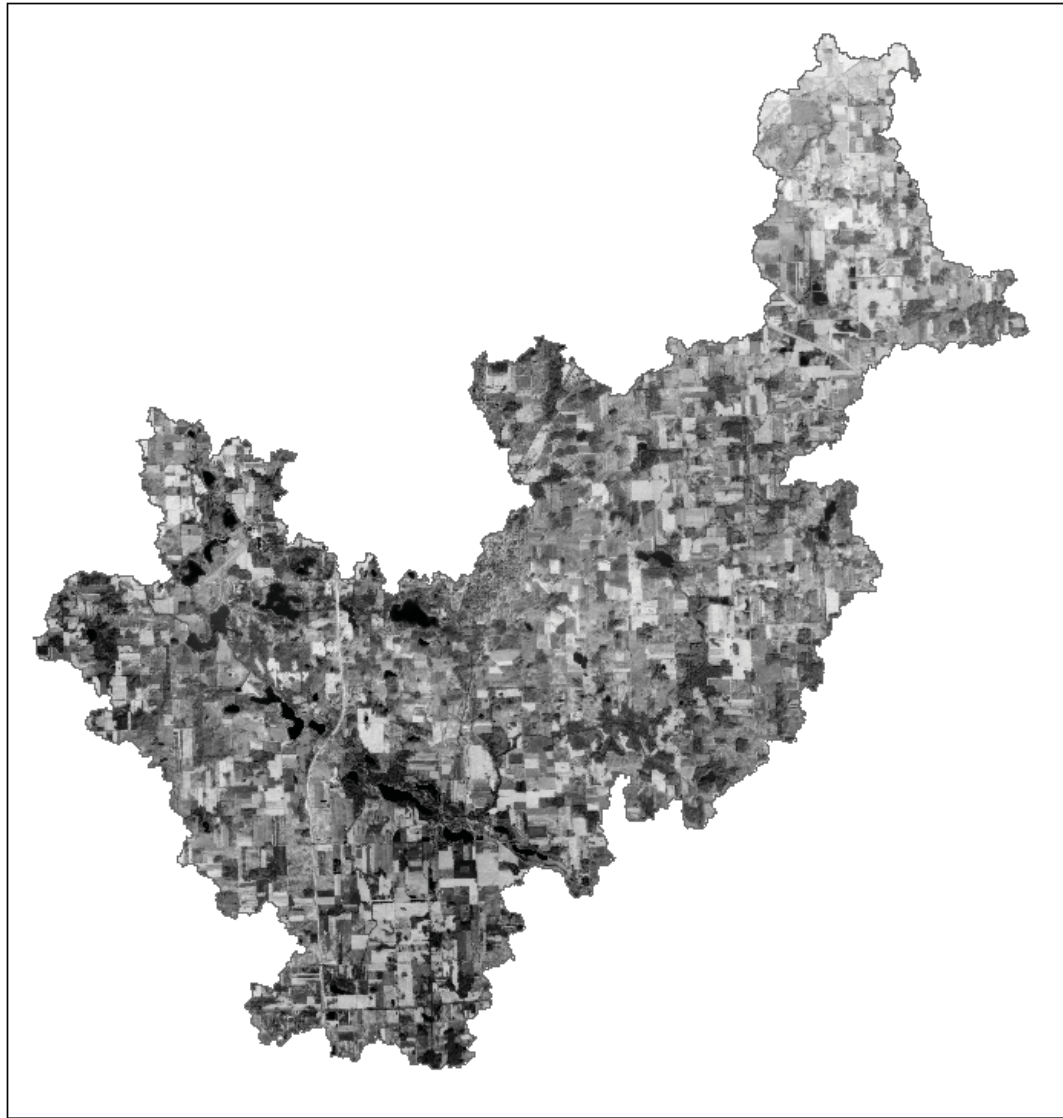


Figure B.7: 1979 mosaic aerial image clipped to watershed boundary for USGS station 04099510. (Image data source: EROS, 2015. Full image created by author).

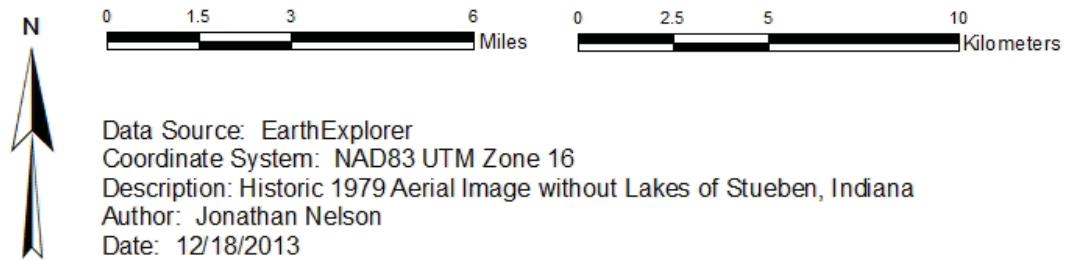
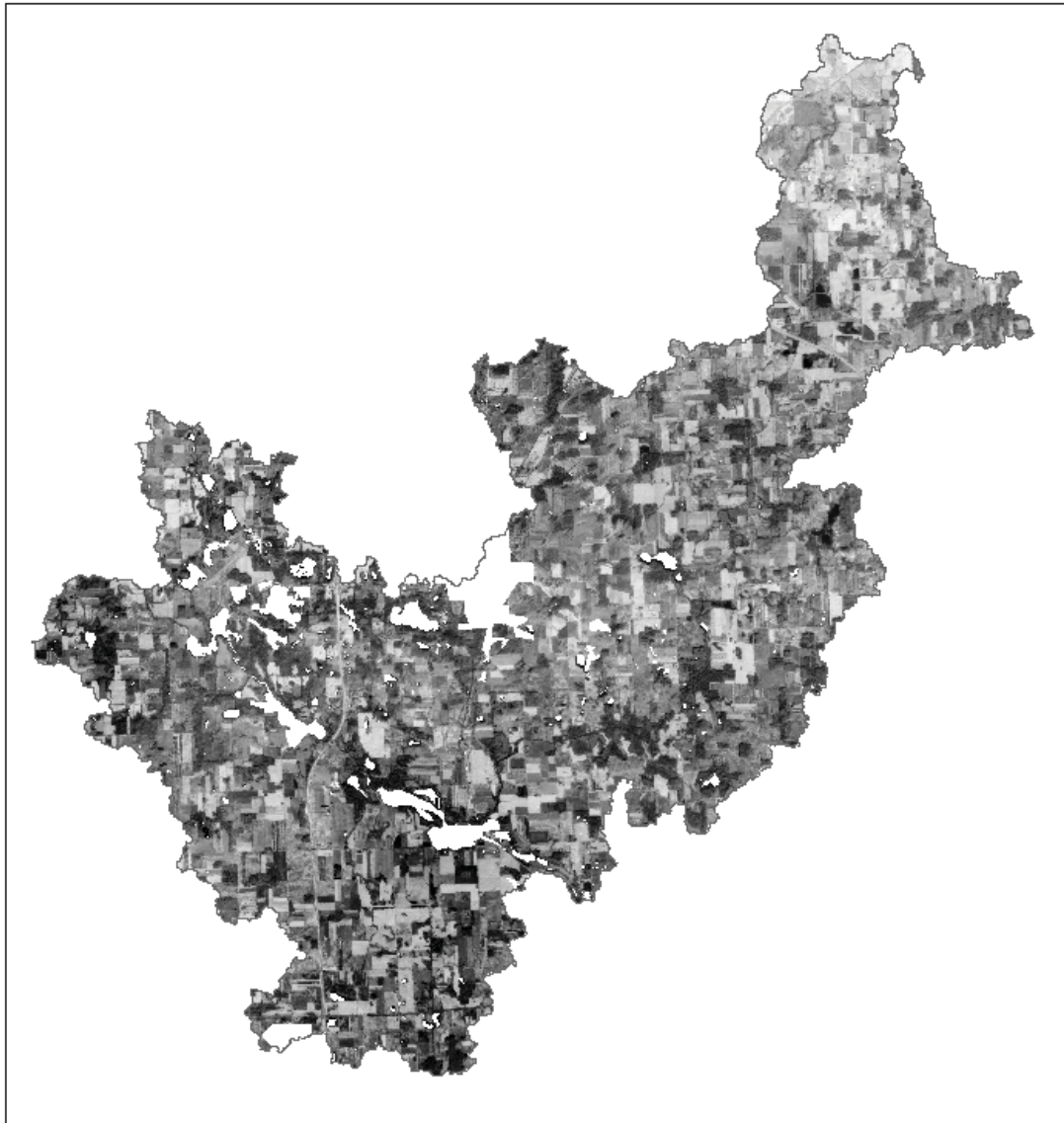


Figure B.8: 1979 mosaic aerial image clipped to watershed boundary for USGS station 04099510, with any open water or urban developed land use class types erased from the image. (Image data source: EROS, 2015. Full image created by author).

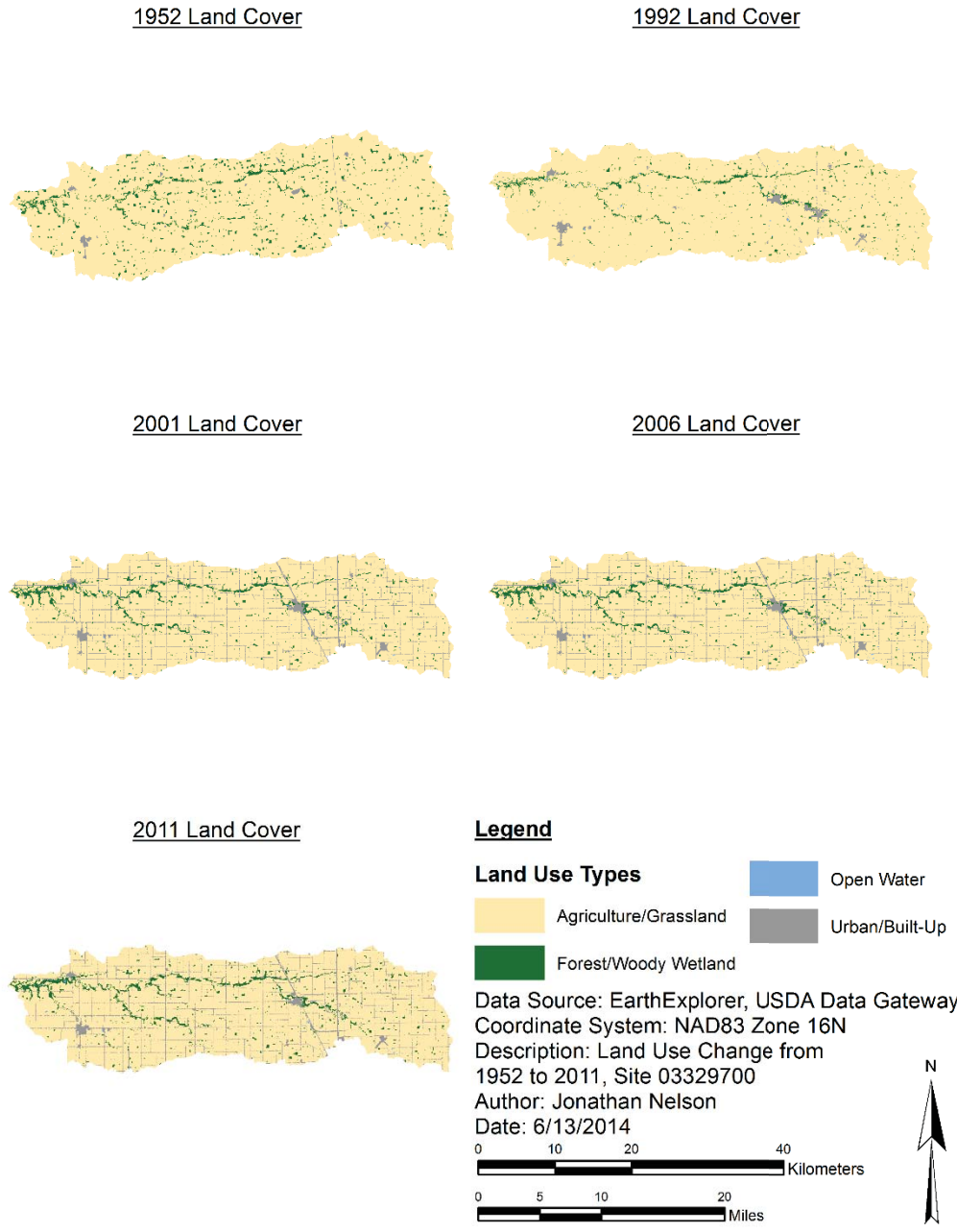


Figure B.9: Land use progression from 1952 to 2011 for USGS station 03329700. Maps for 1992 to 2011 employ generalized NLCD LULC classes.

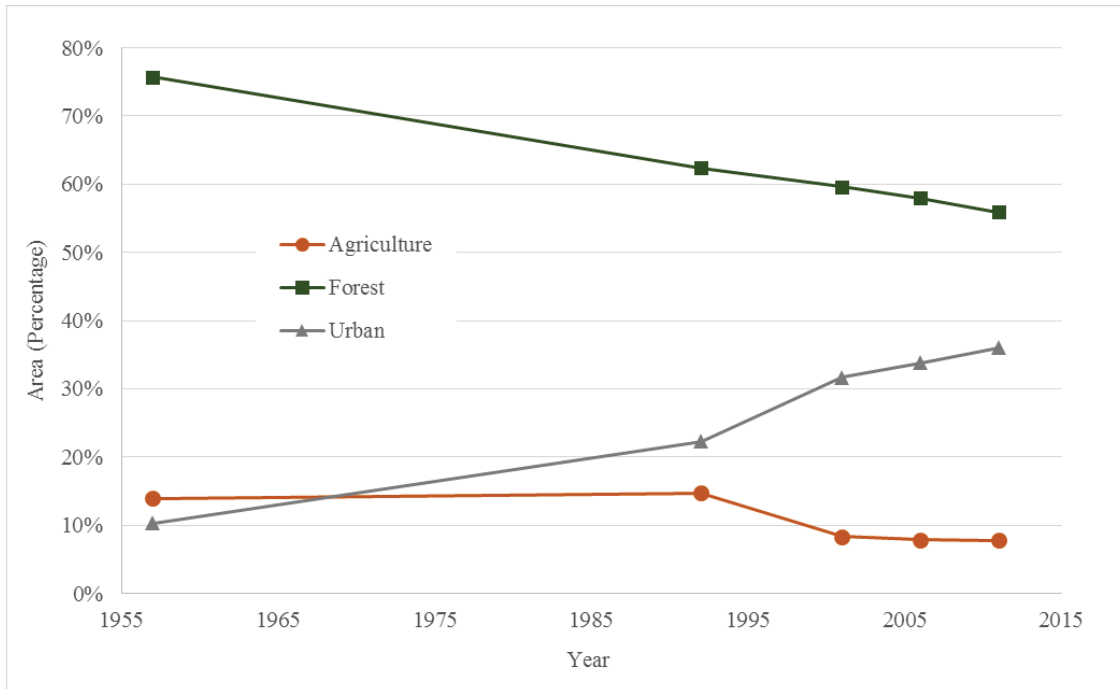


Figure B.10: Graphical representation of LULC change between 1957 and 2011 for Great Egg Harbor River, NJ (USGS station 01411000).

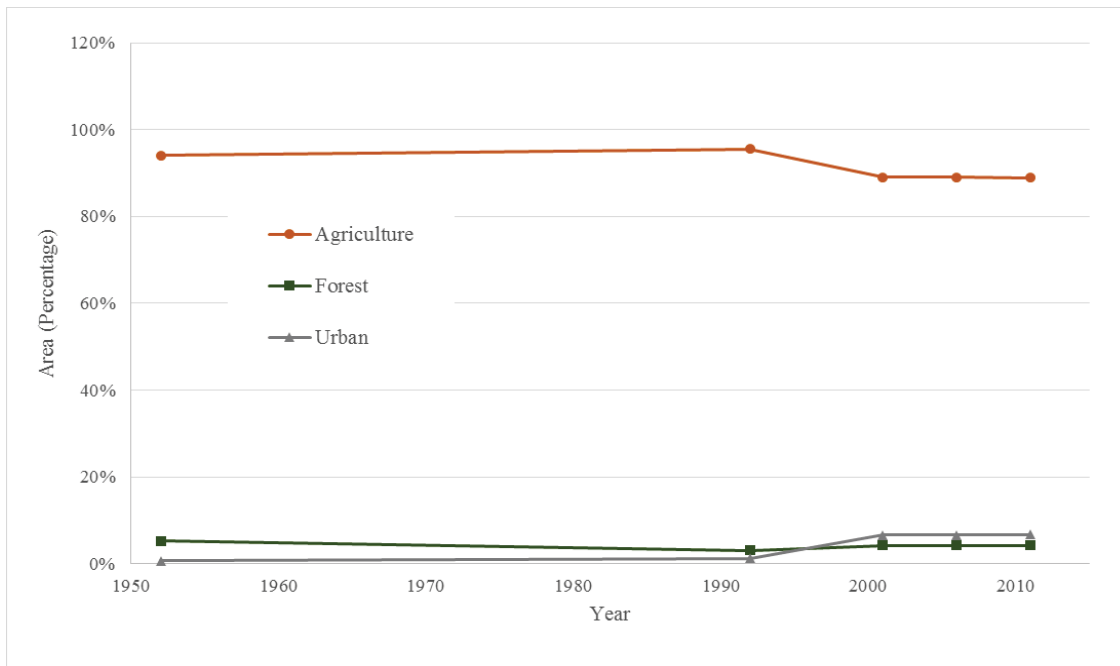


Figure B.11: Graphical representation of LULC change between 1952 and 2011 for Deer Creek, IN (USGS station 03329700).

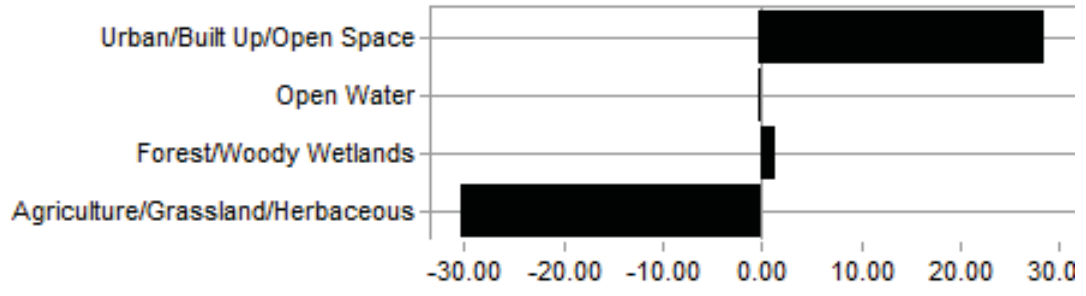


Figure B.12: Net change (mi²) of generalized LULC types observed between 1957 and 2011 for Great Egg Harbor River, NJ (USGS station 01411000) using LCM change analysis.

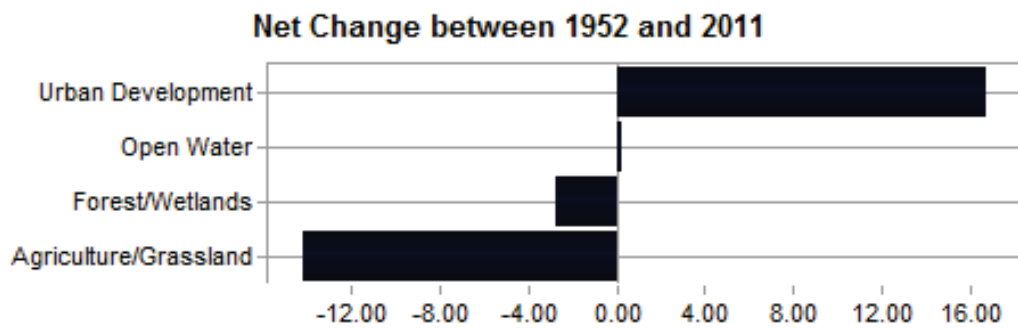


Figure B.13: Net change (mi²) of generalized LULC types observed between 1957 and 2011 for Deer Creek, IN (USGS station 03329700) using LCM change analysis.

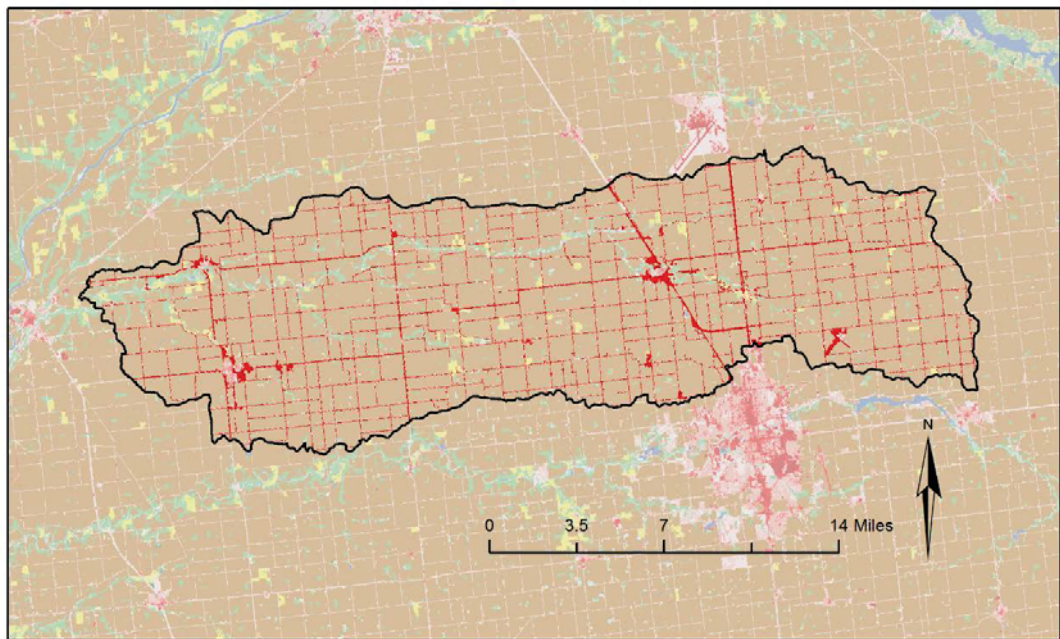


Figure B.14: Change analysis transition from agricultural to urban developed LULC type (in RED) between 1957 and 2011 for Deer Creek, IN (USGS station 03329700).

Appendix C. Future Predictions of LULC Conditions

This appendix includes spatial maps created in ArcMap 10.2 featuring the progression of predicted LULC conditions based on the FORE-SCE scenarios for select watersheds.

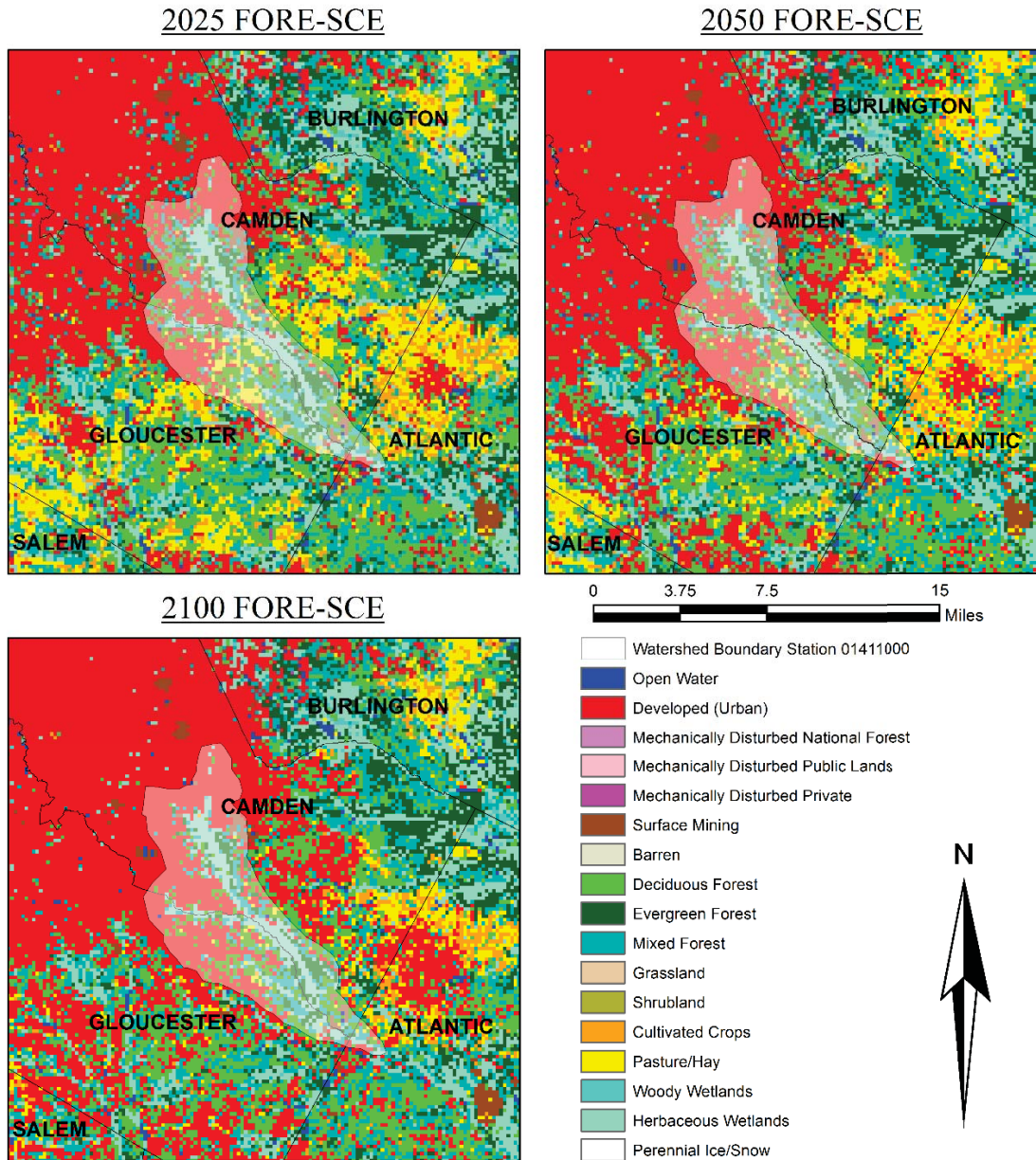


Figure C.1: Projected LULC conditions from FORE-SCE Scenario A1B for Great Egg Harbor River, NJ (USGS station 01411000). (Data Source: USGS, 2014).

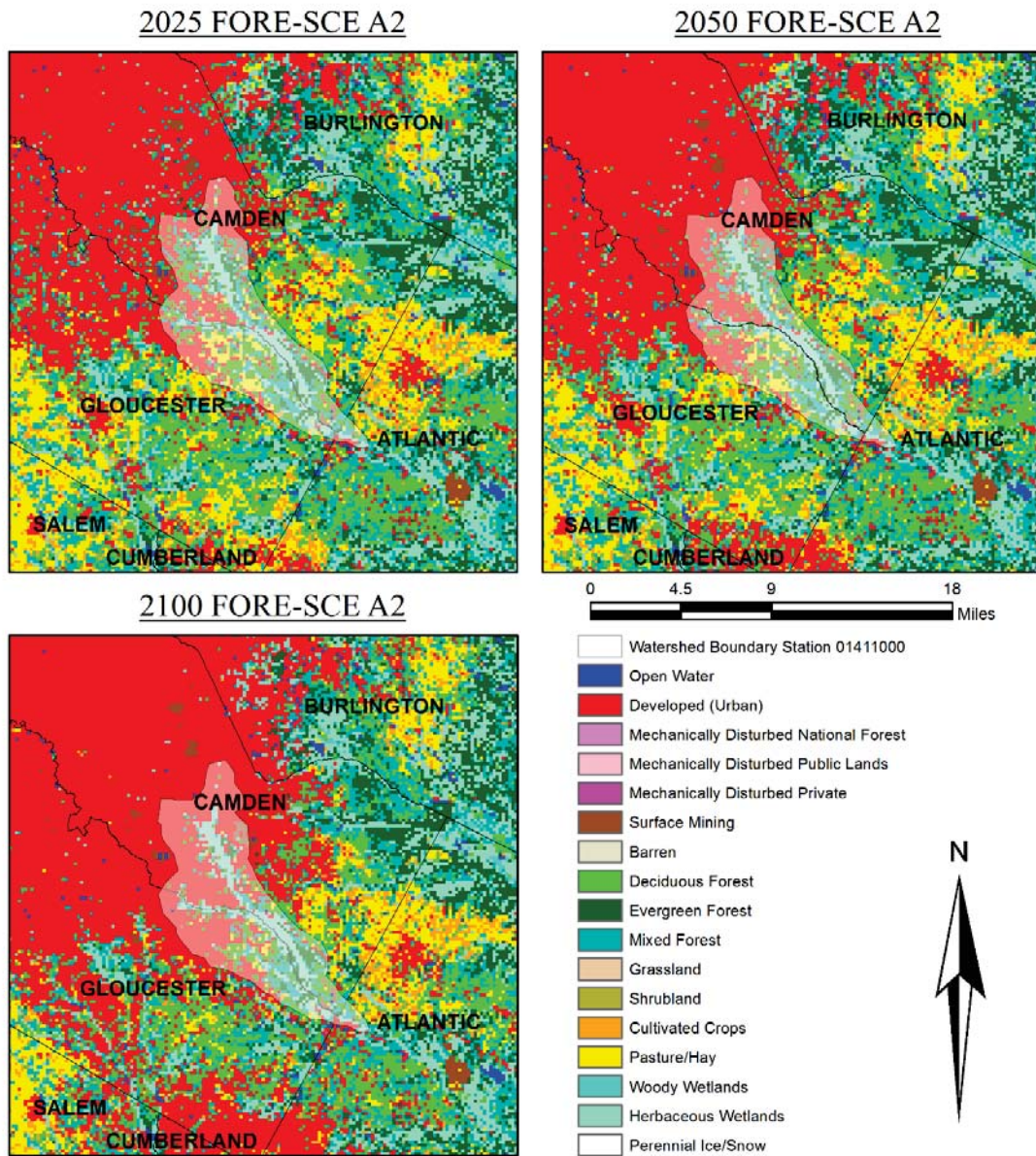


Figure C.2: Projected LULC conditions from FORE-SCE Scenario A2 for Great Egg Harbor River, NJ (USGS station 01411000). (Data Source: USGS, 2014).

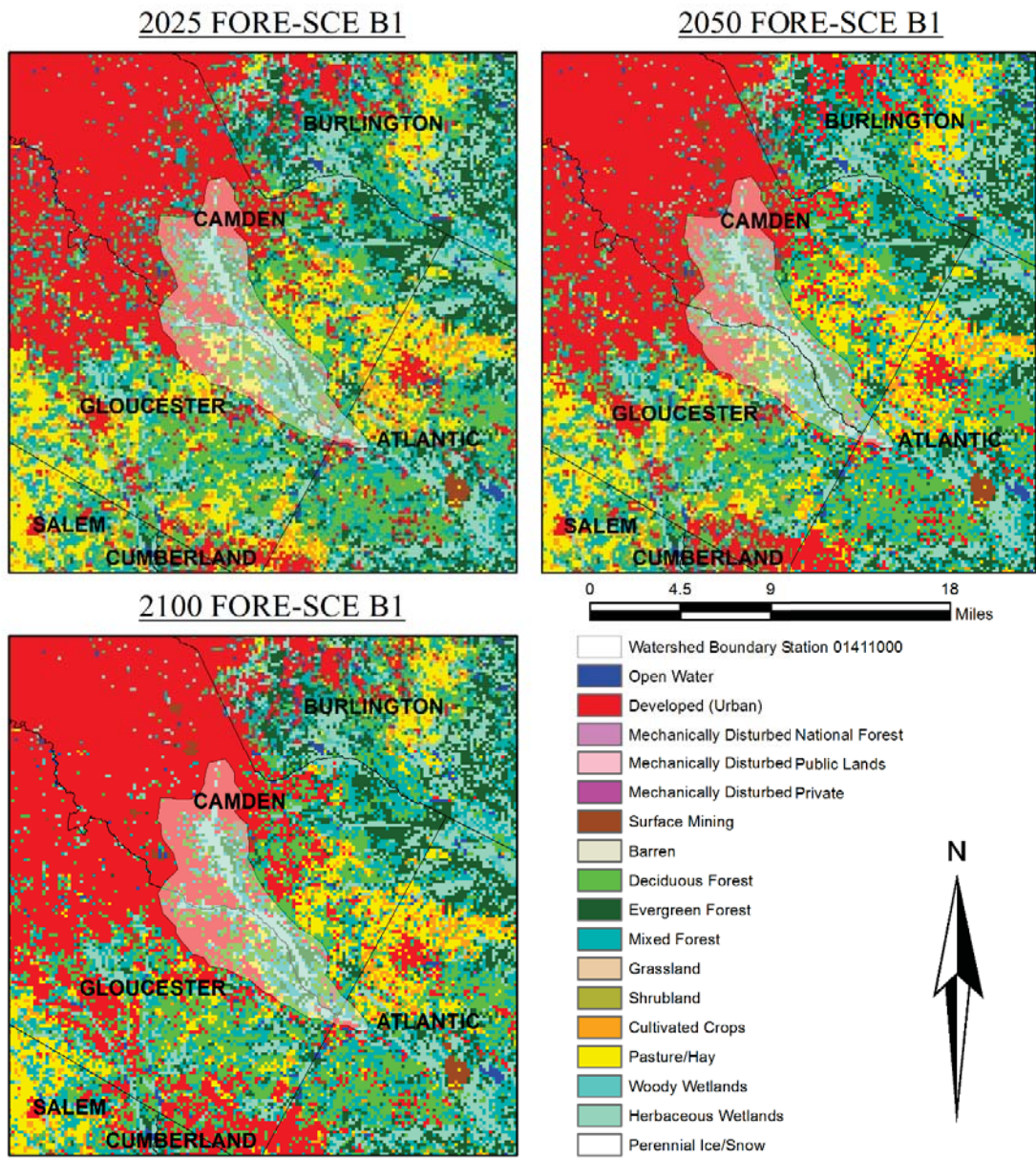


Figure C.3: Projected LULC conditions from FORE-SCE Scenario B1 for Great Egg Harbor River, NJ (USGS station 01411000). (Data Source: USGS, 2014).

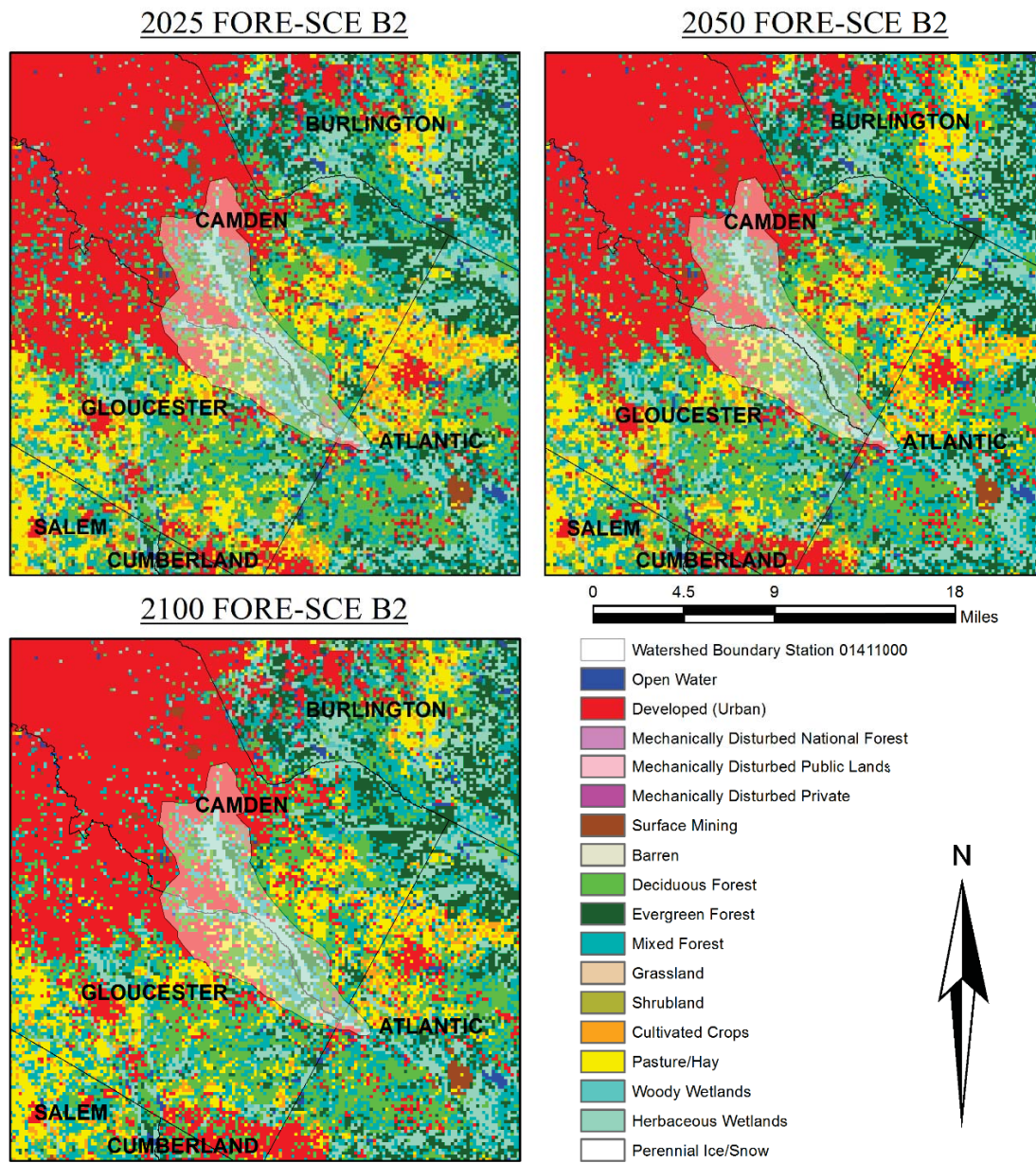


Figure C.4: Projected LULC conditions from FORE-SCE Scenario B2 for Great Egg Harbor River, NJ (USGS station 01411000). (Data Source: USGS, 2014).

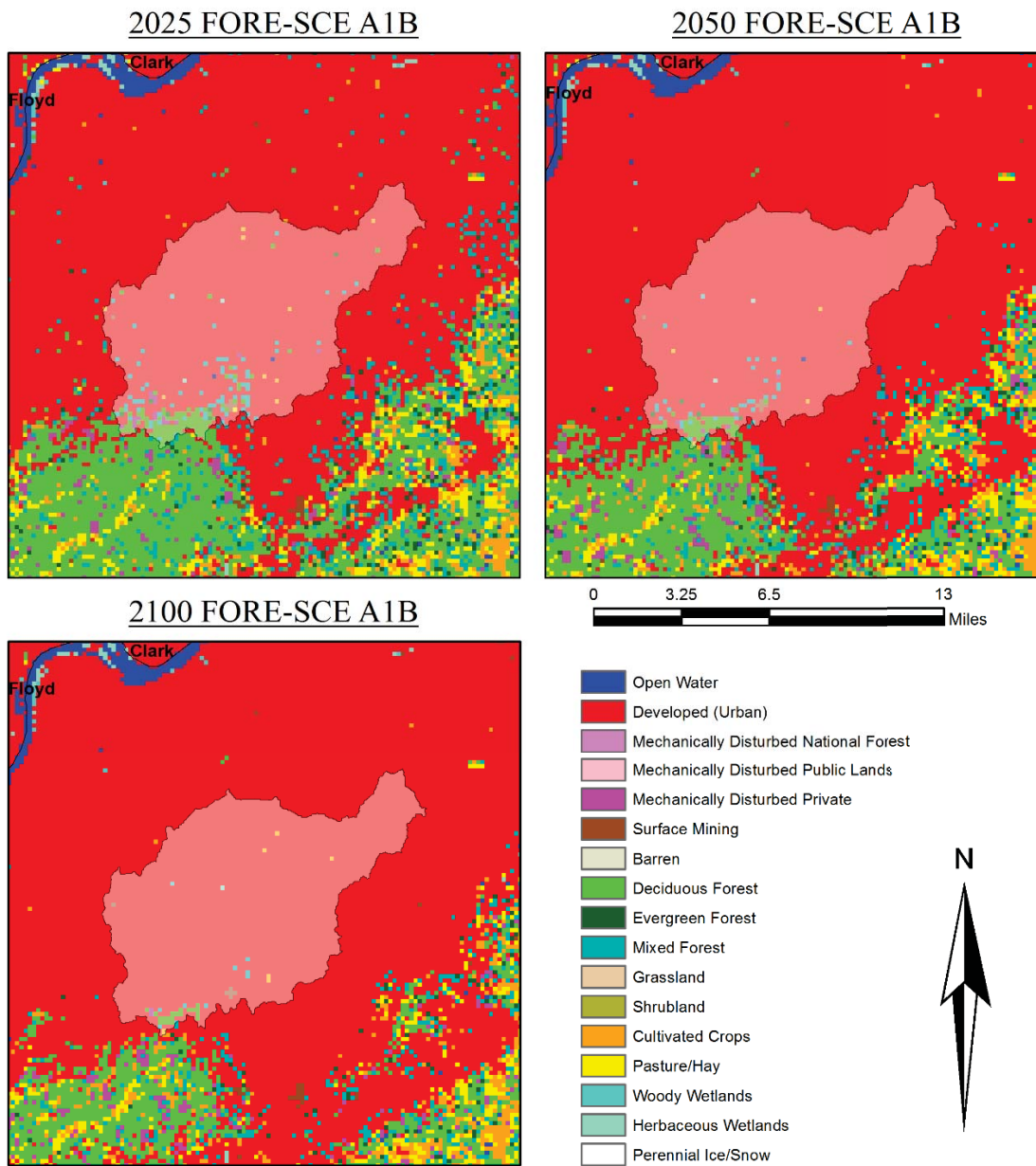


Figure C.5: Projected LULC conditions from FORE-SCE Scenario A1B for Pond Creek, KY (USGS station 03302000). (Data Source: USGS, 2014).

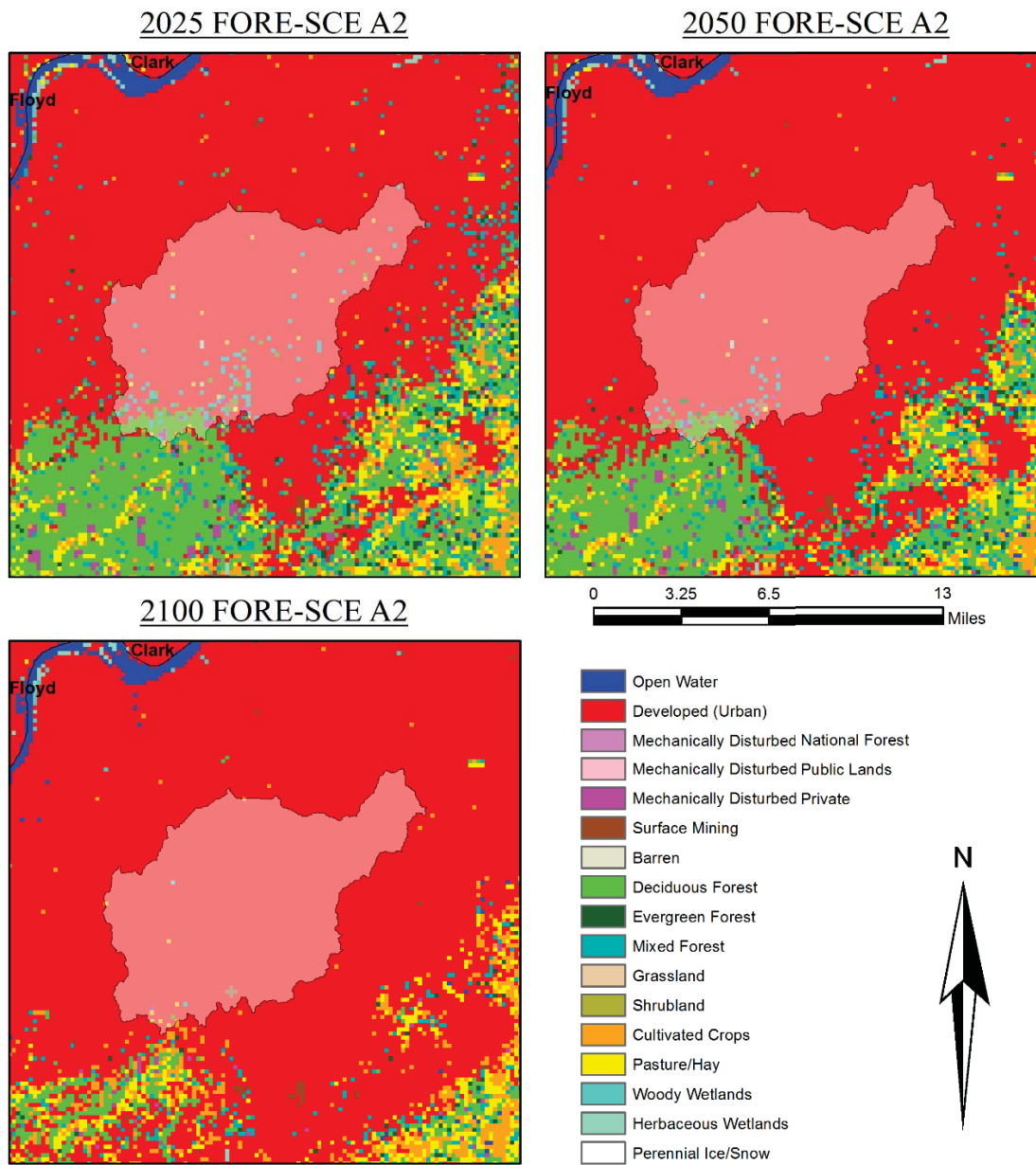


Figure C.6: Projected LULC conditions from FORE-SCE Scenario A2 for Pond Creek, KY (USGS station 03302000). (Data Source: USGS, 2014).

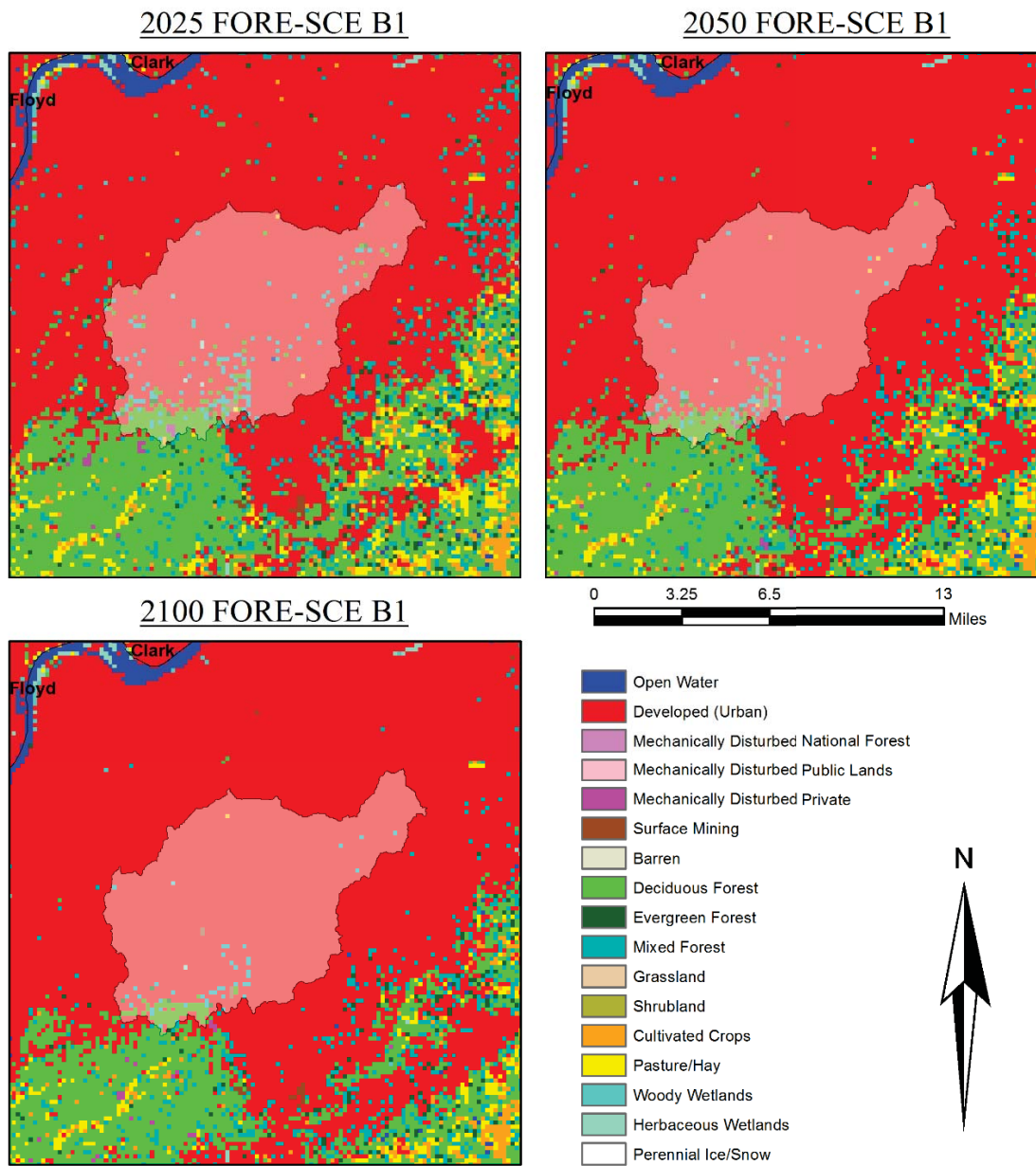


Figure C.7: Projected LULC conditions from FORE-SCE Scenario B1 for Pond Creek, KY (USGS station 03302000). (Data Source: USGS, 2014).

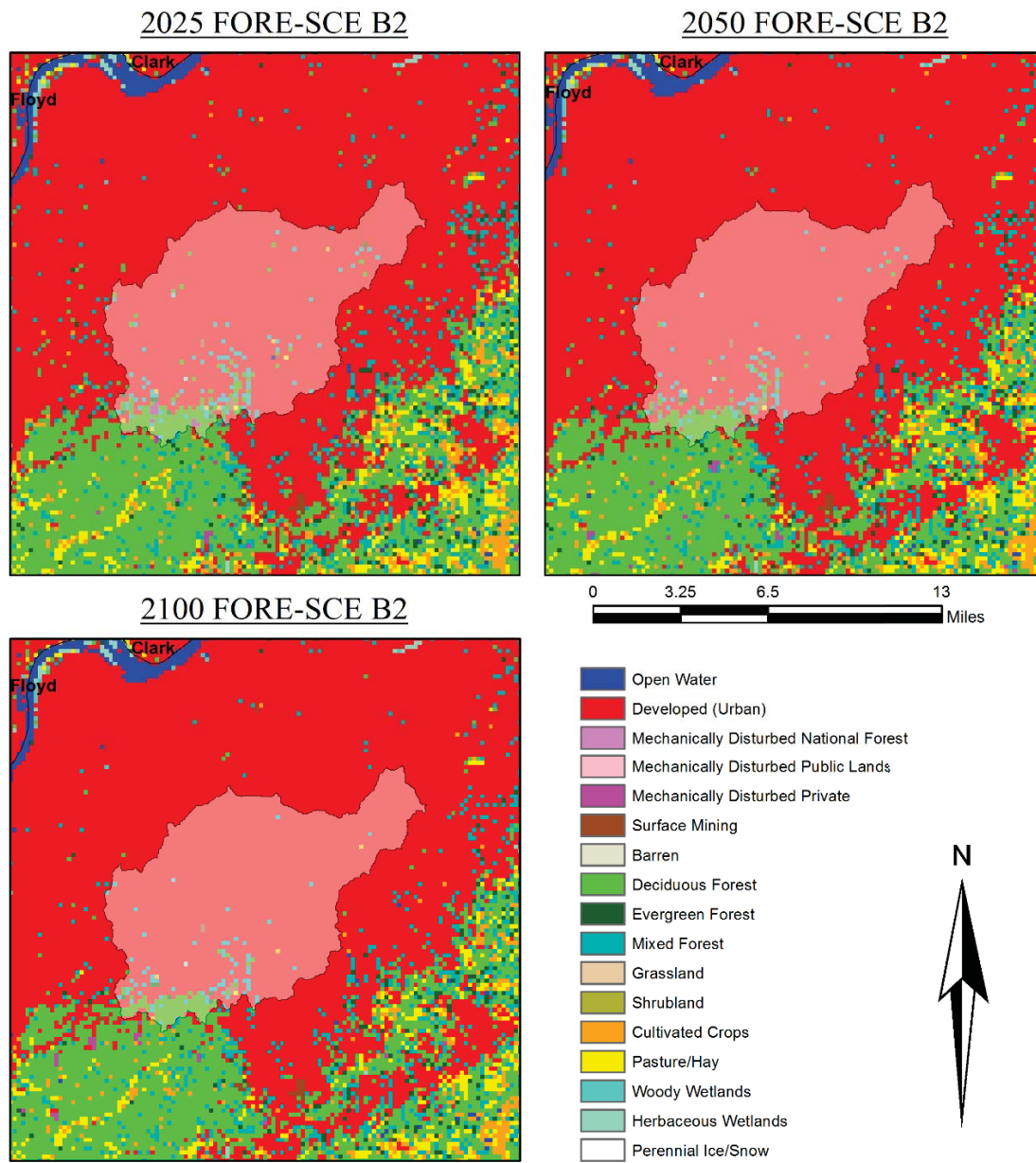


Figure C.8: Projected LULC conditions from FORE-SCE Scenario B2 for Pond Creek, KY (USGS station 03302000). (Data Source: USGS, 2014).

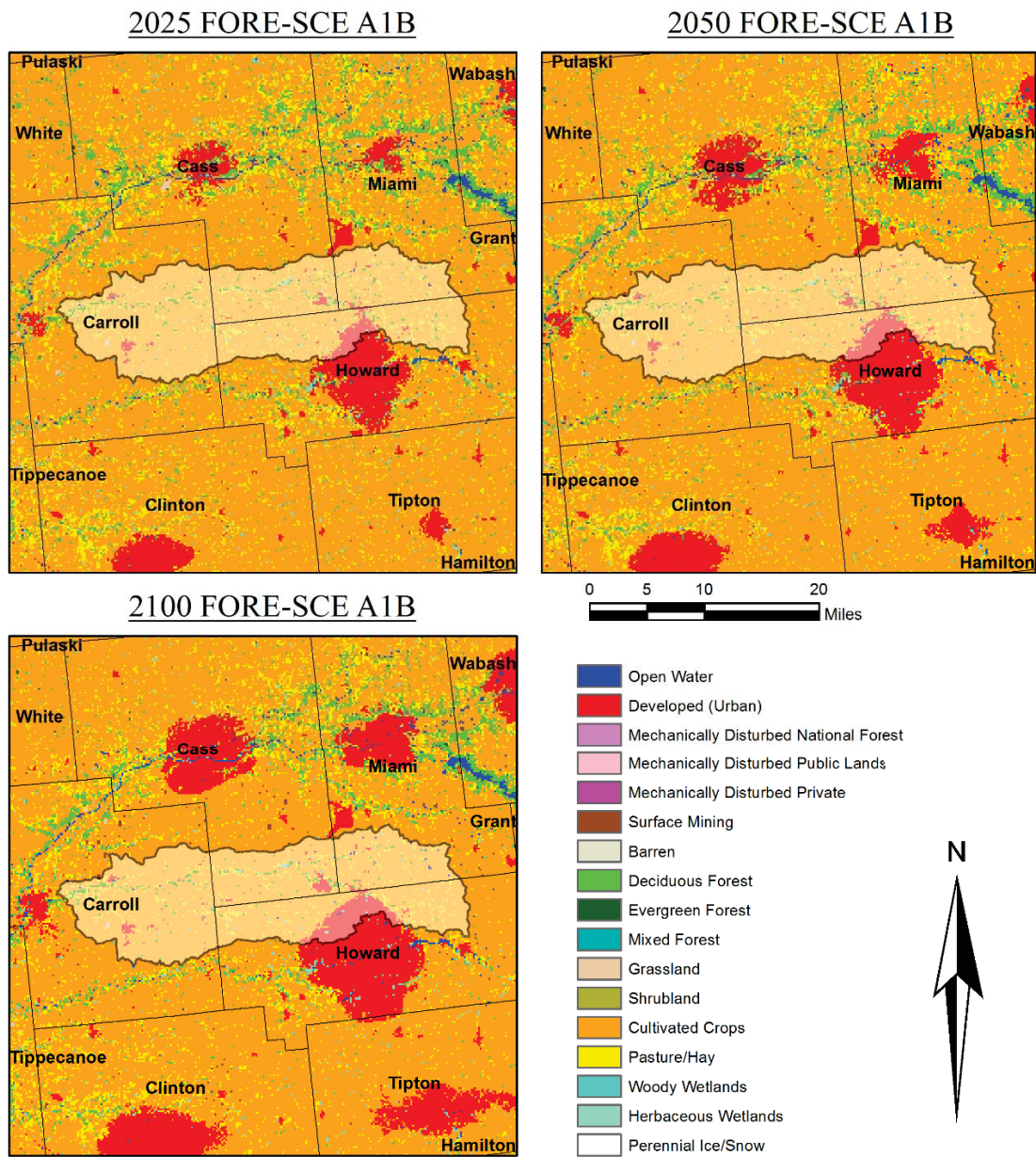


Figure C.9: Projected LULC conditions from FORE-SCE scenario A1B for Deer Creek, IN (USGS station 03329700). (Data Source: USGS, 2014).

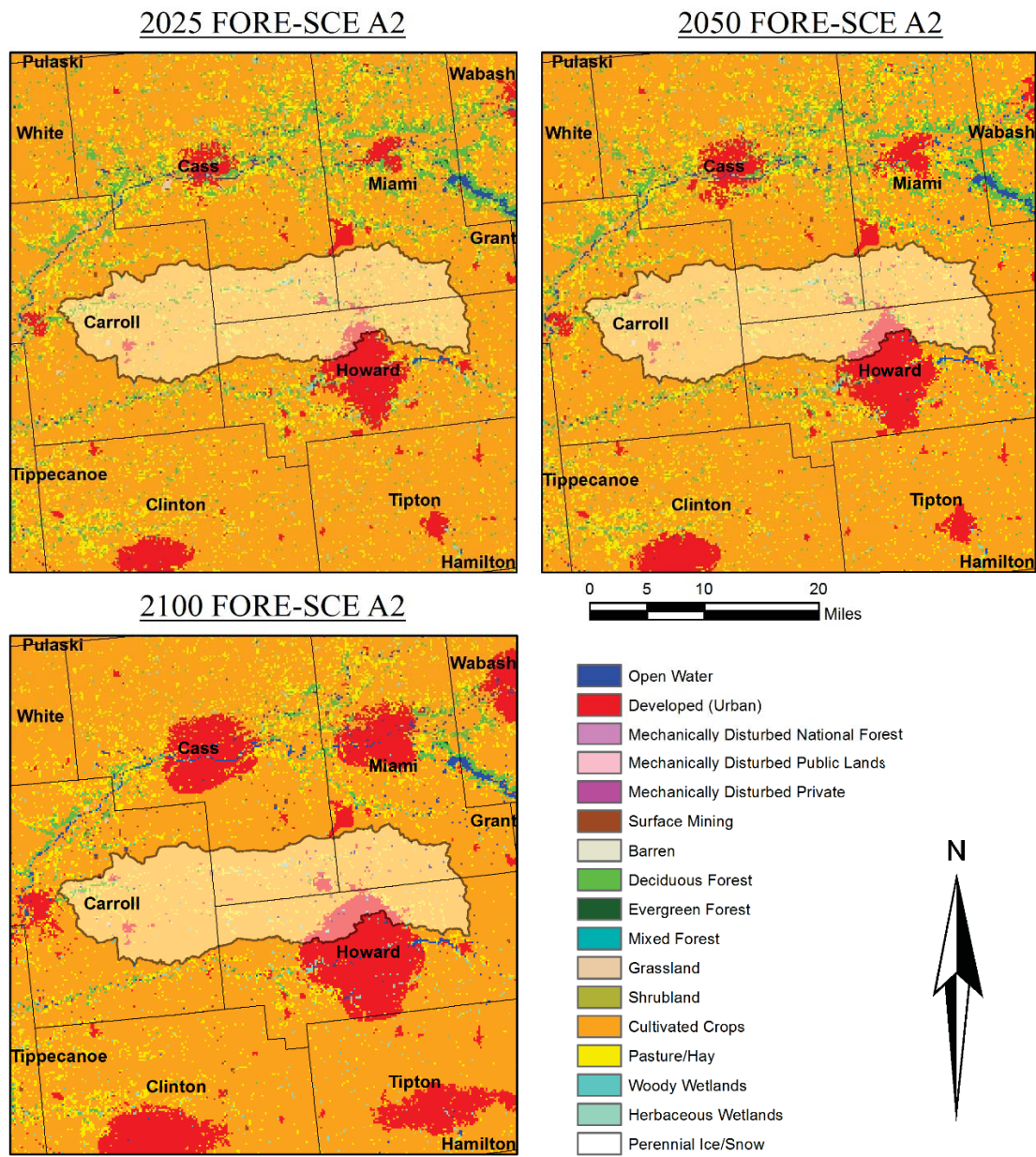


Figure C.10: Projected LULC conditions from FORE-SCE scenario A2 for Deer Creek, IN (USGS station 03329700). (Data Source: USGS, 2014).

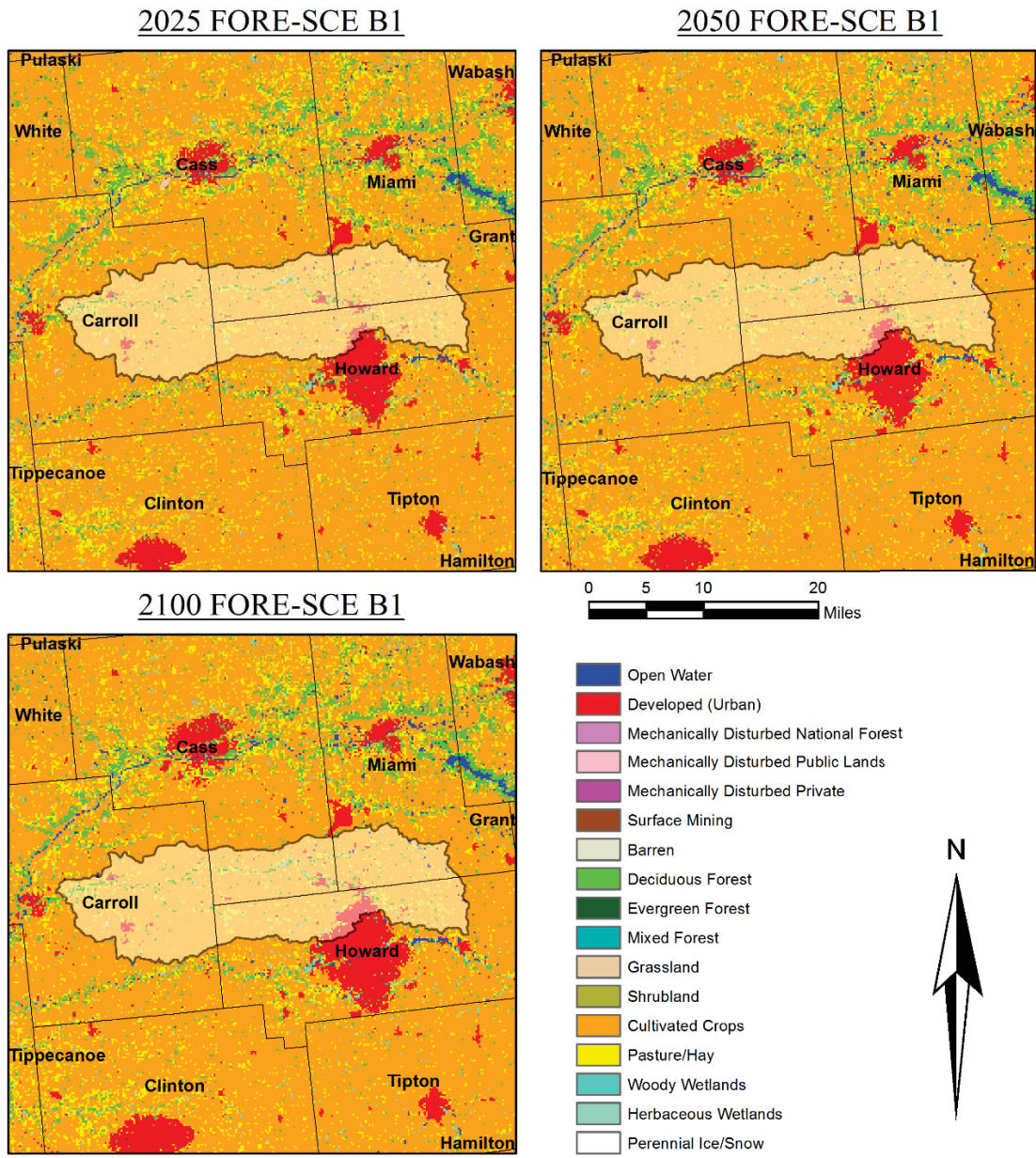


Figure C.11: Projected LULC conditions from FORE-SCE scenario B1 for Deer Creek, IN (USGS station 03329700). (Data Source: USGS, 2014).

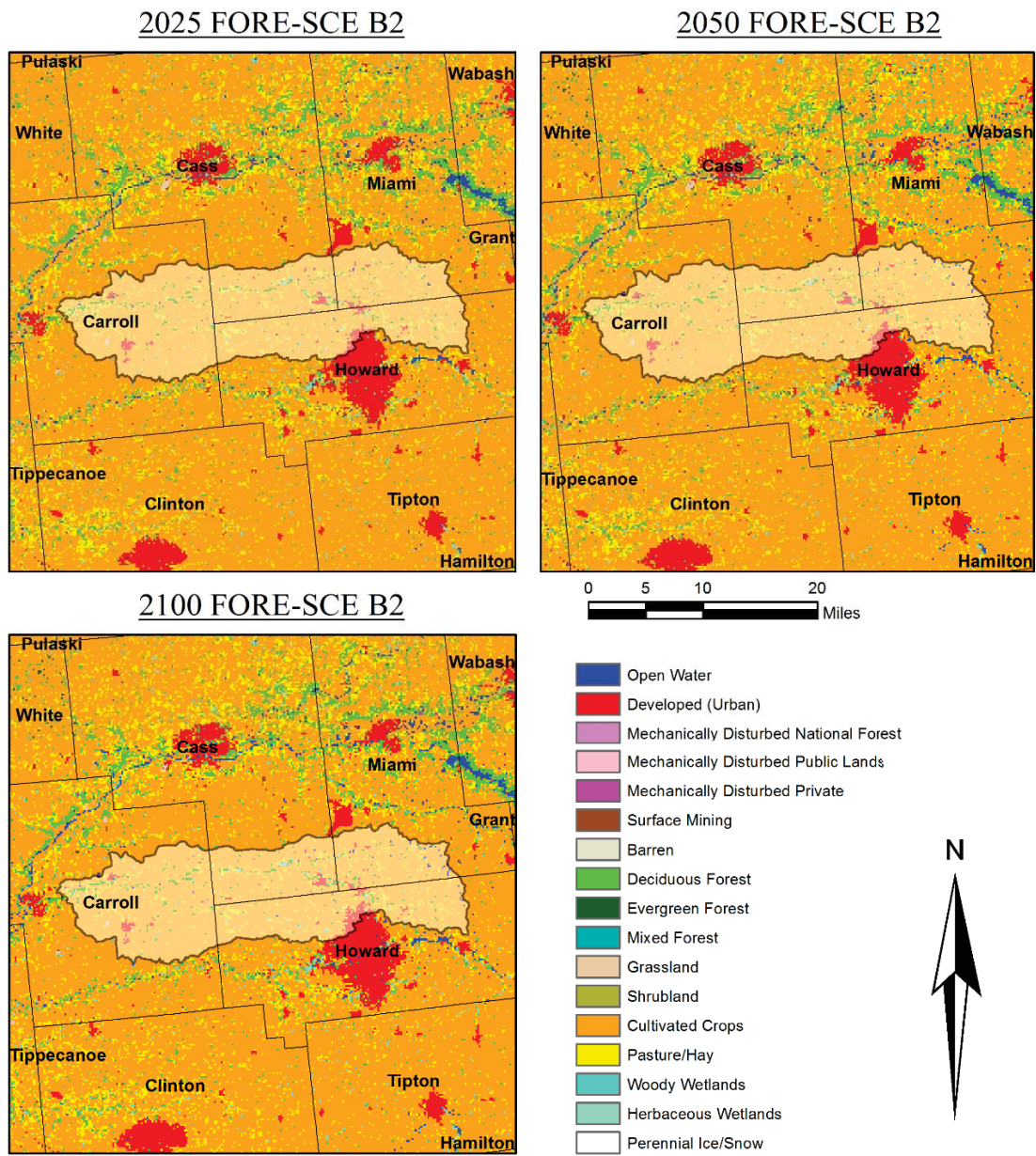


Figure C.12: Projected LULC conditions from FORE-SCE scenario B2 for Deer Creek, IN (USGS station 03329700). (Data Source: USGS, 2014).

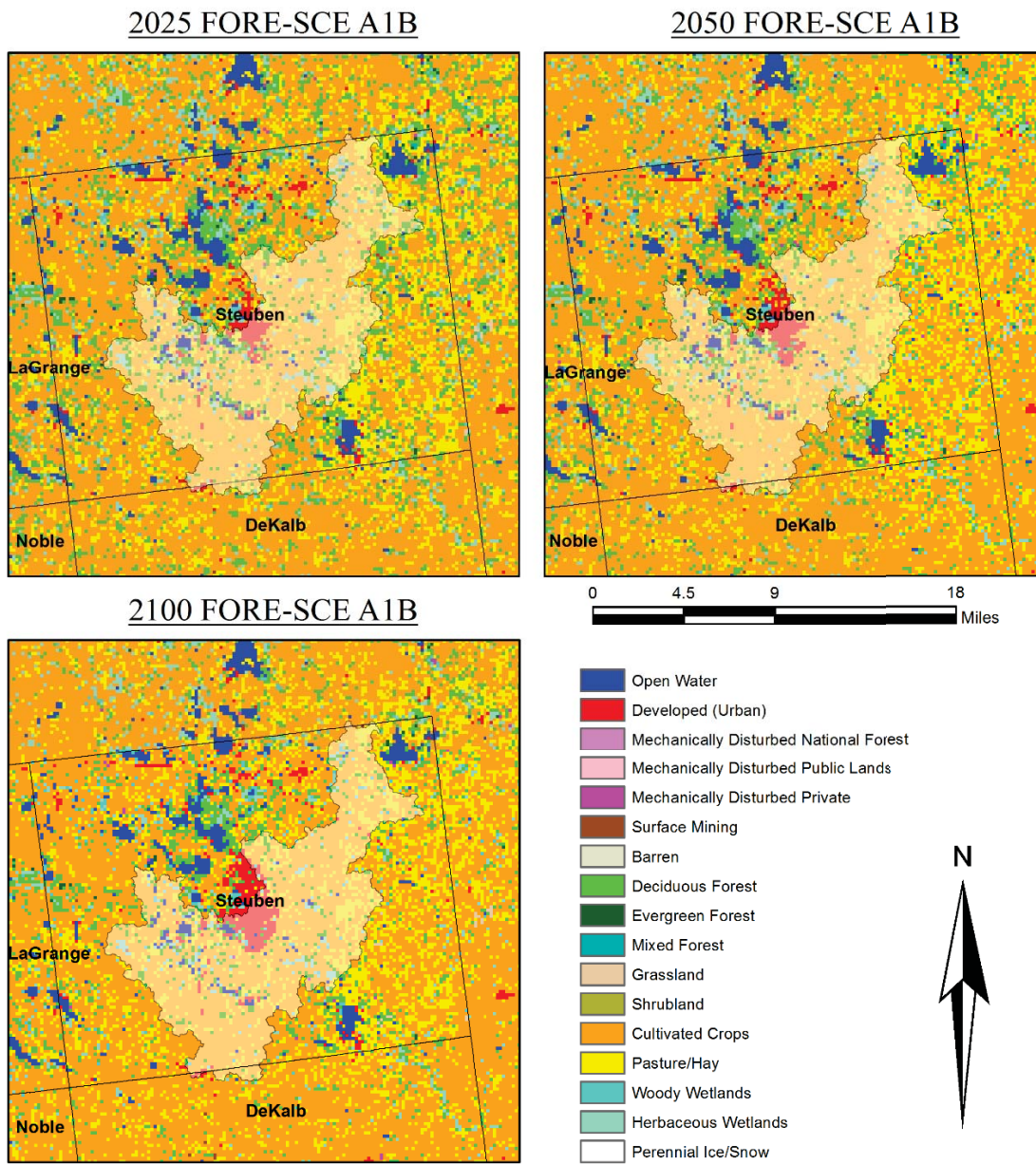


Figure C.13: Projected LULC conditions from FORE-SCE scenario A1B for Pigeon Creek, IN (USGS Station 0499510). (Data Source: USGS, 2014).

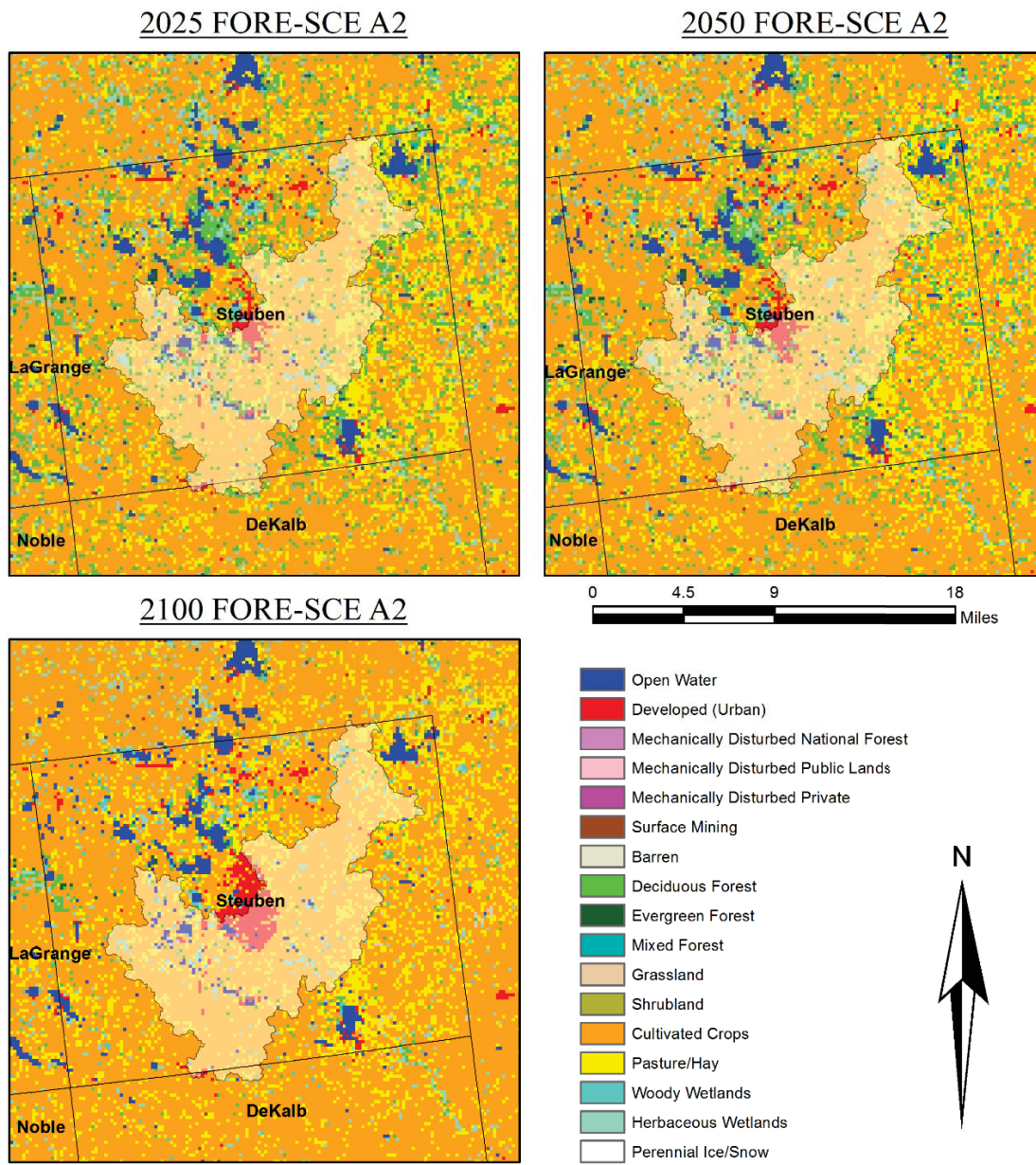


Figure C.14: Projected LULC conditions from FORE-SCE scenario A2 for Pigeon Creek, IN (USGS Station 0499510). (Data Source: USGS, 2014).

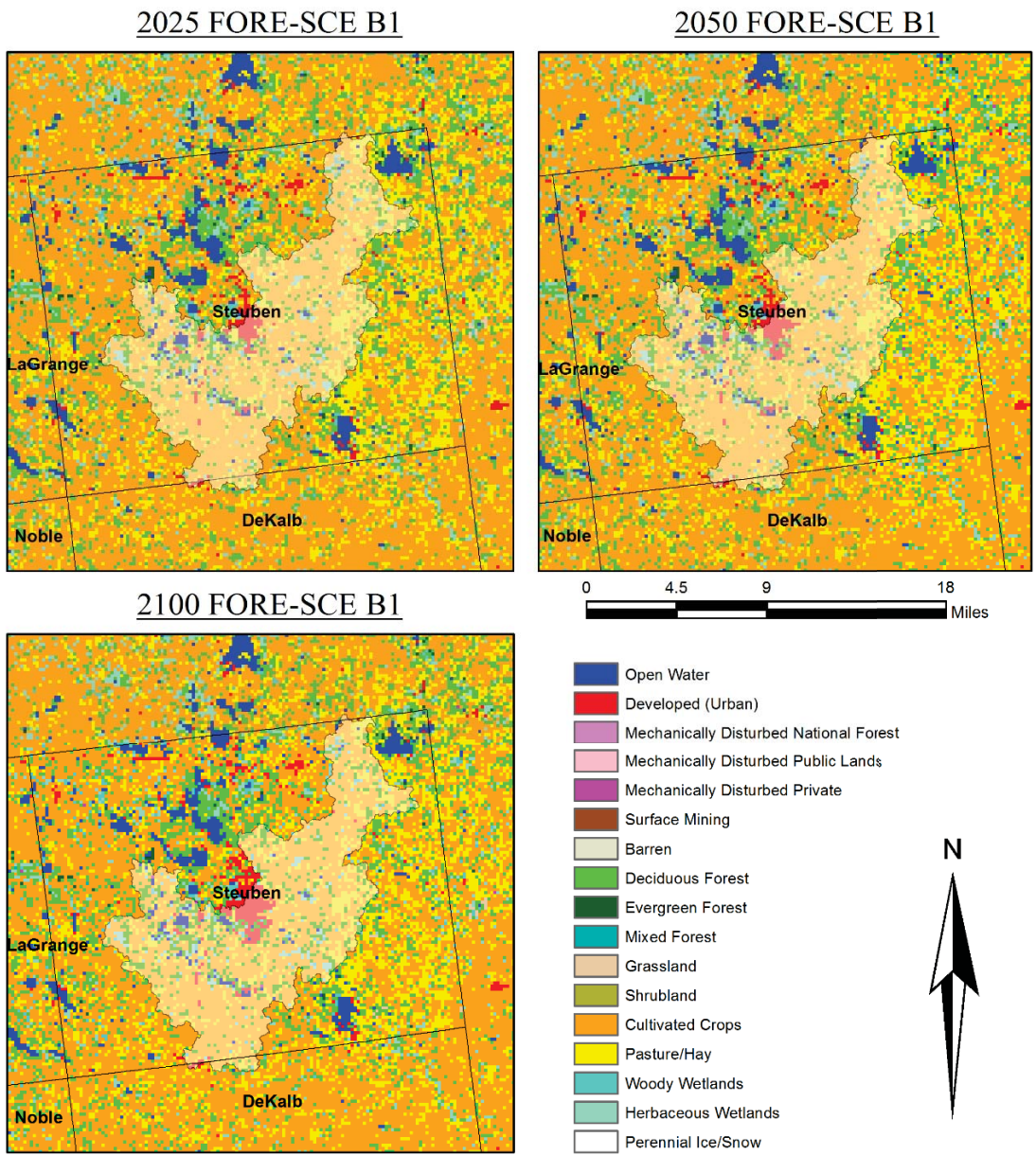


Figure C.15: Projected LULC conditions from FORE-SCE scenario B1 for Pigeon Creek, IN (USGS Station 0499510). (Data Source: USGS, 2014).

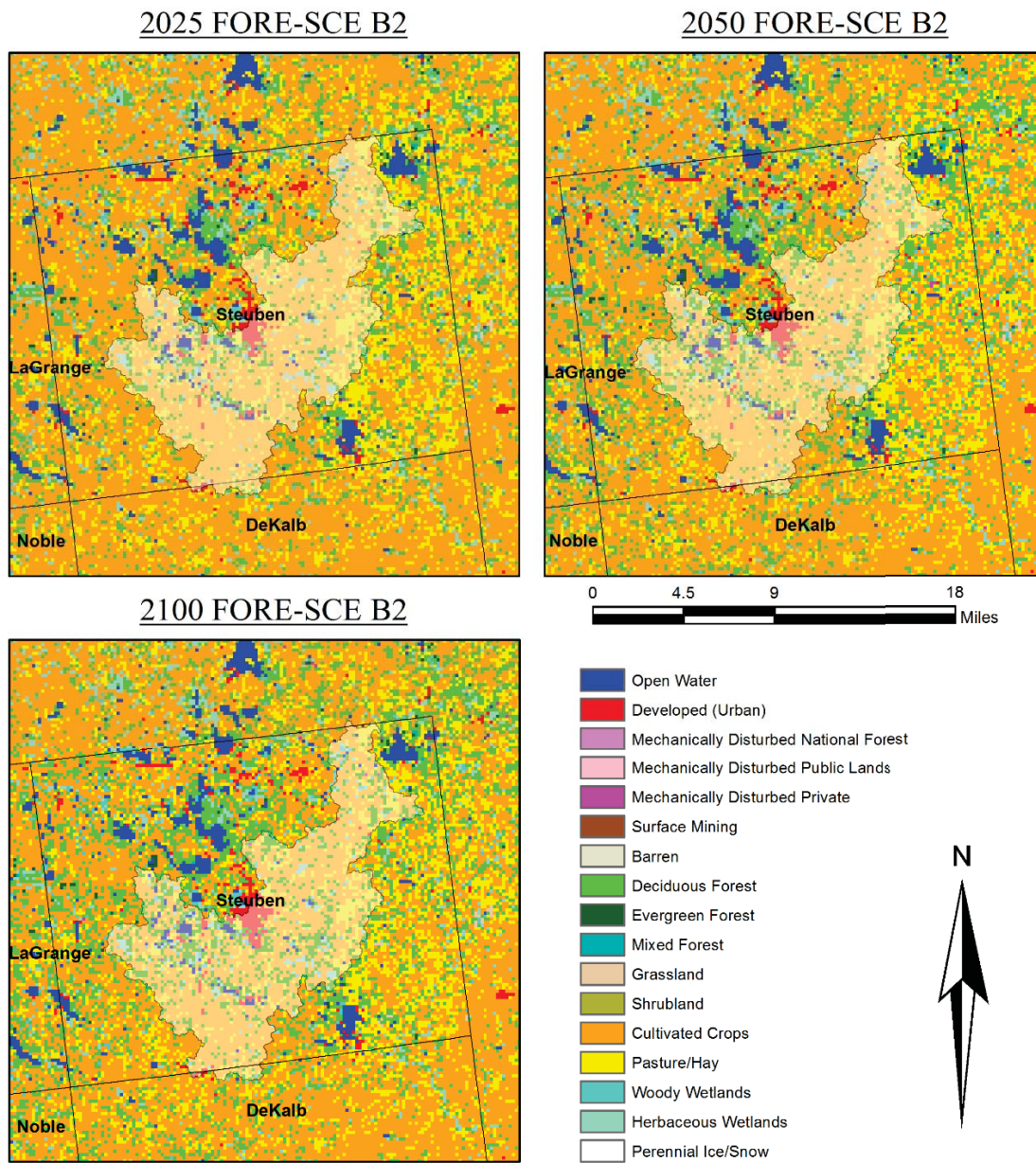


Figure C.16: Projected LULC conditions from FORE-SCE scenario B1 for Pigeon Creek, IN (USGS Station 0499510). (Data Source: USGS, 2014).

Appendix D. Hydrologic SWAT Model

This appendix provides a table with definitions of the NRCS hydrologic soil group classification system, as well as tables with results from SWAT simulations of instantaneous AMF series of both historical and future predicted LULC.

Table D.1: NRCS hydrologic soil groups (NRCS, 2007).

Soil Group	Description
A	Soil with high infiltration rates even when soil is thoroughly wetted and consisting mainly of deep, well-drained sand and gravel. High rates of water transmission
B	Soil with moderate infiltration rates when soil is thoroughly wetted and consisting of moderately deep to deep, moderately well to well-drained soils with moderately fine to moderately coarse textures. Moderate rates of water transmission
C	Soils with slow infiltration rates when thoroughly wetted and consisting mainly of soils with a layer that restricts the downward movement of the water or soils with moderately fine to fine textures. Slow rate of water transmission.
D	Soils having very slow infiltration rates when thoroughly wetted and consisting mainly of clay soils with a high swelling potential. Soils that have permanent high water tables, soils with a clay layer near to the ground surface, and shallow soils over nearly impervious materials. Very slow rates of water transmission

Table D.2: SWAT simulation output for current (base period) and historical AMF series (cms) for Pond Creek Watershed (USGS station 03302000).

Year	Observed	NLCD	Aerial	
	1980-200	1980-2000	1952-1972	1961-1981
1	70.23	17.50	17.20	20.12
2	54.09	49.27	62.30	64.71
3	83.25	74.03	68.80	69.42
4	146.68	64.58	68.09	70.44
5	83.25	92.80	96.00	102.61
6	111.29	79.22	76.05	79.30
7	47.01	25.26	26.00	29.11
8	95.71	37.58	40.44	43.32
9	117.23	114.82	111.97	115.68
10	145.27	107.55	105.37	105.81
11	135.07	150.87	147.55	154.01
12	78.44	80.23	84.11	86.34
13	113.27	60.85	63.38	67.03
14	62.86	71.49	72.02	74.68
15	62.86	33.23	39.38	40.45
16	109.02	85.58	87.73	91.70
17	141.87	61.30	73.87	76.64
18	220.87	351.25	336.17	341.90
19	78.72	37.34	40.34	42.80
20	112.13	95.44	93.00	97.92

Table D.3: SWAT simulation output for current (base period) and historical AMF series (cms) for Pigeon Creek Watershed (USGS station 04099510).

Year	Observed	NLCD	Aerial	
	1980-200	1980-2000	1952-1972	1970-1990
1	10.51	12.20	12.18	12.12
2	12.03	11.28	10.96	10.94
3	22.51	29.55	28.78	28.68
4	9.74	7.41	7.73	7.72
5	10.45	9.45	9.99	9.79
6	19.79	13.54	13.12	13.12
7	9.20	13.11	13.44	13.36
8	7.48	7.71	8.54	8.48
9	7.14	8.48	8.28	8.28
10	12.60	9.81	9.37	9.42
11	14.78	13.67	13.44	13.37
12	16.54	8.51	8.29	8.27
13	7.14	7.75	7.22	6.73
14	22.20	26.78	25.80	25.66
15	9.80	7.00	6.92	6.99
16	8.89	7.14	7.86	7.72
17	28.32	16.40	15.60	15.67
18	15.29	15.66	15.03	15.01
19	18.21	11.91	11.88	11.84
20	15.86	8.02	8.35	8.31

Table D.4: Instantaneous AMF series (cms) based on SWAT simulation output for FORE-SCE scenarios for Pond Creek Watershed (USGS station 03302000).

Year	Hindcast 1980-2000	A1B			A2			B1			B2		
		2000-2020	2040-2060	2080-2100	2040-2060	2080-2100	2040-2060	2080-2100	2040-2060	2080-2100	2040-2060	2080-2100	
1	31.1	40.4	45.9	47.1	45.8	47.5	44.0	45.5	43.6	44.2			
2	69.4	74.8	77.7	78.0	77.6	78.2	76.7	77.3	76.6	76.9			
3	65.2	59.7	60.5	61.1	60.5	61.3	59.5	60.3	59.4	59.7			
4	74.2	78.1	79.8	80.1	79.8	80.1	79.4	79.8	79.3	79.5			
5	126.9	138.1	143.7	144.7	143.7	145.0	141.8	143.2	141.6	142.2			
6	82.1	83.5	84.6	84.8	84.6	84.8	84.2	84.5	84.1	84.3			
7	33.7	35.5	37.0	37.4	37.0	37.4	36.5	36.9	36.4	36.6			
8	47.9	50.6	52.2	52.5	52.2	52.6	51.7	52.1	51.6	51.8			
9	117.6	115.9	116.0	116.2	116.0	116.2	115.8	115.9	115.9	115.8			
10	100.1	94.0	91.2	90.9	91.2	90.8	91.7	91.3	92.0	91.6			
11	158.7	158.0	159.0	159.4	159.0	159.4	158.4	158.8	158.3	158.4			
12	88.7	90.8	92.0	92.2	92.0	92.3	91.7	91.9	91.6	91.8			
13	71.6	72.8	74.1	74.3	74.0	74.3	73.5	73.9	73.6	73.6			
14	75.5	74.2	74.3	74.6	74.4	74.6	74.1	74.3	74.1	74.2			
15	43.0	45.9	47.5	47.9	47.5	48.0	47.1	47.5	46.9	47.2			
16	96.7	98.2	99.4	99.6	99.4	99.7	98.9	99.2	98.9	99.0			
17	83.8	88.7	91.8	92.3	91.7	92.5	90.8	91.5	90.7	91.0			
18	341.5	331.8	328.9	328.9	328.9	328.8	329.1	328.8	329.7	329.0			
19	47.0	49.4	50.9	51.1	50.9	51.2	50.4	50.8	50.3	50.5			
20	113.1	115.0	116.9	117.5	116.9	117.7	116.0	116.6	116.0	116.2			

Table D.5: Instantaneous AMF series (cms) based on SWAT simulation output for predicted FORE-SCE scenarios for Pigeon Creek Watershed (USGS station 04099510).

Year	A1B			A2			B1			B2		
	2000-2020	2040-2060	2080-2100	2040-2060	2080-2100	2080-2100	2040-2060	2080-2100	2080-2100	2040-2060	2080-2100	2080-2100
1	12.18	12.21	12.24	12.22	12.35	12.35	12.16	12.15	12.05	12.02		
2	11.35	11.49	11.62	11.42	11.69	11.69	11.37	11.46	11.34	11.36		
3	29.36	29.43	29.54	29.59	29.99	29.99	29.31	29.29	29.11	28.99		
4	7.44	7.24	7.87	7.30	7.59	7.59	7.48	7.98	7.20	7.55		
5	9.49	9.50	9.56	9.59	9.68	9.68	9.47	9.47	9.45	9.43		
6	13.56	13.97	14.37	14.02	15.14	15.14	13.58	13.59	13.39	13.34		
7	13.04	13.06	13.08	13.06	13.24	13.24	13.03	13.02	12.96	12.95		
8	7.50	7.52	7.56	7.44	7.63	7.63	7.43	7.44	7.43	7.42		
9	8.39	8.34	8.31	8.38	8.32	8.32	8.36	8.34	8.37	8.36		
10	9.89	10.09	10.23	9.97	10.27	10.27	9.92	9.99	9.87	9.87		
11	13.58	13.56	13.70	13.60	13.84	13.84	13.55	13.53	13.43	13.40		
12	8.53	8.62	8.67	8.64	8.90	8.90	8.48	8.48	8.48	8.49		
13	7.73	7.66	7.85	7.70	7.85	7.85	7.69	7.66	7.73	7.70		
14	26.76	27.10	28.17	27.25	29.12	29.12	26.54	26.53	25.82	25.57		
15	7.04	6.67	6.77	6.87	7.11	7.11	7.14	7.18	7.10	7.08		
16	7.81	7.75	7.65	7.83	7.63	7.63	7.84	7.80	7.78	7.81		
17	16.45	17.73	18.88	17.28	19.82	19.82	16.59	17.15	16.27	16.24		
18	15.74	15.87	16.03	15.91	17.35	17.35	15.65	15.65	15.46	15.38		
19	11.95	12.10	12.20	12.08	12.32	12.32	11.94	11.96	11.85	11.81		
20	7.91	7.93	7.92	7.91	7.95	7.95	7.85	7.92	7.85	7.91		